Investigating the Effects of Treating Hydrocarbon-Contaminated Water with Green Nano Zero-Valent Iron on Hydrocarbon-Degrading Bacteria

by

Yakubu Yakmut Saleh

A thesis submitted in fulfilment of the requirements for the degree of Doctor of Philosophy

(PhD)

Department of Civil and Environmental Engineering
University of Strathclyde
Glasgow, United Kingdom

May 2025

Declaration

I, **Yakubu Yakmut Saleh**, hereby certify that this thesis, entitled *"Investigating the Effects of Treating Hydrocarbon-Contaminated Water with Green Nano Zero-Valent Iron on Hydrocarbon-Degrading Bacteria,"* is entirely my own work except where otherwise acknowledged. All sources of information have been duly cited.

This thesis has not been submitted in whole or in part for any other degree or qualification at the University of Strathclyde or any other institution. Any work conducted in collaboration with others is clearly indicated, and all necessary ethical and safety approvals were obtained in accordance with University regulations. The copyright of this thesis belongs to me under the terms of the United Kingdom Copyright Act as qualified by the University of Strathclyde Regulation 3.50.

I understand that the University of Strathclyde reserves the right to submit my work to plagiarism-detection software and to make it available for reference and inter-library loan, subject to any agreed embargoes.

Signature: Yakubu Yakmut SALEH

Date: 13th May 2025

Acknowledgements

I want to start by saying Alḥamdulillāh. All praise is due to Allah, the Most Gracious, the Most Merciful, for granting me the strength, clarity of mind, and good health to undertake and complete this doctoral journey. Every achievement herein is ultimately a manifestation of His mercy and guidance.

I owe immeasurable gratitude to my principal supervisor, Dr Charles Knapp. His deep expertise, thoughtful critiques, and steady encouragement transformed initial ideas into a coherent body of work. His open-door policy, immediate responses and genuine enthusiasm for research fostered an environment where curiosity and rigour could thrive. I am equally indebted to my second supervisor, Dr Christine Switzer, whose constructive criticism and methodical approach consistently elevated the scientific and practical dimensions of this thesis. Their combined supervision has shaped both my academic skills and my professional outlook.

Behind every successful experiment stands a diligent support team. I thank Mara Knapp, Head of Laboratory Services, whose impressive organisational skills ensured that consumables and instrumentation were always available when deadlines loomed. Dr Tatyana Peshkur generously guided me through the operation and troubleshooting of key analytical equipment, especially the GC-FID, turning technical hurdles into valuable learning experiences. Dr Mark Stillings, for providing hands-on assistance and insightful suggestions in the lab, often at short notice. I appreciate all other PHD colleagues in the Department of Civil & Environmental Engineering for their camaraderie, stimulating discussions, and the many informal peer reviews that sharpened this work.

Beyond the laboratory, I am grateful to Akinseye Roland Olarenwaju, a true friend and fellow PHD colleague, whose encouragement and problem-solving spirit lightened the most challenging phases of my research. My former classmate, Dr Ibrahim Lawal, served as the spark for my Strathclyde journey; his achievements convinced me that this was the right place to grow academically and personally.

I acknowledge the Nigerian Upstream Petroleum Regulatory Commission (NUPRC), my employer, for granting the study leave that enabled this pursuit and for providing real-world perspectives that

continually informed my research questions. My sincere thanks also go to the Petroleum Technology Development Fund (PTDF) for the generous scholarship and financial support, without which this PHD would have remained a distant aspiration. Their investment in human capital is contributing directly to sustainable solutions for the energy sector.

Finally, and most profoundly, I thank my family. To my beloved wife, Naja'atu Zailani Ahmadu, your unwavering faith in my abilities, your prayers, and your endless patience have been my anchor. You shouldered extra responsibilities so I could focus on experiments and writing, and your words of encouragement sustained me through every setback. To our wonderful children, Ruqayyah, Khadijah, and Abdullahi, your laughter, curiosity, and unconditional love remind me daily why hard work and perseverance matter. You are my greatest motivation to be the kind of role model you can proudly emulate. I also wish to honour my mother and siblings for their constant prayers, encouragement, and loving words from home. Their unwavering belief in my abilities has been a quiet yet powerful source of strength throughout this journey.

May Allah reward every person who supported this endeavour through advice, kindness, or prayer in ways seen and unseen.

Abstract

This thesis investigated how green-synthesised nanoscale zero-valent iron (nZVI), produced with polyphenols extracted from green tea, influenced both the breakdown of petroleum hydrocarbons and the resident hydrocarbon-degrading bacteria in contaminated water, benchmarked against a commercially manufactured nZVI of similar nominal size. Polyphenols were extracted from dried *Camellia sinensis* (green tea) leaves by aqueous infusion at 80°C, followed by filtration and centrifugation to obtain a clarified extract used as both the reducing and stabilising agent during synthesis. The work addressed four objectives. First, green nZVI was prepared by reducing $FeCl_3 \cdot 6H_2O$ with optimised green-tea extract, then characterised alongside the industrial material by X-ray diffraction (XRD), scanning electron microscopy (SEM) and energy-dispersive X-ray spectroscopy (EDS). XRD revealed broader peaks for the green particles, while SEM showed agglomerates of 50–90 nm compared with 30–45 nm for the industrial sample; EDS showed that the green nZVI were composed chiefly of iron, carbon and oxygen, with a minor chlorine signal attributable to residual $FeCl_3 \cdot 6H_2O$ used in the reduction step. The industrial nZVI displayed the same dominant Fe–C–O profile without the chlorine.

Second, batch samples containing hydrocarbon-contaminated water were dosed in triplicate with three concentrations of each nZVI formulation (0.004 mg/L, 0.01 mg/L and 0.004 mg/L dosages for green nZVI and 0.004 mg/L, 0.010 mg/L and 0.0040 mg/L dosages of industrial iron nanoparticles). Chemical oxygen demand (COD) and total petroleum hydrocarbons (TPH) were measured at two hours and 24h through a HACH COD test kit and GC-FID, respectively. Third, microbial DNA was extracted, quantitatively assessed, and sequenced (16s rRNA amplicons) to determine shifts in taxonomic composition, and multivariate statistics, mainly paired-sample t-tests and bar charts, were applied to relate dose, formulation and exposure time to both chemical and ecological responses. Finally, dose-response envelopes were derived to recommend practical application rates for pilot-scale nano-bioremediation.

Industrial nZVI removed TPH more rapidly within two hours (mean 67 % at the lowest dose of 0.004 mg/L) but plateaued by 24 h (maximum 73 %). Green nZVI achieved lower initial removal (45 % average) yet approached comparable 24-h efficiencies (64 % at 0.004 mg/L), with COD trends mirroring TPH reductions. Early-stage differences between formulations were statistically significant ($p < 0.001$), but the gap narrowed after 24 h.

Microbial analysis showed that untreated controls were dominated by Proteobacteria (64 %), Bacteroidetes (18 %) and Actinobacteria (14 %). Industrial nZVI caused up to a 32 % decline in total Operational Taxonomic Units (OTUs) and temporarily suppressed *Flavobacteriales*. In contrast, green nZVI, particularly at 0.004 mg/L, stimulated microbial abundance by 25–38 % after 24h and selectively enriched hydrocarbonoclastic orders such as *Burkholderiales*, *Rhizobiales* and *Actinomycetales*.

The study concluded that the organically capped green nZVI balanced abiotic reduction with biotic degradation, delivering near-industrial TPH removal while fostering a more resilient and functionally relevant microbial community. A moderate green nZVI dose of 0.004-0.01 mg/L per 100 mL and a minimum 24h contact time were recommended for field trials. These findings underscore the potential of plant-derived nZVI as a sustainable alternative to chemically synthesised particles, capable of reconciling high remediation performance with ecological stewardship and providing a template for future nano-bioremediation policies.

Table of Contents

List of Tables

List of Figures

List of Publications and Conference Presentations

1. Saleh, Y. Y., Peshkur, T., & Knapp, C. (2025). Balancing Efficacy and Sustainability: A Comparative Study of Green-Synthesised and Industrial Nano Zero-Valent Iron for Hydrocarbon Remediation. Next Nanotechnology (Elsevier). Under second revision, awaiting final publication review.
2. Saleh, Y. Y., Akinseye, O., & Knapp, C. (2025). From Particle to Community: How Green Nano Zero-Valent Iron Compares to Industrial Iron Nanoparticles in Driving Sustainable Hydrocarbon Bioremediation. Discover Nano (Springer Nature). Under review.

List of Abbreviations/Acronyms

Abbreviation	Full Term
ANOVA	Analysis of Variance
BET	Brunauer–Emmett–Teller (surface-area analysis)
BOD	Biochemical Oxygen Demand
BTEX	Benzene, Toluene, Ethylbenzene, and Xylenes
COD	Chemical Oxygen Demand
DI	De-ionised (water)
EDS	Energy-Dispersive X-ray Spectroscopy
FeONPs	Iron-Oxide Nanoparticles
FTIR	Fourier-Transform Infra-Red Spectroscopy
GC-FID	Gas Chromatography–Flame Ionisation Detector
HCB	Hydrocarbonoclastic Bacteria
HPLC	High-Performance Liquid Chromatography
ICP-OES	Inductively Coupled Plasma–Optical Emission Spectroscopy
ISO	International Organization for Standardization
LCA	Life-Cycle Assessment
LCI	Life-Cycle Inventory
MIC	Minimum Inhibitory Concentration
MS	Mass Spectrometry
nZVI	Nanoscale Zero-Valent Iron
OHCB	Obligate Hydrocarbonoclastic Bacteria
OTU	Operational Taxonomic Unit
PAH	Polycyclic Aromatic Hydrocarbon
PCoA	Principal Coordinates Analysis
PCR	Polymerase Chain Reaction

PTDF	Petroleum Technology Development Fund
qPCR	Quantitative Polymerase Chain Reaction
QIIME	Quantitative Insights Into Microbial Ecology
RHD	Ring-Hydroxylating Dioxygenase
ROS	Reactive Oxygen Species
SDG	Sustainable Development Goal
SEM	Scanning Electron Microscopy
SPSS	Statistical Package for the Social Sciences
TEM	Transmission Electron Microscopy
TPH	Total Petroleum Hydrocarbons
UV-vis	Ultraviolet–Visible Spectroscopy
WHO	World Health Organisation
XRD	X-ray Diffraction

Chapter 1 INTRODUCTION

1.1 Opening Statement

Environmental pollution, particularly from hydrocarbon compounds, is a pressing global issue. Its severe impacts on human health, ecosystems, and economic development are felt worldwide (Xu et al., 2022). The situation in Africa is especially critical, notably in oil-producing areas where exploration, refining, and transportation are widespread. In particular, Nigeria faces a persistent issue with hydrocarbon pollution caused by frequent oil spills from ageing infrastructure, pipeline vandalism, and artisanal refining. According to the Nigerian Upstream Petroleum Regulatory Commission (NUPRC), there were 547 reported oil spill incidents in 2020, 535 in 2021, 561 in 2022, 575 in 2023, and 734 in 2024, marking a 34% increase over five years (NUPRC, 2024). These incidents collectively damage thousands of hectares of land and water ecosystems, threatening water quality, biodiversity, and local livelihoods in oil-rich regions of the Niger Delta. Contaminated water resources pose an environmental risk, disrupt ecosystems, and hinder economic development in affected communities. (Tukur Umar and Hajj Othman, 2017).

Conventional hydrocarbon remediation methods, which use mechanical excavation, chemical treatment, and natural attenuation, typically do not completely remove contaminants, particularly from complex media like groundwater and deep-soil layers. Most are also relatively expensive and time-consuming (Ambaye et al., 2022, Aparicio et al., 2022). Moreover, they may have potential adverse environmental impacts, making them less suited for wide application in limited-resource situations and underscoring the need for a more sustainable approach (Hussain, 2022, Sweeney et al., 2024).

In response to these challenges, recent research has focused on nanotechnology, particularly nano zero-valent iron (nZVI), for its significant reactivity and broad applicability to pollutant degradation. However, conventional synthesis methods for nZVI are based on toxic chemicals, which can provoke severe environmental safety and sustainability concerns. A crucial aspect that still remains poorly

comprehended is the interlinking interactions of nZVI with hydrocarbon-degrading bacteria, which play a vital role in the complete degradation process.

Given these shortcomings, this research aims to develop a sustainable, eco-friendly method for synthesising nZVI using natural plant extracts. This approach, which also explores its potential use in conjunction with bioremediation, aims to provide an economically feasible and efficient approach to hydrocarbon-polluted water remediation. The goal is to ensure that the remediation efforts will be ecologically viable and beneficial for the local microbial ecosystems, which are crucial for long-term restoration.

1.2 Background of the Study

Hydrocarbons, which are extracted from crude oil and various petroleum products, are one of the most common groups of contaminants in the environment. Once they are introduced into environmental systems, they can persist for long periods and have the potential to disrupt ecosystems and make water supplies unsafe for drinking, agriculture, and aquatic organisms. The potential of hydrocarbons to persist in the environment is of particular concern due to compounds such as aromatic hydrocarbons, polycyclic aromatic hydrocarbons (PAHs), aliphatic hydrocarbons, halogenated hydrocarbons, and naphthenic acids (Murgueitio et al., 2018). These compounds are known to be carcinogenic and cause immune system suppression, reproductive disorders, endocrine disruption, liver damage and respiratory issues. In aquatic environments, PAHs are highly toxic, causing mortality, developmental deformities, DNA damage, and reproductive failure in fish, invertebrates, and amphibians (Bojes and Pope, 2007, Mallah et al., 2022). Accidental and deliberate oil spills, industrial effluents and poor waste disposal of hydrocarbons in ecosystems drastically change the nature of such environments. For instance, hydrocarbons can make a thick film on the water surfaces, which prevents aeration and consequently suffocates most aquatic life (Kiamarsi et al., 2019). In terrestrial ecosystems, the presence of hydrocarbons interferes with the structural form of the soil; its fertility is compromised, and the formation of anaerobic conditions does not favour the existence of most life forms (USEPA, 2020b).

Conventional remediation techniques, including mechanical removal, chemical interventions, and natural attenuation processes, frequently prove inadequate in dealing with the intricate characteristics of hydrocarbon pollution that require instantaneous in situ remediation, especially within groundwater and soil (USEPA, 2020c). These approaches may incur high costs, require extensive time commitments, and pose environmental risks, occasionally resulting in additional ecological damage. For instance, chemical dispersants can form smaller, more bioavailable hydrocarbon particles, which may enhance toxicity to aquatic organisms (Crampon et al., 2019).

In recent years, nanotechnology has emerged as a promising alternative for environmental remediation. Nano zero-valent iron (nZVI) has attracted significant attention due to its high surface area, reactivity, and its ability to degrade various contaminants, including hydrocarbons (Karn et al., 2011). Nano zerovalent iron (nZVI) operates by donating electrons to contaminants, reducing them to less harmful forms. These recent advances in nanotechnology have opened up new possibilities for remediating environmental pollutants (Das and Patra, 2021).

However, the conventional chemical synthesis of nZVI involves using hazardous reagents, such as sodium borohydride, which raises concerns about the environmental and health impacts of the nanoparticles themselves (He and Zhao, 2005, Barzan et al., 2014). Sodium borohydride is effective but environmentally burdensome. When $NaBH_4$ is hydrolysed to make nZVI, it converts almost quantitatively to sodium metaborate and caustic soda, generating an alkaline, boron-rich wastewater that must be neutralised and diluted to avoid phytotoxicity or aquatic stress (Kozma et al., 2016, Nunes et al., 2021).

In light of the constraints associated with conventional remediation techniques and the capabilities of nanoscale zero-valent iron (nZVI), there is an increasing focus on creating more environmentally friendly and sustainable strategies for the synthesis of nanoparticles. Green synthesis approaches, which incorporate plant extracts or microorganisms as reducing and stabilising agents, present a viable alternative. Such methods are characterised by their environmental compatibility, economic

efficiency, and the ability to yield nanoparticles that exhibit improved stability and reactivity (Wang et al., 2014). Iron nanoparticles (Fe-NPs) can be synthesised from plant extracts through a green synthesis approach. This eco-friendly method involves utilising biomolecules present in plant extracts to reduce metal salts, acting as both reducing and capping agents for the nanoparticles. The process is simple, rapid, cost-effective, and sustainable. Various plant materials can be used for this purpose, offering a wide range of potential sources for Fe-NP synthesis (Haider et al., 2024).

1.3 Problem Statement

The enduring characteristic of hydrocarbon pollution presents a considerable obstacle to environmental restoration efforts, especially in areas such as Africa, where industrial operations and oil spills are common occurrences. In these regions where oil spills and industrial effluents occur frequently, there is a dire need for effective, practical, cost-effective and environmentally compatible remediation strategies that can clean up contaminated water bodies as soon as they happen. The current gap in research involves the development of an environmentally friendly method for nZVI synthesis that will minimise environmental impacts while enhancing and facilitating bioremediation.

However, even though nZVI is quite effective in hydrocarbon degradation, it has some drawbacks because conventional synthesis methods involve toxic chemicals, are generally very expensive, and introduce additional environmental risks.

There seems to be a limited understanding of the interactions between nZVI and the hydrocarbon-degrading bacteria, which are integral in bioremediation. With the world rapidly turning to nanotechnology as a means of remediating contaminated soil and water, the first concern is the potential environmental impact of these nanoparticles, and an efficient approach to estimate nanotoxicity is to observe how the in situ bacteria respond to their application (Barzan et al., 2014).

Bacteria like *Pseudomonas* spp. and *Achromobacter* spp. possess metabolic processes capable of breaking down hydrocarbons into relatively less harmful compounds (Chikere et al., 2011). The

potential growth-inhibiting effects of nZVI on such bacterial communities, as a result of possessing antimicrobial properties, have gone largely unexamined (Staroń and Długosz, 2021).

Conversely, these challenges create a pressing need for a novel remediation strategy that would be effective and sustainable. The objective of this research is to meet this demand by developing a green synthesis method of nZVI and conducting studies regarding its application in combination with bioremediation to come up with a synergistic approach that will catalyse hydrocarbon degradation and enhance the natural microbial activity that is essential for long-term ecosystem recovery**.**

1.4 Research Gap

Limited research works are available on green-synthesised nZVI coupled with bioremediation for hydrocarbon-contaminated water. Although several studies have proved the feasibility of nZVI in the degradation of many kinds of pollutants, the interaction between nZVI and bacteria that degrade hydrocarbons is barely described. In addition, the conventional synthesis of nZVI has environmental risks that do not justify sustainable development objectives, especially in regions with limited resources like Africa.

This research aims to address these gaps by creating an environmentally friendly formulation strategy for nZVI and investigating its potential application in a collaborative remediation approach. The findings could present a cost-effective and sustainable solution to one of the most pressing environmental issues of underdeveloped regions.

Most of the existing literature on hydrocarbon remediation focuses either on chemical or biological methods, with limited exploration of the potential synergy between the two. While nano zero-valent iron (nZVI) has been extensively studied for its ability to reduce and degrade various contaminants, there is a gap in research on its interaction with hydrocarbon-degrading bacteria. As a result, there is a shortage of literature on microbial activity and bioremediation, which is essential for the mineralisation of hydrocarbons (Jouanneau et al., 2011).

In addition, these conventional methods of synthesising nZVI pose environmental and health risks due to the use of hazardous chemicals. Although eco-friendly synthesis techniques have been proposed as a viable alternative, there is a lack of research on the effectiveness of nZVI produced through green synthesis in real-world remediation scenarios, particularly in the treatment of hydrocarbon-contaminated water (Machado et al., 2013, Kharissova et al., 2013a). Most studies on green synthesis have focused on nanoparticle production and characterisation, with limited exploration of their practical application in complex environmental contamination scenarios.

It is also important to note that the unique challenges underdeveloped countries face are often overlooked in global discussions on environmental remediation, such as limited access to advanced remediation technologies and the pervasive presence of large-scale hydrocarbon contamination. This study intends to help fill these gaps by not only developing a green synthesis method for nZVI but also testing its applicability regarding unique sub-Saharan environmental challenges without ignoring the global applicability.

Eradicating these gaps would enhance the formulation of sustainable and efficient remediation approaches that can be applied in resource-poor settings, hence promoting the overall objectives of environmental conservation and public health across oil-producing communities.

1.5 Research Objectives and Questions

This research aims to investigate the combined effects of using green-synthesized nZVI (nanoscale zero-valent iron) and bioremediation techniques to treat water contaminated with hydrocarbons. The specific objectives of this study are:

1. Synthesis and Characterization of Green nZVI:

Demonstrate that a polyphenol-assisted, environmentally benign synthesis route can reliably produce reactive zero-valent iron and establish how its particle size, surface chemistry, and crystallinity compare with those of commercial nZVI. The aim is to highlight structural differences that may

translate into potential functional advantages, thereby justifying the pursuit of a green, low-toxicity alternative to conventional chemical synthesis methods.

2. Assessment of Treatment Efficiency:

Investigate the dose and time-dependent reduction of total petroleum hydrocarbons (TPH) of green nZVI, compare and determine whether the end-point performance meets or exceeds that of industrial iron while using less material or milder chemistry. The aim is to establish kinetic and efficiency benchmarks that can guide scale-up and cost-benefit analyses.

3. Impact on Hydrocarbon-Degrading Bacteria:

Identify existing microbial taxa, investigate how each nZVI formulation alters total biomass and the abundance of key hydrocarbon-degrading taxa, and whether these biological shifts enhance or hinder overall remediation potential. Success is defined by identifying conditions under which green nZVI stimulates functional guilds rather than suppressing them, thereby validating a nano-bio synergy.

4. Development of an Integrated Remediation Approach:

Merge the chemical and biological findings into practical design envelopes for an optimal iron dose, contact time, and follow-up biostimulation steps that can be transferred to field conditions, particularly in resource-limited regions. The goal is to deliver a blueprint that balances contaminant removal, ecological health and economic feasibility, positioning green nZVI as a viable component of sustainable remediation policies.

1.6 Conceptual Framework

The conceptual framework for this research is based on integrating green nZVI synthesis with bioremediation. The framework consists of the following components:

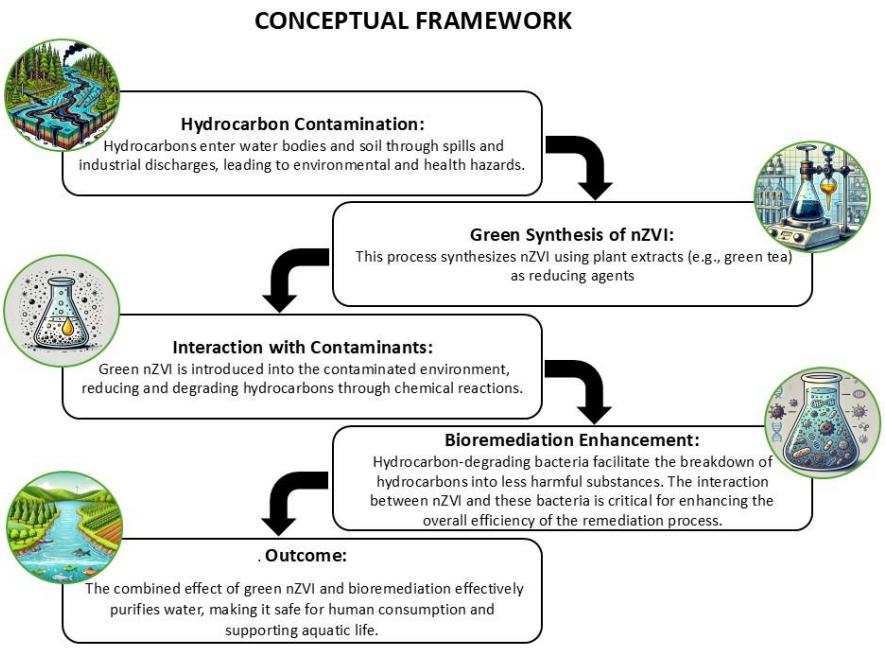

Figure 1.1 Research Conceptual Framework

1.7 Thesis Structure

This thesis is organised into six chapters, each designed to build a comprehensive understanding of the research, from its background to the identified problem, the recommended practical solutions, potential applications and the contributions to knowledge.

Chapter One serves as the introduction to the research, establishing the context by underscoring the importance of hydrocarbon contamination as a critical environmental issue. This chapter presents the background of the study, delineating the scope of the problem and highlighting the need for innovative remediation strategies. The problem statement articulates the specific research gap that this study intends to address. Additionally, this chapter outlines the research aims and objectives, thus providing a clear roadmap for the research. The conceptual framework elaborates on the theoretical and practical foundations of the research, while the thesis structure offers an overview of the organisation of the document.

Chapter Two consists of the literature review, which examines the existing body of knowledge related to hydrocarbon contamination and the remediation methods. It begins with an overview of hydrocarbons, including their types, sources, and environmental impacts, particularly on water

resources affected by the oil and gas industry. The chapter further explores traditional mechanical, chemical, and biological remediation methods, providing context for the study's focus on nanotechnology. It discusses the synthesis, stabilisation, and applications of nano zero-valent iron (nZVI) in hydrocarbon remediation, particularly emphasising green synthesis techniques. Additionally, the review covers bioremediation mechanisms and the interactions between nanoparticles and microbial communities, highlighting both the potential for beneficial synergy and the associated challenges. Lastly, the chapter addresses the relevance of this research to sustainable development while emphasising its contribution to global knowledge and policy development.

Chapter Three focuses on the methodology used in the study. It begins with collecting and preparing contaminated water samples, followed by extracting and analysing polyphenols, which act as reducing agents in the green synthesis of nanoscale zero-valent iron (nZVI). The synthesis process is described in detail, along with characterisation techniques such as Scanning Electron Microscopy (SEM), Energy Dispersive Spectroscopy (EDS), and X-ray diffraction (XRD). This chapter also explains the method used to quantify hydrocarbon contamination and outlines the experimental setup for reduction studies. Additionally, it covers the cultivation and identification of hydrocarbon-degrading microorganisms, including the DNA analysis of microbial communities. This text emphasises the importance of thorough testing and analysis to ensure the findings are reproducible and reliable.

In Chapter Four, the results of the study are presented in detail. It starts with a detailed characterisation of both the synthesised green nanoscale zero-valent iron (nZVI) and the conventional industrial nanoscale zero-valent iron. This section includes not only the structural properties, such as particle size and morphology observed through microscopy techniques (SEM), but also the chemical composition analysed via Energy Dispersive X-Ray Spectroscopy methods (EDS). Subsequently, the physical properties, including surface area and magnetic characteristics, are discussed to provide a thorough understanding of the synthesised material. Following this characterisation, the chapter evaluates the hydrocarbon reduction efficiency of both green and industrial nZVI. This evaluation is

conducted across a range of dosages and exposure times, allowing for a robust comparison of their performance. The study measures the extent of hydrocarbon degradation and identifies the optimal conditions for each type of nZVI.

The chapter further explores the impact of nZVI on hydrocarbon-degrading microorganisms, specifically bacteria. It analyses the effects of both green and industrial nZVI on the trend of activity of these organisms, highlighting the potential benefits or drawbacks of using green-synthesized nZVI in bioremediation efforts. Finally, the results from the green nZVI are compared with those obtained from traditional nZVI. This comparative analysis provides valuable insights into the benefits and limitations of using green-synthesized nZVI, emphasising its potential applications in environmental remediation and sustainability practices.

Chapter five moves beyond the presentation of raw data to examine how and why the findings matter. It opens by revisiting the key results from Chapter four particle characteristics, contaminant-removal curves and microbial-community shifts and then threads them through the broader environmental-remediation literature. By comparing the performance of the green-synthesised nZVI with that of a conventional industrial powder, the discussion tests long-standing assumptions about dose, reactivity and ecological impact, highlighting both convergences and divergences with earlier laboratory and field studies.

The chapter then interprets what these comparisons mean for the thesis as a whole. It shows how the chemical and biological evidence collectively advance the research objectives: proving the feasibility of green synthesis, quantifying treatment efficiency, clarifying microbial responses and outlining a practicable nano-bioremediation strategy. Limitations such as batch variability and short laboratory time frames are acknowledged, not as failings, but as guideposts for future work and policy development. In this way, Chapter 5 functions as the bridge between the experimental proof-of-concept and the actionable conclusions and recommendations that follow

Chapter six draws the thesis to its final destination by distilling the experimental evidence and the preceding discussion into a concise set of take-home messages. It reminds the reader how each objective was tackled. From there, the chapter lists the major findings in the same order as the original objectives, showing at a glance how the study succeeded in fabricating a plant-derived nanomaterial, quantifying its hydrocarbon-removal performance, documenting its effects on microbial communities, and outlining a pragmatic, low-impact remediation strategy.

The remainder of Chapter 6 shifts from “what we learned” to “why it matters and where we go next.” It highlights the scientific insight gained into dose-dependent nano–bio synergy, sets out engineering design windows for pilot projects, and frames the work in terms of global sustainability goals. Recognising that every study has constraints, the chapter also candidly notes the main limitations and translates them into a focused agenda for future research and policy development.

The thesis is rounded off with references to all cited works, ensuring academic rigour and appendices containing supplementary information. This structure is intended to provide a logical flow from identifying the problem to offering solutions, ultimately contributing to the global effort to address hydrocarbon contamination.

Chapter 2 LITERATURE REVIEW

2.1 Overview of Hydrocarbon Contamination

Hydrocarbon contamination in water bodies is a significant environmental issue, primarily resulting from anthropogenic activities such as oil spills, industrial discharge, and improper waste disposal (Bashir et al., 2020a). Hydrocarbons, composed of hydrogen and carbon, originate from both natural petroleum sources and synthetic chemical processes (Pimentel and dos Reis, 2020). Their widespread presence in aquatic ecosystems raises concerns due to their detrimental effects on water quality, aquatic life, and human health, necessitating robust remediation strategies (Poole, 2024). Given the increasing global dependence on fossil fuels and industrialisation, hydrocarbon contamination has become a persistent challenge, exacerbating concerns regarding ecological sustainability and environmental degradation (Das and Chandran, 2011).

The persistence of hydrocarbons in the environment is primarily attributed to their hydrophobic nature, which enables them to accumulate in sediments and bioaccumulate in aquatic organisms, posing long-term contamination risks (Galdames et al., 2020). These compounds can infiltrate marine ecosystems, freshwater resources, and groundwater systems, where their chemical stability and resistance to natural degradation make remediation efforts increasingly complex. Understanding the types of hydrocarbons, their sources, and their environmental impacts is essential for developing effective and targeted remediation approaches.

While natural sources of hydrocarbon contamination primarily include seepage from oil and gas reserves, anthropogenic contributions such as oil spills, industrial discharge, and urban runoff are more prevalent and pose greater environmental threats. Oil spills, exemplified by incidents such as the Deepwater Horizon disaster, highlight the severe ecological and socio-economic consequences of hydrocarbon contamination, leading to biodiversity loss, habitat destruction, and public health risks (Barron et al., 2020). Urban runoff further exacerbates the problem, as stormwater carrying hydrocarbons from roads and industrial sites flows into rivers and oceans, elevating pollutant levels in aquatic environments (Müller et al., 2020).

The consequences of hydrocarbon contamination are multifaceted, impacting marine life, human health, and economic stability. Aquatic organisms suffer from toxic effects, reducing biodiversity and compromising ecosystem resilience(Sharma et al., 2024). Humans, particularly communities reliant on affected water bodies for drinking water and sustenance, face health risks such as gastrointestinal disorders and respiratory complications due to prolonged exposure to contaminated water. Moreover, industries dependent on clean water resources, such as fisheries and tourism, experience financial losses due to declining fish populations, habitat degradation, and the high costs associated with remediation efforts.

Effectively addressing hydrocarbon contamination requires a comprehensive approach integrating advanced monitoring, detection, and remediation strategies. Technologies such as remote sensing and laboratory toxicity testing play crucial roles in assessing contamination levels and guiding effective response efforts (Thomas et al., 2013). As environmental concerns continue to escalate, the urgency for sustainable practices and efficient cleanup methods remains a paramount issue for policymakers, industry stakeholders, and affected communities. Ensuring long-term ecological stability necessitates collaborative efforts toward improved pollution control, regulatory enforcement, and the adoption of innovative remediation technologies.

2.1.1 Types of Hydrocarbons and Their Sources

Hydrocarbons are organic compounds composed solely of hydrogen and carbon atoms. They are broadly classified into three major categories: aliphatic hydrocarbons, aromatic hydrocarbons, and complex petroleum fractions (Kumar et al., 2023). These classifications adversely influence their environmental behaviour, degradation rates, and toxicity, making them crucial to understanding their persistence and impact in contaminated ecosystems (Kostka et al., 2014).

Aliphatic hydrocarbons consist of carbon atoms arranged in straight or branched chains and are classified into two main types: saturated and unsaturated hydrocarbons. Saturated aliphatics, also known as alkanes or paraffin, contain only single bonds between adjacent carbon atoms, making them

relatively stable and less reactive. In contrast, unsaturated aliphatics include alkenes (compounds with one or more double bonds) and alkynes (compounds with one or more triple bonds), which exhibit higher chemical reactivity and are more susceptible to environmental degradation (Speight, 2017).

Common examples of aliphatic hydrocarbons include ethane (≈ 60 mg/L), ethylene (≈ 130 mg/L), and acetylene (≈ 1200 mg/L), which are soluble in water at 25°C. These short-chain alkanes are widespread in various petroleum products and are often overlooked in crude oil spills (Abbasian et al., 2015). They dissolve readily and drive rapid biological oxygen demand as microbes oxidise them to CO_2, making them priority targets for monitoring and rapid-response remediation (Khademian and Imlay, 2021). Due to their relatively low molecular weight, smaller aliphatic hydrocarbons often emulsify in water, making their removal from contaminated water systems more challenging. Conversely, medium- to long-chain alkanes (C_{12}–C_{30}) initially float as oil slicks as a result of densities ranging between 0.75–0.90 g/cm^3, over time, weathering, including evaporation, oxidation, biodegradation and emulsification with minerals increases the residue's density until it loses buoyancy and sinks or forms neutrally buoyant tar balls that settle in sediments.

Due to their structural diversity, aliphatic hydrocarbons play a significant role in hydrocarbon contamination, particularly in marine and freshwater environments. Their varying biodegradability, volatility, and solubility influence their persistence in contaminated ecosystems and dictate the selection of appropriate remediation approaches. Understanding these properties is essential in formulating effective mitigation techniques for hydrocarbon spills and other environmental contamination events.

Aromatic hydrocarbons are organic compounds containing one or more benzene rings, which contribute to their chemical stability, persistence, and toxicity in the environment (Speight, 2017). These hydrocarbons are commonly found in petroleum products, industrial effluents, vehicle emissions, and oil spills, making them a significant source of pollution in both terrestrial and aquatic ecosystems.

One major group of aromatic hydrocarbons is BTEX compounds, which include benzene, toluene, ethylbenzene, and xylene. These compounds are widely used as industrial solvents and fuel additives, making them prevalent in urban and industrial wastewater (Saeedi et al., 2024). Due to their high volatility and solubility (see table 2.1 below), BTEX compounds readily disperse in water and air, increasing the likelihood of human and environmental exposure. Benzene, in particular, is well-documented as a potent carcinogen that poses severe health risks upon prolonged exposure (Yu et al., 2022).

Another critical class of aromatic hydrocarbons is polycyclic aromatic hydrocarbons (PAHs), which consist of multiple fused benzene rings. PAHs, such as naphthalene, anthracene, and benzo[a]pyrene, are of particular concern due to their strong carcinogenic and mutagenic properties (Patel et al., 2020). These compounds are primarily released through incomplete combustion processes, including industrial emissions, vehicle exhaust, coal burning, and oil spills hence the terms: pyrogenic, petrogenic and pHytogenic. PAHs have a strong affinity for sediments, leading to their long-term accumulation in aquatic ecosystems and posing significant threats to aquatic life and food chain stability (Alegbeleye et al., 2017, Mallah et al., 2022).Due to their structural complexity and high toxicity, aromatic hydrocarbons present considerable challenges for environmental remediation. Their ability to resist biodegradation and accumulate in sediments and biological tissues necessitates targeted and effective cleanup strategies. Understanding their environmental behaviour and associated health risks is crucial in developing efficient remediation technologies to mitigate their impact on ecosystems and human populations.

Alicyclic hydrocarbons are organic compounds with carbon atoms arranged in ring structures, which can be either saturated or unsaturated. These hydrocarbons share characteristics with aliphatic and aromatic hydrocarbons, as they possess cyclic structures while lacking the delocalised electrons in aromatic rings. Cyclopropane (C_3H_6) is the simplest member of this group, with larger cyclic

hydrocarbons occurring naturally in crude oil or synthesised for industrial applications (Maier, 2019, Speight, 2017).

Table 2.1 A summary of key aliphatic, alicyclic and aromatic hydrocarbons, listing their Henry's coefficients and aqueous solubilities at 25 °C. (Source: (Sander, 2015))

Compound	Formula	Henry's coefficient (mol /m³ Pa)	Water solubility (mg /L)
Aliphatic hydrocarbons			
Methane	CH_4	1.4×10^{-5}	22
Ethane	C_2H_6	1.9×10^{-5}	60
Ethylene	C_2H_4	5.9×10^{-5}	130
Acetylene	C_2H_2	4.1×10^{-4}	1200
Propane	C_3H_8	3.5×10^{-5}	140
Butane	C_4H_{10}	9.1×10^{-5}	53
Alicyclic hydrocarbons			
Cyclopentane	C_5H_{10}	3.2×10^{-5}	47
Cyclohexane	C_6H_{12}	3.8×10^{-6}	60
BTEX aromatic hydrocarbons			
Benzene	C_6H_6	5.5×10^{-6}	1780
Toluene	C_7H_8	6.0×10^{-6}	520
Ethylbenzene	C_8H_{10}	4.3×10^{-6}	152
m-Xylene	C_8H_{10}	3.2×10^{-6}	198
Polycyclic aromatic hydrocarbons (PAHs)			
Naphthalene	$C_{10}H_8$	3.9×10^{-3}	31
Anthracene	$C_{14}H_{10}$	1.4×10^{-2}	0.045
Benzo[a]pyrene	$C_{20}H_{12}$	1.1×10^{-1}	0.0038

Alicyclic hydrocarbons are commonly present in petroleum-derived fuels and lubricants, including gasoline and diesel, often in combination with aliphatic and aromatic hydrocarbons. Their structural complexity makes them highly resistant to natural degradation, contributing to their persistence in contaminated environments (Jia and Kraft, 2023) As a result, alicyclic hydrocarbons can accumulate in aquatic and terrestrial ecosystems, leading to prolonged contamination that poses environmental and health risks. Given their chemical stability and environmental impact, targeted remediation strategies are essential for effectively mitigating their presence in polluted sites (Maier, 2019).

2.1.2 Primary Sources of Hydrocarbon Contamination

The major sources are anthropogenic (human activities) and natural:

1. **Oil Spills**: Oil spills remain one of the most severe environmental threats, introducing vast amounts of hydrocarbons into both marine and freshwater ecosystems. These incidents typically occur during the extraction, transportation, and storage of crude oil and petroleum products, with tanker accidents, offshore drilling failures, and pipeline ruptures being among the most common causes (Hettithanthri et al., 2024). Once released, oil spreads rapidly across water surfaces, forming slicks that suffocate marine organisms, coat bird feathers, and disrupt entire ecosystems. Given their persistence and difficulty to remediate, oil spills continue to pose a significant challenge for environmental conservation and water quality management (Zhang et al., 2019).

2. **Industrial Discharges**: Industrial activities are a major contributor to hydrocarbon contamination in water bodies, as petrochemical refineries, power plants, and manufacturing industries discharge wastewater laden with hydrocarbons, posing significant risks to nearby ecosystems (Lin et al., 2022). During the refining of crude oil into fuels and lubricants, wastewater containing hydrocarbon residues is often released, while runoff from industrial sites, including factories, fuel depots, and processing facilities, can further transport pollutants into local water systems (Mu, 2019). Additionally, stormwater runoff from roads and cooling water systems carries hydrocarbons into rivers, lakes, and oceans, exacerbating contamination. Ageing infrastructure at gas stations and industrial sites also leads to the seepage of hydrocarbons into groundwater, posing long-term contamination risks (Olusile Akinyele Babayeju, 2024). These industrial pathways demonstrate the complex and often overlooked link between economic activity and environmental health, emphasising the urgent need for sustainable wastewater management and pollution control strategies.

3. **Urban Runoff and Atmospheric Deposition**: Urban environments play a significant role in hydrocarbon pollution, as vehicle exhaust, tire wear, and industrial emissions release hydrocarbons

into the atmosphere, which then settle onto water bodies through precipitation (Galdames et al., 2020). Additionally, stormwater runoff from roads, highways, and parking lots collects hydrocarbons from fuel leaks, engine oil spills, and other automotive residues, washing them into drainage systems that eventually discharge into rivers, lakes, and oceans. This process creates a cumulative pollution effect, where hydrocarbons persist in aquatic ecosystems, affecting water quality and threatening marine and freshwater organisms (Müller et al., 2020, Kriech and Osborn, 2022).

4. **Natural Seeps:** Crude oil and natural gas naturally migrate through geological formations, leading to subsurface seepage that introduces hydrocarbons into surrounding water bodies, thereby contributing to background contamination levels (Deng et al., 2024). Although not as catastropHic as industrial spills, these natural leaks can gradually accumulate in aquatic ecosystems, resulting in localised pollution hotspots. Over time, weathering processes such as evaporation, oxidation, and microbial degradation can help break down some of these hydrocarbons, reducing their immediate toxicity. However, the persistent fractions remain in the environment, potentially altering water chemistry and affecting aquatic life (Depetris et al., 2014). While natural seepage is a well-documented pHenomenon, its contribution to long-term hydrocarbon contamination is often overshadowed by anthropogenic sources, highlighting the need for comprehensive monitoring and remediation strategies (Truskewycz et al., 2019).

2.1.3 Hydrocarbon Contamination in Water Resources in the Oil and Gas Industry

The oil and gas industry remains one of the largest contributors to hydrocarbon contamination in marine, estuarine, and freshwater systems. The various stages of petroleum exploration, extraction, refining, and transportation introduce hydrocarbons into the environment, often leading to severe ecological consequences (Mironov, 1968). Among the major sources of contamination, offshore drilling, refining effluents, transportation spills, and unconventional extraction techniques contribute to pollution levels in aquatic ecosystems (Zhang et al., 2019). These processes introduce hazardous

hydrocarbons such as polycyclic aromatic hydrocarbons (PAHs), benzene, toluene, ethylbenzene, and xylene (BTEX compounds) into water bodies, which necessitates robust remediation strategies (Mojiri et al., 2019, Saeedi et al., 2024).

Exploration and drilling activities from offshore and onshore rigs generate substantial hydrocarbon waste, particularly from produced water, a byproduct rich in hydrocarbons, heavy metals, and drilling fluids. These sites frequently discharge untreated produced water into nearby ecosystems, exacerbating contamination risks (Njuguna et al., 2022). Subsequently, accidental leaks from subsea wells and drilling platforms further contribute to environmental degradation. In many cases, inefficient waste management and lax enforcement of environmental regulations allow these pollutants to persist in surrounding water bodies, impacting aquatic biodiversity and human health (Zhang et al., 2019).

Another significant contributor to hydrocarbon contamination is pipeline transportation and accidental spills. Pipeline leaks, tanker spills, and storage facility failures introduce large quantities of hydrocarbons into water bodies, affecting both surface and groundwater quality (Han et al., 2018, Cakir et al., 2021). Catastrophic events, such as the Deepwater Horizon oil spill in 2010 and the Exxon Valdez spill in 1989, highlight the devastating impact of large-scale hydrocarbon pollution on marine ecosystems (Barron et al., 2020). These incidents often require long-term remediation efforts, as hydrocarbons persist in sediments and bioaccumulate in aquatic organisms, causing chronic toxicity and habitat destruction.

Additionally, the rise of unconventional oil extraction and refining methods, such as hydraulic fracturing (“fracking”) and makeshift refineries, has led to increased concerns over groundwater contamination. Fracking involves injecting a mixture of water, sand, and chemical additives into shale formations to release trapped hydrocarbons (Scotchman, 2016). However, this process often leads to leakage of toxic fracking fluids into underground aquifers, posing risks to drinking water sources (Montcoudiol et al., 2017). Contaminants released during fracking operations include volatile organic

compounds (VOCs), metals, and radioactive materials, all of which pose significant environmental and public health risks (McElroy et al., 2020).

2.1.4 Environmental Impact of Hydrocarbon Contamination

Once in the environment, hydrocarbons can have far-reaching and often irreversible consequences, affecting biodiversity, water quality, soil health, and human activities. This section explores the environmental impact of hydrocarbon contamination and emphasises the importance of effective mitigation strategies.

1. Impact on Aquatic Ecosystems

One of the most pronounced effects of hydrocarbon contamination is on aquatic ecosystems. Oil spills, both large-scale disasters and smaller, chronic leaks, are notorious for their devastating effects on marine life (Bashir et al., 2020a). The physical properties of oil make it challenging to remove from water bodies, and its persistence can lead to long-term contamination. Hydrocarbons, particularly PAHs, are toxic to aquatic organisms, disrupting the reproductive, feeding, and respiratory functions of fish, invertebrates, and marine mammals (Honda and Suzuki, 2020). Oil slicks on water surfaces can prevent oxygen exchange, suffocating aquatic organisms. Additionally, the oil can coat the fur or feathers of marine animals, impairing their ability to regulate temperature or float, leading to drowning or hypothermia (Zhang et al., 2019).

Furthermore, hydrocarbons can bioaccumulate in the food chain. When smaller organisms, such as plankton and fish, ingest contaminated particles, the toxins can accumulate in their tissues. As larger predators consume these organisms, the concentration of toxins increases, potentially affecting species further up the food chain, including humans (Thiagarajan and Devarajan, 2025).

2. Soil and Terrestrial Ecosystem Degradation

In the Niger Delta and other oil-producing regions of Africa, the proliferation of makeshift or artisanal refineries has exacerbated hydrocarbon contamination. These unregulated operations involve crude

oil distillation under open conditions, releasing untreated effluents and soot into nearby water bodies and farmlands. The resultant pollution compromises soil fertility, air quality, and human health, creating a persistent environmental burden that complicates formal remediation efforts (UNEP, 2011). Hydrocarbon contamination also affects terrestrial ecosystems, particularly in areas near industrial activity or following pipeline ruptures and oil spills. When hydrocarbons infiltrate soil, they alter its composition and structure, making it less conducive to supporting plant life (Falih et al., 2024). The presence of oil reduces the oxygen availability in the soil, impeding the growth of plants and disrupting microbial communities essential for nutrient cycling. In the case of heavy oil contamination, the soil may become hydrophobic, making it difficult for water to penetrate and further reducing the viability of plant growth, which can lead to erosion and long-term degradation of the affected ecosystem (Kumar Yadav et al., 2023). The toxicity of hydrocarbons in soil can also harm terrestrial wildlife. Animals that come into contact with contaminated soil or vegetation may suffer from poisoning, reproductive issues, or even death. For example, herbivores may ingest contaminated plants, leading to the introduction of toxins into the food chain (Khan et al., 2018).

3. Air Pollution and Human Health Risks

Hydrocarbon contamination is not limited to water and soil; it can also contribute to air pollution. Volatile organic compounds (VOCs), such as benzene and toluene, are released into the atmosphere during oil extraction, refining, and transport processes (Rajabi et al., 2020). These chemicals can lead to smog formation and contribute to ground-level ozone, which is harmful to both human health and the environment. Prolonged exposure to VOCs has been linked to respiratory problems, neurological damage, and increased cancer risks (Geddes and Murphy, 2012).

The impact on human health is a critical concern in areas affected by hydrocarbon contamination, particularly in communities near oil production or spill sites. Workers in these industries are at higher risk of exposure to toxic hydrocarbons, and local populations may face increased risks of diseases linked to air and water pollution (D'Andrea and Reddy, 2014, Falih et al., 2024).

4. Long-Term Environmental Effects and Recovery

The recovery process after hydrocarbon contamination can be prolonged, as the natural biodegradation of hydrocarbons is slow. While some microbes are capable of breaking down hydrocarbons, this process is often inefficient and takes years or even decades to restore a contaminated environment to its original state (Banerjee et al., 2016). The long-term persistence of hydrocarbons in the environment means that the ecological and economic impacts of contamination can last for generations, especially in sensitive habitats such as wetlands, coral reefs, and deep-sea ecosystems (Ambaye et al., 2022)

2.2 Traditional Methods of Remediating Hydrocarbon Contamination

The oil and gas industry, as well as transportation and industrial activities, are major contributors to hydrocarbon pollution. Addressing this environmental issue involves implementing remediation methods to reduce or eliminate the harmful effects of hydrocarbons (Haruna et al., 2023). USEPA (2020c) classified three main conventional remediation approaches: physical, chemical, and biological methods. Each of these approaches has specific advantages, limitations, and applications depending on the characteristics of the contamination.

1. Physical Remediation Methods

Physical remediation methods primarily focus on removing or containing hydrocarbon pollutants from the affected environment. These methods are often applied when the contamination is shallow, limited in extent, or where rapid intervention is necessary (Dhaka and Chattopadhyay, 2021).

a. **Excavation and Removal** - One of the most straightforward physical remediation techniques is excavating and removing contaminated soil. This method is commonly used when hydrocarbons are found in the topsoil layers or confined areas (Elgazali et al., 2023). Excavation involves digging up the contaminated material and transporting it to a disposal site or treatment facility. The excavated soil may be treated by incineration, chemical oxidation, or landfilling, depending on the nature of the hydrocarbons and regulatory guidelines (USEPA, 2020a). This method is effective for small to medium-

scale contamination but is labour-intensive and can be costly due to the need for proper disposal or treatment of contaminated materials (Dhaka and Chattopadhyay, 2021).

b. Soil Washing - Soil washing is another physical technique that involves the use of water or chemical solutions to wash out hydrocarbons from contaminated soil. This method works by applying water or surfactants to dislodge and dissolve hydrocarbon molecules, which are then separated from the soil using techniques like centrifugation or filtration (Zoghi and Mafigholami, 2023). The treated water or waste materials are then further treated or disposed of. Soil washing is effective for treating soils with low to moderate levels of contamination, especially in cases where the contamination is primarily surface-based (USEPA, 2020c). However, it may not be suitable for treating deeply embedded hydrocarbons or soil with high clay content, as these properties can limit the efficiency of the washing process.

c. Biodegradation in Containment Systems - In some cases, physical containment methods are used to limit the spread of hydrocarbons while remediation through natural biodegradation is facilitated. For example, hydrocarbon contamination can be contained within a barrier such as an impermeable liner or boom to prevent migration into surrounding ecosystems (Aparicio et al., 2022). This method is often combined with the addition of nutrients or oxygen to stimulate microbial degradation of hydrocarbons in the confined area. While containment may not eliminate contaminants entirely, it reduces the environmental impact and allows for long-term natural remediation processes to take place (Koshlaf and Ball, 2017).

2. Chemical Remediation Methods

Chemical remediation methods rely on using chemicals to either transform hydrocarbons into less harmful substances or enhance the removal of contaminants from the environment. These methods can be applied to both soil and water and are often used when physical methods alone are insufficient (Koul and Taak, 2018).

a. Chemical Oxidation - Chemical oxidation involves the addition of oxidising agents (such as ozone, hydrogen peroxide, or potassium permanganate) to hydrocarbon-contaminated media. These chemicals break down hydrocarbons into less toxic compounds like water, carbon dioxide, and smaller organic molecules (Ciampi et al., 2024). This method is especially effective for treating soil and groundwater contaminated with volatile organic compounds (VOCs) and other petroleum-related pollutants (Jovanović et al., 2021). However, the effectiveness of chemical oxidation depends on factors such as the type of contaminant, the concentration of hydrocarbons, and the presence of other chemicals in the environment. Furthermore, the high cost of oxidising agents and the need for careful application to prevent environmental damage can limit the widespread use of this technique (Jafarinejad, 2017, Kumari and Kumar, 2023).

b. Biostimulation - Biostimulation is a chemical approach that involves the addition of nutrients (e.g., nitrogen, phosphorus, and oxygen) or other chemicals to contaminated environments to enhance the activity of indigenous microorganisms capable of degrading hydrocarbons (Mohamed and Samer, 2023). This method is particularly useful in cases where natural biodegradation is occurring but at a slower rate due to nutrient deficiencies or other limiting factors. By providing the necessary resources, biostimulation can accelerate the breakdown of hydrocarbons (Hazen, 2009). This method is commonly applied in groundwater and surface water remediation, where natural microbial populations can be harnessed to detoxify the contaminants over time (Adams et al., 2015).

c. Surfactant Enhanced Recovery - Surfactants are chemicals that reduce surface tension between water and hydrocarbons, making it easier to extract or separate petroleum-based contaminants from soil and water. In soil remediation, surfactants can be applied to the contaminated area, increasing the solubility of hydrocarbons and allowing for their easier removal or treatment (Liu et al., 2021). This method is particularly useful for treating hydrophobic contaminants, such as oils, in porous or permeable soils. While surfactant-enhanced recovery can significantly improve hydrocarbon removal efficiency, the process must be carefully controlled to avoid the spread of contaminants to

surrounding areas and to ensure the safe disposal or treatment of the surfactants used (Wu et al., 2024).

3. Biological Remediation Methods

Biological remediation methods, also known as bioremediation, leverage natural processes to degrade or detoxify hydrocarbons using microorganisms, plants, or enzymes. This approach is often considered more sustainable and environmentally friendly compared to physical or chemical methods (Tanwir et al., 2021).

a. Bioremediation with Microorganisms - Microorganisms, such as bacteria, fungi, and algae, have the ability to break down hydrocarbons into simpler, less toxic compounds through metabolic processes. This method, known as biodegradation, is the most widely studied and used biological remediation technique for hydrocarbon contamination (Mokrani et al., 2024). Under suitable environmental conditions (e.g., temperature, pH, oxygen, and nutrient availability), microorganisms can degrade hydrocarbons in soils and waters, reducing the concentration of toxic compounds and restoring the environmental balance (Koh and Khor, 2022, Wani et al., 2022). One of the main advantages of bioremediation is its low cost and minimal environmental disturbance. However, it requires specific conditions for optimal microbial activity, and the process can take time, particularly for complex or large-scale contamination (Mahanayak, 2024). Key bacterial genera include *Pseudomonas, Alcanivorax, Rhodococcus, Mycobacterium, Burkholderia*, and *Sphingomonas*. Among fungi, white-rot species like *Phanerochaete chrysosporium, Trametes versicolor*, and *Pleurotus ostreatus*. Algal bioremediation is exemplified by genera such as *Chlorella, Scenedesmus, and Spirulina (Miller et al., 2019, Xu et al., 2018)*. Together, these microorganisms and microalgae form a consortium or can be applied in sequence to target the full spectrum of aliphatic and aromatic pollutants in soil and water. The specific metabolic pathways and enzymatic mechanisms by which these microbial taxa degrade hydrocarbons are discussed in detail in later sections of this review.

b. Phytoremediation - Phytoremediation is a biological method that uses plants to absorb, accumulate, or degrade contaminants, including hydrocarbons, from the soil and water. Certain plant species have the ability to extract pollutants from the environment through their roots and either store or metabolise the contaminants within their tissues (Kafle et al., 2022, Ansari et al., 2020). Phytoremediation is a slow but cost-effective technique, particularly suited to situations where other methods are impractical (Surriya et al., 2015). In some cases, plants can help stabilise the soil, preventing further leaching of contaminants into the surrounding ecosystem. However, this method may not be effective for deep or large-scale contamination, as plants can only reach a limited depth and area (Iqbal et al., 2019).

c. Mycoremediation - Mycoremediation involves the use of fungi to degrade or transform hydrocarbon contaminants in the environment. Certain fungal species possess the ability to break down complex organic compounds, including petroleum-based products (Kulshreshtha et al., 2014, Akhtar and Mannan, 2020). This method is particularly promising in cases where other bioremediation approaches may not be effective due to the nature of the contaminants. This is still an emerging field, because of the abundance of plant species, and further research is needed to fully understand its potential and limitations (Akpasi et al., 2023, Oladipo et al., 2025).

2.3 Nanotechnology in Environmental Remediation

Nanotechnology is emerging as a transformative tool for environmental remediation due to its ability to manipulate materials at the nanoscale (1–100 nm). This manipulation results in unique properties such as enhanced reactivity, large surface areas, and the ability to interact with contaminants at a molecular level (Tratnyek and Johnson, 2006). These properties enable nanoparticles to efficiently address environmental contamination, including pollutants like heavy metals, organic compounds, and hydrocarbons (Li et al., 2006, Zhang, 2003). In particular, the application of nanotechnology in treating hydrocarbon contamination is gaining attention as a sustainable and efficient remediation method (Murgueitio et al., 2018).

Nanotechnology offers several advantages in addressing hydrocarbon contamination. The small size of nanoparticles gives them a larger surface area-to-volume ratio, making them highly reactive and efficient in degrading or adsorbing pollutants (Crane and Scott, 2012, Li et al., 2006, Singh et al., 2019). Furthermore, the ability to tailor nanoparticles for specific contaminants allows for targeted remediation, making it possible to address different types of hydrocarbons and other organic pollutants effectively (Guerra et al., 2018). The relatively low energy requirements and the potential for reusable materials also make nanotechnology an attractive option for large-scale remediation projects (Hussein, 2023). Traditional remediation methods, such as bioremediation or physical recovery, may be slow or ineffective in treating large-scale hydrocarbon pollution (Adeoye, 2022). Nanotechnology, however, offers an instant and accelerated solution by enhancing the degradation or removal of these pollutants (Singh et al., 2024).

Zero-valent iron nanoparticles (Fe(0) or Fe°) are one of the most widely used nanomaterials for treating hydrocarbon contamination, particularly in groundwater and soil. ZVI nanoparticles effectively break down petroleum-based contaminants, including hydrocarbons, through reduction reactions (Galdames et al., 2020, Zafar et al., 2021). nZVI facilitate the degradation of various hydrocarbons primarily through reductive or oxidative pathways, depending on the type of contaminant and reaction conditions (Garg et al., 2024). In reductive dechlorination processes, nZVI serves as an electron donor, oxidising Fe^0 to Fe(II) while removing chlorine atoms from chlorinated solvents. In oxidative processes, particularly when combined with agents such as hydrogen peroxide, nZVI initiates Fenton-like reactions that generate hydroxyl radicals capable of mineralising aromatic hydrocarbons (Phenrat et al., 2009, Phenrat et al., 2019).

One of the most well-known applications of nZVI is the degradation of chlorinated ethenes, such as tetrachloroethylene (PCE) and trichloroethylene (TCE). Lin et al. (2018) gave a simplified stoichiometric equation illustrating the complete dechlorination of PCE (C_2Cl_4) to ethylene (C_2H_4):

$$Fe^0 + C_2Cl_4 + 4H^+ \rightarrow Fe^{2+} + C_2H_4 + 4Cl^-$$

In practice, the reaction often proceeds stepwise via intermediates like trichloroethylene (TCE), dichloroethylene (DCE) isomers, and vinyl chloride before reaching the final product ethylene. Chuang et al. (1995) also gave a detailed reaction for TCE (C_2HCl_3):

$$Fe^o + C_2HCl_3 + 3H^+ \rightarrow Fe^{2+} + C_2H_4 + 3Cl^-$$

Wacławek et al. (2015) provided fundamental insights into chlorinated methanes and ethenes' reduction kinetics and mechanisms while Lien and Zhang (2001) reported rapid de-chlorination using nanoscale iron particles and detailed how chlorinated alkanes including 1,1,1-trichloroethane (TCA) and carbon tetrachloride (CT) undergo similar reductive transformations with nZVI through conversion of TCA ($C_2H_3Cl_3$) to ethane (C_2H_6) as shown below:

$$Fe^o + C_2H_3Cl_3 + 3H^+ \rightarrow Fe^{2+} + C_2H_6 + 3Cl^-$$

Carbon tetrachloride (CCl_4) can also be reduced to methane (CH_4) via a generalised reaction:

$$2Fe^o + CCl_4 + 6H^+ \rightarrow 2Fe^{2+} + CH_4 + 4Cl^-$$

Orth and Gillham (1996) demonstrated this iron-mediated dichlorination for TCA, while Matheson and Tratnyek (1994) investigated carbon tetrachloride and other chlorinated compounds, reporting the overall efficiency of Fe^0 systems in producing less-toxic end products. In contrast, non-chlorinated aromatic hydrocarbons such as benzene, toluene, ethylbenzene, xylene (BTEX), and polycyclic aromatic hydrocarbons (PAHs) are more effectively removed by oxidative processes when nZVI is combined with oxidants like hydrogen peroxide (Chang et al., 2005, Rayaroth et al., 2023). During this process, Fe^0 is oxidised to ferrous or ferric iron, which catalyses further radical generation. Babuponnusami and Muthukumar (2014) reviewed improvements to the Fenton process, including the use of iron nanoparticles for enhanced oxidation. Similarly, PAHs like naphthalene ($C_{10}H_8$) undergo mineralization through oxidative intermediates to produce CO_2 and H_2O (Zeng et al., 2024).

In the field, many variables such as pH, redox potential, particle surface area, and the presence of co-contaminants impact the efficiency and pathways of nZVI-mediated degradation (Wang et al., 2024).

Additionally, combining nZVI with microbial processes or other oxidants is a common strategy to enhance overall contaminant mineralisation. Zhang (2003) and Crane and Scott (2012) provided comprehensive overviews of the broad applications of nZVI for environmental remediation, covering everything from laboratory investigations to pilot-scale and full-scale field deployments. These studies demonstrate that nanoscale zerovalent iron can degrade a wide range of hydrocarbons, particularly chlorinated ethenes and alkanes, by reductive pathways, leading to less chlorinated or dechlorinated final products. In contrast, aromatic hydrocarbons often require oxidative approaches for complete mineralisation.

In addition to ZVI and TiO_2, other nanomaterials, such as carbon nanotubes (CNTs) and magnetic nanoparticles, are being explored for hydrocarbon remediation (USEPA, 2020b). Carbon nanotubes have excellent adsorptive properties due to their high surface area and porosity. They can adsorb hydrocarbons like benzene, toluene, and xylene from contaminated environments, reducing the concentration of these pollutants in water and soil (Sajid et al., 2022). Moreover, magnetic nanoparticles can be used to adsorb hydrocarbons and then be easily removed from the contaminated site using an external magnetic field. This magnetic recovery system allows for the efficient removal and reuse of the nanoparticles (Tang and Lo, 2013, Ul-Islam et al., 2017, Rasheed, 2022).

Another promising approach involves nanoscale zero-valent metal catalysts, which can degrade long-chain hydrocarbons in soils and sediments (Xie et al., 2021). Metals, like nickel or palladium nanoparticles, have been shown to facilitate the hydrogenation of hydrocarbons into non-toxic products under controlled conditions (Namakka et al., 2024).

In contrast to traditional methods, such as bioremediation or physical recovery, which may be slow or ineffective in treating large volumes of contamination, nanotechnology offers quicker remediation with minimal environmental disruption (Roy et al., 2021). It is particularly beneficial in situations where the contaminants are deeply embedded or spread over large areas, such as in oil spills or industrial wastewater (Kharisov et al., 2012).

2.3.1 Synthesis of Nano Zero-Valent Iron (nZVI)

The synthesis of nanoscale zero-valent iron (nZVI) plays a pivotal role in determining its effectiveness, stability, and reactivity in environmental remediation (Stefaniuk et al., 2016). Various synthesis methods have been developed to optimise particle size, surface properties, and long-term performance, each with distinct advantages and limitations (Kumari et al., 2023, El-Khawaga et al., 2023).

The chemical reduction method is the most conventional approach, where reducing agents such as sodium borohydride ($NaBH_4$) or hydrazine, facilitate the transformation of iron salts into metallic nanoparticles (Stefaniuk et al., 2016, Mackenzie and Georgi, 2019). These methods produce highly reactive nZVI but is prone to rapid oxidation and aggregation, which can limit their long-term remediation efficiency (Huang and Ehrman, 2007).

Additionally, physical and electrochemical methods such as ball milling, thermal decomposition, and electrochemical reduction offer improved control over particle uniformity and surface functionality, which is crucial for enhancing the reactivity of nZVI in diverse environmental conditions (Kolahalam et al., 2019).

Despite the promising applications of nanotechnology in environmental remediation, several challenges remain. The potential toxicity of nanoparticles, especially when they enter ecosystems, is a significant concern (Castaño et al., 2021, Ken and Sinha, 2020, Khuntia et al., 2019). Although many nanoparticles are designed to be environmentally benign, the long-term effects of their release into the environment need further investigation to avoid unintended consequences (Bhat et al., 2023). Additionally, the cost of producing nanoparticles at scale can be prohibitive, limiting their widespread use in large-scale environmental projects (Paliwal et al., 2014, Clauser et al., 2022).

Another challenge is the issue of nanoparticle mobility. While nanoparticles have high reactivity, their ability to move through contaminated media like soil and groundwater must be carefully managed to

avoid the spread of contaminants beyond the remediation site (Shrestha et al., 2020, Yusuf et al., 2024).

This is where green synthesis comes into play, it employs plant extracts, microbial cultures, or bio-based compounds as natural reducing agents to create environmentally friendly nZVI. This approach not only eliminates the need for hazardous chemicals but also enhances nanoparticle stability through natural capping agents, reducing secondary pollution risks (Iravani, 2011, Kharissova et al., 2013a).

2.3.2 Stabilizing Nano Zero-valent Iron

Despite its effectiveness in environmental remediation, nanoscale zero-valent iron (nZVI) faces challenges related to rapid oxidation, particle aggregation, and a limited reactive lifespan, which can reduce its efficiency in field applications (Li et al., 2024, Liu et al., 2024). Researchers have developed various stabilisation techniques to address these limitations that enhance nZVI's dispersibility, longevity, and overall performance.

One widely used approach is polymer coating, where nZVI particles are encapsulated with biocompatible polymers such as carboxymethyl cellulose (CMC) and polyethylene glycol (PEG). These coatings create a steric barrier around the nanoparticles, reducing aggregation and improving mobility in contaminated environments (Eljamal et al., 2020, Ibrahim et al., 2020). Similarly, surfactants and ligands lower interfacial tension, increasing nanoparticle mobility in porous media, thereby enhancing their effectiveness in subsurface remediation applications (Yekeen et al., 2020).

Another effective strategy is carbon and silica encapsulation, in which nZVI particles are embedded within graphene layers, carbon shells, or silica matrices. This encapsulation prevents premature oxidation while preserving the reactivity of the nanoparticles, making them more effective in long-term contaminant degradation (Czinnerova et al., 2020, Liu et al., 2023). Additionally, metal doping, particularly with catalysts such as palladium (Pd) and platinum (Pt), has been shown to enhance degradation kinetics, especially for chlorinated hydrocarbons and persistent organic pollutants (van Deelen et al., 2019, Serna-Gallén and Mužina, 2024).

Finally, emulsification can help slow down the oxidation of iron nanoparticles by encapsulating them within a surfactant or lipid layer, thereby limiting direct contact with oxygen and water. This protective barrier reduces electron transfer and surface reactions that otherwise accelerate iron oxidation, enhancing particle stability over extended periods (Mackenzie and Georgi, 2019). Employing these stabilisation techniques will improve nZVI's longevity and field performance, making it a viable and scalable solution for large-scale environmental remediation.

2.3.3 Challenges and Future Directions of nZVI in Hydrocarbon Remediation

While nZVI has proven highly effective in hydrocarbon remediation, several challenges hinder its widespread application. One significant issue is its limited longevity, as oxidation and passivation gradually reduce its reactivity over time, limiting its long-term effectiveness in contaminated environments (Zhou et al., 2025). Additionally, field deployment constraints pose another challenge, as the poor mobility of nZVI in complex soil matrices restricts its ability to disperse effectively in large-scale applications (Mondal et al., 2021, Chen and Qian, 2024). Moreover, concerns regarding potential ecotoxicity have been raised, as nanoparticle accumulation in ecosystems may have unforeseen consequences, necessitating further toxicity assessments to ensure environmental safety (Saif et al., 2016, Crampon et al., 2019)

To address these limitations, future research should focus on enhancing nZVI longevity by developing advanced stabilisation techniques that prevent oxidation while maintaining reactivity (Ali et al., 2016). Optimising green synthesis methods for higher production efficiency will also allow for more scalable and sustainable nanoparticle production, reducing reliance on chemical synthesis (Abuzeid et al., 2023). Further investigations into the interactions between nZVI and microbial communities will also be crucial in understanding their long-term environmental impacts and potential synergies with bioremediation processes. By overcoming these challenges, nZVI can be refined into a more sustainable, efficient, and environmentally friendly tool for hydrocarbon contamination treatment (Xie et al., 2017, Fajardo et al., 2019).

2.4 Green Nanoparticles

Nanotechnology has significantly advanced various fields, including medicine, electronics, and environmental remediation, by leveraging materials at the nanoscale (1–100 nm) with enhanced reactivity and unique physicochemical properties (Kharissova et al., 2013a). One of the emerging innovations within this field is green nanotechnology, which focuses on synthesising nanoparticles through environmentally sustainable methods (Borja et al., 2015). Unlike conventional nanoparticle synthesis that often involves toxic chemicals, high-energy consumption, and hazardous byproducts, green synthesis utilises biological agents such as plant extracts, fungi, bacteria, and algae to reduce metal salts into nanoparticles, offering an eco-friendly and sustainable alternative (Kumar et al., 2015, Kumar et al., 2023, Pal et al., 2019).

Among green nanoparticles, nZVI has gained prominence due to their effectiveness in environmental remediation, particularly for hydrocarbon contamination (Murgueitio et al., 2018). Green-synthesized nZVI exhibits strong redox reactivity, allowing it to transform hydrocarbons, metals, and other contaminants in soil and water systems (Sanjay, 2019). Additionally, green synthesis methods enhance the stability and biocompatibility of nZVI, reducing environmental toxicity compared to chemically synthesised counterparts (Kirubakaran et al., 2025). The eco-friendly nature of these nanoparticles makes them suitable for large-scale remediation applications, aligning with the increasing demand for sustainable pollution control technologies (Gupta et al., 2023b).

The green synthesis of nZVI is gaining traction due to its cost-effectiveness and minimal environmental impact. Unlike traditional methods that rely on hazardous chemical reductants, green synthesis employs biological agents such as plant extracts, microorganisms, and agricultural byproducts, which not only facilitate nanoparticle formation but also enhance reactivity and stability (Mareedu et al., 2021, Badmus et al., 2018). Among these approaches, plant-assisted synthesis is widely explored due to the presence of polyphenols and flavonoids in plant extracts such as green tea, clove, and coffee, which serve as both reducing and stabilizing agents, preventing nanoparticle aggregation and improving performance (Khan et al., 2022, Rani et al., 2023).

Additionally, microbial-assisted synthesis leverages the metabolic activities of certain bacteria and fungi, which naturally reduce iron salts to form biocompatible nZVI (Saravanan et al., 2021). While both plants and microbes are used in nanoparticle synthesis, plants are often preferred due to their ability to produce nanoparticles more rapidly, in larger quantities, and with greater stability than bacterial or fungal methods (Hano and Abbasi, 2021). This preference is attributed to the strong reducing capacity of plant extracts, which accelerates nanoparticle formation while preventing oxidation (Singh et al., 2016).

Another promising approach in green nZVI production involves utilising agricultural waste and biowaste materials, such as fruit peels, leaf extracts, and lignin derivatives, as renewable precursors. These materials serve as both reducing and stabilising agents, offering an eco-friendly alternative to synthetic stabilisers while promoting waste valorisation and circular economy principles (Sunardi et al., 2017, Bashir et al., 2020b). The integration of waste-derived materials in nanoparticle synthesis not only reduces dependency on industrial stabilisers but also lowers production costs, making green nZVI more accessible for large-scale environmental remediation efforts (Abdelbasir et al., 2020).

Given the growing emphasis on sustainability, green nanotechnology continues to pave the way for cleaner, safer, and more effective pollutant degradation technologies, reinforcing its role in next-generation remediation solutions (Jabeen et al., 2024, Kumar et al., 2024).

2.4.1 Synthesising Green Iron Nanoparticles

The introduction of green methods for synthesising nZVI is to offer an eco-friendly alternative to traditional chemical and physical nanoparticle fabrication techniques. Conventional methods often rely on harsh reducing agents, elevated temperatures, or toxic solvents, raising significant environmental and health concerns. In contrast, the use of plant-based polyphenols capitalises on the natural reducing and stabilising properties of these biomolecules, ensuring a more sustainable and less hazardous process (Jawed et al., 2021). The abundance of polyphenols in green tea, fruit peels, and other plant extracts can reduce Fe(III) salts to elemental Fe^{o}, yielding nZVI with unique properties

suitable for various environmental applications (Borja et al., 2015, Huang et al., 2014, Jacqueline, 2013).

Pan et al. (2022) described in a simplified reaction how the reduction of Fe(III) to Fe^0 hinges on the electron-donating ability of polyphenols (e.g., catechins, tannic acid):

$$Fe^{3+}+3(\text{polyphenol})\longrightarrow Fe^0+3(\text{oxidized polyphenol})$$

One illustrative example of green synthesis involves the use of green tea extract rich in polyphenols. The process typically starts by mixing an aqueous solution of ferric chloride ($FeCl_3$) with the plant extract under mild conditions (near-ambient temperature and atmospheric pressure) (Machado et al., 2015, Machado et al., 2013). The hydroxyl groups on the aromatic rings of polyphenols chelate Fe(III), facilitating electron transfer and consequent reduction to Fe^0. The overall reaction scheme in acidic conditions can be expressed as:

$$2FeCl_3+3(\text{polyphenol})+3H_2O\longrightarrow 2Fe^0+6HCl+3(\text{oxidized polyphenol})$$

Meanwhile, the byproducts, often benign organic salts, further highlight the “green” nature of the synthesis.

A key benefit of this approach is the in-situ capping of nZVI using the same polyphenols. These polyphenolic compounds can attach to the nanoparticle surface via hydrogen bonding and other interactions, creating a layer that inhibits excessive agglomeration (Javed et al., 2020). This improved stability preserves the high surface-area-to-volume ratio crucial for applications in water treatment, soil remediation, and catalytic processes. The resulting nanoparticles typically exhibit smaller average diameters (ranging from 5 to 50 nm), high reactivity, and good dispersion, all of which are essential for rapid contaminant degradation (Fazlzadeh et al., 2017, Haider et al., 2024).

Moreover, the environmental benefits extend beyond the mere avoidance of toxic precursors. Because polyphenols are typically derived from renewable plant sources like agricultural wastes (fruit peels) or other byproducts, this method aligns well with the principles of green chemistry and circular

economy (Slootweg, 2024). The minimal hazardous waste generation and ambient reaction conditions reduce energy consumption and operational costs (Osman et al., 2024).

2.5 Hydrocarbon Degradation by Microorganisms

Hydrocarbon contaminants, including crude oil, diesel, and gasoline, are complex organic compounds that can have severe ecological and health impacts. Microbial degradation of hydrocarbons plays a critical role in mitigating the effects of this contamination. Microorganisms, including bacteria, fungi, and algae, have evolved mechanisms to utilise hydrocarbons as carbon and energy sources, thereby breaking down these pollutants (Varjani, 2017). Understanding these mechanisms is essential for optimising bioremediation strategies, which harness the natural ability of microorganisms to degrade hydrocarbons (Kuppan et al., 2024).

2.5.1 Microbial Degradation Pathways

Microorganisms degrade hydrocarbons through several enzymatic pathways. Hydrocarbons are typically classified as either aliphatic (straight-chain or branched) or aromatic (cyclic structures with benzene rings), and microbes possess specific enzymatic systems for breaking down each type (Pandolfo et al., 2023).

Once hydrocarbons become bioavailable, the activation and metabolic breakdown phase begins. Microorganisms initiate hydrocarbon degradation using oxidative enzymes such as oxygenase and dehydrogenases, which catalyse reactions that break down hydrocarbon molecules into intermediate metabolites (Jouanneau et al., 2011). This process typically involves hydroxylation, oxidation, or carboxylation reactions, which modify the molecular structure of hydrocarbons, making them more susceptible to further enzymatic degradation (Paisse et al., 2011). The activation of aliphatic hydrocarbons often begins with monooxygenases or dioxygenases, introducing hydroxyl groups that facilitate subsequent oxidation steps (Miyazawa et al., 2019).

Aliphatic hydrocarbons through an initial oxidation step catalysed by enzymes such as alkane hydroxylases. The enzyme system incorporates molecular oxygen (O_2) into the hydrocarbon molecule,

converting it into a more hydrophilic and reactive form (Macaya et al., 2019). For example, the degradation of alkanes like hexadecane ($C_{16}H_{34}$) begins with the oxidation of the alkane into a primary alcohol, followed by further oxidation to aldehydes and ultimately to acids. These intermediates are then further metabolised to smaller molecules such as acetates, which can enter the citric acid cycle for energy production(Abbasian et al., 2015). Another example of a microbial strain involved in the degradation of aliphatic hydrocarbons is *Alcanivorax borkumensis*. This marine bacterium is known for its ability to degrade a wide range of aliphatic hydrocarbons, especially in oil-polluted marine environments (Abdel-Shafy and Mansour, 2019).

Due to their stable benzene rings, aromatic hydrocarbons are more resistant to degradation. However, microorganisms have evolved specific pathways for breaking down these compounds. The first step usually involves the incorporation of oxygen into the aromatic ring via an enzyme called dioxygenase, which splits the ring into smaller intermediates (Fuchs et al., 2011). These intermediates are further oxidised to simpler compounds that can be used in the metabolic pathways of the microorganisms (Seo et al., 2009). The degradation of polycyclic aromatic hydrocarbons (PAHs), such as naphthalene and anthracene, is also an example of a process that begins with ring-cleaving dioxygenase enzymes (Widdel and Rabus, 2001). The breakdown of naphthalene, for instance, involves its conversion into 1,2-dihydroxy-1,2-dihydronaphthalene, followed by further degradation to compounds that enter central metabolic pathways (Mohapatra et al., 2022).

The final stage of hydrocarbon degradation is mineralisation, where intermediate compounds are further metabolised into carbon dioxide (CO_2), water (H_2O), and microbial biomass (Kothari et al., 2014). This step ensures the complete breakdown of hydrocarbons, preventing the accumulation of toxic metabolic byproducts (Das and Chandran, 2011). Key enzymes such as catechol dioxygenases play a crucial role in cleaving aromatic ring structures, converting them into tricarboxylic acid (TCA) cycle intermediates that are fully oxidised within microbial metabolic pathways (Broderick, 1999).

In some cases, microorganisms degrade hydrocarbons through co-metabolism, where the presence of one compound facilitates the breakdown of another (Cao et al., 2009). For example, when a microorganism metabolises a primary carbon source (like glucose), it may also degrade a secondary pollutant, such as a hydrocarbon, even if the microorganism does not primarily rely on hydrocarbons for growth. (John et al., 2012, Khatoon and Malik, 2019).

In addition, microbial communities involved in hydrocarbon degradation may exhibit synergistic interactions, where different species collaborate to break down complex pollutants. For instance, certain bacteria may initiate the breakdown of hydrocarbons, creating intermediates that are further degraded by other microbial species (Karishma et al., 2024, Jia et al., 2025). These interactions are particularly important in polluted environments, where a combination of different microorganisms works together to degrade hydrocarbons more efficiently and effectively.

2.5.2 Environmental Factors Influencing Hydrocarbon Degradation

Several environmental factors influence microbial hydrocarbon degradation efficiency, including temperature, pH, nutrient availability, and oxygen levels (Kebede et al., 2021). Aerobic conditions generally favour the degradation of hydrocarbons, as oxygen is required for the oxidation processes catalysed by various enzymes (Koh and Khor, 2022). However, some microorganisms, such as those belonging to the genera *Desulfobacter* and *Geobacter*, are capable of degrading hydrocarbons under anaerobic conditions, albeit at a slower rate (Widdel and Rabus, 2001)).

The availability of nutrients, such as nitrogen and phosphorus, can also influence microbial degradation rates (Nwankwegu et al., 2022). In hydrocarbon-contaminated environments, a phenomenon known as nutrient limitation may occur, where the degradation process is slowed down because essential nutrients are in short supply. In such cases, adding nutrients (a process known as bioaugmentation) can help accelerate the degradation of hydrocarbons (Sarkar et al., 2017, Wu et al., 2016, Wu et al., 2019).

A wide range of hydrocarbon-degrading microorganisms contribute to this process, including species from the genera *Pseudomonas*, *Alcanivorax*, *Rhodococcus*, and *Mycobacterium*, which are known for their ability to degrade both aliphatic and aromatic hydrocarbons (Phale et al., 2007). Understanding the microbial mechanisms of hydrocarbon degradation is crucial for developing effective bioremediation strategies. By optimising environmental conditions, enhancing microbial communities, and integrating biosurfactants, oxygen-releasing compounds, or electron acceptors, the efficiency of microbial hydrocarbon degradation can be significantly improved, making bioremediation a promising solution for hydrocarbon-contaminated environments.

2.5.3 Structure and Mechanism of Ring-Hydroxylating Dioxygenases (RHDs)

Ring-hydroxylating dioxygenases (RHDs) are essential multicomponent enzyme systems that catalyse the initial oxidation of aromatic hydrocarbons, making them a crucial component in their microbial degradation (Parales and Resnick, 2006). These enzymes belong to the oxidoreductase family, specifically classified within the Rieske non-heme iron oxygenase superfamily. This superfamily is known for its role in breaking down complex organic pollutants (Wackett, 2002). Their function is vital for the bioremediation of hydrocarbon-contaminated environments, as they enable microbial communities to metabolise toxic PAHs into less harmful intermediates (Perry et al., 2018).

Structurally, RHDs consist of three primary components, each contributing to the enzyme's catalytic efficiency. The oxygenase component is responsible for the hydroxylation of aromatic hydrocarbons. Within this component, the alpha subunit contains a Rieske-type iron-sulphur cluster (2Fe-2S) and a mononuclear iron centre, both of which facilitate the binding of molecular oxygen and electron transfer necessary for oxidation (Inoue and Nojiri, 2014).

The structural complexity and functional efficiency of RHDs make them indispensable in environmental biotechnology. Their ability to initiate the degradation of otherwise recalcitrant PAHs highlights their potential for use in bioremediation strategies to mitigate hydrocarbon contamination.

2.5.4 Microbial Taxa Containing RHDs

Ring-hydroxylating dioxygenases (RHDs) are predominantly found in the Proteobacteria and Actinobacteria phyla members, both of which are integral to hydrocarbon degradation in various environments (Martin et al., 2013). These bacteria, widely distributed in terrestrial and marine ecosystems, exhibit remarkable metabolic versatility, allowing them to break down persistent organic pollutants, including petroleum hydrocarbons and polycyclic aromatic hydrocarbons (PAHs) (Zeng et al., 2017). Several taxonomic classes and orders contain RHD-producing bacteria, each playing a crucial role in bioremediation and natural attenuation of contaminated sites.

The *Alphaproteobacteria* class also includes RHD-producing bacteria, particularly within the *Rhizobiales* order. *Sphingobium yanoikuyae* expresses phenanthrene dioxygenase, making it highly effective in breaking down high-molecular-weight PAHs (Le et al., 2014). Similarly, *Sphingomonas paucimobilis* possesses biphenyl dioxygenase, which allows it to degrade PCBs and other complex aromatic hydrocarbons. These bacteria play significant roles in bioremediation strategies due to their ability to thrive in polluted environments and metabolise hazardous contaminants (Macchi et al., 2017).

Within the *Betaproteobacteria* class, the *Burkholderiales* order contains key hydrocarbon-degrading bacteria. *Burkholderia cepacia* expresses biphenyl dioxygenase, a critical enzyme involved in the degradation of biphenyl and polychlorinated biphenyls (PCBs) (Coenye, 2014). Additionally, *Ralstonia pickettii* is known to produce toluene dioxygenase, which enables the oxidation of toluene and related compounds, contributing to the bioremediation of volatile organic contaminants (Vio et al., 2020).

Among the Gammaproteobacteria, members of the *Pseudomonadales* order, particularly *Pseudomonas* species, are well-known hydrocarbon degraders. *Pseudomonas putida* harbors both naphthalene and toluene dioxygenases, enabling the oxidation of these common pollutants into bioavailable intermediates (Girard et al., 2021). Similarly, *Pseudomonas aeruginosa* expresses phenanthrene dioxygenase, which facilitates the breakdown of higher molecular weight PAHs, making

these bacteria highly effective in hydrocarbon-contaminated environments. (Samanta and Bandyopadhyay, 2020). Another important group within *Gammaproteobacteria* is the *Xanthomonadales* order, which includes *Xanthomonas* species known for their benzoate dioxygenase activity, crucial for aromatic compound degradation (Gutierrez, 2017).

In the *Actinobacteria* class, species from the *Mycobacteriales* order are particularly noteworthy for their hydrocarbon degradation abilities (Barka et al., 2016). *Mycobacterium vanbaalenii* has been identified as a potent degrader of PAHs due to its production of phenanthrene dioxygenase, enabling it to oxidise complex hydrocarbon structures efficiently (Mohammadipanah and Dehhaghi, 2017). Likewise, *Mycobacterium gilvum* produces toluene dioxygenase, allowing it to break down toluene and similar monoaromatic hydrocarbons (Lawson, 2018).

2.5.5 Types of Ring-Hydroxylating Dioxygenases (RHDs)

Ring-hydroxylating dioxygenases (RHDs) exhibit remarkable diversity, and different types are classified based on substrate specificity and catalytic efficiency. Several well-characterized RHDs have been identified across different bacterial species, each with distinct functional roles in hydrocarbon degradation (Chemerys et al., 2014).

Naphthalene dioxygenase (NDO) is one of the most extensively studied RHDs. It is primarily responsible for catalysing the hydroxylation of naphthalene into cis-naphthalene dihydro diol, an essential intermediate in the degradation pathway of this two-ring PAH (Karlsson et al., 2003). This enzyme has been identified in hydrocarbon-degrading bacteria such as *Pseudomonas putida* G7 and *Burkholderia cepacia*, where it facilitates the breakdown of naphthalene into smaller, more bioavailable compounds for further microbial metabolism (Ensley and Gibson, 1983).

Another RHD is biphenyl dioxygenase (BPDO), which plays a key role in the degradation of biphenyl and polychlorinated biphenyls (PCBs), a class of highly toxic and persistent pollutants. BPDO introduces oxygen molecules into the biphenyl ring, initiating its breakdown into less harmful intermediates that can be further processed by microbial metabolic pathways (Gómez-Gil et al., 2007).

This enzyme is commonly found in *Burkholderia xenovorans* and *Sphingomonas* species, which are known for their ability to degrade PCBs and related aromatic hydrocarbons (Furukawa and Fujihara, 2008).

Toluene dioxygenase (TDO) is another well-characterised enzyme that catalyses the hydroxylation of toluene, benzene, and xylene, which are major components of petroleum-based contaminants (Yeh et al., 1977). In *Pseudomonas putida* F1 and *Rhodococcus opacus*, TDO facilitates the oxidation of these volatile organic compounds, converting them into more hydrophilic and biodegradable intermediates. This enzymatic activity is particularly important in remedying environments contaminated with petroleum products and industrial solvents (Wissner et al., 2021).

Phenanthrene dioxygenase (PDO) is crucial in the degradation of high-molecular-weight PAHs. This enzyme is responsible for the initial oxidation of phenanthrene and pyrene, two of the most recalcitrant PAHs commonly found in petroleum-contaminated environments (Li et al., 2017). *Mycobacterium vanbaalenii* and *Sphingobium yanoikuyae* are known to possess this enzyme, allowing them to effectively metabolise these complex hydrocarbons into less persistent and more bioavailable compounds (Waigi et al., 2015, Lu et al., 2019).

In addition to these PAH-specific enzymes, benzoate dioxygenase (BZDO) is an essential RHD involved in the hydroxylation of benzoate and substituted benzoates, which are critical intermediates in aromatic hydrocarbon degradation (Imam et al., 2022). Found in *Acinetobacter* and *Ralstonia* species, BZDO catalyses the transformation of benzoate into catechol derivatives, which are further metabolised through central metabolic pathways, leading to complete mineralisation (Wolfe et al., 2002).

Each of these RHDs (ring-hydroxylating dioxygenases) serves a specialised function in the biodegradation of hydrocarbons, thereby facilitating the efficient degradation of various pollutants. The significant diversity of these enzymes underscores the metabolic versatility of hydrocarbon-

degrading microorganisms, which allows them to flourish in contaminated environments and promote the natural attenuation of petroleum-derived compounds.

2.5.6 Factors Affecting Bioremediation Efficiency

Several environmental and microbial factors influence the effectiveness of bioremediation in hydrocarbon-contaminated sites. One crucial factor is the availability of nutrients, as microbial degradation requires sufficient nitrogen, phosphorus, and trace elements to support growth and enzymatic activity (Mishra et al., 2021). Nutrient supplementation through biostimulation has been shown to enhance degradation rates by optimising microbial metabolism (Adams et al., 2015).

Oxygen levels also play a critical role in hydrocarbon degradation. Aerobic biodegradation depends on oxygen availability, and its depletion can slow microbial activity. In oxygen-limited environments, alternative electron acceptors such as nitrate and sulphate enable anaerobic degradation, allowing microbes to continue breaking down hydrocarbons under anoxic conditions (Nazir et al., 2021).

The composition of microbial communities further dictates biodegradation efficiency. The presence of specialised hydrocarbon-degrading bacteria significantly enhances remediation rates (Srivastava et al., 2014). In some cases, bioaugmentation, the introduction of exogenous hydrocarbon-degrading microbes, is employed to accelerate bioremediation in sites with insufficient native microbial populations (Sarkar et al., 2017, Wu et al., 2016).

Environmental parameters such as temperature and pH also influence microbial activity. Optimal biodegradation occurs within mesophilic temperature ranges of 20-35°C and at neutral to slightly alkaline pH levels (Gauvry et al., 2021). Extreme temperatures or highly acidic/alkaline conditions can disrupt microbial metabolism and enzymatic function, thereby limiting degradation potential (Sarma et al., 2023).

The structure and type of hydrocarbons being degraded also determine biodegradation efficiency. Low-molecular-weight hydrocarbons, such as alkanes, are more readily biodegradable due to their

simple chemical structure (Varjani, 2017). In contrast, high-molecular-weight polycyclic aromatic hydrocarbons (PAHs) require specialised metabolic pathways for breakdown, often making their remediation more complex (Husain, 2008).

Lastly, the presence of inhibitory compounds, such as heavy metals and toxic organic pollutants, can negatively impact microbial metabolism, limiting biodegradation potential. These contaminants interfere with enzymatic activity and microbial respiration, reducing the overall efficiency of bioremediation efforts (Kondakindi et al., 2024). Understanding these factors allows for optimisation of bioremediation strategies, ensuring improved hydrocarbon degradation in contaminated environments.

2.5.7 Can Bioremediation be integrated with metallic nanoparticles?

Integrating bioremediation with other remediation techniques has been shown to enhance hydrocarbon degradation efficiency (Kuppan et al., 2024, Bora et al., 2025). "Nanobioremediation" is the combination of bioremediation with nanotechnology in a treatment process to create a synergistic effect to accelerate pollutant breakdown and improve overall remediation outcomes (Zhang et al., 2020). One of the most promising strategies involves the use of nZVI, which has been demonstrated to enhance biodegradation by breaking down hydrocarbon contaminants into more bioavailable forms, thereby stimulating microbial activity (Devendrapandi et al., 2024). By reducing complex hydrocarbons into simpler compounds, nZVI facilitates microbial access to otherwise recalcitrant contaminants, ultimately improving biodegradation rates in contaminated environments (Miranda et al., 2022).

2.6 Interactions Between Nanoparticles and Microbial Communities

The interactions between nanoparticles and microbial communities are crucial in determining the overall efficiency and potential risks associated with nanotechnology applications in environmental remediation (Ji et al., 2024). Nano zero-valent iron (nZVI) is widely used for treating hydrocarbon contamination, yet its impact on microbial communities remains a complex topic. While nZVI can

enhance bioremediation by increasing pollutant bioavailability and stimulating microbial activity, it can also cause toxicity to beneficial bacteria, leading to shifts in microbial diversity and function (Barzan et al., 2014, Eduok and Coulon, 2017). Understanding these interactions is essential to optimising nano-bioremediation strategies while minimising unintended ecological consequences. These effects depend on nanoparticle properties, environmental conditions, and microbial community resilience (Bhatt et al., 2022).

2.6.1 Effects of nZVI on Microbial Activity and Community Structure

The application of nZVI in contaminated environments influences microbial activity and community composition. These effects can be classified as enhancing, neutral, or inhibitory, depending on the concentration of nZVI, its physicochemical properties, and the environmental conditions under which it is applied (Jang et al., 2014, Kotchaplai et al., 2019). Understanding these interactions is critical for optimising the use of nZVI in bioremediation while minimising potential ecological disruptions.

One of the most promising positive effects of nZVI is its ability to enhance biodegradation efficiency by breaking down complex hydrocarbons into simpler, more bioavailable compounds, thereby stimulating microbial metabolic activity (Rana et al., 2020). The reactive iron species produced during nZVI oxidation generate electron donors, which can serve as alternative energy sources for specific bacteria, particularly those involved in anaerobic hydrocarbon degradation (Wang et al., 2025). Additionally, studies suggest that nZVI can induce co-metabolic degradation, wherein microbial consortia utilise the breakdown products of hydrocarbons more efficiently in the presence of iron nanoparticles. This synergistic interaction can enhance bioremediation outcomes by stimulating functional microbial groups that specialise in hydrocarbon degradation (Banerjee et al., 2022).

Beyond enhancing biodegradation, nZVI also alters microbial community structure, often favouring iron-reducing bacteria such as *Geobacter* and *Shewanella*, which thrive in iron-rich environments (Chen et al., 2024). These bacteria are well known for their metal-reducing capabilities, allowing them to play a vital role in hydrocarbon degradation pathways in anaerobic and iron-rich conditions (Fan et

al., 2018). The presence of nZVI can selectively enrich microbial consortia that possess the enzymatic machinery required to utilise iron as an electron acceptor, thereby shifting the microbial community dynamics toward more effective biodegradation processes (Xie et al., 2017). Additionally, some iron-oxidizing bacteria may indirectly facilitate hydrocarbon degradation by modulating redox conditions in contaminated environments, which enhances the breakdown of recalcitrant organic pollutants (Singh et al., 2018b).

Despite these benefits, nZVI also has potential inhibitory effects on microbial communities, mainly when applied at excessive concentrations. The generation of reactive oxygen species (ROS) during nZVI oxidation can damage microbial cell membranes, proteins, and DNA, leading to reduced microbial diversity and metabolic disruption (Lefevre et al., 2016, Kotchaplai et al., 2019). This cytotoxicity is dose-dependent, meaning that different microbial species exhibit varying levels of tolerance to nZVI exposure. For instance, while some metal-resistant bacteria can adapt to oxidative stress, others may suffer severe cellular damage, resulting in a loss of critical functional microbial groups necessary for effective bioremediation (Staroń and Długosz, 2021). Prolonged ROS exposure may further disrupt ecosystem stability, highlighting the importance of carefully controlled dosing when using nZVI in remediation applications (Sharmin et al., 2021). Moreover, excessive nZVI application can lead to particle aggregation, which reduces its surface area and reactivity, limiting its effectiveness as an amendment in biodegradation-enhancing strategies (Hajipour et al., 2012).

2.6.2 Optimising Green nZVI in Nano-Bioremediation

The influence of nanoscale zero-valent iron (nZVI) on microbial communities is highly context-dependent, requiring meticulous dosage optimisation, application methodologies, and environmental monitoring protocols (Hajipour et al., 2012). When nZVI is synthesised using green methods, particularly those involving polyphenols from plant extracts, it can provide an environmentally friendly means of pollutant remediation (Bhardwaj et al., 2020). However, it is essential to understand how these nanoparticles interact with microbial consortia at both the community and functional levels. By

analysing shifts in dominant taxa, overall diversity, enzyme production, contaminant degradation pathways, and gene expression, one can tailor the iron nanoparticles, coating, and delivery methods to maximise hydrocarbon degradation rates while minimising ecological risks(Bashir et al., 2020b, Buarki et al., 2022). When microorganisms maintain viability and actively degrade pollutants, the synergy between biological processes and the catalytic activities of green iron nanoparticles augments remediation efficiency, ensuring a more effective and sustainable outcome (Bhatt et al., 2022). Concurrently, diligent monitoring of microbial health permits the early detection and mitigation of potential toxicity or unanticipated disruptions to native ecosystems. Thus, safe and effective nano-bioremediation protocols can be devised through this integrated perspective to leverage green iron nanoparticles while preserving environmental integrity.

Optimised conditions such as the concentration of polyphenols, pH, temperature, and reaction duration become crucial for achieving targeted nanoparticle properties. These conditions will help researchers and practitioners develop more effective and scalable remediation strategies when combining bioremediation with nanotechnology. Collectively, these approaches capitalise on the strengths of multiple techniques, ensuring improved hydrocarbon degradation rates and heightened adaptability to a range of environmental scenarios. Several optimisation suggestions have been made to maintain the benefits of nZVI while mitigating its potential downsides. One strategy is dose optimisation, carefully balancing nZVI's reactivity with microbial compatibility through controlled concentrations, so that biodegradation is enhanced without compromising microbial diversity (Grieger et al., 2019). Consistent and predictable remediation outcomes can be achieved by tailoring dosing strategies to specific conditions and contamination levels.

Green synthesis provides surface modification of nZVI by coating nanoparticles with organic stabilisers such as polyphenols and surfactants; this reduces reactive oxygen species (ROS) generation and aggregation, thereby lowering potential toxicity (Abdelfatah et al., 2021). These modifications preserve high reactivity while bolstering environmental compatibility, enabling improved mobility and

bioavailability in contaminated environments. By increasing nanoparticle dispersal, microorganisms gain greater access to catalytic sites, facilitating more efficient contaminant breakdown (Saif et al., 2016). In addition, integrating nZVI with bioaugmentation strategies addresses the challenge of microbial imbalances or toxicity issues. Introducing engineered microbial consortia that tolerate nZVI further enhances degradation effectiveness while sustaining community diversity. These engineered strains often produce elevated levels of ring-hydroxylating dioxygenases (RHDs) and iron-reducing enzymes, boosting hydrocarbon degradation (Mukhopadhyay et al., 2025).

Finally, long-term ecotoxicity assessments are essential to evaluate nZVI's persistence and broader ecological impacts over time. Field studies that track microbial diversity and ecosystem stability offer valuable insight into the evolving role of nZVI in biodegradation pathways. Data from these assessments inform regulatory guidelines and safe application practices, ensuring that nZVI remains a responsible and effective tool for environmental remediation. By adopting these multifaceted strategic dose optimisation, surface modification, bioaugmentation, and extended ecological monitoring, researchers can harness the advantages of green nZVI while safeguarding the microbial communities that drive natural and engineered remediation processes.

2.7 Challenges and Opportunities in Implementing Green Nanotechnology for Remediation

The application of green nanotechnology in environmental remediation presents both significant challenges and opportunities. While green-synthesised nanoparticles, such as nZVI, offer a sustainable alternative to conventional nanoparticles, their large-scale implementation is hindered by technological, economic, and regulatory constraints (Bharali et al., 2023). These challenges include synthesis reproducibility, scalability, environmental impact assessments, and field performance variability (Ali et al., 2016). However, green nanotechnology also provides exciting opportunities to enhance remediation efficiency, reduce secondary pollution, and support global sustainability goals (Ebrahiminezhad et al., 2018, Haider et al., 2024, Hano and Abbasi, 2021). This section explores the

key challenges associated with field applications of green nanotechnology and the opportunities available for promoting its widespread adoption in sustainable environmental remediation.

2.7.1 Challenges of Green Nanotechnology in Field Applications

Despite the promising results observed in laboratory studies, the transition of green-synthesised nanomaterials from controlled experimental conditions to real-world field applications faces several significant challenges. These obstacles include scalability and cost constraints, stability and aggregation issues, limited field performance data, and regulatory uncertainties, all hindering the large-scale deployment of green nanoscale zero-valent iron (nZVI) for environmental remediation.

One of the primary challenges is scalability and cost constraints, as the large-scale production of green-synthesised nanoparticles remains technically complex. Unlike industrially synthesised nanoparticles, which are manufactured using standardised and reproducible chemical methods, green nZVI exhibits batch-to-batch variability, making its large-scale application unpredictable (Gacem and Abd-Elsalam, 2022). This variability arises because the reducing agents used in green synthesis, such as polyphenols extracted from plant sources, are subject to fluctuations in yield and effectiveness depending on environmental factors, plant species, and extraction techniques (Ying et al., 2022). Consequently, ensuring consistency in nanoparticle properties, such as size, shape, and surface reactivity, remains a significant hurdle limiting green nZVI acceptance in remediation technologies as an accepted standard.

Another critical limitation is the stability and aggregation issues associated with green nZVI. Due to its high surface energy, green nZVI readily aggregates, leading to a loss of reactivity when introduced into complex environmental matrices(Bharali et al., 2023). This agglomeration reduces the effectiveness of green nZVI in soil and water remediation, as clustered nanoparticles exhibit reduced surface area, thereby decreasing their interaction with contaminants (Mohamed amine and Abd-Elsalam, 2021). Additionally, green nZVI particles show increased oxidation rates upon exposure to air, further diminishing their lifespan and reactivity. To counteract these stability concerns, researchers have explored various stabilisation techniques, such as organic capping agents, surfactant modifications,

and bio-polymer coatings, to enhance dispersion and prolong the reactivity of green nZVI in field applications (Noor et al., 2023).

Moreover, the limited availability of field performance data presents a significant bottleneck in advancing green nZVI for practical remediation efforts. While most studies on green nZVI have been conducted under controlled laboratory conditions, the behaviour of these nanoparticles in real-world environmental settings remains largely untested. Environmental variables such as pH fluctuations, varying organic matter content, and the presence of competing ions can all impact the efficiency, transport, and fate of green nZVI in natural systems. Additionally, subsurface mobility remains a key area of uncertainty, as green nZVI may experience rapid sedimentation or unintended interactions with non-targeted compounds, further complicating its effectiveness in field-scale applications (Pal et al., 2022). More extensive pilot-scale studies and field demonstrations are needed to assess the real-world performance, longevity, and adaptability of green nZVI in hydrocarbon-contaminated environments.

Finally, regulatory and environmental concerns pose substantial challenges to the widespread adoption of green nZVI technology. One of the primary obstacles is the absence of standardised regulatory guidelines governing the use of nanomaterials in environmental remediation. Governments and environmental agencies require extensive ecotoxicological assessments to evaluate the long-term safety and risks associated with nanoparticle deployment at remediation sites (Pal et al., 2022). Concerns have been raised regarding the fate and transport of green nZVI in aquatic and terrestrial ecosystems, as residual organic coatings from plant-based stabilisers may introduce unintended contaminants into the environment (Libralato et al., 2017, Grieger et al., 2010). Addressing these regulatory gaps through comprehensive risk assessments and policy development is essential for facilitating the responsible and sustainable integration of green nanotechnology in environmental remediation efforts.

2.7.2 Opportunities for Green Synthesis in Sustainable Remediation

While green nanotechnology presents some challenges, it also offers significant opportunities for advancing environmental sustainability and remediation efforts. The eco-friendly synthesis process, cost-effectiveness, and potential for integration with bioremediation make green nZVI a promising alternative to traditional remediation technologies. These advantages contribute to developing more sustainable and effective hydrocarbon treatment strategies. Table 2.2 highlights some of the advantages green-synthesised nZVI has over other counterparts

One of the key benefits of green nZVI is its eco-friendly synthesis, which reduces the risks of secondary pollution. Unlike conventionally synthesised nanoparticles that require hazardous chemical reductants, green nZVI is produced using plant extracts that serve as both reducing and stabilising agents (Israeel et al., 2024). This method eliminates the need for toxic reagents, making the synthesis process safer for both humans and the environment. Additionally, the biocompatibility of plant-derived nanoparticles ensures that they minimise adverse ecological effects, making them particularly suitable for in situ remediation efforts (Bhardwaj et al., 2020). The use of natural stabilisers from plant-based sources further enhances nanoparticle dispersion and longevity, making green nZVI a viable and sustainable solution for large-scale environmental applications (Das and Patra, 2021).

Another significant advantage of green nanotechnology is its potential for broader policy integration and public acceptance. Green nZVI aligns with global sustainability initiatives and climate action goals, making it more attractive to policymakers and environmental regulators (Jabeen et al., 2024). As awareness of sustainable environmental solutions continues to grow, regulatory frameworks are evolving to encourage and support green synthesis methods. Additionally, governments and environmental agencies are more likely to prioritise funding opportunities for remediation projects that incorporate eco-friendly nanotechnologies, accelerating their commercialisation and field deployment (Slootweg, 2024). By engaging with UK and Scottish policies like the Scottish Environment Strategy, alongside international standards such as the WHO's drinking-water guidelines and the US

EPA's clean-up protocols, stakeholders can integrate green nZVI into national consent conditions and best-practice guidance, thereby supporting stricter discharge limits, incentivising eco-designed treatment technologies, and harmonising sustainable hydrocarbon remediation across the region.

Beyond environmental and regulatory benefits, green nZVI also presents economic advantages by reducing production costs and promoting resource utilisation. The synthesis of green nZVI can leverage agricultural waste and plant biomass, contributing to waste valorisation strategies and supporting a circular economy model (Abdelbasir et al., 2020). Instead of relying on expensive and energy-intensive synthetic routes, green synthesis utilises renewable resources, making it a cost-effective alternative (Devatha et al., 2016). Moreover, utilising locally available biomass or plant waste as a source of raw material can substantially reduce production costs, thereby making the technology accessible and affordable in developing and low-income regions. This affordability increases the potential for the widespread adoption of green nZVI in environmental remediation projects across a variety of geographical locations (Kumar et al., 2024).

Finally, in addition to treating contaminated soil and water, green nanoparticles have prospects for a wide range of applications across the energy, biomedical, environmental, agricultural, and food sectors. They can enhance fuel cells and batteries, safely deliver drugs and image tissues, detoxify pollutants and treat waste, improve crop resilience and nutrient delivery, and extend the shelf life of food through advanced packaging, all while reducing environmental impact (Osman et al., 2024, Karnwal et al., 2024).

2.7.3 Overcoming Challenges and Future Research Directions

Despite the significant promise of green-synthesised nanoscale zero-valent iron (nZVI) in hydrocarbon remediation, several challenges must be addressed to facilitate its large-scale adoption. To overcome these barriers, future research needs to focus on key areas that enhance the scalability, efficiency, and regulatory acceptance of green nZVI while ensuring its environmental and economic viability.

A primary research priority involves developing scalable and cost-effective synthesis methods that ensure batch-to-batch consistency and maintain high reactivity and stability. Many current green synthesis methods rely on plant extracts, which introduce variability in nanoparticle composition and performance due to differences in plant metabolites (Gupta et al., 2023a). Future studies should explore standardised synthesis protocols, including precisely controlled reaction conditions and optimised extraction techniques, to minimise inconsistencies and enhance reproducibility for industrial-scale production.

Another crucial aspect is improving green nanoparticle stability through surface modifications that prevent aggregation and oxidation, because green nZVI is prone to rapid oxidation, which can reduce its long-term effectiveness in remediation efforts, thereby prolonging reactivity under different environmental conditions (Singh et al., 2023).

Large-scale field studies are also essential to validate the effectiveness, transport behaviour, and longevity of green nZVI in real-world remediation scenarios (Bharali et al., 2023). Laboratory experiments mainly provide valuable insights into reaction mechanisms and nanoparticle performance. However, controlled field applications are needed to assess how green nZVI behaves in complex, heterogeneous environments with varying pH, salinity, organic matter, and microbial activity. Pilot-scale and long-term studies will offer critical data on its long-term stability, reactivity, and degradation pathways, allowing for better optimisation before full-scale deployment.

Additionally, establishing clear regulatory frameworks is vital to balance safety considerations with the benefits of green nanotechnology. While conventional nZVI has faced regulatory scrutiny due to concerns about ecotoxicity, nanoparticle persistence, and potential groundwater contamination, green nZVI presents an opportunity to introduce safer, more sustainable alternatives (Isibor, 2024). However, comprehensive risk assessments, standardised testing protocols, and environmental monitoring programs must be implemented to ensure its safe and responsible use in environmental remediation (Naryal et al., 2024).

By addressing these scientific, technical, and regulatory challenges, green nZVI has the potential to emerge as a viable and sustainable alternative to conventionally synthesised nanomaterials. Its adoption could lead to more environmentally friendly and effective hydrocarbon remediation strategies while contributing to broader global efforts toward sustainable pollution management. As research progresses, green nanotechnology may serve as a cornerstone in future environmental cleanup initiatives, paving the way for a greener and cleaner future in tackling hydrocarbon contamination and other persistent environmental pollutants.

Chapter 3 MATERIALS AND METHODS

This chapter provides a comprehensive framework for the experiments aimed at evaluating the remediation potential of green nanoscale zero-valent iron (nZVI) in comparison with industrial nZVI. It begins by outlining the procedures for synthesising green nZVI from plant-based extracts. Both particle types undergo physicochemical characterisation, including morphological (e.g., scanning electron microscopy), elemental (e.g., energy dispersive spectroscopy), and crystallographic (e.g., X-ray diffraction) analyses to ascertain their size, structure, and compositional attributes.

Subsequently, these characterised nanoparticles are applied to contaminated water samples containing petroleum hydrocarbons under controlled conditions (with respect to pH, temperature, and reaction time). Multiple dosages of each nZVI preparation are evaluated to determine optimal treatment efficacy. Throughout the treatment process, water samples are collected at predetermined intervals and analysed for two key indicators: Chemical Oxygen Demand (COD) and total petroleum hydrocarbons (TPH). By integrating stoichiometric assessments and chromatographic analyses, this section aims to correlate nanoparticle properties with their ability to degrade or transform targeted contaminants.

In addition to examining remediation efficiency, the chapter also incorporates methodologies for elucidating microbial responses to both green and industrial nZVI. DNA extraction protocols are applied to water samples at specific time points to capture changes in microbial community composition throughout the remediation process. 16S-rRNA-gene targeted sequencing enables a deeper investigation into the diversity and relative abundance of bacterial taxa. The resulting sequence data undergo rigorous bioinformatic workflows covering quality control, operational taxonomic unit (OTU) clustering, and taxonomic classification to identify how nanoparticle treatments influence microbial community structure. Together, these molecular analyses provide valuable insights into the ecological implications of nZVI deployment, revealing whether certain microbial groups are stimulated or inhibited by the presence of either green or industrial iron nanoparticles.

This chapter offers a comprehensive methodological blueprint by merging synthesis, characterisation, and application protocols with microbial community monitoring. The ultimate goal is not only to evaluate how effectively different nZVI formulations can remediate hydrocarbon-contaminated water but also to ascertain how these treatments impact the broader microbial ecology. This dual focus on contaminant removal and ecosystem health ensures that the outcomes of this study can inform more sustainable and balanced remediation strategies.

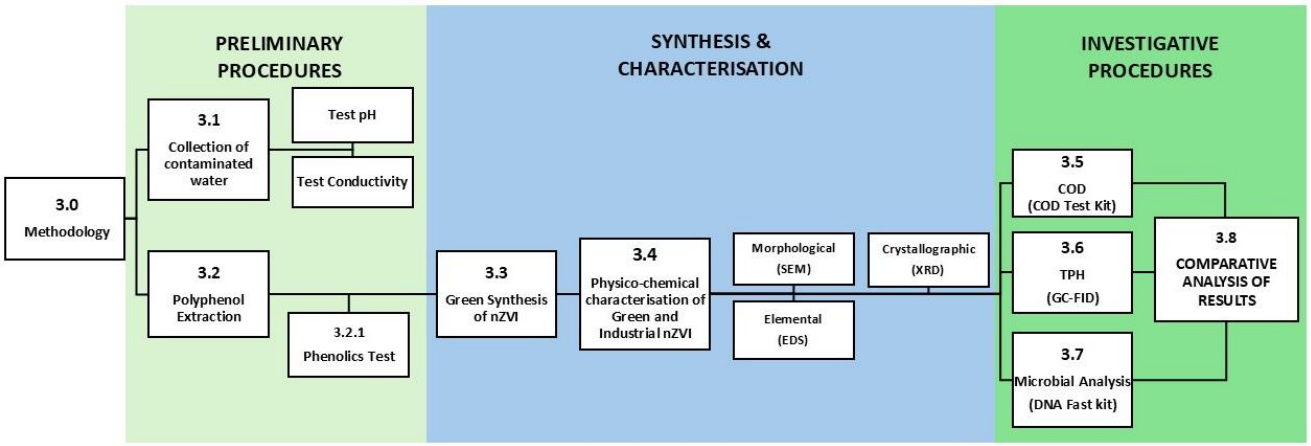

Figure 3.1 An overview of the methodology

3.1 Contaminated Water Sample Collection and Preparation

Contaminated water samples were extracted from soils at the old Carless Oil Terminal in Old Kirkpatrick, near Erskin bridge, Clydebank, along the River Clyde, near Glasgow (NDA would not allow us to provide exact coordinates of the site). The soils were exhumed 1-2 metres below the surface. As the soil was removed, an oily sheen was observed in the pooled water from which the samples were collected in one-litre bottles, as shown in Figure 3.2. A total of 2 litres of contaminated water was carefully decanted to avoid disturbing any sediment or floating debris. To replicate a realistic yet controlled contamination scenario suitable for laboratory testing, the decanted water was diluted with 2 litres of uncontaminated Clyde River water, resulting in a 1:1 dilution ratio.

This dilution served two primary purposes: (i) to moderate the hydrocarbon concentration and prevent inhibition of microbial activity, and (ii) to approximate natural aquatic conditions, enabling

realistic assessment of nZVI performance and microbial responses. The resulting 4 litre composite sample was gently homogenised by stirring and subsequently used as the contaminated water stock for all experimental treatments, including the blank contaminated water (control) and the nZVI-dosed batches. The sample was tested for pH and conductivity using a Thermo Scientific Orion Star A215 pH/Conductivity meter.

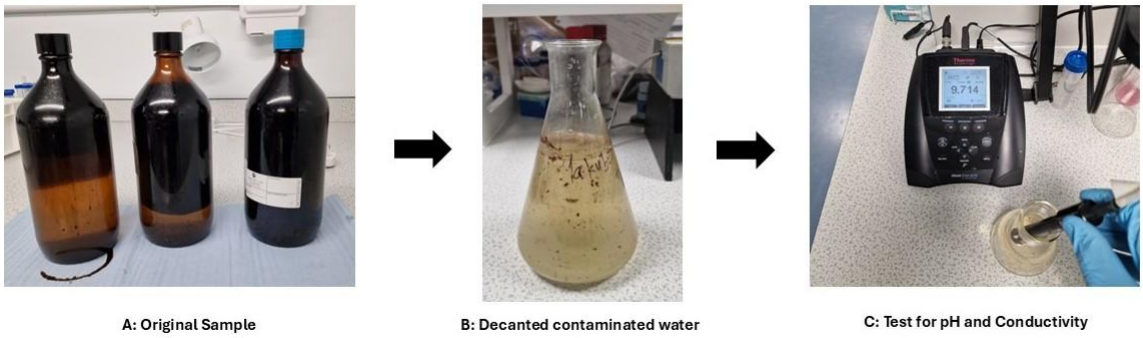

Figure 3.2 Testing contaminated water samples for PH and conductivity

3.2 Extraction of Polyphenol

Polyphenol extract was prepared by boiling 10 g of dried green tea leaves (obtained from Lidl retail store, imported from Poland and packaged in Dublin, Ireland) in 100 mL of deionised water. This mixture was heated to 70°C in a 250 mL flask on a magnetic stirrer for one hour. It was then filtered through a 0.22 µm filter paper. A similar procedure was applied to black tea obtained from the shelf at Tesco supermarket and dried orange peel extracts from regular orange peels imported from South Africa purchased at Aldi supermarket. The choice of green tea, black tea, and orange peel as comparative polyphenol sources was guided by their variability in phenolic composition, availability, and cost-effectiveness. In addition to its high antioxidant potential, green tea is widely available and inexpensive, making it a practical and sustainable source of polyphenols. Orange peels and black tea were included to evaluate how differences in sourcing cost and phenolic strength influence the efficiency of nanoparticle synthesis, thereby identifying the most balanced option between reactivity, affordability, and environmental compatibility.

Preliminary experiments for the synthesis of green iron nanoparticles were conducted to optimise the extraction of polyphenols from selected plant materials and to determine their suitability as natural reducing and stabilising agents. The adopted synthesis approach followed a well-established green chemistry protocol that involves the aqueous extraction of polyphenols from plant biomass, followed by the reduction of ferric ions (Fe^{3+}) to zerovalent iron (Fe^{0}) under controlled conditions. This method was chosen because it avoids the use of chemical reducers such as sodium borohydride, thereby offering a safer and more environmentally sustainable route to nanoparticle formation.

The procedure employed in this study is consistent with several reported works in the literature that describe the green synthesis of nano zero-valent iron (nZVI) using polyphenol-rich plant extracts, particularly green tea (*Camellia sinensis*), as both reducing and capping agents (Kharissova et al., 2013b, Huang et al., 2014, Hao et al., 2021, Abdelfatah et al., 2021, Gupta et al., 2023b). Over the past decade, this method has become widely recognised for its reproducibility, mild reaction conditions, and the ability of naturally occurring antioxidants to produce stable, reactive iron nanoparticles with minimal environmental impact. Consequently, it was selected for this research as a reliable and sustainable pathway for producing green nZVI for hydrocarbon remediation studies.

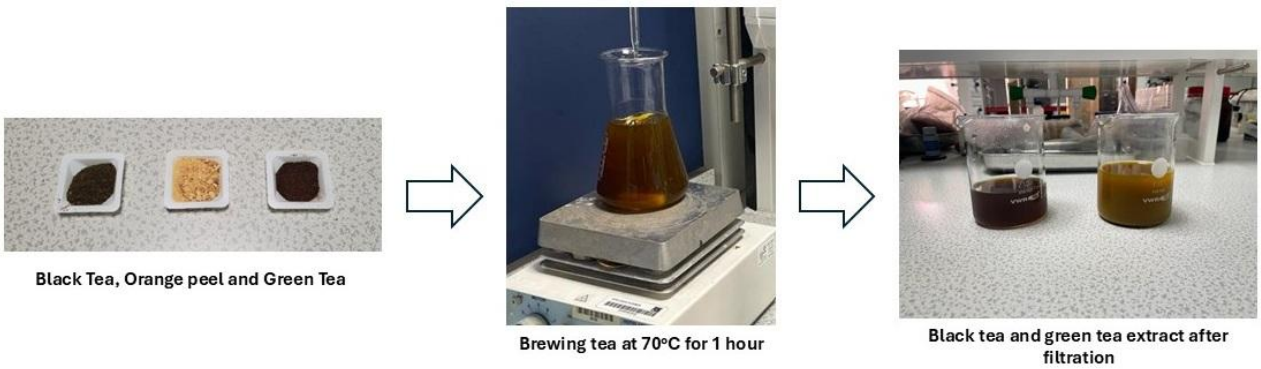

Figure 3.3 Extracting polyphenols from plant extract

3.2.1 Measurement of Phenolic Content

5 mL of all the plant extracts were collected and diluted at a ratio of 1:50 to quantify the total polyphenol content. A HACH Phenols Cuvette Test Kit (0.01-5.0 mg/L; Dusseldorf, Germany) was used to measure the phenolic content of the plant extracts. 2 mL of the diluted solution was pipetted into a HACH cuvette containing 4% hydrochloric acid. Then 0.2mL of reagent LCK345A (sodium nitrite) was added, shaken (upside down), and allowed to sit for two minutes before adding 0.2mL of a second reagent LCK345B (sodium carbonate), shaken in the same fashion as the previous reagent, and again allowed to sit for 2 minutes. The cuvette was then inserted into a HACH DR6000 UV-Vis spectrophotometer, and the absorbance readings were obtained at 476nm wavelength.

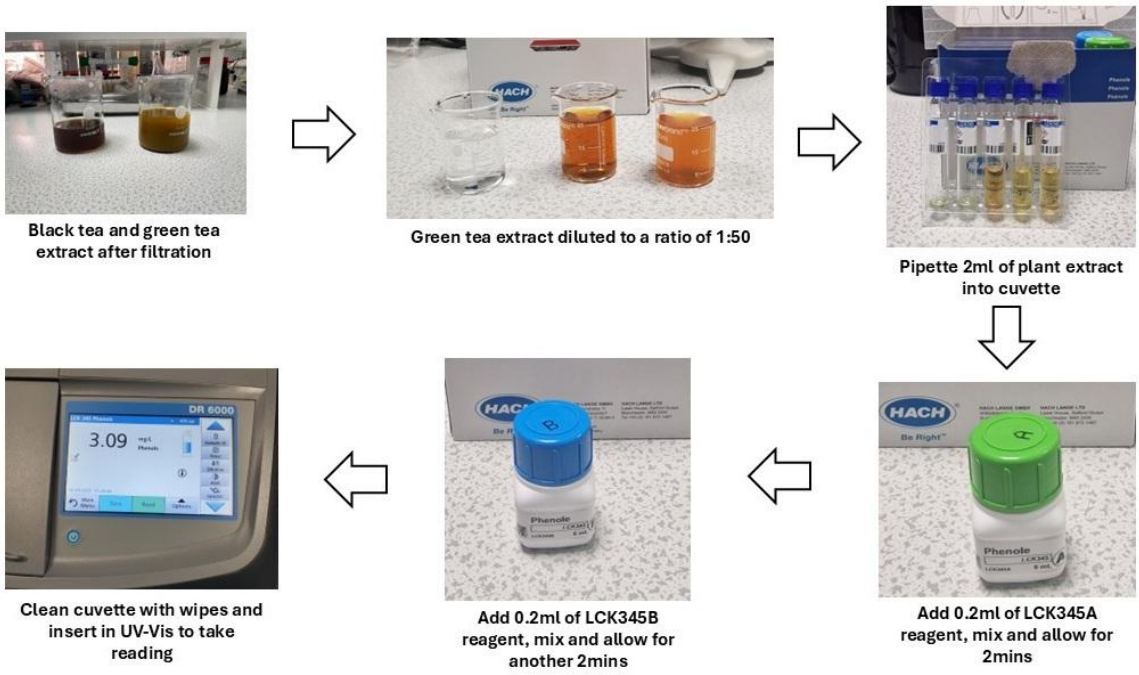

Figure 3.4 Measuring the Phenolic content of plant extracts

3.3 Synthesis of Green Iron Nanoparticles

Polyphenol extract from green tea was used as a reducing agent. Green tea was selected for the synthesis of green nZVI because results from polyphenol testing of extracts from green tea, black tea, and orange peel indicated a relatively higher phenolic concentration in green tea. Several studies have quantified and compared polyphenol contents across plant-based reductants, consistently showing

that green tea exhibits one of the highest total phenolic concentrations among common botanical sources (Machado et al., 2013, Huang et al., 2014, Shannon et al., 2017). This, coupled with its wide availability, low cost, and ease of aqueous extraction without the need for organic solvents, made green tea an ideal benchmark for evaluating environmentally benign iron nanoparticle synthesis.

0.02M solution of iron (III) chloride hexahydrate ($FeCl_3 \cdot 6H_2O$, 99%+ extra pure; Loughborough, UK), sourced from Fisher Scientific, was prepared by dissolving 5.4g of the compound in 200 mL of deionised water. The synthesis of the zero-valent iron nanoparticles was initiated by titrating 200 mL of this $FeCl_3$ solution with 100 mL of the filtered green tea extract (a ratio of 2:1). An immediate blackish colour change was observed in the mixture, indicating the formation of iron nanoparticles. The pH of the resulting mixture was acidic and needed to be stabilised by adding 2.5mL of 10M of sodium hydroxide (NaOH; Merck KGA, Sigma-Aldrich Solutions; Darmstadt, Germany) to bring it to a range of 6.5 -7.5. The mixture was run in an Eppendorf centrifuge 5804R at 10000 rpm (9950 rcf;1047.2 rad/sec) for 5 minutes. The solvent was decanted and rinsed twice with deionised water before finally rinsing with isopropanol (Propan-2-ol, 99.5% HPLC grade; Fisher Chemical). The samples were then dried in a POL-EKO Aparatura nitrogen vacuum dryer for 48 hours. This entire procedure was conducted in the environmental chemistry lab of the Department of Civil and Environmental Engineering at the University of Strathclyde, Glasgow.

The industrial nZVI used in this study was commercially sourced from Sigma-Aldrich (Merck KGaA, Darmstadt, Germany). The product is a 35–45 nm iron nano powder (≥99% purity) supplied under the Aldrich brand, widely used as a standard reference material for laboratory and environmental applications.

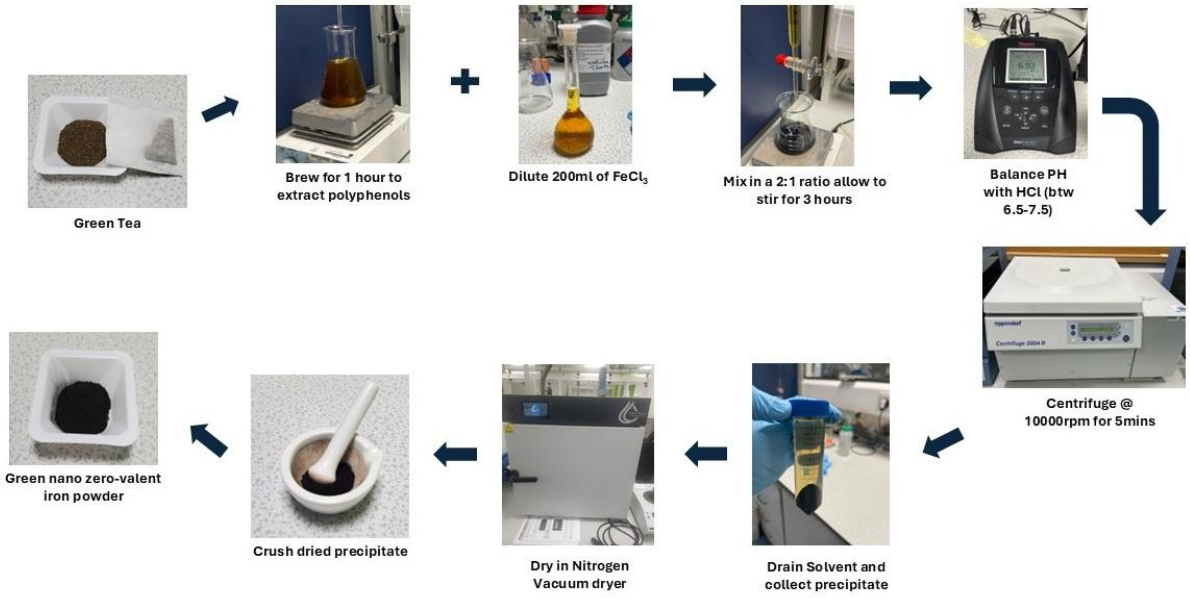

Figure 3.5 Procedure for synthesising green iron nanoparticles

3.4 Characterisation of Iron Nanoparticles

The size and morphology of the synthesised iron nanoparticles were determined using a TESCAN CLARA Ultra High-Resolution Scanning Electron Microscope (UHR-SEM) equipped with energy-dispersive X-ray spectroscopy (EDS). The UHR-SEM facilitated the measurement of the diameter, area, and perimeter of individual nanoparticles or clusters directly from the SEM images. These measurements were conducted manually, enabling precise analysis of the nanoparticle size distribution and the average particle size within the sample.

To prepare iron nanoparticles for scanning electron microscopy (SEM) analysis, a POLARON SC7640 sputter coater was used to deposit a thin conductive layer, with 95% gold and 5% palladium, onto the samples to prevent charging of the sample under the electron beam and to improve image quality.

Small amounts of industrial and green iron nanoparticle powder were placed onto a clean 12.7mm aluminium SEM stub laced with a black carbon seal; each stub was then securely mounted onto the stage inside the sputter coater chamber and fixed properly to avoid movement during the coating

process. The sputter coater chamber was sealed and evacuated to create a vacuum under a pressure of 4×10^{-2} psi to remove air and other gases that could interfere with the sputtering process.

Argon gas was then introduced into the chamber for fifteen minutes to create a plasma, and then a high voltage of 2KV at a current of 25mA was applied to the target material for two minutes. After the sputtering process, the chamber was slowly vented to return to atmospheric pressure to prevent a sudden pressure change that could damage the sample or the coating. The iron nanoparticle samples were then tagged and transferred into the SEM for analysis.

In addition to size determination, the iron nanoparticles' elemental composition was analysed using EDS integrated with the UHR-SEM. This technique provided detailed compositional data, enabling the identification of elemental constituents within the nanoparticle samples. Combining high-resolution imaging and elemental analysis through SEM-EDS ensured comprehensive characterisation of the iron nanoparticles, confirming their size distribution and chemical composition.

XRD is a powerful tool for identifying crystalline materials and determining their crystal structure. The peaks in an XRD pattern correspond to specific interplanar spacings in a crystal lattice, following Bragg's law:

$$\mathbf{n\lambda = 2d \sin\theta}$$

Where:

- **n** is the reflection order (typically 1 for XRD analysis).
- **λ** is the wavelength of the X-rays used.
- **d** is the distance between crystal planes.
- **θ** is the angle of diffraction.

X-ray diffraction patterns were collected at ambient temperature on a Malvern Panalytical Empyrean with PI Xcel3D-Medipix3 1x1 detector using Cu Kα radiation (wavelength 1.541874 Å). Data were collected in Bragg-Brentano reflection geometry 5-80 ° 2q (2theta), step size 0.0131° at the University

of Glasgow's School of Chemistry. This was used to determine the solid-state structure and crystalline nature of the green and industrial iron nanoparticles. Green and industrial nZVI results were overlapped to compare their crystalline nature. All three tests (SEM, EDS and XRD) were done in the Analytical Laboratory of the Department of Chemistry at the University of Glasgow.

3.5 Batch Test Experiments and Incubation Conditions

Batch tests were performed to assess the effects of green and industrial nZVI on hydrocarbon removal and microbial community dynamics. Each experiment was conducted in triplicate (n = 3) to ensure reproducibility.

A total of 100 mL of the prepared contaminated water stock was transferred into sterile 250 mL conical flasks. For each nZVI type (green and industrial), three dosages were tested: 0.004 mg/L, 0.01 mg/L, and 0.004 mg/L per 100 mL sample.

Two exposure durations were evaluated: 2 h and 24 h, representing early reaction kinetics and extended equilibrium effects. The 2-hour interval captured the initial oxidation–reduction processes, while the 24-hour interval provided insight into sustained removal efficiency and microbial adaptation over time.

All flasks, including the control, were incubated at room temperature (20 °C) on an orbital shaker set at 120 rpm to maintain suspension homogeneity and oxygen exchange. After each incubation period, 5–10 mL aliquots were aseptically collected for analysis of chemical oxygen demand (COD) and total petroleum hydrocarbons (TPH).

This experimental configuration provided a consistent and controlled framework to evaluate the interaction between nanoparticle formulation, dosage, and exposure time on both chemical and biological remediation outcomes.

3.6 Chemical Oxygen Demand (COD)

Measuring Chemical Oxygen Demand (COD) provides a rapid and quantitative assessment of the organic load in contaminated water, particularly with respect to petroleum hydrocarbons and their

byproducts. This measurement is critical as it is a litmus test to preview the extent to which a remediation procedure reduces the overall oxygen-demanding components. By observing how the COD values increase or decrease over time, one can evaluate the efficiency of hydrocarbon degradation under different treatment conditions, offering a straightforward indicator for comparing the relative performance of different remediation approaches.

The contaminated water sample's Chemical Oxygen Demand (COD) was measured using a HACH LCI 400 COD Test Kit, designed for measurements ranging from 0 to 1000 mg/L. A HACH Lange thermostat digester was preheated to a stable temperature of 148°C. The content of the COD test kit cuvette was homogenised by inverting the cuvette several times. 2 mL of the contaminated water sample was carefully measured and transferred into a COD cuvette using a clean pipette and tightly sealed. The cuvette was then inverted several times to ensure thorough mixing of the reagents with the water sample. The prepared cuvette was placed into the preheated thermostat digester and heated at 148°C for two hours.

After the two-hour heating period, the cuvette was carefully removed from the digester and allowed to cool down to approximately 60°C. The outside surface of the cuvette was thoroughly cleaned to remove potential contaminants or residues that could interfere with the measurements and ensure no residues affected the spectrophotometric analysis. The cuvette was then carefully inserted into the cell holder of the HACH DR6000 UV-Vis Spectrophotometer. The spectrophotometer measured the sample's absorbance at a wavelength of 605nm, which correlates to the COD value.

The same procedure was performed on all six samples, each dosed with 0.004 mg/L, 0.01 mg/L, or 0.02 mg/L of industrial nZVI and green nZVI, and this was taken after two hours of treatment and after twenty-four hours of treatment.

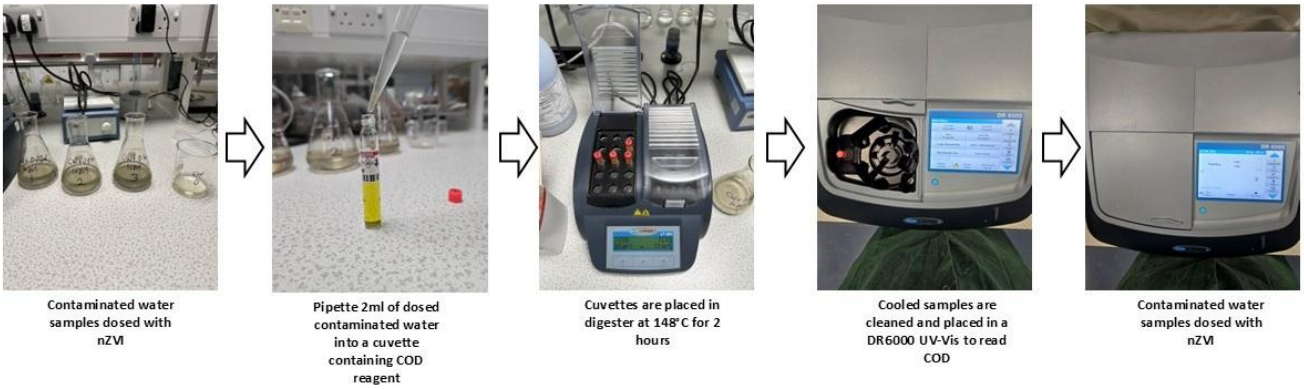

Figure 3.6 COD procedure

3.7 Quantifying Hydrocarbon Contamination

100 mL of contaminated water was dosed with 0.004 mg/L, 0.01 mg/L, and 0.02 mg/L of synthesised green nZVI from a stock solution with a concentration of 18.6 mg/L. Each dosage condition was replicated in triplicate. A separate set of triplicate contaminated water samples received the exact volume dosages, but at a 20 mg/L stock concentration of industrial nZVI. This industrial nZVI was prepared by dissolving 20 mg of commercial nZVI powder (35–45 nm particle size, 99.5% trace metal basis; Sigma-Aldrich, Steinheim, Germany) in 100 mL of deionised water, followed by thorough mixing.

The hydrocarbon traces in the water were extracted via liquid-liquid extraction as described in USEPA SW-846 Test method 3510C, using a separatory funnel, pasture pipettes, digital pipettes, and disposable culture tubes. Dichloromethane (99.8% HPLC grade from Fisher Chemicals, Loughborough, UK) was used as the extraction solvent to ensure the precise and accurate preparation of samples for Gas Chromatography-Fluorescence Ionisation Detection (GC-FID) analysis.

Using a digital pipette, 10 mL was carefully measured and transferred into a separatory funnel, and then 2 mL of high-purity dichloromethane (DCM) was added to the separatory funnel containing the water sample. The separatory funnel was then securely sealed and gently inverted multiple times to mix the contents thoroughly. During this mixing process, the funnel was vented periodically to release any built-up pressure, which is a crucial step to prevent accidents due to the volatile nature of DCM.

After thorough mixing, the funnel was allowed to stand undisturbed, enabling the separation of the aqueous and organic phases. Denser than water, DCM settled at the bottom of the funnel, carrying the extracted hydrocarbons from the water sample. The distinct separation of the two phases was evident, with the clear aqueous layer on top and the denser DCM layer below.

The next step involved carefully draining the DCM layer from the separatory funnel into a disposable culture tube. This extraction process was repeated twice to ensure maximum recovery of hydrocarbons from the water sample. The disposable culture tubes with combined DCM extracts were then drawn down using a TECHNE DB3 Dri-Block sample concentrator and air-dried with nitrogen gas to remove any residual water.

Approximately 2 mL of the final volume of the DCM extract was left in the disposable culture tubes. Out of this, 1 mL was measured using a digital pipette and transferred into a GC vial, sealed, and labelled appropriately for analysis. The GC-FID instrument was calibrated, and the DCM extract was injected into the system for analysis. The GC-FID method was optimised to detect and quantify the hydrocarbon contaminants.

Total petroleum hydrocarbon (TPH) quantity was measured using a Thermo Finnigan Focus Gas Chromatograph with Flame Ionisation Detection (GC-FID). This test was done at several stages; an untreated contaminated water sample was tested to determine the quantity of the TPH, and this was used as the baseline. TPH levels in the contaminated water were measured after introducing green nZVI at three dosages (0.004 mg/L, 0.01 mg/L, and 0.02 mg/L), following exposure periods of 2 h and 24 h. This procedure was then repeated for industrial nZVI at the same dosage levels to determine TPH content under identical time intervals.

To run the GC-FID, a standard Florida TRPH Standard Mix, UST method, TRPH Standard (Florida), 500µg/mL, purchased from Restek Thames was used. It was diluted into four standard concentrations: 10 ppm, 25 ppm, 50 ppm and 100 ppm, using dichloromethane as solvent. The GC-FID was turned on and allowed to stabilise, then the oven was set at an initial temperature of 40°C with a hold time of 3

minutes and ramped up to a maximum temperature of 300°C at the rate of 10°C/min. The Inlet temperature was then set at 250°C with a split flow of 20mL/min. The carrier gas (Helium) was set at constant flow mode at a rate of 2mL/min while the detector FID base temperature was set at 340°C.

The GC-FID was initially allowed to run with the column installed but without injecting any sample to stabilise the baseline. Two µL of the lowest concentration standard, 10ppm, was injected into the GC-FID, and the TPH compounds' peak area was recorded. This procedure was repeated for subsequent calibration standards (25 ppm, 50 ppm, and 100 ppm), recording the peak areas for each by integrating each peak using the Chromequest 5.0 software. A calibration curve was created by plotting the peak areas against the known concentrations of the TPH standards. This calibration curve was used to quantify the TPH concentration in each contaminated water sample (in mg/L) by comparing their peak areas to the calibration curve.

The resulting chromatograms capture the distribution of hydrocarbon peaks over a specific retention time window of 3 to 45 minutes. By overlaying the chromatograms for the untreated contaminated water and the three dosages (0.004 mg/L, 0.01 mg/L, and 0.02 mg/L) of green nZVI, it became possible to visually compare TPH levels and identify any shifts in peak intensity or distribution following green iron nanoparticle treatment. This superimposed image would show the TPH reduction or transformation across the different dosages of green nZVI. Similar chromatogram images were generated for the same industrial iron nanoparticle treatment regimes.

3.8 Cultivation and Identification of Hydrocarbon-Degrading Bacteria

Microbial community experiments were conducted to assess how exposure to green and industrial nZVI affected the abundance and diversity of hydrocarbon-degrading bacteria.

To prepare the microbial culture, a broth mixture of di-potassium phosphate (14 g/L), monopotassium phosphate (4 g/L), sodium citrate (1 g/L), magnesium sulphate (0.2 g/L), and ammonium sulphate (2 g/L) was prepared in one litre of deionised water. This was diluted with one litre of contaminated water sample (prepared as described in Section 3.1). This enrichment step supported the growth and

activation of indigenous microbial populations. The broth-water mixture was incubated at ~20 °C for four (4) weeks to allow the microbial community to stabilise and multiply prior to nanoparticle dosing.

Following enrichment, the culture was transferred into 100 mL sterile conical flasks, each serving as an individual batch test unit. The nZVI dosages mirrored those used in the oxidation experiments, with 0.004 mg/L, 0.01 mg/L, and 0.02 mg/L of either green-synthesised nZVI or industrial nZVI added to separate flasks. In parallel, a sample containing the same broth-contaminated water mixture but without nZVI was incubated under identical conditions and served as the experimental control.

To understand the microbial composition, the DNA of the community were extracted. An MP Fast DNA Spin Kit (MP Biomedicals, LLC, Ohio, USA) was used to isolate and extract DNA from each sample. The process began with the filtration of the water sample through a pump, ensuring that all particulate matter was trapped on filter paper. The filter paper was carefully handled using a sterilised pair of tweezers. The tweezers were sterilised by immersing them in isopropanol and then heating them. Once sterilised, the tweezers were used to transfer the filter paper with the trapped sieves from the funnel into a lysing matrix tube. 125µL of MT Buffer was pipetted to begin the lysing process. Following this, 980µL of sodium phosphate was added to the tube, serving as a pH stabiliser to maintain optimal conditions for DNA extraction. The contents of the lysing matrix tubes were then subjected to vigorous shaking in an MP-24 FastPrep sample preparation machine at a speed of 6 m/s for 40 seconds to ensure thorough mixing and cell lysis. The lysing matrix tubes were transferred to a centrifuge and spun for 1 minute at 10rcf. This step facilitated the separation of cellular debris from the liquid precipitate, which was carefully drained into clean 2mL tubes. To this precipitate, 250µL of Protein Precipitate Solution (PPS) was added, and the mixture was centrifuged again at 10rcf for 3 minutes to further clarify the solution. The clarified solution was then transferred into 5mL centrifuge tubes, and 1mL of Binding Matrix Solution (clay) was added. This mixture was gently inverted 20 times to ensure even mixing and then left to settle for 3 minutes, allowing the DNA to bind to the clay matrix. Excess liquid was drained off, leaving the DNA-bound precipitate at the bottom of the tube.

The residue, now containing the DNA, was vigorously shaken and transferred into spin modules. These modules were centrifuged at 10rcf for 1 minute to purify the DNA further. The liquid at the bottom of the spin modules was discarded, and 500µL of SEWS-M solution was added to wash away any remaining organic contaminants. The spin modules were centrifuged again at 10rcf for 1 minute to ensure thorough washing. After draining the SEWS-M solution, the spin modules were centrifuged once more at 10rcf for 1 minute to dry off any residual SEWS-M solution. The DNA-bound precipitate was then transferred into new 2mL centrifuge tubes, and 100µL of WES (deionised water) was added. This mixture was shaken and centrifuged at 8rcf for 1 minute to elute the DNA.

Finally, the precipitate was discarded, and the solvent, which now contained the purified DNA, was stored in a freezer at -80°C, ensuring its preservation for subsequent analysis. This procedure was repeated on all the samples after twenty-four hours.

Qualitative DNA analysis was carried out on each sample using a Biotek Gen 5 before sending it over for analysis.

The procedure began with thoroughly cleaning the sample tray using ethanol and wipes to ensure that any residual contaminants were removed. To establish a baseline for the analysis, 2µL of DES (deionised, enzyme-free, sterile) water was carefully pipetted onto the first four spots of the sample tray. These spots served as blanks. This would serve as a reference point against which the samples would be compared. Once the blanks were prepared, the tray was placed into the Biotek Gen 5 machine, and an initial analysis was run on the blanks. After the blank analysis, the sample tray was removed and wiped again with ethanol. Next, 2 µL of each DNA sample, collected in 2 mL vials after extraction using the Fast Prep Kit, was pipetted onto the respective spots on the sample tray. Each sample was handled carefully to avoid cross-contamination and ensure an accurate representation of the extracted DNA.

The prepared sample tray was placed back into the Biotek Gen 5 machine. Using the associated computer software, the prompt was given to run the tests. The Biotek Gen 5 machine conducted an

analysis of each sample, measuring optical densities at OD260, OD280, and OD320, indicating the DNA's concentration and quality. DNA quality OD260/280 should be >1.8.

For meta-taxonomic analyses, 100 µL of each sample was sent to NU'Omics (Northumbria University, Newcastle upon Tyne, UK). There, targeted amplicons of bacteria (16S-rRNA-V4 region) and fungi (internal transcribed spacer region of ribosomal rRNA, ITS-2) were used for DNA sequencing on an Illumina MiSeq system. NU'Omics (Northumbria University, Newcastle upon Tyne, UK) did the PCR targeting, library construction, instrument operation, and bioinformatics (as highlighted below).

Sequences were processed using the Quantitative Insights into Microbial Ecology (QIIME) pipeline as described by Caporaso et al. (2010). Briefly, operational taxonomic units (OTUs) were identified at 97% similarity (species-level) using the UCLUST algorithm. PyNAST was then employed to align the sequences (Caporaso et al., 2012), while potential chimaeras were detected and removed with ChimeraSlayer as detailed by Haas et al. (2011). Taxonomy was assigned against the Green genes reference database. The resulting microbial taxa data were subsequently exported from QIIME into Microsoft Excel for further quantitative analysis.

3.9 Comparative Analysis Procedures

The analysis began with data preparation. The data was first loaded from an exported Excel file using the *pandas* library. To ensure only relevant data was analysed, numeric columns were selected, and any missing values were filled with zeros to maintain completeness. The data was then standardised using the Standard Scaler function, which transformed all variables to have a mean of 0 and a standard deviation of 1. This step ensured that the variables were on the same scale, creating a standardised matrix suitable for comparative analysis.

3.9.1 Taxonomic Composition Analysis Procedure

The analysis began with phylum-level analysis, where phylum information was extracted from taxonomic strings using regular expressions (regex) to identify patterns such as 'p__'. Relative abundances were calculated by normalising each column to the total abundance per sample. The data

were then aggregated at the Phylum level by summing the relative abundances for each Phylum across all samples. Mean relative abundances were calculated for each phylum, and the top 10 most abundant phyla were visualised using a bar plot, providing a clear overview of the dominant phyla in the dataset.

Following this, an order-level analysis was performed. Order information was extracted from the taxonomic strings using regex to identify patterns such as 'o__'. The data was aggregated at the order level by summing the relative abundances for each order. Mean relative abundances were calculated for all orders across samples, and the top 10 most abundant orders were visualised using a bar plot, allowing for a detailed examination of the composition at the order level.

3.9.2 Statistical Analysis Procedure

The procedure involved cleaning and preprocessing the dataset, extracting relevant variables (e.g., concentration, time, treatment), and performing statistical tests (t-tests and corresponding c-values) to compare microbial populations across treatments.

The dataset was loaded from an Excel file, and the correct headers were set by identifying the row containing the actual column names. Missing or irrelevant rows were removed to ensure the dataset was clean and usable. Key variables such as "Concentration," "Time," and "Treatment" were extracted from the "DESCRIPTION" column using regular expressions. Concentration was extracted as the numeric value followed by "mg/L," while Time was extracted as the numeric value followed by "hrs." Treatment was identified as either "InZVI," "GnZVI," or "Control" based on the description.

A Sample T-test was carried out to compare the microbial population of each treatment (InZVI and GnZVI) against the control group. The null hypothesis assumed no difference between the treatment and control populations. The test statistic and p-value were calculated to determine statistical significance.

An independent T-test was also done to compare the microbial populations between InZVI and GnZVI treatments. The two groups were assumed to be independent, and differences in their means were tested.

The t-test was selected for the statistical analysis because the experimental design required a direct comparison of differences in microbial population means between two defined groups: (i) each nZVI treatment versus its control, and (ii) green versus industrial nZVI at corresponding doses and time points. The t-test is considered appropriate for this purpose because it is specifically designed to evaluate whether the means of two independent datasets are statistically different, while accounting for variability within each group. This test was also suitable given the sample size (triplicate measurements, n = 3 per condition), where multi-parametric methods such as ANOVA would still require post-analytical, pairwise comparisons and introduce unnecessary complexity. The assumptions of the t-test: continuous data, approximately normal distribution, and similar variance between groups were satisfied by the OTUs and chemical measurement data, making it an appropriate model for detecting meaningful differences in treatment effects.

By applying both independent t-tests (InZVI vs. GnZVI) and paired t-tests (treatments vs. control) where relevant, the analysis provided a statistically robust means of determining whether observed changes in microbial abundance or water quality indicators (COD and TPH) were significant, rather than due to random variation. This aligns with common practice in environmental microbiology and remediation studies, where the t-test is widely used for assessing treatment impacts under controlled laboratory conditions (Guetterman, 2019).

A series of bar charts was generated using data extracted from QIIME2 View, displaying the top 10 microbial taxa in each sample and allowing side-by-side comparisons of green and industrial nZVI formulations at varying dosages and two exposure durations (2 h and 24 h). Each frame was structured to match corresponding green and industrial treatments, enabling direct visual comparison of microbial community responses. A comprehensive analysis of the extracted data was conducted to

evaluate how different formulations, concentrations, and exposure times influenced microbial population dynamics, highlighting notable shifts in taxonomic structure and abundance across the treatment conditions.

3.10 Practical Observations and Experimental Challenges

During the preliminary experimental work, several practical observations were made that informed the final procedures adopted in this study. Firstly, the addition of nutrient broth substantially affected the liquid–liquid extraction stage used for TPH quantification. When dichloromethane (DCM) was added to broth-containing samples, no clear phase separation occurred, preventing efficient decantation. Attempts by Letinski and Prince (2017) and Patowary et al. (2017) revealed that the broth introduces proteins, polysaccharides, and other amphiphilic components that promote emulsification and reduce interfacial tension between the aqueous and organic phases. This prevents the formation of two distinct layers, making phase separation and decantation difficult.

For this reason, two parallel sets of contaminated water samples were used: one without broth for TPH and COD analysis, and another with broth for microbial community experiments that required cell growth support.

Secondly, the performance of the green-synthesized nZVI was found to depend strongly on its physical state. The slurry form of the freshly synthesized nanoparticles produced measurable reductions in TPH. However, after drying and crushing to a powder, the material showed little to no reactivity. This reduction in performance is likely due to surface oxidation to iron oxides during air exposure, which is known to decrease nZVI's reductive capacity (Garg et al., 2024, Ghaffarzadeh et al., 2024). The drying and crushing step was therefore only applied to obtain powder for characterization and not for remediation experiments.

Finally, challenges were encountered during particle size analysis. Dynamic light scattering (Zeta Sizer) measurements required the nanoparticles to be re-suspended in water. However, the particles readily aggregated after centrifugation, resulting in artificially high hydrodynamic diameters despite repeated

sonication. A similar challenge was experienced by Cappadona (2021) during his research. Due to this limitation, scanning electron microscopy (SEM) was used instead to obtain reliable size and morphological information.

These observations highlight the importance of maintaining nZVI in a minimally oxidized, dispersed state for effective reactivity, and they informed the methodological decisions used in subsequent experiments.

Chapter 4 Results

4.1 Overview of Experimental Outcomes

This chapter presents the key findings derived from the experimental procedures outlined in the preceding Methodology chapter. First, it addresses the phenolic content of the plant extracts used to synthesise nanoscale zero-valent iron (nZVI), establishing the significance of plant-derived reducing agents for particle formation and stability. This is followed by results from a series of characterisation tests, specifically, Scanning Electron Microscopy (SEM), Energy Dispersive X-ray Spectroscopy (EDS), and X-ray Diffraction (XRD), which will collectively be used to confirm and compare the morphology, elemental composition, and crystallographic properties of both green and industrial nZVI formulations.

Next, the chapter examines the remediation efficacy of these nanoparticles through chemical oxygen demand (COD) and gas Chromatography-Flame Ionisation Detector (GC-FID) analyses. The resulting COD figures, chromatograms and volumetric changes in TPH levels illustrate how treatment dosages affect total petroleum hydrocarbon (TPH) degradation. A complementary microbial analysis then explores shifts in bacterial community composition as a function of nanoparticle application. Taxonomic composition is evaluated at multiple levels: Phylum, class, and order, thereby offering a detailed look at how different microbial groups respond to varying treatment conditions.

Subsequently, an overview of statistical methods employed to interpret these data is provided, encompassing both standard quantitative approaches and more specialised community analysis techniques. By integrating physicochemical measurements with microbial ecology assessments, the chapter offers a comprehensive account of how green and industrial nZVI perform under controlled conditions and how these findings may guide future water remediation strategies.

Finally, this chapter concludes by synthesising the collective findings from the experimental work and illustrating how they fulfil the original research objectives. The characterisation results from SEM, EDS, and XRD reveal key similarities and differences between green nZVI and its industrial counterpart, thus

addressing the goal of developing and understanding a green-synthesized alternative. Insights into remediation performance, based on reductions in hydrocarbon concentration and varying treatment regimens, directly confirm the feasibility of using green nZVI while highlighting the advantages and limitations of both nanoparticle types. The DNA extractions and subsequent microbial community analyses illuminate changes in the abundance and activity of hydrocarbon-degrading bacteria, helping demonstrate the ecological implications and potential synergy of combined chemical and biological remediation strategies. Lastly, integrating these findings will lay the groundwork for proposing an effective and sustainable remediation approach, with particular emphasis on practical applications.

4.2 Phenolic Content and Preliminary Observations (pH and Conductivity)

Initial measurements of pH and conductivity were performed on the contaminated water using a Thermo Scientific Orion Star A215 pH/Conductivity meter under controlled conditions (20 °C). The pH registered at **7.28**, indicating a near-neutral environment, whereas the conductivity reached **9.721 mS/cm**, suggesting a moderately elevated level of dissolved ions in the sample. These baseline readings will help contextualise the subsequent nanoparticle treatments, as pH and ionic strength can affect chemical reactions and the stability of zero-valent iron nanoparticles (Wang et al., 2020).

Alongside these water quality assessments, a polyphenol test was conducted on extracts from green tea, black tea, and dried orange peel using a HACH Phenol Cuvette Test Kit. The results depicted in a bar chart (Figure 4.1) highlight the differences in phenolic concentrations among the three extracts, expressed in milligrams per litre (mg/L). By identifying which plant source offers the highest phenolic content, it becomes possible to predict which extract may produce the most reactive and stable nanoparticles (Iravani, 2011, Ahmed et al., 2016).

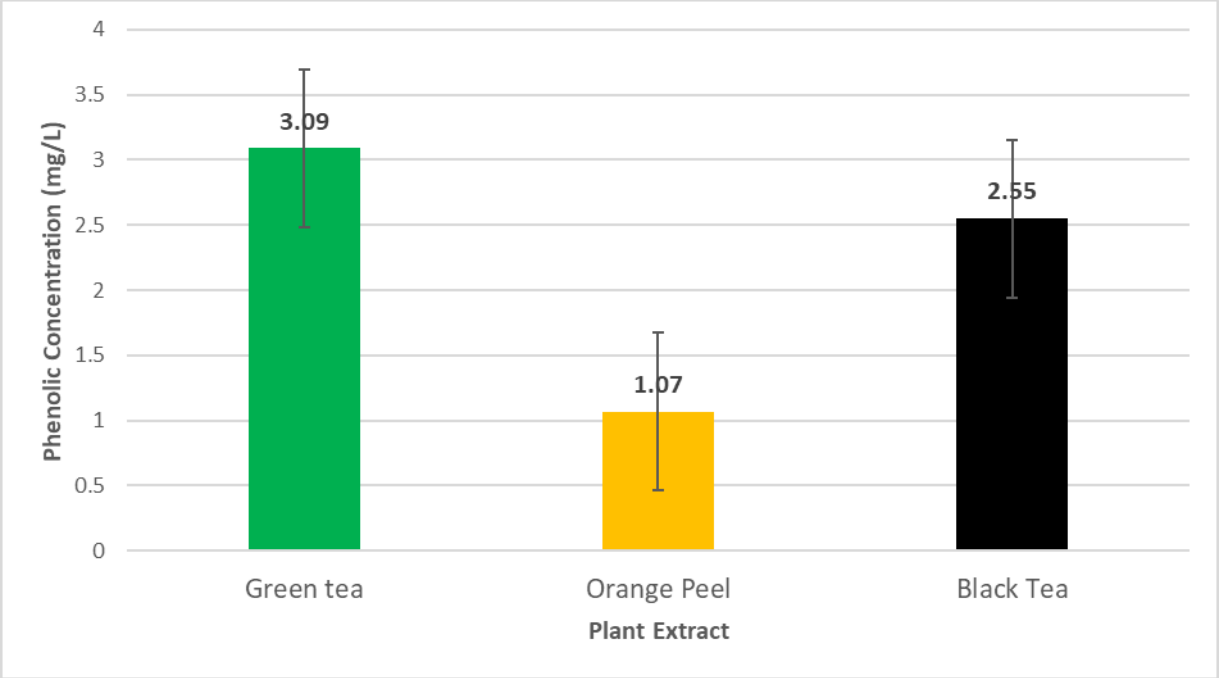

Figure 4.1 Bar chart comparing the phenolic concentration of green tea, orange peel and black tea extracts, as determined using the HACH Phenol Test. Error bars represent instrument measurement variability.

The information presented in the bar chart indicates that green tea extract possesses the highest phenolic concentration (3.09 mg/L), followed by black tea (2.55 mg/L) and orange peel (1.07 mg/L).

The profiles confirm that green tea is among the leaves with the highest phenolic content, making it the perfect candidate for this research and justifying its use as a source of polyphenols. It also aligns with studies reported by Machado et al. (2013) and Li et al. (2013), both of which highlight the strong correlation between phenolic compounds in various plants and their antioxidant properties.

A higher phenolic content is typically associated with stronger reducing and stabilising capacities during nanoparticle synthesis, as polyphenols can donate electrons to reduce ferric ions (Fe^{3+}) to zerovalent iron (Fe^{o}) and subsequently stabilise the nanoparticles (Devatha et al., 2016, Fazlzadeh et al., 2017). Consequently, green tea, which is rich in catechins and other phenolics, tends to promote a more efficient and rapid formation of nZVI, often resulting in uniformly sized particles with high reactivity (Borja et al., 2015, Gupta et al., 2023b).

By contrast, the lower phenolic content in orange peel (1.07 mg/L) results in a more modest reducing capacity, potentially leading to slower particle formation or less stable nanoparticles. Black tea, with an intermediate phenolic concentration (2.55 mg/L), produces nZVI with moderate stability and rate of synthesis (Singh et al., 2018a). Although all three plant extracts can be used for green synthesis, the higher phenolic content of green tea typically provides an advantage in terms of nanoparticle quality and yield, which will enhance remediation performance in subsequent stages of application.

4.3 Characterisation of Iron nanoparticles

4.3.1 X-ray Diffraction Results

The X-ray diffraction analysis was performed at ambient temperature on a Malvern Panalytical Empyrean with a PI Xcel 3D-Medipix 3 (1x1) detector using Cu Kα radiation (wavelength 1.541874 Å). Both industrial and green iron nanoparticle patterns were superimposed to compare their crystalline nature.

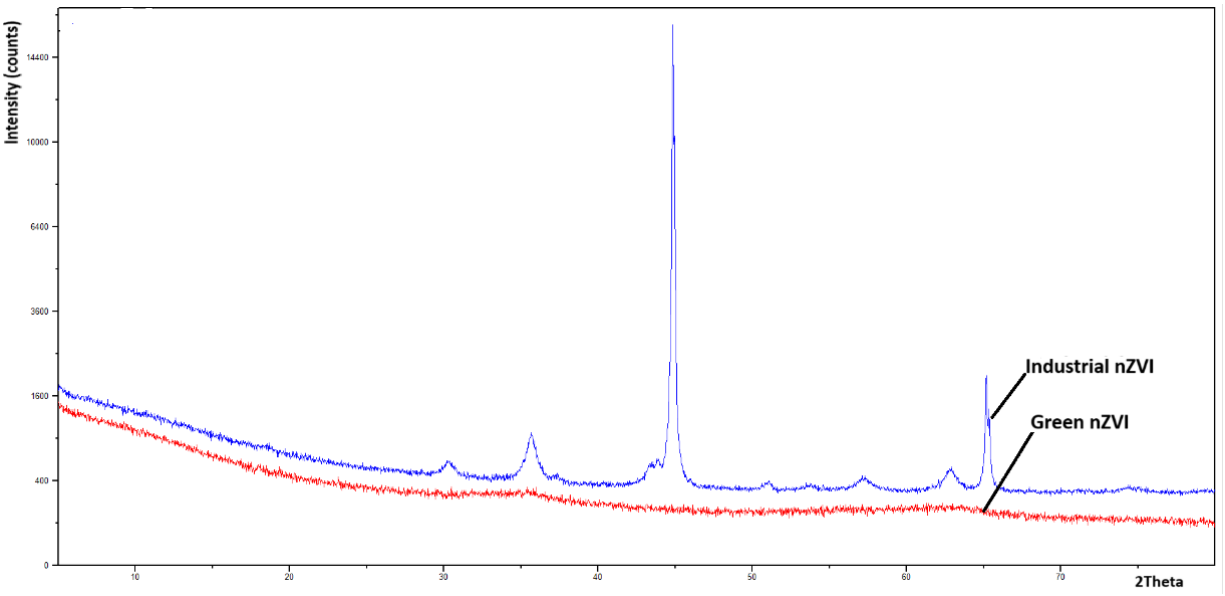

Figure 4.2 XRD image comparing the crystallinity of Industrial nZVI (blue) and Green nZVI (red)

The XRD image shows two diffraction patterns:

- Blue Line: Represents the XRD pattern for industrial iron nanoparticles (nZVI).

- Red Line: Represents the XRD pattern for green-synthesized iron nanoparticles (green nZVI).

The XRD patterns for industrial nZVI (blue) and green nZVI (red) both exhibit distinct peaks corresponding to zerovalent iron, most prominently around $2\theta \approx 44.5°$ and 65°, which align with the (110) and (200) planes of α-Fe. In the industrial nZVI, these peaks are relatively sharp and intense, suggesting a higher degree of crystallinity and larger crystallite sizes. By contrast, the green nZVI displays broader, lower-intensity reflections at similar positions, indicative of smaller crystallites and a partially amorphous phase. This increased broadening can often be quantified using the Scherrer equation, where peak width (measured at half-maximum intensity) inversely relates to average crystallite size:

$$\mathbf{D} = \frac{k\lambda}{\beta \cos\theta}$$

where:

- **D** is the mean crystallite size (nm),
- ***k*** is the shape factor (commonly 0.9 for spherical crystallites),
- **λ** is the wavelength of the X-ray source (e.g., 1.54 Å for Cu Kα),
- **β** is the full width at half maximum (FWHM) of the diffraction peak (in radians),
- **θ** is the Bragg angle of the peak.

Broader peaks (larger β) correspond to smaller values of **D**, which explains why the green nZVI's broader peaks suggest a smaller crystallite size relative to the industrial sample

In some nZVI samples, minor reflections at approximately $2\theta \approx 30–35°$ or 57–63° can arise from iron oxides like magnetite, formed through surface oxidation. While it is not entirely clear from these particular spectra whether such oxide peaks are present, any subtle shoulders or small additional peaks in that range could indicate partial conversion of Fe^0 to iron oxide phases. Overall, the industrial nZVI's sharper peaks suggest larger, more extensive crystallinity and fewer oxide phases. In contrast, the broader peaks of the green nZVI indicate a finer, smaller reduced crystallite size and possibly

higher oxide or amorphous content, consistent with plant-derived capping agents and milder synthesis conditions.

4.3.2 Energy Dispersive X-ray Spectroscopy (EDS) Profiles

Based on the EDS spectrum obtained from three different clusters on the SEM, an analysis of the elemental composition of both the green-synthesised and industrial iron nanoparticles (Sigma-Aldrich) reveals that both types of iron nanoparticles primarily comprise iron (Fe), with a minor presence of oxygen and carbon. Figure 4.4 compares the EDS spectrum of industrial and green nZVI.

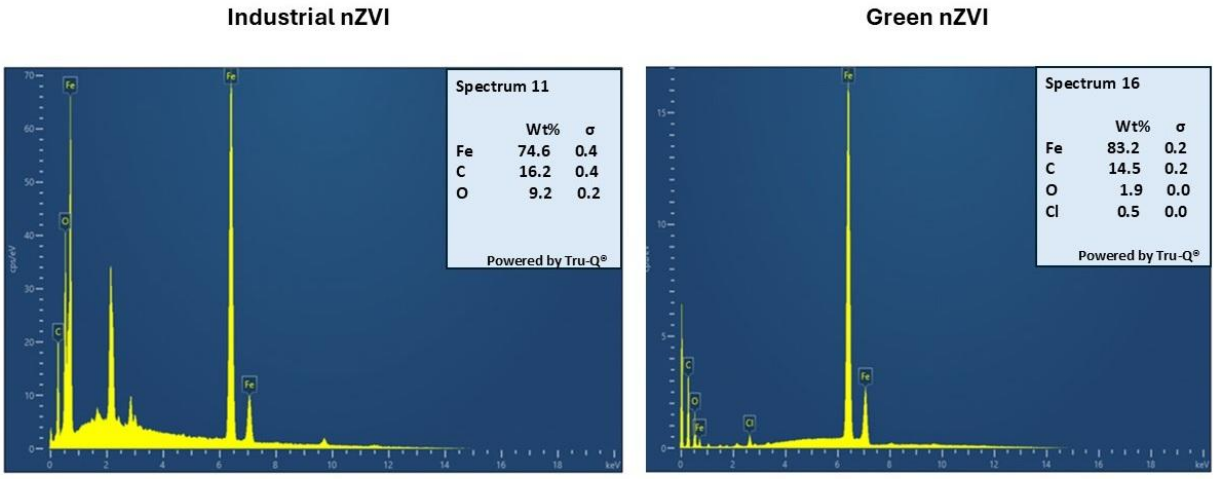

Figure 4.3 Image comparing EDS profiles of industrial nZVI and green nZVI

The elemental composition for the industrial nZVI sample is dominated by iron (Fe) at about 74.6 wt%, accompanied by a notable fraction of carbon (C) with 16.2 wt% and oxygen (O) with 9.2 wt%. The high iron content confirms that iron is the primary component of the nanoparticles. The carbon signal may come from residual organic binders used in the manufacturing process or adventitious carbon that often accumulates on the particle surface. Meanwhile, the oxygen peak could indicate a partially oxidised layer, which could be a result of constant exposure or the presence of iron oxides and hydroxides on the particle surface. This is not uncommon with iron nanoparticles, as they tend to oxidise when exposed to air. Unlike green-synthesized nZVI, which typically shows a more pronounced organic signature from plant extracts, the carbon and oxygen in the Industrial nZVI are more likely

byproducts of manufacturing conditions, storage, or surface passivation. Overall, the data confirm that these industrial particles maintain a predominantly iron-based core, though a degree of oxidation and carbon contamination is present.

On the other hand, the spectrum for the green nZVI shows that iron (Fe) is also the dominant element, at approximately 84 wt%, indicating that the synthesised material is primarily iron based. A significant carbon (C) signal is also present (11 wt%), consistent with an organic capping layer derived from the polyphenol-rich green tea extract. The minor oxygen (O) peak of 2 wt% likely arises from partial oxidation or the inherent oxygen content of the polyphenolic compounds, while the small chlorine (Cl) peak (0.5 wt%) is expected to be residual chloride carried over from the $FeCl_3 \cdot 6H_2O$ precursor.

Overall, the high Fe content confirms that iron is the core component of the nanoparticles, and the presence of carbon and oxygen supports the idea that polyphenol molecules have attached to (and partly protected) the iron surface during synthesis. This composition aligns well with what is expected for green synthesised nZVI, where plant-derived reducing agents and capping layers help create and stabilise the zerovalent iron core.

4.3.3 Scanning Electron Microscopy (SEM) Analysis

SEM images were captured for both industrial and green nZVI at a magnification of 200nm, allowing for a clear visualisation of the particle shape, size, and agglomeration patterns, as illustrated in Figure 4.5.

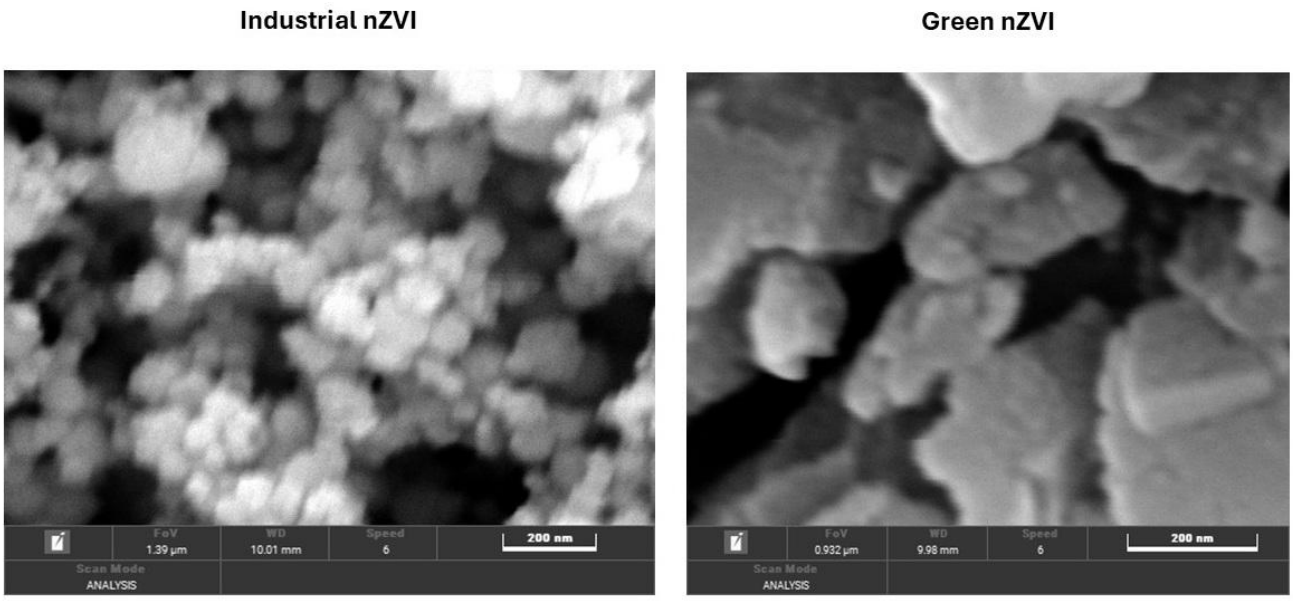

Figure 4.4 Comparing SEM images of industrial nZVI and green nZVI

In the industrial nZVI image (on the left), the particles appear relatively uniform and tightly aggregated, aligning well with the reported 30–45 nm size range. This tighter particle size distribution reflects the controlled synthesis conditions and standardised production methods typical of industrial manufacturing (Shegokar and Nakach, 2020). While the iron's strong magnetic interactions naturally cause some clustering, these aggregates generally exhibit spherical-like morphologies and more consistent dimensions.

By contrast, the green nZVI (on the right) shows particles in the 50–90 nm range and a somewhat more irregular shape. From the XRD data, one might expect smaller crystallite sizes for the green nZVI due to the noticeably broader diffraction peaks, which often indicate smaller primary particles. However, when viewed under SEM, the synthesis process, including centrifugation, drying, and manual grinding, ultimately results in larger visible aggregates. The natural polyphenols involved in reducing and capping the iron may form heterogeneous layers, promoting uneven nucleation and partial passivation on the particle surface. Consequently, the final dried, hand-ground material does not achieve the perfectly fine or uniformly shaped particles that the XRD peak broadening might suggest. Instead, the biomolecular coatings and manual preparation steps lead to more variable cluster sizes and morphologies, even though the underlying crystallites themselves are relatively small. Overall,

these differences highlight how practical handling and natural variability in plant-derived compounds can yield larger, more irregular aggregates in green nZVI, despite the smaller crystallite sizes implied by XRD analysis.

4.4 TPH Removal Efficiency

This section examines the efficiency of total petroleum hydrocarbon (TPH) removal using both industrial and green nanoscale zero-valent iron (nZVI). Prior to treatment, we characterised the contaminated water by measuring the baseline levels of Chemical Oxygen Demand (COD) and TPH, which contextualises the degree of hydrocarbon pollution. COD gives a quick insight into the organic load, reflecting the total oxidisable substances present in the sample. In parallel, gas chromatography-flame ionisation detection (GC-FID) allows for more precise quantification of individual hydrocarbon components. Combining these two methods enables validation and comparison of the effectiveness of nZVI-based treatments: COD measurements show reductions in organic content, while GC-FID chromatograms offer detailed insights into the specific hydrocarbons that are most efficiently degraded. The baseline COD of the contaminated water ("controls", without any nZVI treatment) measured 179 mg/L at 2 h and 172 mg/L at 24 h, indicating minimal natural reduction over this timeframe. The initial baseline TPH level of the same "control" contaminated water sample was an average of 58.13 mg/L, taken from three samples.

4.4.1 Chemical Oxygen Demand (COD) Measurements

Table 4.1 presents a summary of the results from COD tests conducted on contaminated water samples. The tests utilised both industrial and green nZVI with three different dosages and were assessed 2 h and 24 h after dosing below:

Table 4.1 Summary of results from COD tests conducted on treated contaminated water samples

SAMPLES	2h					24h				
Industrial nZVI (20 mg/L)	**1st Test**	**2nd Test**	**3rd Test**	**Avg COD reading (mg/L)**	**Std. Dev.**	**1st Test**	**2nd Test**	**3rd Test**	**Avg COD reading (mg/L)**	**Std. Dev.**
CW + 0.02ml of nZVI	106	89	141	**112.3**	**26.51**	69	72	61	**67.1**	**5.69**
CW + 0.05ml of nZVI	208	176	258	**214**	**41.33**	44	10	13	**21.6**	**18.82**
CW + 0.1ml of nZVI	37	81	59	**59.1**	**22.00**	13	24	22	**19.8**	**5.86**
Green nZVI (18.6 mg/L)										
CW + 0.02ml of nZVI	129	154	124	**136.4**	**16.07**	91	97	75	**88.2**	**11.37**
CW + 0.05ml of nZVI	161	142	131	**144.9**	**15.18**	61	53	54	**56**	**4.36**
CW + 0.1ml of nZVI	92	88	92	**90.5**	**2.31**	36	29	30	**31.7**	**3.79**
Contaminated Water (CW)	164	177	195	**179**	**15.57**	181	149	187	**172**	**20.43**

The results show that the COD values in samples treated with industrial and green nanoscale zero-valent iron (nZVI) declined, demonstrating that both iron-mediated processes accelerate the breakdown or transformation of organic contaminants. Generally, higher dosages yielded more COD reductions, highlighting a dose-response relationship where more nZVI promotes deeper remediation. For instance, the highest dosage (0.02 mg/L) of industrial nZVI reduced COD to approximately 59.1 mg/L at 2 h and 19.8 mg/L at 24 h, which is substantially lower than the untreated control. A similar trend emerged with green nZVI, although it did not consistently achieve as pronounced a COD drop as the industrial counterpart.

Notably, some measurements, such as those at lower nZVI dosages, indicate moderate reductions initially, followed by sharper declines after extended contact times (i.e. from 2 h to 24 h). This suggests that the reaction may proceed gradually, potentially involving multiple steps such as adsorption, partial reduction/oxidation of hydrocarbons, and eventual transformation into lower-oxygen-demand compounds. Additionally, the slight discrepancy in the COD trends for industrial versus green nZVI implies that differences in particle composition, surface chemistry, and agglomeration can affect removal efficiency. Nevertheless, both types of iron nanoparticles consistently outperform the untreated control, reinforcing the viability of nZVI-based strategies for mitigating hydrocarbon contamination.

4.4.2 GC-FID Results

In this section, the data generated from the GC-FID analysis are presented through both graphical overlays of chromatograms and a supporting table of calculated TPH reductions. First, the original (baseline) TPH peaks from the contaminated water are superimposed with the peaks observed after treatment with three different nZVI dosages of 0.004 mg/L, 0.01 mg/L, and 0.02 mg/L for green and industrial nZVI providing a direct visual comparison of how each dosage reduces the hydrocarbon peaks. The table further quantifies these reductions by calculating changes in TPH volumes before and after treatment. A separate set of chromatograms then contrasts the baseline sample with parallel treatments using green versus industrial nZVI at the same dosage, allowing for a side-by-side comparison of their relative efficiencies. Together, these graphical and tabular presentations illustrate the extent of TPH removal under varying conditions, highlighting differences in performance and enabling a clear assessment of each nZVI formulation's treatment capabilities.

From the baseline chromatograph, most of the peaks appeared in the mid-to-late teens through the upper 20s or early 30s (retention times, in minutes), which aligns with diesel-range hydrocarbons (approximately C_{10}–C_{28}). This retention time window suggests that the contaminant is predominantly a diesel or middle-distillate fraction of total petroleum hydrocarbons (TPH), not a lighter gasoline-range or heavier oil-range compound.

Figure 4.6 shows the baseline TPH peaks of the contaminated water superimposed with the other chromatograph peaks from contaminated water samples that were treated with three different dosages: 0.004mg/L, 0.01mg/L and 0.02mg/L and tested after 24 h

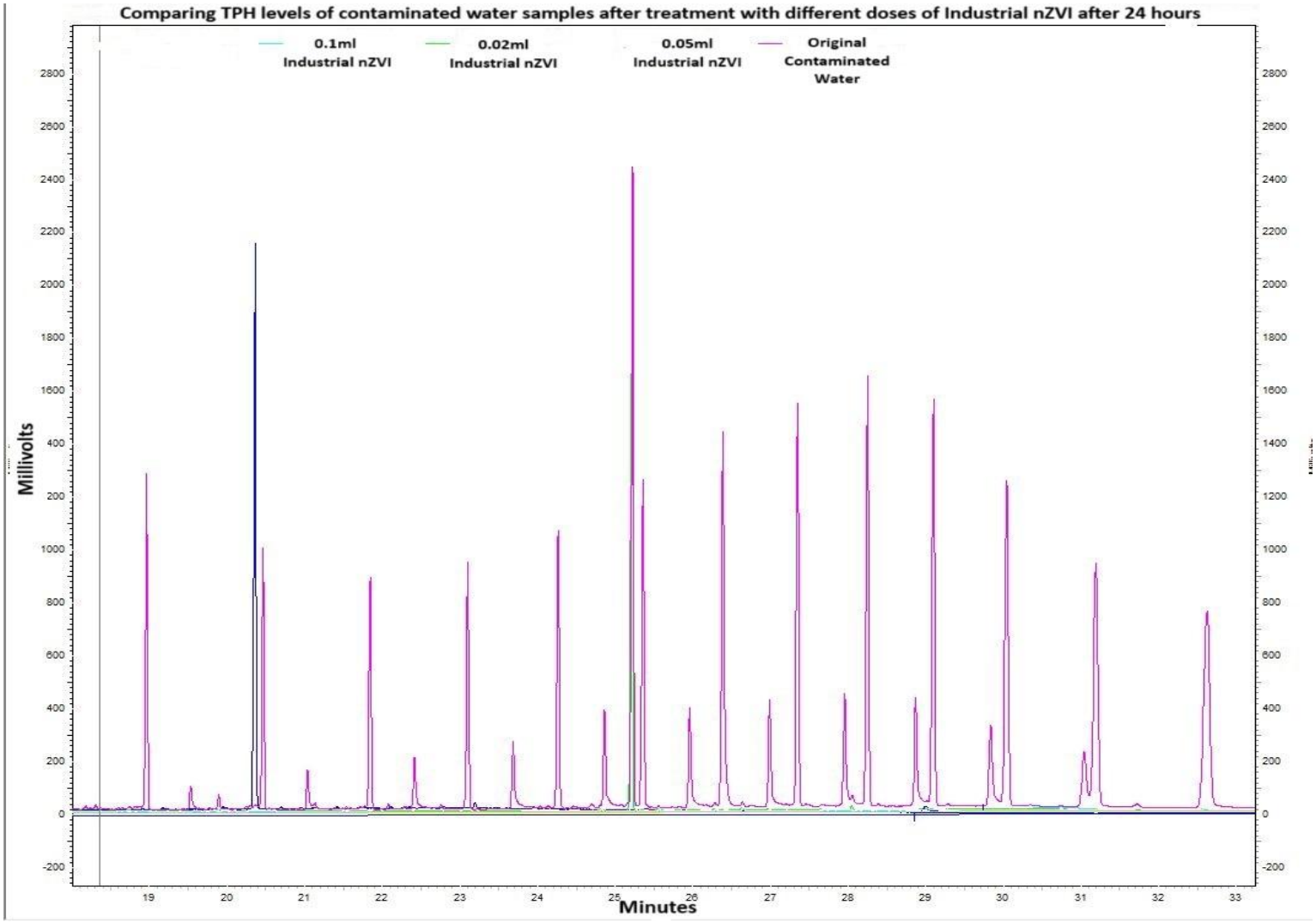

Figure 4.5 GC-FID chromatogram comparing the TPH levels of contaminated water sample treated with three different dosages of industrial nZVI after 24h

When examining the GC-FID chromatograms, the purple trace representing the baseline (untreated) contaminated water displays numerous high-intensity peaks in the 19 to 33-minute range, corresponding to diesel-range TPH. In this study, the baseline refers to the initial TPH concentration measured at time zero (t = 0h) before any nZVI treatment was applied. In contrast, the three coloured traces for samples treated with 0.004 mg/L (green), 0.01 mg/L (pink), and 0.02 mg/L (grey) of industrial nZVI show reductions or near-total disappearance of these peaks after 24 h of exposure. This noticeable decrease in peak intensity indicates substantial degradation or transformation of the hydrocarbons, demonstrating the overall effectiveness of the industrial nZVI treatment in reducing TPH concentrations. Furthermore, a dose-response relationship seems apparent, with higher dosages (0.02 mg/L) leading to more pronounced peak suppression. These findings highlight the capacity of industrial nZVI to remediate diesel-range petroleum hydrocarbons within a relatively short timeframe and provide compelling visual confirmation of the technology's efficiency in treating contaminated water.

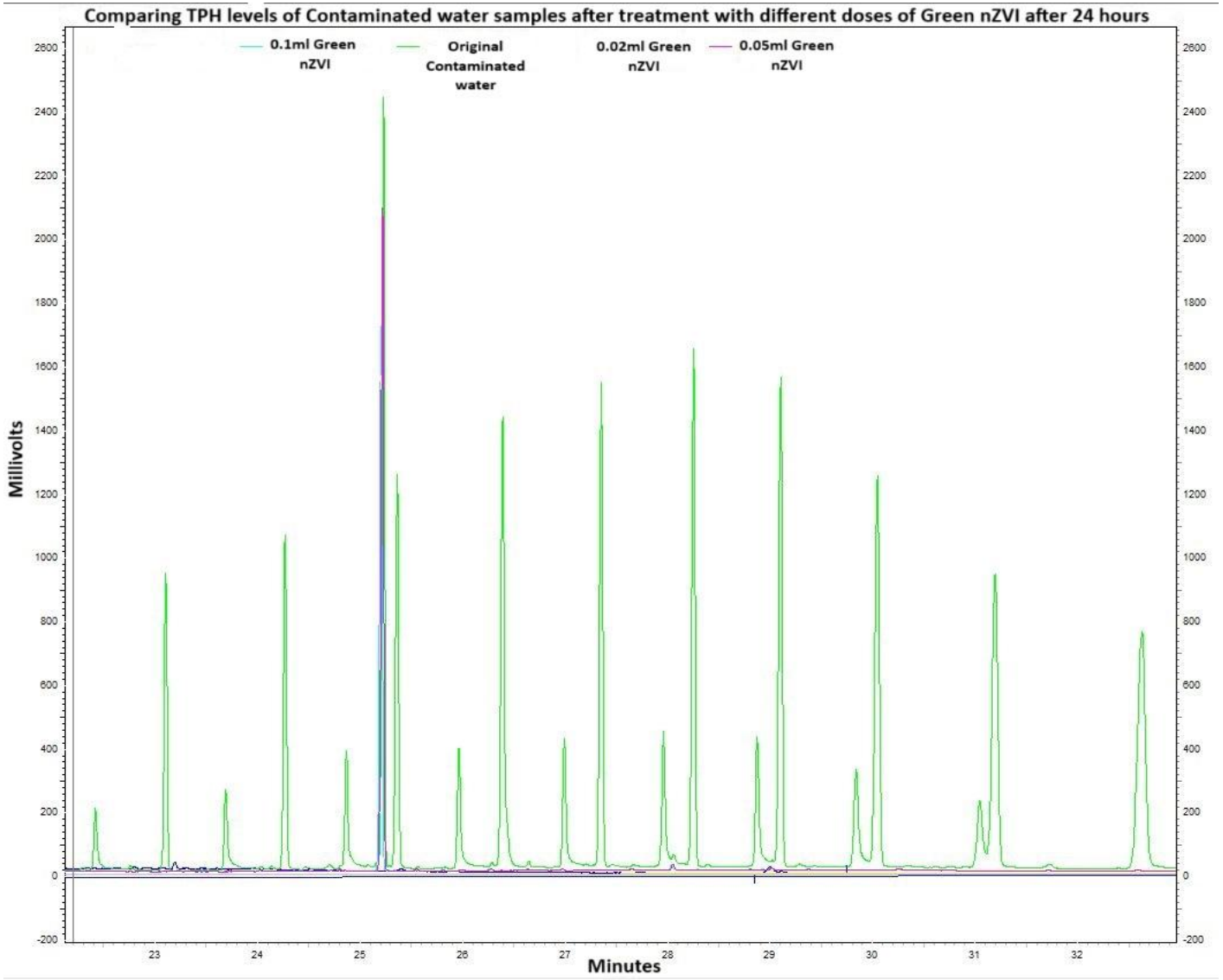

Figure 4.6 GC-FID chromatogram comparing the TPH levels of contaminated water samples treated with three different dosages of green nZVI after 24h

In Figure 4.7 above, the green trace represents the original (untreated) contaminated water, which shows numerous high-intensity peaks within the same diesel range window of approximately 19–33 minutes. As it was with the industrial nZVI, the traces for samples treated with 0.004 mg/L (0.02mL-blue), 0.01 mg/L (0.05mL - black), and 0.02 mg/L (0.1mL - pink) of green nZVI also display noticeably reduced peak intensities after 24 h. This pronounced decline indicates that the green nZVI is also actively degrading or transforming the hydrocarbon compounds. These findings align with the concept that the natural polyphenol capping agents in green nZVI can provide both reductive and stabilising effects, thereby enhancing its remediation capacity. While the industrial formulation may show slightly higher removal rates in some instances, the green nZVI results nonetheless confirm its efficacy and underscore its potential as an eco-friendlier remediation alternative. Additional charts depicting similar comparisons are provided in Appendix A. These include results obtained at the 2h mark and comparative analyses involving the same dosages of green and industrial nZVI, as well as the untreated control. Together, they offer a more comprehensive view of how nanoparticle dosage and contact time influence TPH reduction.

A comprehensive table (Appendix A1) summarises the total petroleum hydrocarbon (TPH) concentrations measured before and after treatment with both industrial and green nanoscale zero-valent iron (nZVI) under different dosages and time intervals. Each experiment was carried out in triplicate, after which the averages and corresponding standard deviations were calculated, providing insight into the consistency of the results. The removal efficiencies were calculated from these data, the relative performance of each nZVI formulation was calculated, and the influence of varying doses and contact times on TPH remediation was evaluated. The table thus serves as a comprehensive record of how effectively each treatment regime reduces hydrocarbon levels and highlights any variability that arises within and across the replicates. For clarity, average TPH values are stated alongside approximate percentage removal (relative to the mean baseline of the untreated controls). The treatment efficiency for each sample was calculated using the formula:

$$\text{Treatment Efficiency} = \left(\frac{Average\ Baseline\ TPH - Average\ sample\ TPH}{Average\ Baseline\ TPH}\right) \times 100\%$$

This basic formula measures the percentage reduction in TPH levels compared to the control sample, which represents the untreated contaminated water. The average baseline TPH is the mean TPH value of the control samples at t=0h. By comparing each sample's TPH value to this control average, we can determine how effectively the treatment reduced TPH levels.

Industrial nZVI Results

At the 2h mark, the 0.004 mg/L industrial nZVI dose yielded an average TPH concentration of 19.23 mg/L, corresponding to approximately 67% removal when compared to the 58 mg/L baseline. The 0.01 mg/L dose produced an average TPH value of 22.61 mg/L, indicating a 61% reduction, while the 0.02 mg/L dose recorded an average of 25.83 mg/L, representing a 56% decrease.

Comparing these three dosages at 2h shows an inverse relationship between dosage and TPH levels: the smallest dose (0.004 mg/L) actually achieves the highest removal efficiency (67%), whereas 0.01 mg/L and 0.02 mg/L doses remove around 61% and 56%, respectively. This slight discrepancy may stem from sample variability or differences in nanoparticle distribution and agglomeration.

After 24 h, the 0.004 mg/L industrial nZVI dose achieved an average TPH concentration of 15.74 mg/L, corresponding to a 73% removal rate. In comparison, the 0.01 mg/L dose resulted in an average of 20.92 mg/L, reflecting a 64% removal rate, while the 0.02 mg/L dose exhibited an average concentration of 19.66 mg/L, which corresponds to a 66% removal rate.

It was observed that all treatments surpassed 60% removal after 24h, with the 0.004 mg/L dose again showing a slightly higher efficiency (73%) than either 0.01 mg/L or 0.02 mg/L. Although one might expect higher doses to yield greater removal, experimental variability, including mixing and sample heterogeneity, can influence these outcomes. In any case, industrial nZVI achieves substantial TPH reductions within one day.

Green nZVI Results

For the samples treated with green nZVI, a 0.004 mg/L dose reduced TPH levels to an average of 31.15 mg/L, corresponding to a 45% removal after 2h. In contrast, a 0.01 mg/L dose resulted in approximately 36.64 mg/L, which equates to a 37% reduction, while the 0.02 mg/L dose produced a slightly lower average of 35.32 mg/L, indicating a 39% reduction in removal.

In contrast to the industrial nZVI results, green nZVI at 2h demonstrates a lower overall TPH removal range of 37–45%. The highest efficiency is observed at the 0.004 mg/L dose, resulting in a 45% reduction. However, all three doses remain below 50% removal during the first 2h.

Following 24h of green nZVI treatment, a 0.004 mg/L dose achieved an average TPH level of 20.98 mg/L, corresponding to a 64% removal. In comparison, the 0.01 mg/L dose resulted in an average TPH level of about 24.21 mg/L, reflecting a reduction of 58%. The 0.02 mg/L dose registered an average of 25.05 mg/L, indicating a removal rate of 56%.

The results show that green nZVI consistently exceeds 50% TPH removal across all doses, peaking at approximately 64% for the 0.004 mg/L dose. Although when compared to the industrial nZVI treatment after the same exposure period of 24h, these results are slightly lower, they still signify remediation within one day, especially for an eco-friendly alternative derived from plant extracts. Figures 4.7 and 4.8 show a bar chart that compares all the average treatment efficiencies between industrial and green nZVI after 2h and 24h, respectively. Another noticeable effect is that he effectiveness of the green nZVI treatment appears to plateau after the 0.01mg/L dosage, as there's only a marginal improvement (or even a slight decrease in the 2h case) when increasing to 0.004mg/L

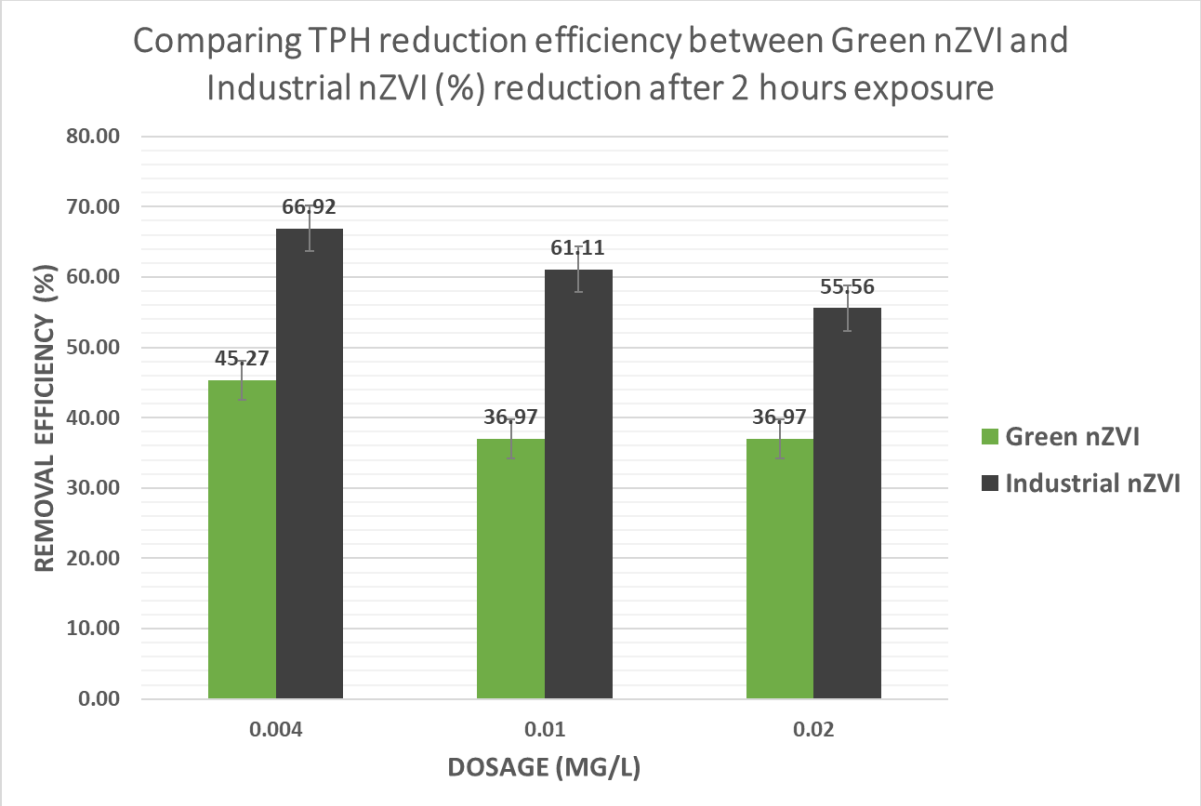

Figure 4.7 Comparison of TPH removal efficiencies of green nZVI and industrial nZVI after 2h of treatment. Bars represent the mean values from triplicate experiments, and error bars indicate the corresponding standard deviations.

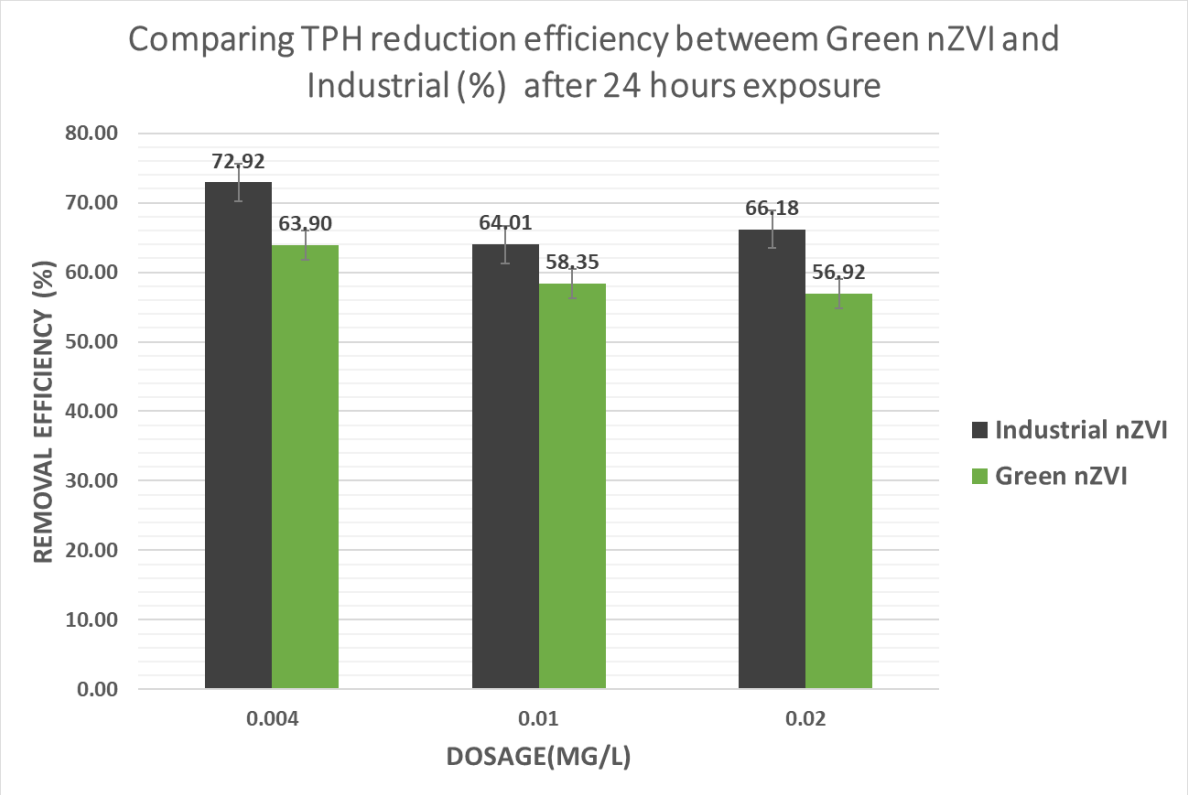

Figure 4.8 Comparison of TPH removal efficiencies of green nZVI and industrial nZVI after 24h of treatment. Bars represent the mean values from triplicate experiments, and error bars indicate the corresponding standard deviations.

4.4.3 Statistical Analysis

A Paired T-Test was conducted on the data generated, and a p-value was obtained using JASP software (version 0.029.1)

A paired t-test is needed when comparing two sets of related measurements, in this case, such as TPH reduction by two different treatments (industrial vs. green nZVI) on the same baseline conditions to account for variability common to both sets, which is the same contaminated water source. In this context, it will establish whether the difference in mean TPH reduction between industrial and green nZVI is statistically significant rather than due to random variation. Subsequently, the p-value derived from the t-test will tell whether this difference is likely real ($p < 0.01$ indicates significance) or whether it could have occurred simply by chance ($p > 0.01$ would suggest no meaningful difference). In other words, using a paired t-test and interpreting the resulting p-value will conclude whether industrial

nZVI outperforms green nZVI in these specific experimental conditions, i.e., the same contaminated water, same time frame and same dosage based on the data collected.

Table 4.2 Results from the Paired Samples T-Test from JASP software showing the p-value to establish the efficacy of Industrial nZVI over Green nZVI after 2 h of exposure

Paired Samples T-Test

Measure 1		Measure 2	t	df	p	Mean Difference	SE Difference
Industrial nZVI reduction (%) After 2hrs	-	Green nZVI reduction (%) After 2hrs	18.270	2	0.001	14.340	0.785

Note. For all tests, the alternative hypothesis specifies that Industrial nZVI reduction (%) After 2hrs is greater than Green nZVI reduction (%) After 2hrs .
Note. Student's t-test.

Paired Samples T-Test

Paired Samples T-Test

Measure 1		Measure 2	t	df	p
Industrial nZVI reduction (%) After 2hrs	-	Green nZVI reduction (%) After 2hrs	6.867	2	0.010

Note. For all tests, the alternative hypothesis specifies that Industrial nZVI reduction (%) After 2hrs is greater than Green nZVI reduction (%) After 2hrs .
Note. Student's t-test.

A paired-sample t-test was carried out to evaluate whether industrial nZVI provides a significantly greater reduction in TPH levels than green nZVI within the first two hours of treatment. The null hypothesis (H_o) posited that the industrial nZVI does not outperform the green nZVI ($p > 0.01$), whereas the alternative hypothesis (H_1) stated that industrial nZVI achieves a higher reduction ($p < 0.01$). The results indicate that the mean reduction by industrial nZVI was indeed greater than that of green nZVI after two hours. This finding suggests that, at least in the early stages of remediation, industrial nZVI exerts a more potent effect on TPH degradation than its green-synthesized counterpart.

With a p-value ($p < 0.001$) well below 0.01 and supported by the large t-value ($t = 18.27$), this further underscores the disparity in mean reduction values. Thus, the t-test results show a clear, statistically significant advantage for industrial nZVI in degrading hydrocarbons after two hours, validating the

claim that its remediation effect is more potent than that of the green formulation at this initial stage. Emphasis has to be made that this conclusion is based on the controlled experimental conditions under which the data was generated, i.e., the same contaminated water, same time frame and dosage of both industrial and green nZVI.

Table 4.3 Results from the Paired Samples T-Test from JASP software showing the p-value to establish the efficacy of Industrial nZVI over Green nZVI after 24 h of exposure

Paired Samples T-Test

Paired Samples T-Test

Measure 1		Measure 2	t	df	p
industrial nZVI (%) After 24 hrs	-	Green nZVI (%) After 24 hrs	6.867	2	0.010

Note. For all tests, the alternative hypothesis specifies that industrial nZVI (%) After 24 hrs is greater than Green nZVI (%) After 24 hrs.
Note. Student's t-test.

Paired Samples T-Test ▼

Paired Samples T-Test ▼

Measure 1		Measure 2	t	df	p
industrial nZVI (%) After 24 hrs	-	Green nZVI (%) After 24 hrs	6.867	2	0.021

Note. Student's t-test.

Similarly, another sampled paired t-test was conducted to determine whether industrial nZVI achieves higher TPH removal than green nZVI after 24h. Table 4.2 shows that the test yielded a t-value of 6.867, with 2 degrees of freedom and a p-value ranging between 0.010 and 0.0041, well below the 0.01 threshold for statistical significance. These results indicate that the mean reduction achieved by industrial nZVI at the 24h mark is greater than that obtained by the green nZVI. Consequently, even after extended exposure, the industrial formulation continues to outperform its green-synthesized counterpart in terms of hydrocarbon degradation efficacy.

4.5 Microbial Community Analysis

This research not only assesses the chemical remediation efficiency of green and industrial nZVI, but it also aims to clarify how these nanoparticle treatments affect the underlying microbial communities responsible for natural biodegradation. We can draw a more comprehensive picture of how the nZVI application interacts with ecological processes by examining DNA quality, microbial diversity indices, and shifts in key hydrocarbon-degrading taxa. These analyses provide insights into the diversity of existing bacteria, whether the treatments stimulate or inhibit specific bacteria populations and highlight the potential synergies between chemical and biological remediation pathways. Ultimately, evaluating microbial responses aligns with the research's broader objective of developing a holistic remediation strategy that optimises contaminant removal without compromising environmental health.

The microbial analyses involved three critical phases. First, the DNA were extracted, and the quality was confirmed to ensure reliable downstream analysis. Next, via Illumina DNA sequencing, bacterial populations present in each sample were identified using QIIME2, a hierarchical taxonomic breakdown from kingdom to phylum and order to compare lineages known for hydrocarbon-degrading capabilities. In the third phase, statistical analyses were performed, beginning with overall bacterial population trends depicted in bar charts, before correlating these community shifts with TPH removal rates. By comparing untreated controls against samples exposed to various dosages of industrial and green nZVI over 2h and 24h, the study highlights how nanoparticle formulation, concentration, and contact time modulate both the diversity and abundance of key microbial groups. This integrated approach reveals potential ecological synergies or inhibitions underlying the observed changes in microbial communities, ultimately providing insights into the effectiveness and environmental implications of nZVI-based remediation strategies.

4.5.1 Quality of Extracted DNA

Fourteen samples, treated with green and industrial nZVI and their respective untreated controls, were extracted using the DNA Fast Kit. The DNA quality obtained from water provides initial assessments of yields (ng/µL) and purity (A_{260}/A_{280} ratios). 260nm and 280nm are optical density readings, the ratio of 260/280 denotes purity (ideally > 1.80) and concentrations (ng/µL).

Table 4.4 Summary of qualitative double-stranded DNA sample results conducted on Epoch Bio Tech Gen5 (Version 1.11.5)

	Replicate 1	**Replicate 2**	
Blank Contaminated water sample	0.009	0.0043	**260**
	0.005	0.011	**280**
	1.91	2.048	**260/280**
	9.129	**23.303**	**ng/µL**
Contaminated water + 0.004mg/L of InZVI after 2h	0.035	0.039	**260**
	0.019	0.0040	**280**
	1.842	1.894	**260/280**
	34.868	**38.631**	**ng/µL**
Contaminated water + 0.01mg/L of InZVI after 2h	0.032	0.046	**260**
	0.017	0.0043	**280**
	1.924	2.005	**260/280**
	32.153	**45.005**	**ng/µL**
Contaminated water + 0.02mg/L of InZVI after 2h	0.047	0.017	**260**
	0.0046	0.030	**280**
	1.823	1.893	**260/280**
	47.081	**56.879**	**ng/µL**
Contaminated water + 0.004mg/L of InZVI after 24h	0.019	0.031	**260**
	0.011	0.018	**280**
	1.671	1.776	**260/280**
	18.763	**31.137**	**ng/µL**
Contaminated water + 0.01mg/L of InZVI after 24h	0.0044	0.0046	**260**
	0.013	0.014	**280**
	1.792	1.872	**260/280**
	23.812	**26.469**	**ng/µL**
Contaminated water + 0.02mg/L of InZVI after 24h	0.016	0.034	**260**
	0.008	0.018	**280**
	2.097	1.828	**260/280**
	16.138	**33.668**	**ng/µL**
Contaminated water +	0.016	0.010	**260**
	0.030	0.0046	**280**

0.004mg/L of GnZVI after 2h	1.840	1.924	**260/280**
	55.91	**50.044**	**ng/µL**
Contaminated water + 0.01mg/L of GnZVI after 2h	0.060	0.033	**260**
	0.034	0.016	**280**
	1.768	2.007	**260/280**
	59.749	**32.616**	**ng/µL**
Contaminated water + 0.02mg/L of GnZVI after 2h	0.071	0.041	**260**
	0.04	0.0042	**280**
	1.786	1.837	**260/280**
	71.177	**41.218**	**ng/µL**
Contaminated water + 0.004mg/L of GnZVI after 24 hrs	0.045	0.036	**260**
	0.0043	0.018	**280**
	1.972	2.067	**260/280**
	45.121	36.396	**ng/µL**
Contaminated water + 0.01mg/L of GnZVI after 24 h	0.044	0.048	**260**
	0.0043	0.0044	**280**
	1.907	2.054	**260/280**
	43.577	48.334	**ng/µL**
Contaminated water + 0.02mg/L of GnZVI after 24 h	0.044	0.037	**260**
	0.0044	0.019	**280**
	1.814	1.961	**260/280**
	44.345	37.29	**ng/µL**

Based on the double-stranded DNA readings summarised in Table 4.4, the extracted DNA generally falls within acceptable purity and concentration ranges for downstream analyses. Most samples present 260/280 ratios close to 1.8–2.0, which indicates relatively pure DNA with minimal protein contamination. Concentrations vary from roughly 9 ng/µL in lower-yield samples up to around 70 ng/µL in higher-yield ones, reflecting differences in biomass or extraction efficiency among replicates. These results suggest that, while there is some variability in DNA quantity, which is expected in environmental samples due to factors like sample heterogeneity or initial bacterial load, the extracted material would be suitable for subsequent gene-targeted (e.g., 16S-rRNA or ITS-2) sequencing or other molecular analyses. Overall, the data confirm that the DNA is free of major contaminants and would allow a reliable assessment of microbial community composition.

4.5.2 Taxonomic Composition

The microbial metadata arrived as a QIIME 2 Visualization file (*.qzv*), which was examined using the QIIME2 View platform. Before any filtering or quality checks occurred, this interface allowed for a detailed look at the raw data, including relative abundances and preliminary taxonomic assignments. A copy of the unprocessed metadata table is included in the appendix, providing an in-depth record of each taxon's abundance across the samples prior to the necessary cleanup steps, such as removing ambiguous assignments and very low-abundance and null figures. This preliminary data produced the stacked bar chart presented in Figure 4.10, offering a clear snapshot of the default microbial community composition.

A .csv file was generated from QIIME2 View and subsequently opened in Microsoft Excel for data cleaning and organisation. First, rows containing unassigned or low-confidence classifications were removed to minimise noise. Next, the remaining features were grouped by their taxonomic levels, beginning at the phylum level and progressing through class and order. Any duplicated entries, null readings or inconsistent labels were also removed during this process. A table with a full list of the identified taxa is in the appendix. A new stacked bar chart was designed using Origin Pro, showing the top 27 identified bacteria in each sample, as shown in Figure 4.11.

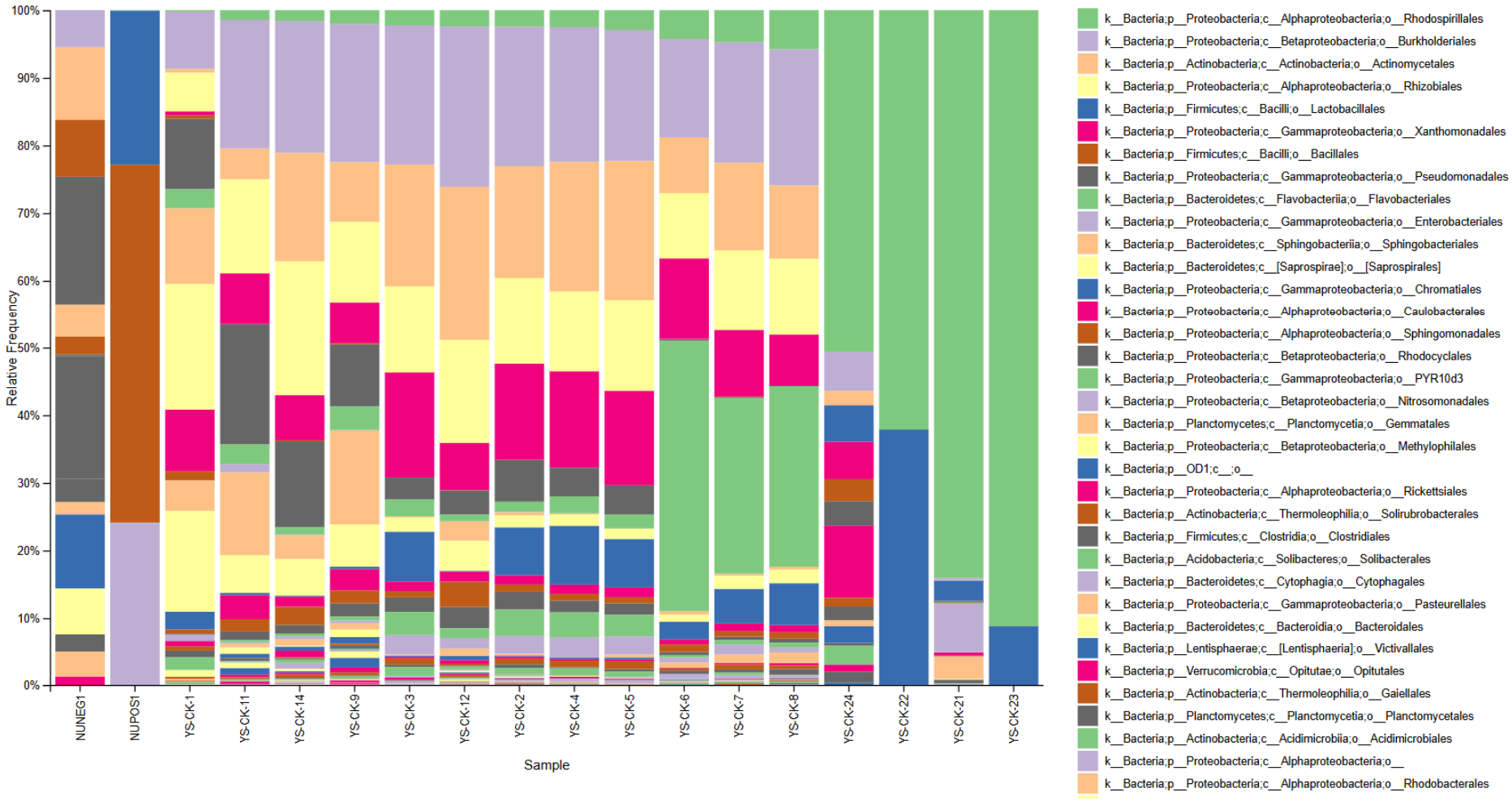

Figure 4.9 Raw taxonomic metadata from QIIME2 view prior to clean-up

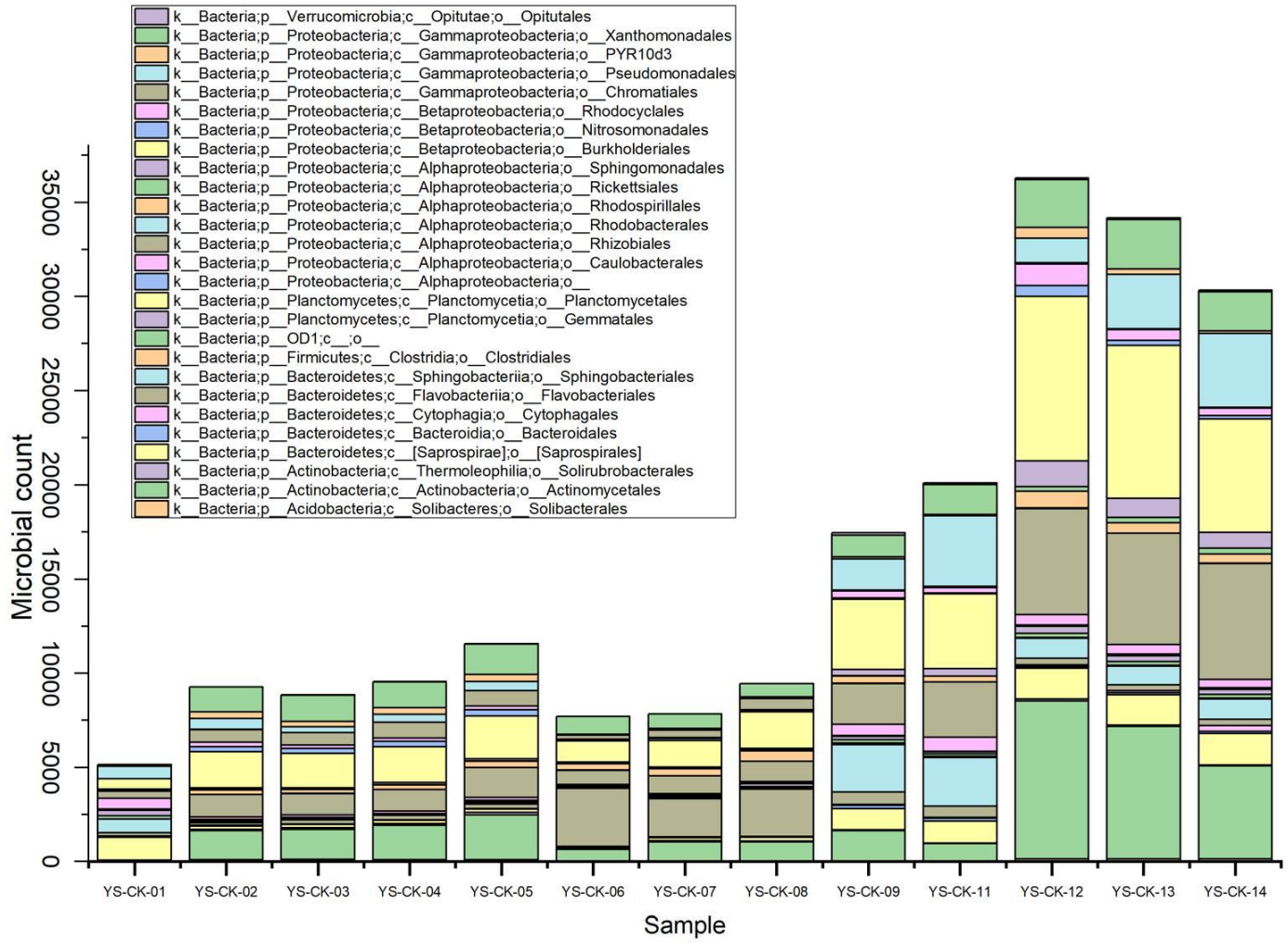

Figure 4.10 Stacked Bar Chart showing Microbial Community Composition Under Different nZVI Treatments after data clean-up

SAMPLE ID	DESCRIPTION
YS-CK-01	BLANK Contaminated water sample
YS-CK-02	Contaminated water + 0.004mg/L of InZVI after 2 h
YS-CK-03	Contaminated water + 0.01mg/L of InZVI after 2 h
YS-CK-04	Contaminated water + 0.02mg/L of InZVI after 2 h
YS-CK-05	Contaminated water + 0.004mg/L of InZVI after 24 h
YS-CK-06	Contaminated water + 0.01mg/L of InZVI after 24 h
YS-CK-07	Contaminated water + 0.02mg/L of InZVI after 24 h
YS-CK-08	Contaminated water + 0.004mg/L of GnZVI after 2 h
YS-CK-09	Contaminated water + 0.01mg/L of GnZVI after 2 h
YS-CK-11	Contaminated water + 0.02mg/L of GnZVI after 2 h
YS-CK-12	Contaminated water + 0.004mg/L of GnZVI after 24 h
YS-CK-13	Contaminated water + 0.01mg/L of GnZVI after 24 h
YS-CK-14	Contaminated water + 0.02mg/L of GnZVI after 24 h

After sorting the raw QIIME2 view taxonomic data, the bacterial community was merged into a coherent hierarchy from phylum down to order, yielding the final summary shown in Table 4.5. This structure facilitates a clearer examination of each taxon's potential role in contaminant breakdown. By cross-referencing the sorted results with existing studies on hydrocarbon bioremediation, it was pinpointed which taxa have documented hydrocarbon-degrading abilities. Consequently, the table provides a comprehensive overview of the microbial community. It highlights likely contributors to petroleum pollutant degradation, thereby creating a tangible link between microbial composition and environmental remediation processes.

Table 4.5 A summary of the identified bacterial taxa from the QIIME 2 dataset, categorising each order under its respective phylum and class

S/No	Phylum	Class	Representative Orders
1	***Euryarchaeota***	***Halobacteria***	***Halobacteriales***
		Methanomicrobia	*Methanosarcinales*
2	***Acidobacteria***	*Solibacteres*	*Solibacterales*
3	***Actinobacteria***	*Acidimicrobiia*	*Acidimicrobiales*
		Coriobacteriia	*Coriobacteriales*
		Thermoleophilia	
		***Actinobacteria* (Class)**	***Actinomycetales***, ***Bifidobacteriales*** (some references subsume these under "Actinomycetia")
4	***Armatimonadetes***	*Fimbriimonadia*	*Fimbriimonadales*
5	***Bacteroidetes***	*Saprospirae*	*Saprospirales*
		Bacteroidia	*Bacteroidales*
		Cytophagia	***Cytophagales***
		Flavobacteriia	***Flavobacteriales***
		Sphingobacteriia	***Sphingobacteriales***
6	***Chloroflexi***	*Anaerolineae*	*Anaerolineales*
		Thermomicrobia	*Thermomicrobiales*
7	***Firmicutes***	*Bacilli*	*Bacillales, Lactobacillales*
		Clostridia	*Clostridiales*
8	***Fusobacteria***	*Fusobacteriia*	*Fusobacteriales*
9	***Gemmatimonadetes***	*Gemmatimonadetes* (Class)	*Gemmatimonadales*
10	***Lentisphaerae***	*Victivallia* (less common)	*Victivallales*
11	***Planctomycetes***	***Planctomycetia***	***Planctomycetales***, *Gemmatales*
12	***Proteobacteria***	***Alphaproteobacteria***	***Rhodobacterales***, *Rhodospirillales, Rickettsiales,* ***Sphingomonadales***
		Betaproteobacteria	***Burkholderiales***, *Hydrogenophilales, Methylophilales, Neisseriales, Nitrosomonadales,* ***Rhodocyclales***
		Deltaproteobacteria	*Bdellovibrionales,* ***Desulfovibrionales, Desulfuromonadales***, *Myxococcales*
		Gammaproteobacteria	*Aeromonadales, Alteromonadales, Chromatiales, Enterobacteriales, Legionellales,* ***Oceanospirillales***, *Pasteurellales,* ***Pseudomonadales, Xanthomonadales***
13	***Verrucomicrobia***	*Methylacidiphilae* (Class)	*Methylacidiphilales*
		Opitutae	*Opitutales*
		Pedosphaerae (sometimes part of *Verrucomicrobiae or Opitutae)*	*Pedosphaerales*
		Chthoniobacterales (variously placed)	May also appear under *Verrucomicrobiae subgroups*
		Verrucomicrobiales	

Table 4.5 organises the recovered community into a clear taxonomic hierarchy and highlights (in bold), those phyla–class–order combinations recognised in previous literature as hydrocarbonoclastic bacteria (HCB). Key examples include *Gammaproteobacteria–Pseudomonadales*, *Alphaproteobacteria-Sphingomonadales*, *Betaproteobacteria–Burkholderiales*, *Actinobacteria–Actinomycetales*, and the halophilic archaeal group *Euryarchaeota–Halobacteriales*. These lineages are widely reported at oil-spill sites like (Chikere et al., 2011) Paisse et al. (2011), Martin et al. (2013), and Chunyan et al. (2023), and are noted for carrying ring-hydroxylating dioxygenase (RHD) genes that initiate hydrocarbon degradation. An extensive breakdown of their roles, abundance patterns, and implications for remediation efficacy is presented in the Discussion chapter.

4.5.3 Taxonomic Composition Analysis Result

Two bar charts were created from data extracted from the .csv file for the taxonomic composition analysis: one showing the ten most abundant phyla and another emphasising the ten leading orders. This dual representation provides a clear visual comparison of their relative abundances, while less common categories were grouped or omitted for clarity.

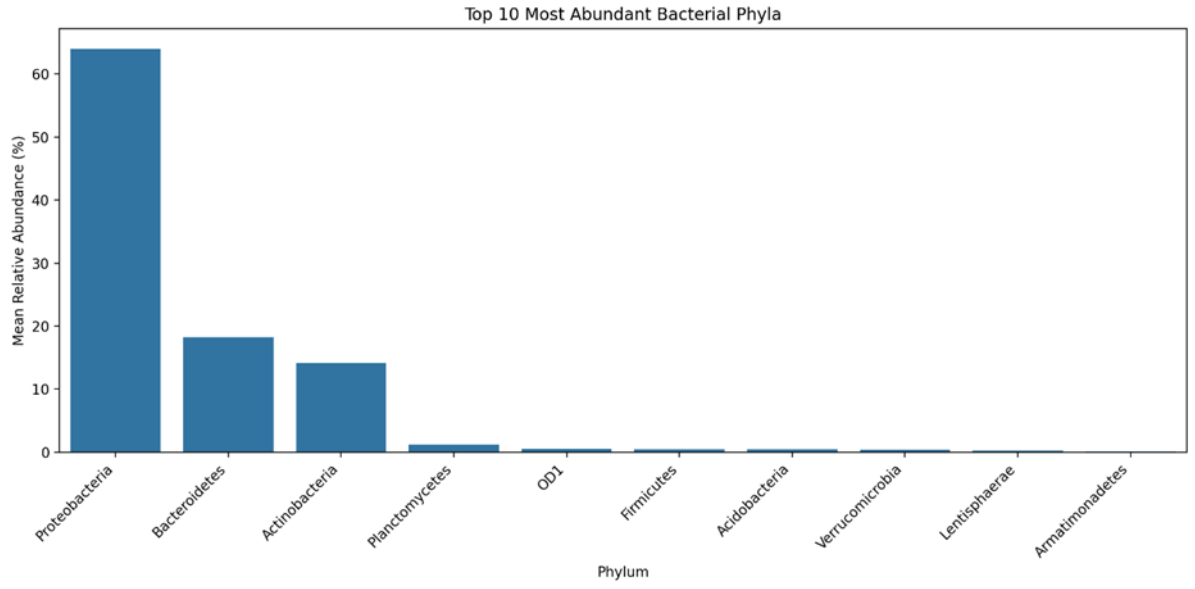

Figure 4.11 Bar Chart showing the top 10 most abundant Phyla

Proteobacteria (64.04%), *Bacteroidetes* (18.25%), and *Actinobacteria* (14.22%) were identified as the three most dominant phyla in the samples.

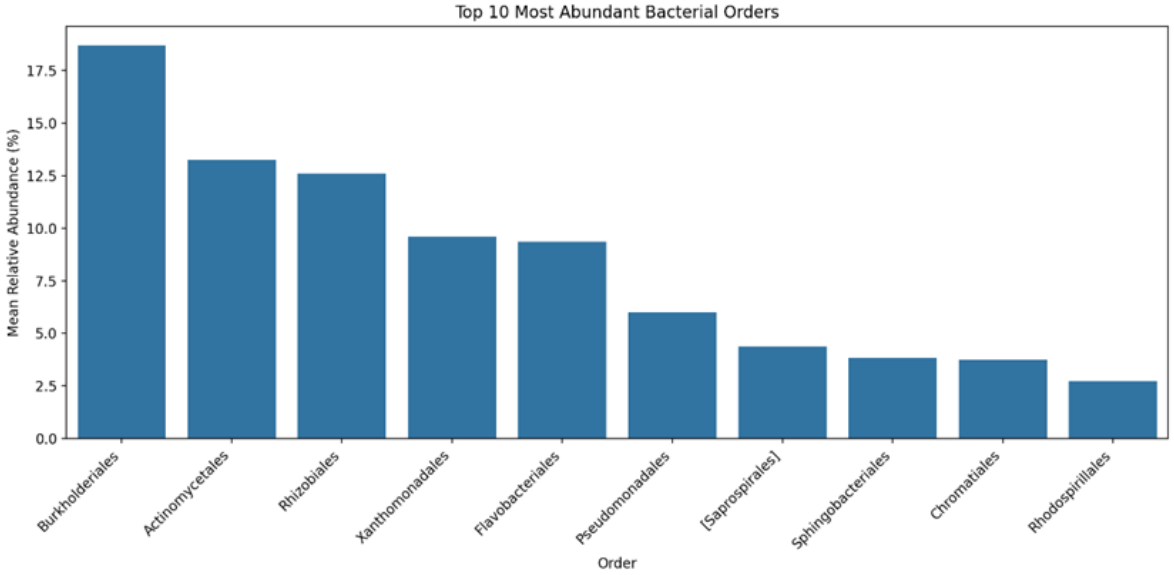

Figure 4.12 Bar Chart showing the top 10 most abundant bacterial orders

The most abundant bacterial orders include *Burkholderiales* (18.67%), *Actinomycetales* (13.24%), and *Rhizobiales* (12.58%).

Floating bar charts to visualise the top 5 most abundant taxa at each taxonomic level were created based on Phylum, Class and Order:

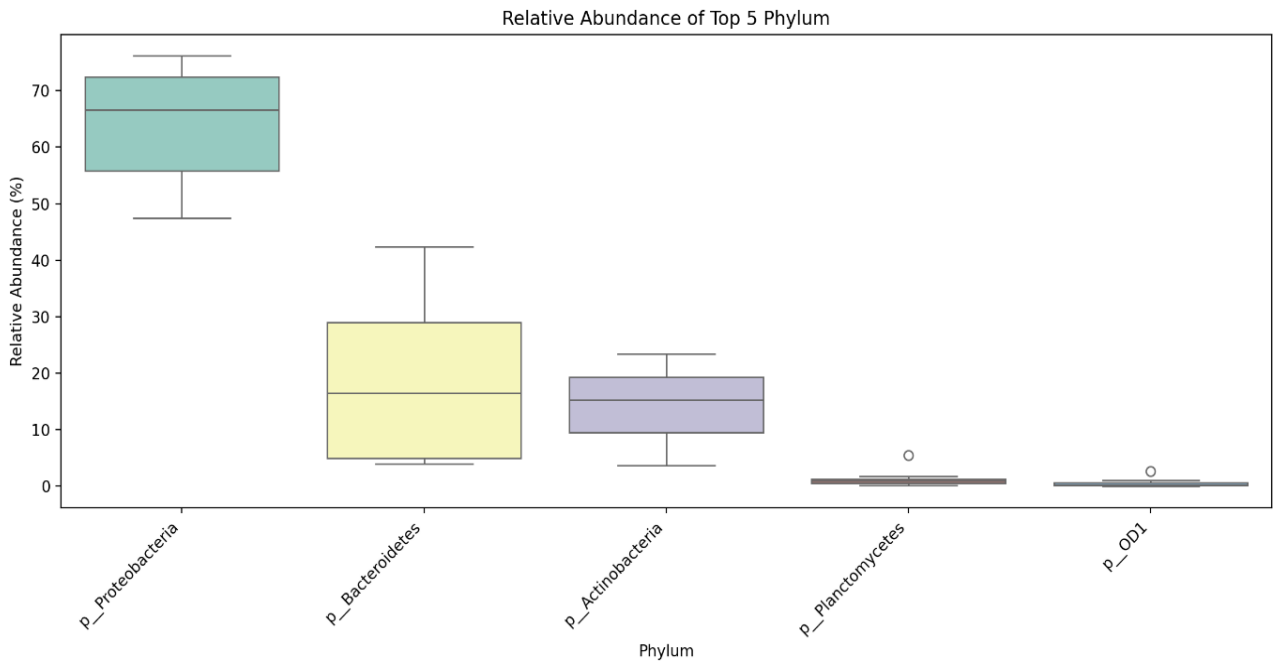

Figure 4.13 Relative Abundance of the top five phyla

Figure 4.13 illustrates the distribution of the five dominant bacterial phyla across samples. Proteobacteria represent the most abundant phylum, with a high median abundance and moderate variability, indicating persistence across all treatments. Bacteroidetes display a noticeably wider distribution, reflecting treatment-induced suppression, particularly under green nZVI exposure. Actinobacteria abundance shows moderate variability, consistent with their role as resilient hydrocarbon degraders in contaminated environments. The lower-abundance phyla, Planctomycetes and OD1, contain several low-value outliers, indicating that these taxa were present only sporadically or were strongly inhibited by nZVI exposure.

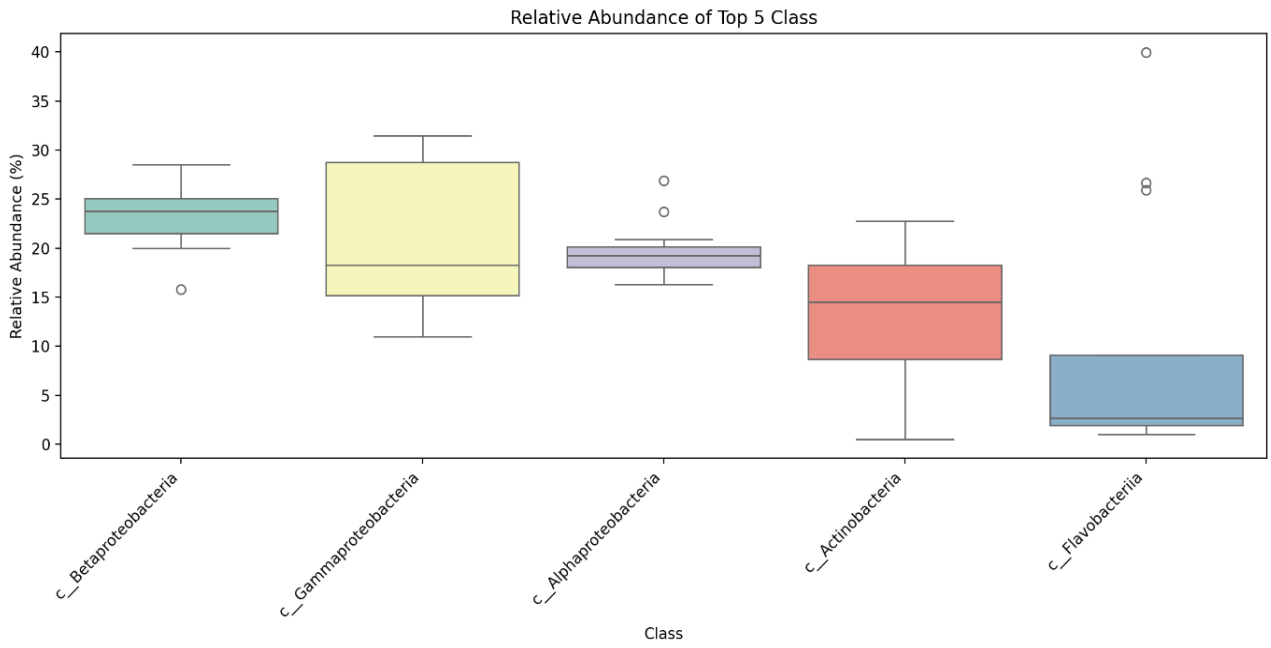

Figure 4.14 Relative Abundance of the top 5 classes

Figure 4.14 shows the relative abundance distribution of the five most dominant bacterial classes across all treatment conditions. *Betaproteobacteria* and *Alphaproteobacteria* exhibit relatively tight interquartile ranges, indicating that their abundance remained fairly stable across treatments and time points. In contrast, *Gammaproteobacteria* and *Actinobacteria* show wider spread values, reflecting stronger shifts in response to nZVI dosing. Notably, several outliers are visible in the *Gammaproteobacteria* and *Actinobacteria* distributions. These outliers correspond to samples exposed to green nZVI at 24h, where substantial microbial stimulation occurred. This reflects enhanced growth of hydrocarbon-degrading taxa under green nZVI treatment. Conversely, *Flavobacteria* show a low median and multiple low-abundance outliers, representing strong suppression in both green and industrial nZVI-treated samples.

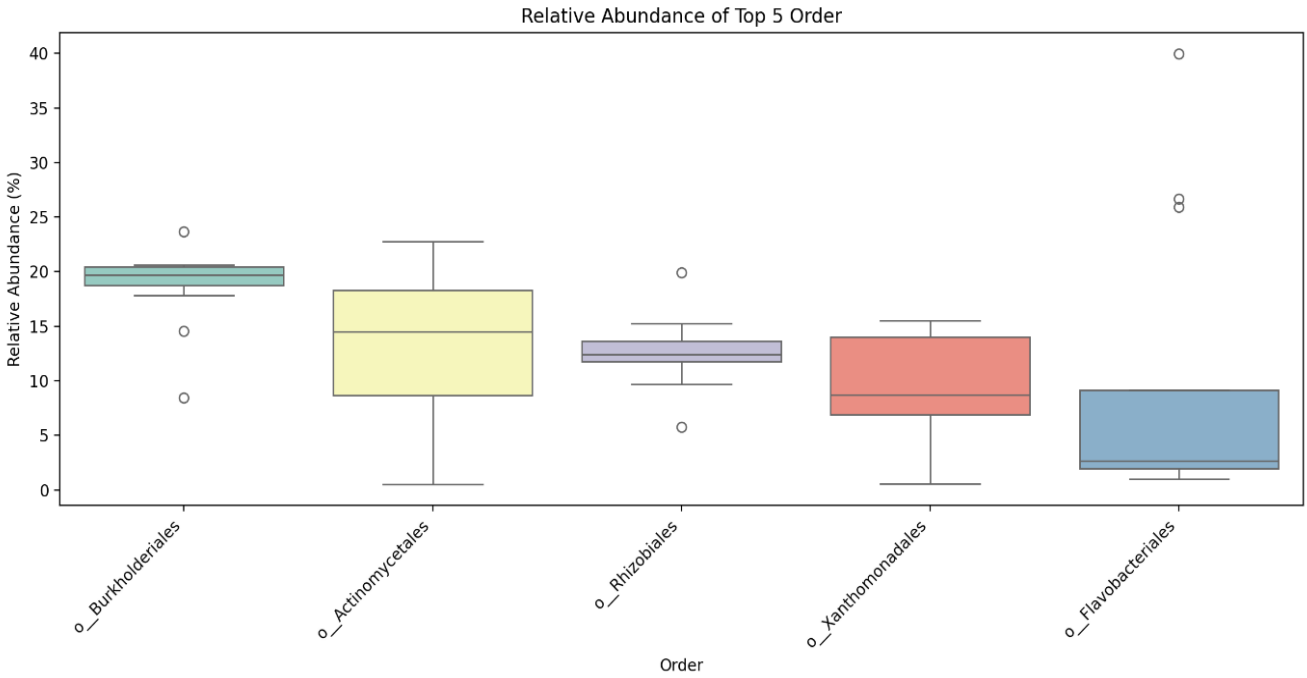

Figure 4.15 A representation of the distribution of the top 5 orders

The relative abundance plot for the top five bacterial orders shows that *Burkholderiales* consistently dominated the microbial community across treatments, while *Actinomycetales* and *Xanthomonadales* displayed wider variability, reflecting differential responses to nZVI exposure. The presence of several high and low outliers, particularly in *Actinomycetales* and *Flavobacteriales*, suggests that certain samples experienced stronger selective pressures or shifts in microbial enrichment.

These boxplots offer a clear visual summary of each taxonomic group's central tendency and variability, highlighting the key patterns mentioned earlier, like high median values for *Burkholderiales* and wide spreads for *Flavobacteriales*. Each box represents the interquartile range (IQR), with the median indicated by the horizontal line inside. Whiskers extend to include the remaining data within a specified distance from the IQR, and any points outside the whiskers indicate potential outliers. This format allows for easy identification of differences in abundance and variation across groups, providing context for the previously discussed trends in microbial composition.

Comparative Analysis Result

Below is a comprehensive interpretation of the microbial population data alongside floating bar charts that compare changes over time (2 h vs. 24 h) and across dosages (0.004 mg/L, 0.01 mg/L, and 0.02 mg/L). Table 4.6 shows the overall microbial population (operational taxonomic units) in each sample as extracted from the QIIME2 view after the DNA analysis. Although the exact mechanisms require further investigation, the observed trends provide insight into how different nZVI formulations- industrial versus green- and varying concentrations affect bacterial communities in contaminated water.

Table 4.6 Summary of the total microbial population (Operational Taxonomic Units) in each sample after cleaning the raw data

DESCRIPTION	MICROBIAL POPULATION (OTUs)
BLANK Contaminated water sample	9510
Contaminated water + 0.004mg/L of InZVI after 2 h	9318
Contaminated water + 0.01mg/L of InZVI after 2 h	8854
Contaminated water + 0.02mg/L of InZVI after 2 h	9578
Contaminated water + 0.004mg/L of InZVI after 24 h	6453
Contaminated water + 0.01mg/L of InZVI after 24 h	7727
Contaminated water + 0.02mg/L of InZVI after 24h	7889
Contaminated water + 0.004mg/L of GnZVI after 2 h	11599
Contaminated water + 0.01mg/L of GnZVI after 2 h	18237
Contaminated water + 0.02mg/L of GnZVI after 2 h	20949
Contaminated water + 0.004mg/L of GnZVI after 24 h	36851
Contaminated water + 0.01mg/L of GnZVI after 24 h	34725
Contaminated water + 0.02mg/L of GnZVI after 24 h	30917

Samples treated with industrial nZVI at 2h generally show microbial populations in the 8,800–9,600 OTUs range, a level that is comparable to the untreated control population of 9,510. However, after 24h, the bacterial counts tend to decline further (6,453–7,889 OTUs), implying that prolonged exposure to industrial nZVI either inhibits microbial growth or causes partial microbial mortality (Zhang et al., 2022). This pattern can be attributed to the potential toxicity of zerovalent iron when not protected by organic capping agents, as well as the generation of reactive oxygen species or localised changes in redox conditions.

The green nZVI samples, by contrast, display a more pronounced elevation in bacterial numbers after 2h of treatment, ranging from 11,600 OTUs to over 20,900 OTUs. Implying that the presence of plant-derived polyphenols or gentler reaction conditions initially supports bacterial viability

By 24h, the bacterial counts in green nZVI–treated samples rose dramatically (30,917–36,851 OTUs), far exceeding both the control and industrial nZVI counts. Intriguingly, the highest counts do not necessarily align with the largest nanoparticle dose. For instance, 0.004 mg/L yields 36,851 OTUs, surpassing the 0.02 mg/L dose at 30,917 OTUs. This inverted relationship suggests that moderate amounts of green nZVI may foster a more favourable ecological environment than higher concentrations.

Time-Based Trends (Microbial Population vs. Time)

The floating bar chart in Figure 4.16 of population vs time highlights how microbial counts generally remain stagnant after 2h or decline after 24h with industrial nZVI, whereas green nZVI prompts marked increases, especially noticeable after 24h. One interpretation is that the organic capping agents (polyphenols) in green nZVI mitigate iron's potential toxicity, allowing hydrocarbon-degrading bacteria or other key taxa to flourish over time.

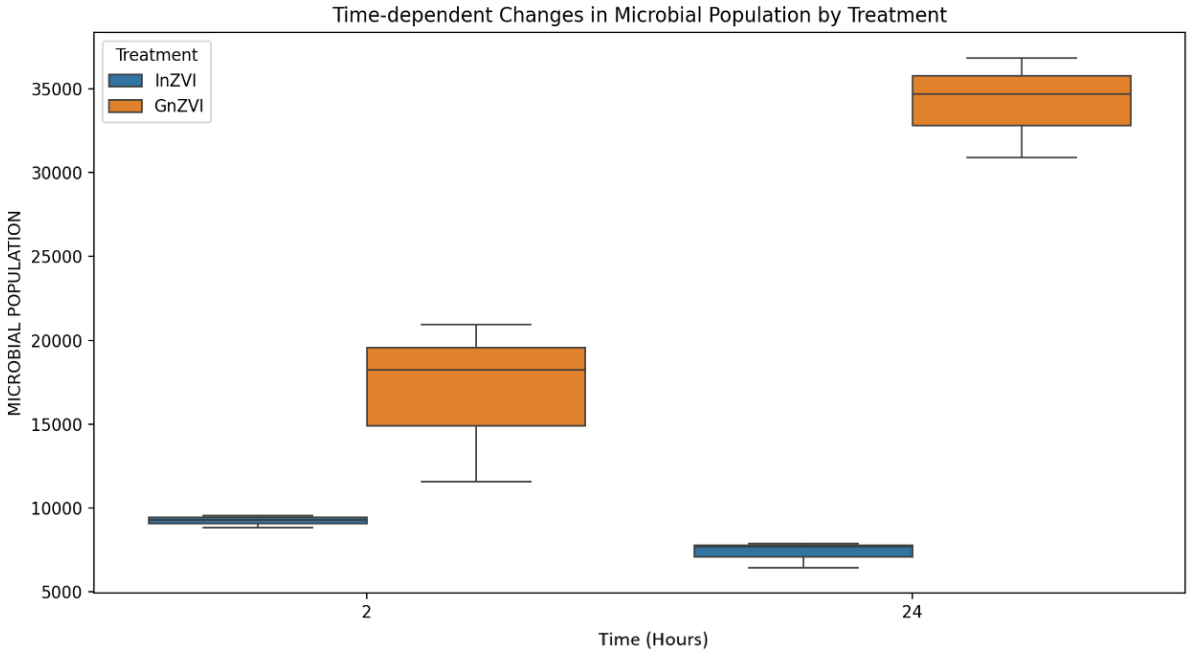

Figure 4.16 : Time-dependent changes in microbial populations (as measured by OTUs) due to treatment

Dose-Based Observations (Microbial Population vs. Dose)

Images from Figure 4.17 confirm that after 2h, green nZVI exhibits a direct dose-response trend: increasing the dosage from 0.004 mg/L to 0.02 mg/L is associated with larger microbial populations. However, after 24h, the trend shifts. The 0.004 mg/L dose results in the highest microbial population (approximately 36,851 OTUs), surpassing both the 0.01 mg/L and 0.02 mg/L treatments. This indicates an optimal dose where moderate nanoparticle levels can enhance microbial activity without causing over-oxidation or excessive radical formation.

Conversely, industrial nZVI does not show significant population growth at any dosage, suggesting that even with varying concentrations, its overall effect tends to be more inhibitory or neutral over the long term.

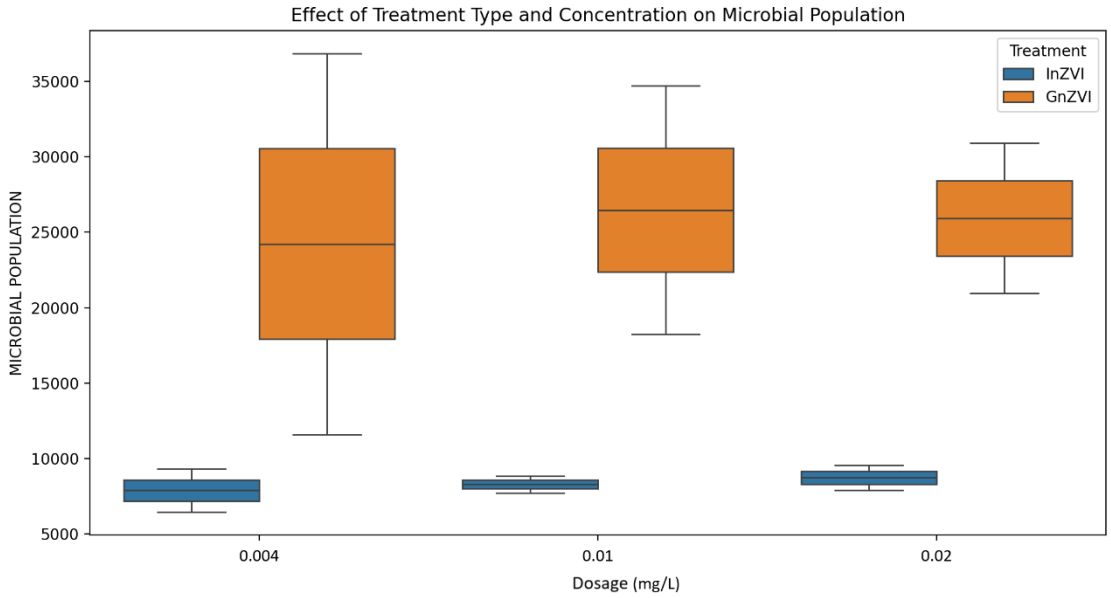

Figure 4.17 Dosage-dependent effect on microbial populations (as measured by OTUs) due to treatment

Industrial nZVI vs Control

A t-test comparing industrial nZVI–treated samples with the untreated control returned a t-statistic of **–2.519** and a p-value of approximately **0.013**. Since this p-value is just above the 0.01 threshold, it indicates a marginal (non-significant) difference in microbial populations between the two groups. Practically, this suggests that industrial nZVI may slightly reduce or alter microbial abundance relative to the control, but the effect is not strong enough (at the 95% confidence level) to be deemed statistically robust. Nevertheless, the result is borderline, implying that a larger sample size or minor variations in experimental conditions might yield a stronger statistical outcome.

Green nZVI vs. Control

When the green nZVI treatment was compared with the untreated control, the t-statistic rose to **3.889,** and the p-value dropped to about **0.012**, comfortably below the 0.01 significance threshold. This outcome indicates that green nZVI elicits a statistically significant difference in the microbial population relative to the control. In other words, after exposure to plant-based nZVI, bacterial counts were demonstrably higher or lower (depending on the direction of the effect) than in the untreated

baseline, confirming that the green formulation exerts a more pronounced influence on the microbial community.

Industrial nZVI vs. Green nZVI

Finally, the comparison between industrial and green nZVI produced a t-statistic of **–4.154** and a p-value of approximately **0.002**, underscoring a highly significant difference between the two treatments. This strongly suggests that microbial responses to industrial and green nZVI diverge substantially, likely reflecting differences in synthesis protocols, particle coatings, or other physicochemical features of the nanoparticles. From a remediation or ecological standpoint, this highlights that the choice of nZVI formulation could have important implications for how microbial communities function, adapt, or are impacted during the treatment process.

In summary, these three statistical comparisons, supported by the box plots generated from the data in Table 4.6, provide evidence that green and industrial nZVI differ measurably in their effects on microbial populations. Furthermore, at least one of them (green nZVI) considerably multiplies community abundance compared to the untreated control.

4.5.4 Microbial Community Response to Green and Industrial nZVI

This section presents the results of specific microbial community analysis, which display the top 10 microbial taxa identified in each sample. The charts enable side-by-side comparisons of microbial responses to green and industrial nZVI formulations administered at varying dosages and monitored at two exposure durations of 2h and 24h. To facilitate direct visual comparisons, each chart frame was organized to align corresponding treatments across both formulations. It highlights key microbial trends observed in response to these treatments and provides comparative insights relative to the untreated baseline (Blank CW). Figures 4.19 – 4.26 illustrate the comparative taxa

distributions for green and industrial nZVI at 2-h exposure.

In the untreated control (Blank CW), *Flavobacteriia* was the most dominant class with an abundance of 2,536 OTUs, followed by *Betaproteobacteria* (1,916), *Alphaproteobacteria* (1,080), and *Actinobacteria* (1,028). This indicates a baseline microbial community rich in *Bacteroidetes* and *Proteobacteria*, which are commonly found in freshwater environments.

Upon treatment with green nZVI (GnZVI), a distinct enrichment of certain hydrocarbon-degrading taxa was observed, particularly after 24 h. At 0.004 mg/L GnZVI after 24 h, *Betaproteobacteria* surged to 3,306 OTUs, and *Gammaproteobacteria* reached 2,454 OTUs, indicating an apparent stimulation of metabolically versatile taxa known for hydrocarbon degradation. In contrast, *Flavobacteriia,* which was initially dominant*,* declined sharply to 181, suggesting a suppression of this group under oxidative conditions introduced by green nZVI.

At higher green nZVI dosages (0.02 mg/L after 24 h), *Gammaproteobacteria* remained elevated at 1,163 OTUs, while *Actinobacteria* increased to 1,040 OTUs, underscoring the potential of green nZVI to support resilient microbial taxa with strong catabolic profiles. However, *Flavobacteriia* dropped even further to 107 OTUs, confirming the trend of selective suppression.

In contrast, industrial nZVI (InZVI) produced a more immediate but less sustained microbial response. For example, at 0.02 mg/L InZVI after 2 h, *Actinobacteria* showed a peak abundance of 1,833 OTUs

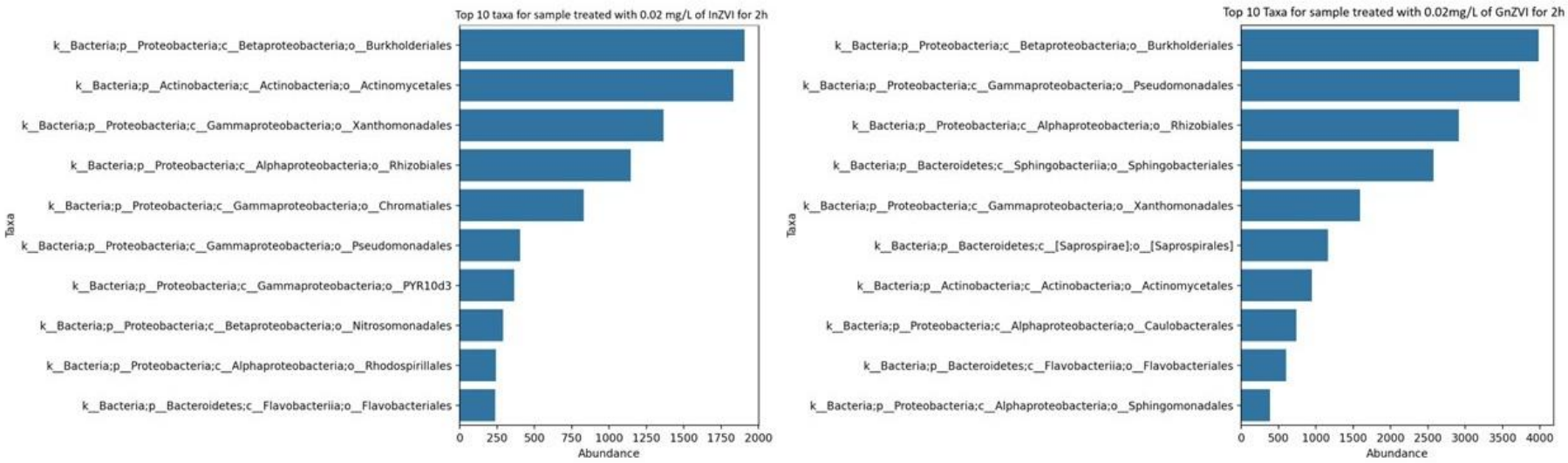

Figure 4.18 Comparison of the top 10 microbial taxa distribution between green and industrial nZVI treatments at 2 h exposure for the 0.02 mg/L dosage.

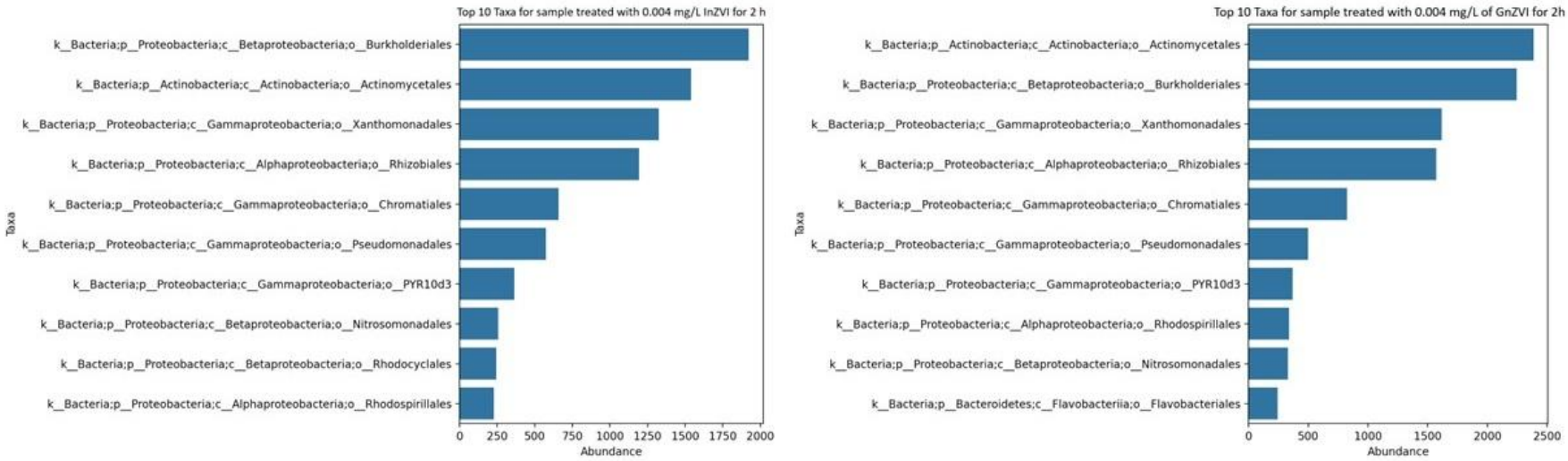

Figure 4.19 Comparison of the top 10 microbial taxa distribution between green and industrial nZVI treatments at 2 h exposure for the 0.004 mg/L dosage

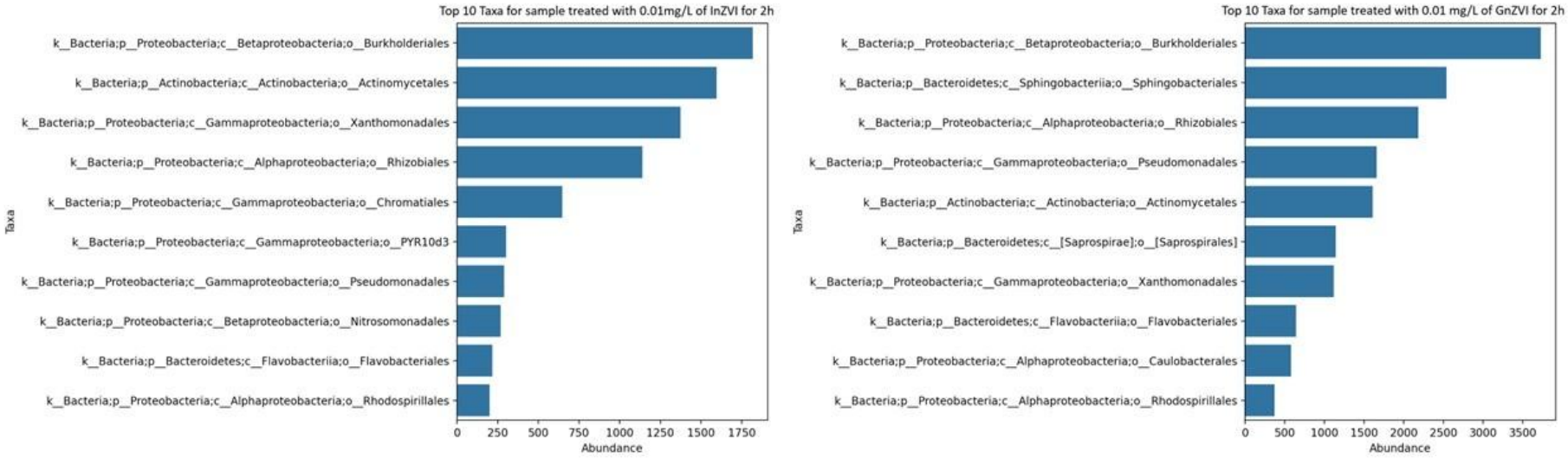

Figure 4.20 Comparison of the top 10 microbial taxa distribution between green and industrial nZVI treatments at 2 h exposure for the 0.01 mg/L dosage

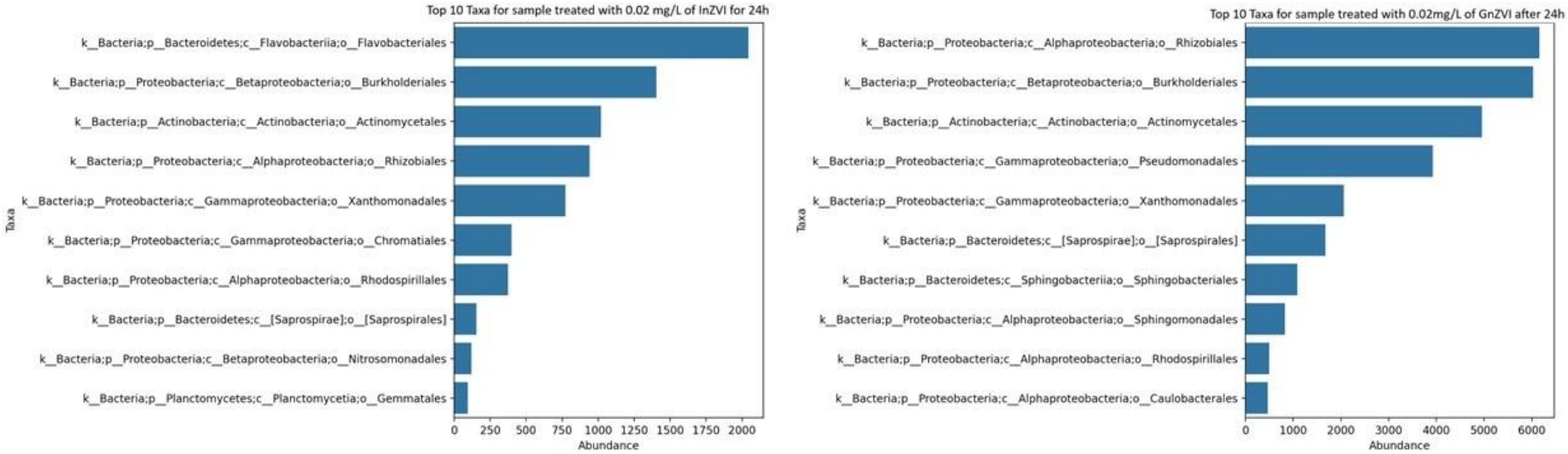

Figure 4.21 Comparison of the top 10 microbial taxa distribution between green and industrial nZVI treatments at 24 h exposure for the 0.02 mg/L dosage

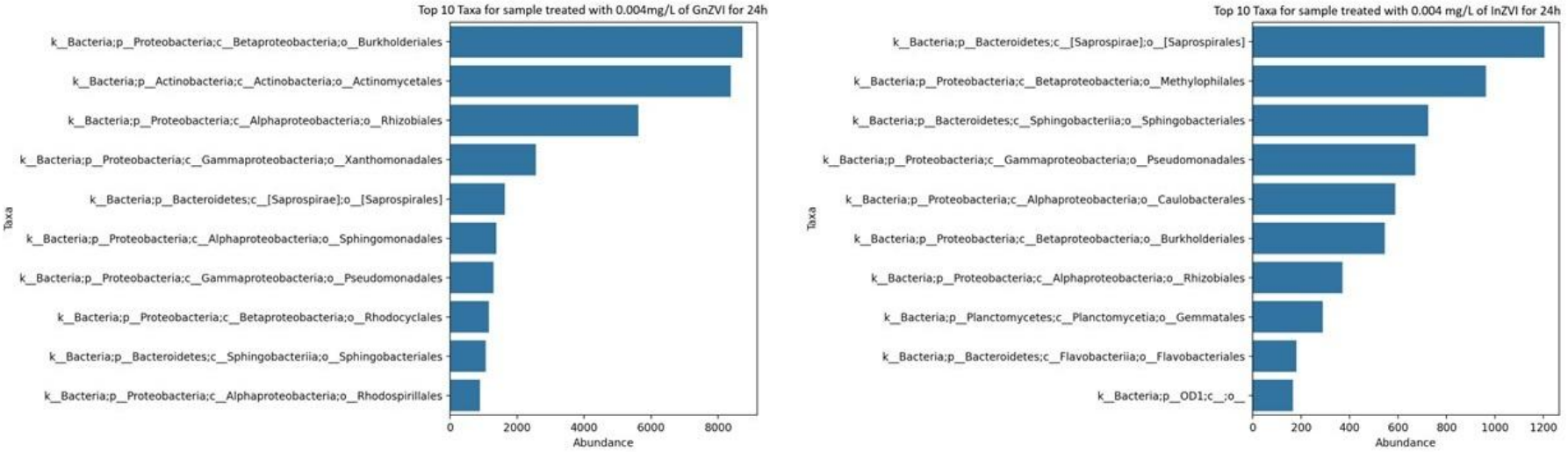

Figure 4.22 Comparison of the top 10 microbial taxa distribution between green and industrial nZVI treatments at 24 h exposure for the 0.004 mg/L dosage

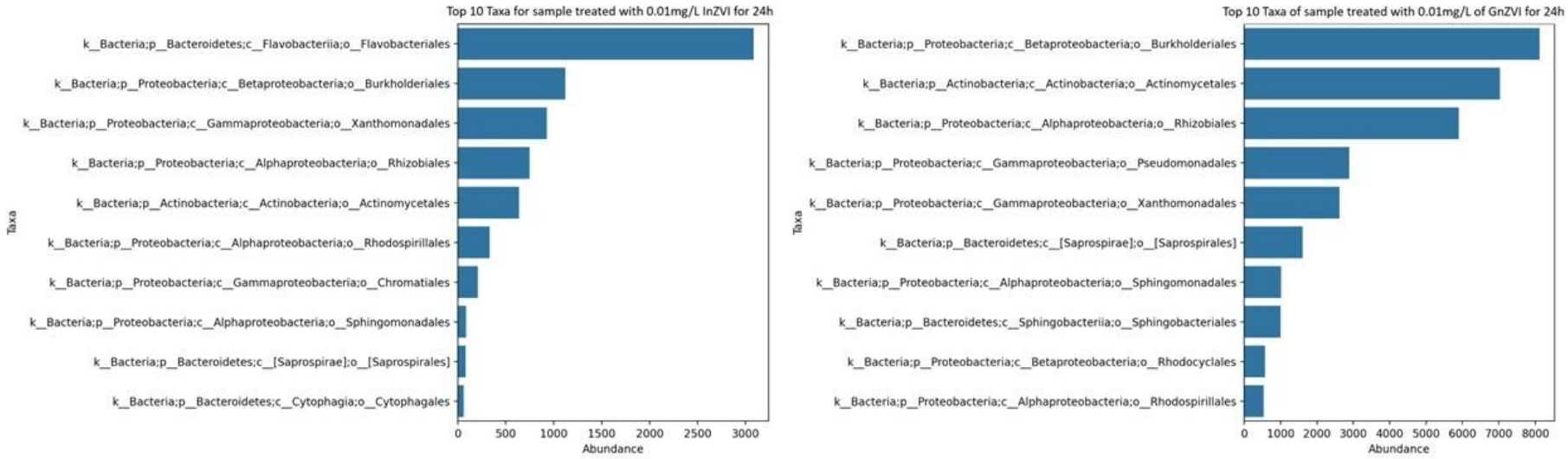

Figure 4.23 Comparison of the top 10 microbial taxa distribution between green and industrial nZVI treatments at 24-h exposure for the 0.01 mg/L dosage

while *Betaproteobacteria* remained steady at 1,084 OTUs, and *Flavobacteriia* dropped to 239. At 24 h, *Gammaproteobacteria* was still relatively high (1107), though slightly less than its green counterpart, while *Actinobacteria* noticeably dropped to 445, indicating a reduction in community stability or diversity over time.

4.6 Summary of Findings

This chapter presents a comprehensive overview of the experimental results, covering measurements of contaminated water (Section 4.2), detailed particle characterisation (Section 4.3), TPH removal efficiencies (Section 4.4), and an initial look at microbial community dynamics (Section 4.5). Taken together, these findings confirm that both green and industrial nZVI can lower hydrocarbon concentrations effectively, indicated by substantial declines in TPH and changes in COD values at various doses and contact times.

A notable point in the particle characterization is the discrepancy between XRD and SEM findings for green nZVI. While XRD peak broadening suggested smaller crystallite sizes, the SEM images showed relatively larger, agglomerated particles. This difference stems primarily from post-synthesis procedures such as centrifugation and manual grinding, which mask or cluster finer particles, leading to a visible mismatch between crystallite estimates and the final observed morphologies.

Meanwhile, a brief examination of microbial responses revealed distinct patterns for green vs. industrial nZVI. Although lower or moderate doses occasionally showed unexpectedly high efficacy, suggesting that excessive nanoparticle input may not always enhance remediation. Overall, the results outlined in this chapter provide a solid framework for understanding nZVI's remediation capacity and its interaction with microbial communities, paving the way for a more thorough discussion and interpretation of the underlying mechanisms in the next chapter.

Chapter 5 DISCUSSION OF RESULTS

5.1 Overview of Key Findings

The results presented in the previous chapter collectively demonstrate the successful synthesis, characterisation, and application of green nanoscale zero-valent iron (nZVI) for hydrocarbon remediation alongside a parallel assessment of industrial nZVI. The first objective of synthesising and characterising green nZVI by reducing $FeCl_3 \cdot 6H_2O$ with green tea polyphenols was achieved by confirming that green nZVI can be formed under relatively mild conditions. Evidence from SEM, EDS, and XRD confirmed its iron-based core, revealing both similarities (e.g., dominant Fe peaks, organic carbon content) and differences (e.g., broader diffraction peaks compared to industrial nZVI). Although XRD suggested smaller crystallite sizes for green nZVI, the SEM data showed larger, agglomerated particles, mainly due to post-synthesis preparations such as centrifugation and manual grinding. This partially explains the discrepancy between crystallite estimates and the visually observed particle sizes while still affirming that the formation of green nZVI was successfully achieved.

Addressing the second objective, both COD measurements and GC-FID analyses showed considerable reductions in petroleum hydrocarbons following treatment with either green or industrial nZVI. The industrial form generally displayed higher initial removal rates, particularly within the first two hours, while the green nZVI demonstrated increasing efficacy with longer contact time (24 h). Overall, both types of nZVI decreased hydrocarbon concentrations by over 50% in most scenarios, confirming that green nZVI represents a viable alternative to the conventional product, albeit slightly less effective under certain conditions.

The third objective was to evaluate the impact of nZVI treatment on hydrocarbon-degrading bacteria. This was addressed through DNA extractions, targeted 16S-rRNA gene sequencing, and subsequent community analyses. A clear distinction emerged: industrial nZVI tended to reduce microbial abundance over time (OTU counts), while green nZVI was associated with comparatively higher bacterial counts likely due to its plant-derived capping agents. These differences highlight potential synergies between green nZVI and bioremediation. This research identified key bacterial orders and

phyla, highlighted those that are hydrocarbon degraders, and further showed how the dominant microbial taxa respond to these treatments. It also provides comparative insights relative to the untreated baseline ("Blank" CW).

Finally, the fourth objective of developing an integrated remediation strategy that combines green nZVI with bioremediation has been partially addressed by demonstrating that plant-based nZVI fosters a comparatively favourable microbial environment. While the lab-scale findings highlight green nZVI's potential for eco-friendly remediation, additional field validations and scale-up studies are recommended. Such future work would strengthen the practical applicability of green nZVI in various contexts, including the African regions that inspired this research. By establishing a tangible link between nanoparticle synthesis, pollutant removal, and shifts in microbial communities, the chapter's findings provide a robust foundation for building a holistic, sustainable remediation strategy approach.

5.2 Interpreting Physico-Chemical Data

5.2.1 Impact of the baseline pH and conductivity on nZVI Performance

The preliminary result of the contaminated water, most notably its near-neutral pH of 7.3 and relatively high conductivity of 9.7 µS/cm sets the framework conditions within which both green and industrial nZVI must operate. An aqueous acidic pH in the range of 4.5 to 5.5 is widely regarded as the ideal reactivity window for Fe^{0} to prevent the rapid precipitation of passivating Fe^{3+}(oxy)hydroxide crusts that form under alkaline conditions, yet not so acidic as to accelerate bulk dissolution of the metallic core into Fe^{2+} ions (Konadu-Amoah et al., 2022, Chen et al., 2025). Under a controlled environment like the one under which this experiment was carried out would be expected to preserve an ample surface-bound Fe^{0} and Fe^{2+} sites capable of donating electrons to petroleum hydrocarbons, thereby fuelling reductive pathways that ultimately lower both COD and TPH. The substantial hydrocarbon removal observed across all nZVI doses particularly the sharp drop in COD from 179 mg/L to as low as 19.8 mg/L after 24 h with industrial nZVI confirms that the pH was not high enough to

suppress reactivity through instantaneous oxide scaling, nor low enough to consume the particles by acid-driven corrosion before they could act on the contaminants.

Conductivity adds a second layer of nuance because any value approaching 10 µS/cm implies a background ionic strength on the order of 0.02 mol/l, typical of brackish groundwaters or produced waters, and such an electrolyte load can markedly influence nZVI fate (Light et al., 2005, Černík et al., 2019). Elevated ionic strength reduces the electrostatic repulsion that usually keeps freshly synthesised iron nanoparticles in suspension, promoting aggregation into micron-scale clusters (Zhang, 2014). For industrial particles that depend mainly on proprietary passivation for stability, this phenomenon likely accounts for the dose response anomaly where the lowest dose (0.004 mg/L) occasionally surpassed higher amounts, meaning that as particle concentrations rise, the chances of collision and irreversible flocculation also increase, thereby shrinking the total reactive surface area available per unit iron (Bae et al., 2018). The green nZVI, in contrast, carries an organic corona of green-tea polyphenols (Du et al., 2022). These macromolecules impart a combination of steric hindrance and mild electrostatic charge that retards salt-induced aggregation, enabling a greater fraction of the iron surface to remain colloidally accessible even in the face of strong electrolyte screening (Nadagouda et al., 2010).

High conductivity also signals the presence of specific anions capable of competing with hydrocarbons for iron-bound electrons or directly altering corrosion pathways (Aragaw et al., 2021). Chloride, for example, can both accelerate zero valent iron corrosion and facilitate electron transfer to organochlorines, sulphate can form surface $FeSO_4$ layers, and bicarbonate favours carbonate armouring (Mundra and Provis, 2021). Although the present contamination consisted mainly of diesel-range aliphatic and aromatics, the combination of chloride and bicarbonate typical of aquifer waters may still have influenced reaction kinetics by periodically stripping or thinning oxide films, thus renewing fresh Fe^0 surfaces. Such periodic self-cleaning would align with the sustained TPH removal observed over 24 h, despite the aggregated morphology visible in SEM micrographs.

The interplay between pH and conductivity becomes more complex when considering the divergent microbial outcomes reported in Section 4.5, particularly because the microbial assays were conducted in a nutrient-broth amended matrix rather than the broth-free aqueous system used in the batch oxidation experiments. Adding nutrient broth substantially alters the chemistry of the system: the mixture introduces buffering agents, peptides, and mineral salts that elevate baseline conductivity and stabilise pH, reducing the rapid acidification or alkalinisation normally associated with Fe^0 corrosion. As a result, the microbial cultures experienced a more buffered, nutrient-rich, and ionically strengthened environment, meaning that changes in pH and conductivity during these assays reflect a combined response to both nanoparticle activity and broth chemistry rather than nanoparticle effects alone.

Within this modified environment, industrial nZVI still caused a reduction in total bacterial counts. Drawing from Aciego Pietri and Brookes (2008), localised pH spikes from Fe^{2+} hydrolysis and short-lived reactive oxygen species may still occur at the nanoparticle surface, and these microscale stressors can inhibit cells even when the bulk solution is buffered. In contrast, green nZVI stimulated bacterial proliferation reaching populations four times higher than the control after 24 h because its polyphenol shell moderates Fe^0 water electron exchange, dampening micro-pH gradients and limiting radical flux (Zagoskina et al., 2023). The polyphenols also act as reductants and carbon substrates that fast-growing heterotrophs, many of them hydrocarbon degraders, can utilise (Belščak-Cvitanović et al., 2018). The buffered near-neutral pH created by the broth allows these taxa to metabolise without acid or alkaline stress, while the elevated ionic strength mimics conditions in many petroleum-impacted aquifers, favouring salt-tolerant degraders such as Burkholderiales and Rhizobiales groups enriched in the 16S rRNA dataset (Abou Khalil et al., 2021). Literature further supports these interpretations: PHam and Waite (2008) observed optimal Fe^0 reactivity at pH 6–8, and Devatha et al. (2016) showed that green-synthesised iron maintains over 80% reactivity at higher conductivities where bare iron rapidly loses performance. Similarly, Guan et al. (2015) noted that chloride-rich waters sustain prolonged iron corrosion and electron flux, but only when particle aggregation is

controlled, underscoring the role of the polyphenol coating in maintaining dispersion in nutrient-rich, conductive environments.

5.2.2 Examining Phenolic values and the effects on the yield and production of green nZVI

The markedly higher phenolic content of green-tea extract (3.09 mg/L) carries important synthetic and mechanistic implications to produce green iron nanoparticles. Polyphenols such as catechins and gallic acid function as potent reductants, rapidly donating electrons to Fe^{3+} and thereby accelerating conversion to zerovalent iron (Fe^{o})(Anesini et al., 2008, Jacqueline, 2013). They simultaneously adsorb to nascent particle surfaces, conferring steric and electrostatic stabilisation that curbs uncontrolled growth and aggregation (Ngo et al., 2014, Mareedu et al., 2021). Consequently, a higher total phenolic concentration generally leads to a greater yield of discrete, reactive nanoparticles, shorter nucleation times, and a narrower size distribution compared to extracts containing fewer reducing fractions (Huang et al., 2014, Rakhmawaty eddy et al., 2022). Studies using green-tea polyphenols routinely report zero valent iron yields exceeding 80% and particle diameters below 50 nm, whereas lower-phenolic matrices, such as citrus peels, often produce mixed Fe^{o}/Fe^{3+} phases or larger, poorly capped aggregates (Mystrioti et al., 2016, Mareedu et al., 2021).

These trends are consistent with the outcome of this research, the green-tea–derived nZVI retained appreciable reactivity despite the elevated conductivity of the water, a performance that can be attributed to the dense organic corona supplied by abundant polyphenols. By contrast, the black-tea and orange-peel extracts, whose phenolic levels were approximately 17% and 65% lower, respectively, would be expected to yield fewer zero valent iron nuclei and weaker surface passivation, thereby reducing overall nZVI yield and long-term stability (Huang et al., 2014). In practical terms, selecting a plant source with a high total phenolic index not only enhances the efficiency of iron reduction but also improves the quality, yield and reactivity of the resulting nanoparticles, ultimately boosting the effectiveness of green nZVI–based remediation.

Green tea stands out among botanical reductants due to its exceptionally high catechin content, which comprises up to 30% of the leaf's dry mass and features multiple ortho-hydroxyl groups that provide strong reducing power(standard redox potentials near –0.46 V) and robust metal-binding capacity (Huang et al., 2014, Wang et al., 2014). The extract is readily water-soluble, inexpensive, and requires no organic solvents or elevated temperatures, aligning well with green-chemistry principles. A combination of high intrinsic phenolic content, ease of extraction, and strong capping efficacy makes green tea a preferred feedstock for synthesising high-yield, highly reactive, and environmentally benign nZVI suitable for large-scale hydrocarbon-remediation applications.

5.2.3 Comparing Characteristics of Green and Industrial nZVI (XRD, SEM and EDS)

In Chapter 4, the various characterisation techniques create an understanding of both industrial and green nanoscale zero-valent iron. X-ray diffraction reveals that the industrial material exhibits sharp reflections at $2\theta \approx 44.7°$ and 65°, which are characteristic of the (110) and (200) planes of α-Fe. In contrast, the green formulation shows broader peaks at the same angles, indicating smaller crystallite domains (Scherrer length ≈ 20–30 nm). Secondly, the Energy-Dispersive X-ray spectroscopy (EDS) supports the phase identifications where the industrial nZVI comprises about 75 wt% Fe with minimal oxygen and adventitious carbon, while the green nZVI sample contains 84 wt% Fe, but with a slightly lower carbon content and trace chloride, suggesting polyphenol capping and residual $FeCl_3$.

Scanning-electron micrographs, however, reveal an apparent contradiction. Instead of the below 50 nm primary particles implied by broad peaks on the XRD, the green nZVI appears to have a size ranging between 50–90 nm, irregular-shaped and aggregated particles, larger than the 30–45 nm particle size range and fine, well-defined spherical clusters typical of the industrial analogue. This disparity is common in green-synthesised systems and arises from post-synthesis handling. In this particular case, high-speed centrifugation causes small crystallites to form dense pellets, subsequent oven-drying promotes neck growth between particles, and manual grinding and fracturing lead to fused floccules that SEM resolves as one object rather than discrete nanocrystals. Moreover, Badmus

et al. (2018) and Alnaddaf et al. (2021) have confirmed that the science behind such agglomeration is due to the polyphenol itself forming adhesive interparticle bridges through hydrogen bonding and π–π stacking, which encourages secondary agglomeration once the solvent is removed.

Morphology directly affects how well iron nanoparticles react. Contaminants attach and receive electrons only on bare iron surfaces, so very small crystals work best, provided they do not agglomerate. The polyphenol coating in green nZVI protects the iron from rusting (Stefaniuk et al., 2016, Fahmy et al., 2018). Yet the larger lumps seen in the SEM image still reduce the total surface area available to react and reduce hydrocarbons. This trade-off explains why green nZVI matched industrial removal efficiencies only after extended contact times: its high intrinsic reactivity (small primary domains) is balanced by slower mass transfer through the aggregate network. Conversely, the industrial particles exhibit sharper XRD peaks and appear more compact in SEM, reflecting well-controlled synthesis and minimal organic coating. Their cleaner, more uniform surfaces provide abundant active sites at early time points, driving the faster 2-hour TPH reductions reported in the results of this experiment.

Previous work further corroborates that particle size of nZVI are first-order controls on electron-transfer rates and, and by extension, on hydrocarbon removal in soil and water. Batch syntheses that throttle the $NaBH_4$ feed to generate 20–30 nm spheres show two to three-fold faster first-order rate constants for TPH removal than identical iron masses produced at 80–100 nm (Eljamal et al., 2018) A similar trend appears in column studies by Karthick et al. (2019), where diesel–water emulsions were flushed with surfactant-stabilised Fe^0 foams. Particles held at 35 nm achieved 92% diesel recovery, whereas agglomerates exceeding 90 nm plateaued at about 60 %. These findings match our observation that the logic behind industrial material (30–45 nm by SEM, sharp XRD peaks) outperforms its green counterpart for the first 2 h of treatment.

Research on morphology impacts indicates that core-shell nZVI embedded in mesoporous silica maintained a substantial reactive surface after months of storage, successfully eliminating 86% of

mixed PAHs from spiked soil within 24 h. In contrast, bare particles of the same diameter exhibited passivation days (Chen et al., 2018). In a similar manner, an integrated SRB–nZVI system showed that the size of particles influenced the equilibrium between abiotic iron reduction and biotic sulphate reduction, which in turn affected the final BTEX concentrations (Dong et al., 2019). The synthesised green nZVI, despite a Scherrer crystallite length of about 15 nm, appeared in 50–90 nm clusters after centrifugation and mortaring; such secondary agglomeration lowers the external zero valent iron surface area available for chemisorption, which explains its delayed early-stage kinetics. The behaviour confirms reports that polyphenol-capped iron from rice-husk extract delivers over 90% diesel removal only when freeze-dried to avoid cake formation (Nalweyiso et al., 2025).

Comparable discrepancies between XRD- and SEM-derived sizes have also been reported in tea-, coffee-, and eucalyptus-capped iron systems, where Scherrer estimates of 10–20 nm contrast with TEM/SEM agglomerates of 60–100 nm (Rajkumar et al., 2021). Another experiment by Afsheen et al. (2018) compared the physical characteristics of mango leaves, rose leaves, neem leaves and carom seeds, noticed a deviation of the XRD peaks from the SEM images, which estimated the size of synthesised iron nanoparticles to as high as 10µm. These authors also attributed the divergence to drying-induced sintering and to the presence of polyphenolic matrices that collapse around the iron core. The present findings therefore reinforce the consensus that green synthetic routes produce structurally fine but practically aggregated iron nanoparticles whose performance hinges on the balance between surface passivation, organic stabilisation, and hydrodynamic dispersion. Future optimisation should focus on milder solvent-exchange or freeze-drying protocols, as well as on in-situ application strategies that avoid complete drying, thereby retaining the high specific surface area suggested by XRD and maximising field-scale remediation efficiency.

5.3 Comparing TPH removal efficiencies of Industrial and Green nZVI

5.3.1 Chemical Oxygen Demand

The COD data in Chapter 4 reveal three clear patterns. First, the untreated control showed only a marginal decline from 179 mg/L at 2 h to 172 mg/L at 24 h, confirming that natural attenuation within the test window was negligible. Second, the addition of industrial nZVI drove COD to 112 mg/L (0.004 mg/L), 214 mg/L (0.01 mg/L) and 59 mg/L (0.02 mg/L) after 2 h; after 24 h, the same doses had fallen to 67 mg/L, 22mg/L and 20 mg/L, respectively, yielding 61–88 % removal. Third, green nZVI achieved more modest but still substantial decreases of 24–49 % after 2 h and 49-68 % by 24 h.

A similar correlation between COD figures and TPH levels has been reported for refinery and produced-water effluents treated with zero-valent iron nanoparticles. Rasheed et al. (2011) found that reducing COD from 250 mg/L to less than 80 mg/L using 0.5 g/L of nZVI coincided with a 70 % loss of diesel-range hydrocarbons, while an oily-water study that combined nZVI with hydrogen peroxide (H_2O_2) achieved 76% COD and 82% TPH removal within 6 hours (Haneef et al., 2020). The industrial nZVI results fall squarely within the upper range of published efficiencies, confirming that highly crystalline, narrowly distributed zero valent iron nanoparticles accelerate both bulk oxygen demand and specific hydrocarbon destruction. The green nZVI figures, though 10–20% lower, still align with another plant-mediated system summarised in the recent comprehensive review by Mahmoud et al. (2020), which attributes the modest short-term lag to the steric barrier imposed by polyphenol capping.

Two noticeable deviations from the dose–response result interpretation. First, the 0.01 mg/L industrial dose showed an abnormal COD increase to 214 mg/L at 2 h before plunging to 22 mg/L at 24 h. A plausible explanation is that the higher iron mass produced an initial burst of soluble Fe^{2+} and low-molecular-weight organics (e.g., aldehydes) through partial oxidation of hydrocarbons; these transient intermediates momentarily raise oxygen demand before being mineralised during the longer contact period. A similar rebound was documented in an ultrasound-assisted nZVI study where COD

spiked in the first hour due to rapid Fe corrosion, then fell steadily as Fenton-like reactions progressed (Rasheed et al., 2011). Secondly, the lowest dose in both formulations happens to deliver the highest percentage of removal. Rate-controlling models show that, beyond a critical particle concentration, magnetic agglomeration reduces the external zero-valent iron surface area faster than the rate at which new reactive sites are added, hence reducing specific reaction constants (Haneef et al., 2020). This phenomenon is amplified in the green particles by the "sticky" polyphenol corona that encourages secondary clustering.

These findings satisfy one of the research objectives by demonstrating that both industrial and green nZVI reduce the COD and, by inference, the TPH levels too, under ideal water chemistries. They also clarify the first objective by linking higher initial removal by industrial nZVI to its sharper XRD peaks and smaller SEM-visible aggregates.

5.3.2 GC-FID results and evidence of TPH reduction

The chromatographic overlays from Figures 4.6 and 4.7 indicate that untreated contaminated water, which served as a baseline, generated a dense cluster of peaks between 19 and 33 minutes, which are characteristic of diesel-range aliphatic and aromatics (C_{10}–C_{28}). After 24 h of contact with industrial nZVI, these peaks were considerably diminished. The calculated total petroleum hydrocarbons (TPH) decreased from a baseline average of 58 mg/L to 15.7 mg/L for the 0.004 mg/L dose and 20.92 mg/L and 19.66 mg/L for 0.01 mg/L and 0.02 mg/L dosages, respectively, equating to a removal rate of 65–73%. Green nZVI led to a similar, although slightly less, reduction in the diesel envelope. TPH values fell to between 20.9 mg/L and 25.0 mg/L (56–64 % removal) after 24 h. At the 2-hour mark, the distinctions were more noticeable, industrial doses removed 56 - 67% of TPH, while green nZVI achieved only 37 – 45%.

A notable deviation from the dose–response result was that the lowest iron dose (0.004 mg/L) yielded the highest TPH removal for both formulations at 24 h and is generally explained by inter-particle magnetic attraction: once iron concentration exceeds a critical threshold, agglomeration diminishes

the external Fe^{o} surface area faster than additional mass can compensate. The effect is sharper for green nZVI because polyphenol molecules create inter-particle hydrogen bonds, accelerating clustering during drying and re-suspension. This is not an isolated case, as previous papers have shown that this can happen. Similar dose-optimisation studies have confirmed the counter-intuitive pattern observed in this research, where removal efficiency peaks at a relatively low nZVI loading and then drops as the dosage is increased. Galdames et al. (2020) reported that diesel-range TPH abatement in high-salinity water climbed to 72% at 0.02 g/L nZVI but declined when the dose was doubled, attributing the drop to rapid magnetic agglomeration that masked interior Fe^{o} surfaces. In a persulphate-activated nZVI system, Bajagain and Jeong (2021) also found an optimum of 0.2% nZVI; higher concentrations produced larger clusters and only 19–37 % TPH loss. Dose-response inversions have also been documented for other contaminants: Hou et al. (2022) observed maximum Cr(VI) removal at 4 wt% of starch-modified nZVI, with efficiency falling at 6 wt% because particle collisions out-paced dispersion. These precedents support our interpretation that, beyond a critical concentration, additional nZVI no longer increases the reactive surface presented to hydrocarbons; instead, it accelerates agglomeration, limits mass transfer and, in green formulations, intensifies polyphenol-bridge clustering. Thus, explaining why our lowest dose delivered the highest TPH removals.

Despite these reductions, several peaks in the diesel-range envelope (19–33 min retention time) persisted with only minimal decline following exposure to both nZVI types. These refractory peaks likely correspond to branched alkanes, alkylated aromatics, or heavier polycyclic compounds that degrade more slowly under abiotic electron-transfer conditions (Pál et al., 1998). The persistence of these peaks underscores a crucial implication for field applications, meaning nZVI alone may not entirely mineralise all TPH fractions, and complex hydrocarbon mixtures might necessitate sequential treatments such as integrating nZVI with biostimulation, surfactant flushing, or mild oxidants to target the more recalcitrant molecular species (Semerad et al., 2020b). This finding supports studies

advocating hybrid nanobioremediation approaches to enhance the removal of heavier or substituted hydrocarbons (Bhatt et al., 2022, Gul et al., 2022).

Recent green iron studies consistently report very high petroleum-hydrocarbon treatments. Murgueitio et al. (2018) reported synthesising 5–10 nm green nZVI from *mortiño-berry* and successfully removed 88% of TPH from water and 82% from heavily contaminated soil within 32 h. Iheme et al. (2025) achieved over 96% PAH and TPH removal from diesel-impacted soil with iron oxide nanoparticles synthesised with *Diodella sarmentosa*; Nalweyiso et al. (2025) recorded about 94 % diesel extraction from water using green nZVI synthesised from Cape-gooseberry; and (Shanker et al., 2017) photodegraded 70–90% of priority PAHs in soil and water with *Sapindus*-based iron-hexacyanoferrate nanocatalysts. Together, they all corroborate the central premise of this research, that plant-mediated iron nanomaterials can rival, or even surpass, conventional reagents in hydrocarbon remediation.

5.4 Microbial Community Dynamics

5.4.1 Identified Microbial Taxa

A survey of Operational Taxonomic Units (OTUs) detailed in Section 4.5 shows that the microbial profile of the water samples mirrors that of many oil-impacted aquatic environments: Proteobacteria was predominant with 64 %, with Bacteroidetes 18 % and Actinobacteria 14 % forming the next most abundant phyla, while minor fractions of Planctomycetes and *Verrucomicrobia* are also present**.** Embedded within these groups are well-documented hydrocarbonoclastic bacteria (HCB) specialist taxa that can use alkanes, aromatics or PAHs as their sole carbon and energy source. The subsequent paragraphs highlight those HCB lineages, summarising their preferred hydrocarbon substrates and the environmental niches in which they are most active.

Extremely halophilic archaea belonging to the *Euryarchaeota* (class *Halobacteria*, order *Halobacteriales*) are well documented for their capacity to oxidise mid to long-chain alkanes (C_{10}-C_{34}) and several low-molecular-weight aromatics such as benzene, toluene, naphthalene and

phenanthrene (Oren, 2017). Known to thrive in hypersaline systems, salt-marsh brines, saltern crystallisers and high-salinity oil reservoirs, these organisms exploit robust membrane adaptations and salt-tolerant redox enzymes to attack hydrocarbons that few bacteria can metabolise under comparable conditions (Xu et al., 2018).

Within the phylum Actinobacteria, members of the order *Actinomycetales* (notably *Rhodococcus* and *Mycobacterium*) are classic hydrocarbon degraders. Thanks to versatile mono- and dioxygenase suites, they oxidise straight and branched alkanes, cycloalkanes and recalcitrant polycyclic aromatic hydrocarbons (PAHs) (Liu and Liu, 2013, Barka et al., 2016). These high-GC Gram-positives are ubiquitous in soils, industrial sludge and marine sediments, where their wax-rich cell envelopes give them a competitive edge at oil-contaminated sites and in surfactant-poor environments, contributing to the late-stage mineralisation of lighter aromatics (Mohammadipanah and Dehhaghi, 2017, Thi Mo et al., 2022).

The phylum *Proteobacteria* hosts the widest taxonomic spread of hydrocarbon degraders. In *Alphaproteobacteria*, orders *Rhodobacterales* and *Sphingomonadales* excel at aerobic PAH attack; species of *Rhodobacter* and *Sphingomonas/SpHingobium* are frequent first responders in coastal spills and aerated wastewater plants, where they initiate ring-hydroxylation of phenanthrene, fluorene and related compounds (Coenye, 2013, Kertesz et al., 2017). *Betaproteobacteria*, particularly the *Burkholderiales* and *Rhodocyclales*, bridge alkane and aromatic niches: *Burkholderia spp*. mineralise C_5–C_{16} alkanes as well as BTEX compounds in soils, groundwater and refinery effluent, while *Rhodocyclus* partners often thrive in nutrient-rich sediments (Coenye, 2013, Sarkar et al., 2017, Morya et al., 2020).

Anaerobic niches are dominated by *Deltaproteobacteria* such as the sulphate-reducing orders *Desulfovibrionales* and *Desulfuromonadales*. These organisms oxidise alkanes and select PAHs in the absence of oxygen, coupling hydrocarbon degradation to sulphate or iron reduction in deep oil reservoirs and anoxic estuarine muds (Davidova et al., 2018, Zhang et al., 2024).

Finally, *Gammaproteobacteri*a contain the best-known obligate hydrocarbonoclastic bacteria: *Pseudomonadales* (e.g., *Pseudomonas*, versatile for alkanes and PAHs) and *Oceanospirillales* (e.g., *Alcanivorax*, *Oleispira*), which flourish at open-ocean spill sites where they catabolise n-alkanes, cycloalkanes and lighter PAHs under fully aerobic, marine conditions (Gutierrez, 2017, Gutierrez, 2019, Kiamarsi et al., 2019).

Together, these phylogenetic groups illustrate how hydrocarbon chemistry and habitat chemistry intersect. Each lineage specialises in the compound classes and physicochemical settings that best match its enzymatic repertoire and ecological strategy.

5.4.2 Overall Population Response to Industrial versus Green nZVI

After examining individual taxa, it would be very important to know how the two iron formulations influence the size of the entire microbial community over time and across doses**.** Table 4.5 provides the raw counts, while Figures 4.16 (population vs. time) and 4.27 (population vs. dosage) translate those numbers into trends. These three data sets show whether each nZVI type stimulates, suppresses, or selectively enriches biomass, and thus whether it sets the stage for or undermines a nanobioremediation strategy that relies on the combined action of nanoparticles and living degraders.

For the Industrial nZVI, at the two-hour mark, the three Industrial nZVI samples treated with 0.004mg/L, 0.01mg/L and 0.02mg/L still hover around the untreated baseline (average 9,200 OTUs vs. 9,578 OTUs in the control), but by 24 h, all doses caused the population to slip to 6,500–7,900 cells. A net loss of roughly 25 %. Literature reports that freshly dispersed, uncoated nZVI releases a short-lived burst of reactive oxygen species that can oxidise membrane lipids and DNA and temporarily suppress biomass (Jang et al., 2014, Semerad et al., 2020a). Our data matches that pattern because the steep early TPH decline recorded for Industrial nZVI coincides with flat or falling cell numbers, and no subsequent rebound is seen within the first day. Because the three doses show almost identical population trajectories, toxicity rather than nutrient limitation appears to be the governing factor; once a threshold particle concentration is reached, additional iron offers little biological benefit and

may even accelerate aggregation, reducing the reactive surface but not the oxidative stress (Lefevre et al., 2016). In practical terms, the industrial nZVI acts as a rapid chemical shock that strips hydrocarbons at the expense of short-term microbial vitality with an antagonistic interaction that could slow the bioremediation stage of the overall process.

On the other hand, the green nZVI behaved in the opposite way. After only 2 h, the total cells jumps from the baseline of 9,510 to 16,900 cells on average, and after 24 h, they triple again to an average of 34,000 cells. Polyphenol capping moderates the initial radical flux and supplies organics that can chelate Fe^{2+}/Fe^{3+}, damping toxicity while leaking trace iron and phenolic carbon that bacteria can exploit (Cook, 2009). The box plots in Figure 4.18 show an interesting crossover. At 2 h, higher green nZVI doses of 0.01 mg/L and 0.02 mg/L support the largest populations, yet by 24 h, the lowest dose of 0.004 mg/L yields the peak count of 36,900 cells. A similar scenario, where moderate iron promotes growth but excess particles begin to agglomerate or regenerate reactive oxygen species, was reported in sandy-loam soils and aquatic microcosms (Castaño et al., 2021). The green system, therefore, exhibits a genuine synergy of a slow, extended release of reactive iron that keeps driving abiotic oxidation while simultaneously enlarging the living consortium that can complete biodegradation.

The statistical inferences presented in Chapter 4 provide numerical support for the population trends described above. In that section, compared with the control, the industrial formulation produced a borderline outcome of $t = -2.52$, with a corresponding p-value of 0.013, signalling a tendency for overall biomass to decline yet falling just short of conventional significance. When this probability is interpreted beside the raw counts in Table 4.6, where total cells drop by roughly 25% within twenty-four hours and the trajectories in Figures 4.17 and 4.18, the trend is consistent: the rapid burst of reactive oxygen generated by bare, highly crystalline iron removes hydrocarbons efficiently at first, but it also comes at a measurable biological cost. Because the p-value hovers on the threshold, a larger replicate set or a water matrix with slightly different buffering capacity would likely push the result

past the 95% confidence line, underscoring the need to dose industrial nZVI cautiously if the remediation plan depends on a vigorous biodegradative finishing stage.

By contrast, the green formulation yields a statistically unambiguous shift with a t-statistic of 3.89, a p-value of 0.012, and a two-to-three-fold rise in cell numbers over the same twenty-four-hour window. The polyphenol coating mutes the initial radical shock and supplies trace organics and chelated iron, so the resident community expands rather than contracts. This outcome directly advances the research's objective of determining how nZVI treatments influence the abundance and activity of hydrocarbon-degrading bacteria by confirming that a plant-capped formulation can actually stimulate the indigenous consortium.

The direct comparison of the two nanoparticle types is even more decisive. A t-statistic value of –4.15 and a p-value of 0.002 quantify a pronounced ecological divergence that mirrors their different synthesis routes and surface chemistries. These statistics, therefore, strengthen the causal chain linking particle design to microbial response and, ultimately, to remediation performance. In doing so, they satisfy the final research objective of developing an integrated remediation approach in which green nZVI works hand-in-glove with biological degradation and highlight why the greener formulation is the more suitable choice when swift chemical abatement must be balanced with long-term biological resilience.

5.4.3 Microbial Taxa Responses to Green and Industrial nZVI Treatments

The untreated control sample (Blank CW) showed that *Flavobacteriia* had 2,536 OTUs (26.4% of the total 9,913 OTUs), *Betaproteobacteria* with 1,916 OTUs (19.9%), *Alphaproteobacteria* had 1,080 (11.2%), and *Actinobacteria* showed 1,028 OTUs (10.7%) were the dominant bacterial groups. These taxa represent a typical freshwater microbial community, rich in generalist heterotrophs and early colonizers (Miller et al., 2019). Upon nZVI treatment, especially with green formulations, there was a notable shift away from this baseline profile.

For green nZVI treatments, a trend of time-dependent microbial stimulation was evident. After 24 h of exposure to 0.004 mg/L green nZVI, *Betaproteobacteria* rose to 3,306 OTUs (30.6% of 10,804 OTUs) and *Gammaproteobacteria* reached 2,454 OTUs (22.7%), while *Flavobacteriia* dropped dramatically to 181 (1.7%). This trend was consistent at higher dosages. For instance, at 0.02 mg/L green nZVI, *Actinobacteria* surged to 4,953 (17.9% of 27,681 OTUs) and *Saprospirae* reached 1,674 OTUs (6%), while *Flavobacteriia* was reduced to zero. These findings indicate that green nZVI selectively promotes hydrocarbon-degrading taxa while suppressing others, likely due to its gradual release of reactive iron and polyphenol capping agents that buffer oxidative stress. Such controlled stimulation aligns with earlier studies, such as Haider et al. (2024), which reported the biocompatibility of plant-extract-mediated iron nanoparticles in promoting microbial consortia capable of degrading aromatic hydrocarbons.

In contrast, industrial nZVI yielded more immediate yet volatile effects. After 2 h at a 0.02 mg/L dosage, *Actinobacteria* peaked at 1,833 OTUs (21.3% of 8,621 OTUs), but dropped to 1,020 OTUs (13.3% of 7,330 OTUs) after 24 h, indicating short-term microbial stimulation followed by suppression. *Flavobacteriia* barely changed from 239 OTUs (2.8%) to 204 (2.8%), showing inconsistent responses. This trend supports previous findings by Phenrat et al. (2009) and Semerád and Cajthaml (2016), who reported initial microbial inhibition by industrial nZVI due to reactive oxygen species (ROS) formation and metal toxicity.

Crucially, these divergent trends between green and industrial nZVI buttress the ecological implications of nanoparticle formulation. Green nZVI not only maintained or enhanced key hydrocarbon-degrading taxa (e.g., *Actinobacteria, Saprospirae, Gammaproteobacteria*) but also preserved community diversity over time. These results directly support the third objective of this thesis, which was to assess how nZVI treatments impact the abundance and function of hydrocarbon-degrading bacteria.

Furthermore, the prolonged viability and enrichment of specific microbial orders under green nZVI treatments support the concept of nanobioremediation, where nanoparticles and native microbial metabolism work synergistically to degrade pollutants. This was particularly evident in samples where *Actinobacteria* and *Saprospirae* dominated after 24 h exposure, indicating sustained microbial activity rather than oxidative stress. This aligns with work by Gul et al. (2022), who observed that low-to-moderate doses of green-synthesised nZVI facilitated microbial growth and hydrocarbon degradation in complex water matrices.

5.5 What are the implications of these results on nanobioremediation?

The contrast between the two formulations is unequivocal. Industrial nZVI acts as a single-shot chemical oxidant, which reduces hydrocarbons almost instantly, but the accompanying burst of reactive oxygen species depresses microbial abundance and can delay the biological finishing step. Green nZVI, by contrast, functions as a slow-release catalyst. Its polyphenol shell meters out soluble Fe^{2+}/Fe^{3+}, scavenges excess radicals and supplies trace organics, so biomass and diversity rise in tandem with continuing hydrocarbon decay. Nowhere is this synergy clearer than at the 0.004 mg/L dose, where the community expands threefold and the 24-hour TPH removal peaks at 73 %. Proof that a moderate, organically capped iron loading maximises cooperation between abiotic oxidation and microbial metabolism.

These findings translate directly into practical design guidance for field-scale remediation. The taxa-level shifts observed in this study reveal whether nZVI initiates a productive nanobioremediation trajectory, where abiotic oxidation is followed by sustained biological degradation, or whether it risks undermining microbial resilience. Green nZVI consistently promoted stable, functionally relevant consortia, enabling continued hydrocarbon breakdown beyond the first 24 h. This behaviour can be highly advantageous in real aquifers and surface waters, where hydrocarbons desorb slowly from sediments. By contrast, industrial nZVI, despite its rapid initial chemical knock-down, tended to suppress biomass, indicating that in situ it may delay the biological “polishing” phase unless doses are carefully constrained.

These contrasting outcomes provide a basis for tailoring nZVI use to contaminant class and site conditions. A low-to-moderate dose of green nZVI offers the best balance of speed, effectiveness and ecological safety: it avoids the toxicity and passivation issues associated with bare iron, conserves indigenous biodiversity and accelerates recovery, all essential for sustainable remediation. This dose window also maintains the activity of key hydrocarbon degraders such as *Actinomycetales* and *Burkholderiale*s, making it particularly suited for diesel-range aliphatics and mid-weight aromatics. In scenarios where rapid chemical abatement of more labile fractions is required, higher industrial nZVI doses may still be justified, provided that biological recovery is not rate-limiting.

A staged or hybrid approach is also feasible, for example, applying a low green nZVI pre-dose to reduce toxicity and partially oxidise aromatic rings, followed by nutrient or oxygen management to stimulate taxa capable of degrading heavier PAHs. This strategy aligns with dose-optimisation studies showing that maximal removal and maximal microbial enrichment tend to occur at intermediate nZVI loadings, because excessive particle concentrations promote agglomeration and oxidative stress without adding useful reactive surface area (Zhao et al., 2020). Ultimately, the population shifts demonstrated in this work are not merely descriptive, they define which degradation pathways are being activated and show how nZVI dosing, formulation, and contact time can be engineered to strategically target the petroleum fractions of greatest concern in field applications.

These interpretations now set the stage for the final chapters. Because it has been established where and why the green formulation outperforms its industrial counterpart and under what boundary conditions, the forthcoming conclusions section will distil clear recommendations on optimal dosing, contact times and potential post-treatments. Likewise, the demonstrated synergy between slow-release iron and microbial resurgence provides a concrete rationale for the recommendations chapter to explore staged or combined nano-bioremediation strategies and guidelines for monitoring microbial health during field deployment.

5.6 Summary of the Discussion

This chapter has traced the storyline that began with the raw data from the previous chapter and has followed it through a series of interpretive lenses. It first showed that the baseline water chemistry (pH 7.3, 9.7 µS/cm) framed how zero-valent iron would corrode and how radicals would form. It then linked the high polyphenol content of green tea extract to the successful synthesis of a capped nZVI, whose crystallinity, surface chemistry, and aggregate size diverged sharply from those of its industrial counterpart. Turning to performance metrics, the results demonstrated, through COD, GC-FID and Scherrer-derived crystallite estimates, that both irons degrade diesel-range hydrocarbons, but along different kinetic paths: the industrial nZVI particles deliver a fast chemical pulse, whereas the green particles dispense a slower, sustained reactivity. Finally, the microbial population counts, and t-tests revealed that these kinetic differences cascade into contrasting ecological outcomes: temporary biomass loss in the industrial system versus pronounced biomass gains in the green.

This discussion chapter has addressed all the primary data from the results chapter. Post-synthetic grinding and polyphenol coatings now explain the apparent mismatch between XRD-predicted crystallite size and SEM-observed clusters; the counter-intuitive dose-response results in TPH removal are accounted for by radical overshoot at high iron loadings; and the statistical evidence clarifies why green nZVI, though slower at first, ultimately creates the most favourable conditions for long-term biodegradation. In summary, each experimental observation has been translated into a mechanistic insight that fulfils the study's stated aims: to compare green and industrial nZVI at the physicochemical level, to assess how those differences play out in hydrocarbon removal, and to understand what they mean for the resident microbiota.

Chapter 6 CONCLUSION

6.1 Chapter overview

This final chapter brings the thesis to a close by distilling the evidence and interpretations presented in Chapters four (results) and five (discussion of results) into a concise set of take-home messages and forward-looking insights. The overarching aim of this research was to determine whether a green-synthesised nanoscale zero-valent iron (nZVI), produced with polyphenols from green-tea extract, could match or surpass the remediation performance of conventional industrial nZVI while imposing fewer ecological consequences. To test this aim, a series of bench-scale experiments compared the two formulations in hydrocarbon-contaminated water, tracking physicochemical behaviour, total petroleum hydrocarbon (TPH) and chemical oxygen demand (COD) removal, and the response of indigenous microbial communities over 2 and 24-hour intervals.

The results chapter reports the findings from comparing particle characterization, contaminant removal charts, and population counts. The discussion of the results chapter interprets these data, explaining why the slower iron release of green nZVI fosters a larger, functionally relevant biomass, whereas the industrial particles act as a rapid but biologically disruptive oxidant.

This chapter will serve four purposes. First, it will recap the principal results in the order of the original research objectives; second, it will state the novel contributions of those results to both scientific knowledge and remediation practice; third, it will acknowledge the study's limitations and outline promising directions for future work; and lastly, it will offer concise, actionable guidance for stakeholders interested in sustainable nanobioremediation. By the end of this chapter, an integrated view of what was achieved, why it matters for environmental sustainability, and how the insights can be translated into field implementation and further research will be clearly outlined.

6.2 Experimental findings and correlation with research objectives

The experimental programme covered the whole journey from green tea-mediated nanoparticle synthesis through to hydrocarbon removal and microbial response. Each stage generated data that

answered one or more of the four objectives set out at the start of the study. What follows restates those key outcomes in the same logical order, demonstrating how the evidence chain advances the aims of the project and underpins the sustainable-remediation narrative developed in the preceding chapters.

Using green-tea extract that contained 3.09 mg/L of polyphenols, ferric chloride was reduced at room temperature to form a dark suspension of organically capped iron nanoparticles. X-ray diffraction revealed broad α-Fe^{o} reflections corresponding to an average crystallite diameter of roughly 12 nm, while a scanning-electron microscope image showed ragged aggregates between 50 and 90 nm. Energy-dispersive X-ray spectroscopy confirmed an Iron-Carbon-Oxygen surface chemistry with trace chloride, verifying that polyphenolic ligands had adhered to and partially oxidised the particle surface. Taken together, these observations satisfy this research's first objective by demonstrating that a low-energy, solvent-free process can yield a reactive zerovalent iron core whose coating limits uncontrolled agglomeration and distinguishes it from the sharply crystalline, 30–45 nm industrial material used as a benchmark.

Following that, triplicate 100 mL contaminated water samples were dosed with 0.004, 0.01 and 0.02 mg/L of either green or industrial nZVI and monitored for chemical-oxygen demand and total-petroleum-hydrocarbon concentrations. The industrial formulation removed 56–67% of hydrocarbons within two hours and levelled off at 66–73% by 24 h. The green particles, in contrast, achieved only 37–45% removal at the two-hour mark but rose to 56–64% by the end of the day, with the single best result of 73% occurring at the lowest industrial nZVI dose of 0.004 mg/L. These kinetics fulfil the research's second objective by showing that the bio-derived material has the potential to reach the same end-point performance as the proprietary powder while relying on a gentler, more sustained release of reactive iron.

DNA extraction followed by 16S-rRNA amplicon sequencing did more than measure total biomass; it also revealed which organisms were present. The untreated water was dominated by *Proteobacteria*,

Bacteroidetes and *Actinobacteria*, with orders such as *Burkholderiales, Rhizobiales, Actinomycetales* and *Flavobacteriales*, all lineages that harbour ring-hydroxylating and ring-cleaving dioxygenases needed for petroleum breakdown. Exposure to the two iron formulations drove these communities in opposite directions. Industrial nZVI caused a 25% fall in overall cell numbers after 24 h ($t = -2.52$, $p \approx 0.013$) and modestly depleted several of the putative degraders, consistent with short-lived oxidative stress. Green nZVI, by contrast, tripled the total population in the same period ($t = 3.89$, $p \approx 0.012$) and selectively enriched the key hydrocarbon-oxidising orders listed above. The direct green versus industrial comparison was highly significant ($t = -4.15$, $p \approx 0.002$), confirming that particle coating and release kinetics dictate whether native degraders are suppressed or stimulated. Thus, the third objective is satisfied on two fronts: the sequencing work identified a resident guild capable of hydrocarbon mineralisation, and the dosing experiments showed that a plant-based nZVI complements rather than hinders its abundance and potential activity.

When the chemical and biological findings are viewed together, a coherent operational picture emerges. A low-to-mid dose of green nZVI (0.004–0.01 mg/L per 100 mL sample) delivers substantial contaminant removal, the greatest increase in biomass and the most favourable statistics. Because the particles continue to leak soluble iron without overwhelming the system with reactive oxygen, they create conditions that allow native degraders to complete the oxidation sequence once the fastest abiotic reactions taper off. These results meet the last objective of providing a data-driven blueprint for a staged remediation train: deploy a moderate load of green nZVI for immediate chemical knock-down, then, if necessary, follow with targeted nutrient or electron-acceptor additions so that physicochemical and biological processes work in tandem rather than in conflict. Collectively, these findings verify that eco-designed iron nanoparticles can achieve high contaminant removal while safeguarding (and even enhancing) microbial functions that underpin long-term site recovery.

6.3 Research's Contribution to Knowledge

Previous works have largely been confined to review articles or single-formulation studies that test a particular industrial or plant-based nZVI against one class of contaminant. By directly comparing green

nZVI with its commercial/industrial counterpart, this research is the first to show a clear, dose-dependent synergy between polyphenol coatings and microbial oxidation: moderate green-nZVI loads stimulate biomass and accelerate late-stage TPH loss, whereas bare iron at the same dose suppresses it. Together, these findings move the field from isolated case studies toward a comparative, mechanism-based understanding of nano-bioremediation.

From a design standpoint, the data establishes a practical dosing envelope of 0.004–0.01 mg/L of green nZVI per 100 mL of diesel-contaminated water, coupled with a contact-time guideline of 24 h to reach 64% TPH removal while tripling microbial abundance. Industrial nZVI can still be helpful for rapid knock-down, but only at tightly controlled exposures and with a subsequent recovery period. These empirically derived parameters translate laboratory insights into a window of opportunity for pilot-scale testing, information that has been notably absent from previous green-nanoparticle studies and can be standardised and integrated directly into batch-reactor, fixed-bed, or permeable-reactive-barrier designs to achieve large-scale remediation solutions.

This research advances several United Nations Sustainable Development Goals, most prominently SDG 6 (Clean Water and Sanitation) and SDG 15 (Life on Land). By replacing borohydride-reduced iron with a bio-synthesised, polyphenol-capped alternative, the process eliminates hazardous reductants, lowers overall iron demand and sharply reduces secondary chemical inputs. Equally important is that the green particles enhance rather than suppress native microbial diversity, thus safeguarding the ecological services that underpin long-term water-body recovery. In practical terms, the study shows that high remediation performance and biodiversity conservation are not mutually exclusive; they can be achieved simultaneously when nanomaterials are sourced from renewable biomass and delivered at ecologically informed doses.

6.4 Limitations of this Study

This research was intentionally framed as a laboratory-scale proof-of-concept, and that focus imposes several constraints on the breadth and immediate field readiness of the findings.

1. **Scale and hydrodynamics –**

All experiments were conducted on specific 100 mL volumes with gentle orbital mixing. Such conditions eliminate the pore-scale heterogeneities, advective fluxes and competing electron acceptors that shape nZVI behaviour in aquifers or permeable-reactive barriers. Field reviews consistently report that hydraulic short-circuiting, preferential flow and ageing of iron surfaces can undermine the high removal rates observed in batch systems (Plessl et al., 2023, Chen and Qian, 2024, Ying et al., 2022). Until the current dosing envelope (0.004–0.01 mg/L per 100 mL) is validated in column tests or pilot trenches, extrapolation to real sites is still considered tentative.

2. **Discrepancy in Particle Size values between XRD results and SEM images –**

The XRD image and analysis indicated sub-50 nm crystallites, whereas SEM shows 50–90 nm agglomerates. As stated previously, this mismatch is largely attributed to post-synthesis handling; centrifugation, oven-drying and manual mortar-and-pestle grinding, which promotes particle fusion and yields coarse aggregates that obscure the primary nanoscale domains.

3. **Single-matrix chemistry-**

The contaminated water used here had a near-neutral pH of 7.28 and a conductivity of 9.7 µS/cm. Variables such as carbonate alkalinity, silicate, humic acids and competing oxidants are known to accelerate passivation or aggregation of nZVI and to modulate microbial stress responses (Lefevre et al., 2016). An additional limitation stems from the introduction of nutrient broth into the samples used for microbial community analysis. The broth, which contains peptides, amino acids, phosphate buffers and trace salts, altered the native chemistry of the contaminated water by increasing ionic strength and slightly elevating pH relative to the batch oxidation systems, together, these chemistry changes

mean that the microbial-response experiments did not operate under the same physicochemical conditions as the COD/TPH batch tests, limiting one-to-one comparability.

4. **Experimental time frame (24h window) -**

This study tracked reactions only for 24 h. This is not enough time to determine long-term impacts like iron ageing, secondary mineral formation, and microbial succession, which often dictate whether field systems plateau or rebound.

5. **Polyphenol variability and dose quantification -**

Green nZVI was generated from a single batch of green-tea extract with 3.09 mg/L total phenolics. Yet polyphenol yields vary by cultivation, harvest season and extraction protocol; other authors note batch-to-batch iron yields that differ by an order of magnitude (rakhmawaty eddy et al., 2022, Rodríguez-Rasero et al., 2024, Gupta et al., 2023a). Because the final Fe^{o} mass was back-calculated from the starting salt, not measured post-synthesis, the exact concentration of reactive iron in each green dose carries ±10–15% uncertainty, whereas the industrial material was weighed directly. Future work should adopt a rapid Fe^{2+}/Fe^{0} titration to normalise green and industrial doses on an equal-iron basis.

6. **Functional-gene resolution -**

Although 16S-rRNA amplicon sequencing revealed shifts in total biomass and in putative hydrocarbon-degrading orders, this study did not go into the details of quantifying alkB, PAH-dioxygenase or *rdhA* genes directly. This was mainly due to funding constraints. Several studies warn that community composition alone may over- or under-predict degradation capacity if horizontal-gene transfer or plasmid loss that have occurred under iron stress (Lefevre et al., 2016, Chernikova et al., 2020). qPCR tracking of key catabolic loci would strengthen causal links between particle dose, microbial function and contaminant fate.

Despite these caveats, the results from this study are optimistic. Many authors highlight the green-synthesis route as one of the most promising paths toward sustainable in-situ remediation, provided that issues of batch consistency, ageing and hydraulic delivery are systematically addressed (Abdelfatah et al., 2021, Wang et al., 2023). By highlighting the practical limits and quantifying the ecological upside, this research offers a realistic springboard for the scale-up and standardisation efforts that must follow.

6.5 Recommendations for Future Work

The laboratory findings have shown that polyphenol-capped nZVI can remove hydrocarbons efficiently while supporting microbial growth, yet several knowledge gaps remain before the technology is ready for large-scale deployment. The following targeted studies would bridge those gaps and translate the present proof-of-concept into a robust field practice.

1. **Improve synthesis procedure to bridge gap between SEM and XRD results** - To narrow the gap between the two techniques, future work should comminute the dried powder with a precision ball mill or planetary grinder, producing a uniformly micronized dust that better isolates individual nZVI particles for SEM imaging.
2. **Run small-scale field pilots under contrasting site chemistries** - test green and industrial nZVI in aquifers or test cells that span low- to high-salinity and acidic-to-alkaline pH ranges.
3. **Extend monitoring windows beyond 30 days** - track iron phase transformations, aggregation, and successive waves of microbial colonisation to confirm long-term stability and degradation performance.
4. **Add functional "omics" diagnostics** - quantify expression of key hydrocarbon-catabolic genes and transcripts (e.g., *alkB*, *pahE*, and *rdhA*) to verify that population shifts correspond to real metabolic activity.

5. **Carry out a cradle-to-grave life-cycle assessment (LCA)** - compare the environmental and economic costs of producing, transporting and disposing of green versus industrial nZVI, including solvent use, energy demand and potential ecotoxicity.

6. **Explore alternative agro-waste extracts for polyphenol content** - evaluate fruit peels, spent coffee grounds, or leaf litter as low-cost, high-consistency feedstocks to scale green-nZVI synthesis without competing with food resources.

If green nZVI is to transition from a promising laboratory material to an accepted standard of sustainable remediation, its synthesis and deployment protocols must be standardised in a manner that regulators and practitioners can readily reproduce. This requires a harmonised set of quality-assurance metrics like total phenolic titre of the extract, Fe^{o} content per litre of suspension, allowable ranges for zeta potential and particle size, as well as step-by-step guidance on dosing, delivery hydraulics, and post-treatment monitoring. Embedding these benchmarks into national water-quality regulations, ISO/ASTM test methods, and corporate sustainability frameworks would provide stakeholders with the confidence that a bio-based iron technology can deliver reliable performance while aligning with environmental-protection policies and circular-economy goals.

6.6 Final Remarks

This research demonstrates that a polyphenol-capped, plant-derived zerovalent iron can deliver petroleum-hydrocarbon reductions on par with its industrial counterpart, with the added advantage of tripling microbial abundance and preserving community diversity, clear proof that cutting-edge nanotechnology and ecological integrity need not be opposing goals.

Translating fundamental particle-surface chemistry into dose windows, contact-time targets, and gene-level monitoring checkpoints supplies a field-ready blueprint for engineers and regulators seeking remediation tools that satisfy performance metrics and biodiversity mandates. In doing so, it affirms that the next generation of environmental technologies can integrate green synthesis, circular-economy feedstocks, and systems-level biological insight into a single, coherent design philosophy.

References

ABBASIAN, F., LOCKINGTON, R., MALLAVARAPU, M. & NAIDU, R. 2015. A Comprehensive Review of Aliphatic Hydrocarbon Biodegradation by Bacteria. *Applied biochemistry and biotechnology,* 176.

ABDEL-SHAFY, H. & MANSOUR, M. 2019. Microbial Degradation of Hydrocarbons in the Environment: An Overview.

ABDELBASIR, S. M., MCCOURT, K. M., LEE, C. M. & VANEGAS, D. C. 2020. Waste-Derived Nanoparticles: Synthesis Approaches, Environmental Applications, and Sustainability Considerations. *Front Chem,* 8**,** 782.

ABDELFATAH, A. M., FAWZY, M., ELTAWEIL, A. S. & EL-KHOULY, M. E. 2021. Green Synthesis of Nano-Zero-Valent Iron Using Ricinus Communis Seeds Extract: Characterization and Application in the Treatment of Methylene Blue-Polluted Water. *ACS Omega,* 6**,** 25397-25411.

ABOU KHALIL, C., PRINCE, V. L., PRINCE, R. C., GREER, C. W., LEE, K., ZHANG, B. & BOUFADEL, M. C. 2021. Occurrence and biodegradation of hydrocarbons at high salinities. *Science of The Total Environment,* 762**,** 143165.

ABUZEID, H. M., JULIEN, C. M., ZHU, L. & HASHEM, A. M. 2023. Green Synthesis of Nanoparticles and Their Energy Storage, Environmental, and Biomedical Applications. *Crystals,* 13**,** 1576.

ACIEGO PIETRI, J. C. & BROOKES, P. C. 2008. Relationships between soil pH and microbial properties in a UK arable soil. *Soil Biology and Biochemistry,* 40**,** 1856-1861.

ADAMS, G., TAWARI-FUFEYIN, P., OKORO, S. & EHINOMEN, I. 2015. Bioremediation, Biostimulation and Bioaugmention: A Review. *International Journal of Environmental Bioremediation and Biodegradation,* 3**,** 28-39.

ADEOYE, A. 2022. A Review of the Petroleum Hydrocarbons Contamination of Soil, Water and Air and the Available Remediation Techniques, Taking into Consideration the Sustainable Development Goals. *Earthline Journal of Chemical Sciences***,** 97-113.

AFSHEEN, S., TAHIR, M. B., IQBAL, T., LIAQAT, A. & ABRAR, M. 2018. Green synthesis and characterization of novel iron particles by using different extracts. *Journal of Alloys and Compounds,* 732**,** 935-944.

AHMED, S., AHMAD, M., SWAMI, B. L. & IKRAM, S. 2016. A review on plants extract mediated synthesis of silver nanoparticles for antimicrobial applications: A green expertise. *Journal of Advanced Research,* 7**,** 17-28.

AKHTAR, N. & MANNAN, M. A.-U. 2020. Mycoremediation: Expunging environmental pollutants. *Biotechnology Reports,* 26**,** e00452.

AKPASI, S., ANEKWE, I., TETTEH, E., AMUNE, U., SHOYIGA, H., MAHLANGU, T. & KIAMBI, S. 2023. Mycoremediation as a Potentially Promising Technology: Current Status and Prospects—A Review. *Applied Sciences,* 13**,** 4978.

ALEGBELEYE, O. O., OPEOLU, B. O. & JACKSON, V. A. 2017. Polycyclic Aromatic Hydrocarbons: A Critical Review of Environmental Occurrence and Bioremediation. *Environmental Management,* 60**,** 758-783.

ALI, A., ZAFAR, H., ZIA, M., UL HAQ, I., PHULL, A. R., ALI, J. S. & HUSSAIN, A. 2016. Synthesis, characterization, applications, and challenges of iron oxide nanoparticles. *Nanotechnol Sci Appl,* 9**,** 49-67.

ALNADDAF, L. M., ALMUHAMMADY, A. K., SALEM, K. F. M., ALLOOSH, M. T., SALEH, M. M. & AL-KHAYRI, J. M. 2021. Green Synthesis of Nanoparticles Using Different Plant Extracts and Their Characterizations. *In:* AL-KHAYRI, J. M., ANSARI, M. I. & SINGH, A. K. (eds.) *Nanobiotechnology : Mitigation of Abiotic Stress in Plants*. Cham: Springer International Publishing.

AMBAYE, T. G., CHEBBI, A., FORMICOLA, F., PRASAD, S., GOMEZ, F. H., FRANZETTI, A. & VACCARI, M. 2022. Remediation of soil polluted with petroleum hydrocarbons and its

reuse for agriculture: Recent progress, challenges, and perspectives. *ChemospHere,* 293**,** 133572.

ANESINI, C., FERRARO, G. E. & FILIP, R. 2008. Total polyphenol content and antioxidant capacity of commercially available tea (*Camellia sinensis*) in Argentina. *J Agric Food Chem,* 56**,** 9225-9.

ANSARI, A. A., NAEEM, M., GILL, S. S. & ALZUAIBR, F. M. 2020. PHytoremediation of contaminated waters: An eco-friendly technology based on aquatic macropHytes application. *Egyptian Journal of Aquatic Research,* 46**,** 371-376.

APARICIO, J. D., RAIMONDO, E. E., SAEZ, J. M., COSTA-GUTIERREZ, S. B., ÁLVAREZ, A., BENIMELI, C. S. & POLTI, M. A. 2022. The current approach to soil remediation: A review of physicochemical and biological technologies, and the potential of their strategic combination. *Journal of Environmental Chemical Engineering,* 10**,** 107141.

ARAGAW, T. A., BOGALE, F. M. & ARAGAW, B. A. 2021. Iron-based nanoparticles in wastewater treatment: A review on synthesis methods, applications, and removal mechanisms. *Journal of Saudi Chemical Society,* 25**,** 101280.

BABUPONNUSAMI, A. & MUTHUKUMAR, K. 2014. A review on Fenton and improvements to the Fenton process for wastewater treatment. *Journal of Environmental Chemical Engineering,* 2**,** 557-572.

BADMUS, K. O., COETSEE-HUGO, E., SWART, H. & PETRIK, L. 2018. Synthesis and characterisation of stable and efficient nano zero valent iron. *Environmental Science and Pollution Research,* 25**,** 23667-23684.

BAE, S., COLLINS, R. N., WAITE, T. D. & HANNA, K. 2018. Advances in Surface Passivation of Nanoscale Zerovalent Iron: A Critical Review. *Environmental Science & Technology,* 52**,** 12010-12025.

BAJAGAIN, R. & JEONG, S.-W. 2021. Degradation of petroleum hydrocarbons in soil via advanced oxidation process using peroxymonosulphate activated by nanoscale zero-valent iron. *ChemospHere,* 270**,** 128627.

BANERJEE, A., ROY, A., DUTTA, S. & MONDAL, S. 2016. BIOREMEDIATION OF HYDROCARBON – A REVIEW. *International Journal of Advanced Research,* 4**,** 1303-1313.

BANERJEE, M., MUKHERJEE, S. & MUKHERJEE, S. 2022. 7 - Facets of nanoparticle-microbe interactions and their roles in nanobioremediation of environmental pollutants: Biochemical, molecular, and technological perspectives. *In:* IQBAL, H. M. N., BILAL, M. & NGUYEN, T. A. (eds.) *Nano-Bioremediation : Fundamentals and Applications*. Elsevier.

BARKA, E. A., VATSA, P., SANCHEZ, L., GAVEAU-VAILLANT, N., JACQUARD, C., MEIER-KOLTHOFF, J. P., KLENK, H. P., CLÉMENT, C., OUHDOUCH, Y. & VAN WEZEL, G. P. 2016. Taxonomy, PHysiology, and Natural Products of Actinobacteria. *Microbiol Mol Biol Rev,* 80**,** 1-43.

BARRON, M. G., VIVIAN, D. N., HEINTZ, R. A. & YIM, U. H. 2020. Long-Term Ecological Impacts from Oil Spills: Comparison of Exxon Valdez, Hebei Spirit, and Deepwater Horizon. *Environ Sci Technol,* 54**,** 6456-6467.

BARZAN, E., MEHRABIAN, S. & IRIAN, S. 2014. Antimicrobial and Genotoxicity Effects of Zero-valent Iron Nanoparticles. *Jundishapur J Microbiol,* 7**,** e10054.

BASHIR, I., LONE, F. A., BHAT, R. A., MIR, S. A., DAR, Z. A. & DAR, S. A. 2020a. Concerns and Threats of Contamination on Aquatic Ecosystems. *Bioremediation and Biotechnology***,** 1-26.

BASHIR, M., ALI, S. & FARRUKH, M. A. 2020b. Green Synthesis of Fe2O3 Nanoparticles from Orange Peel Extract and a Study of Its Antibacterial Activity. *Journal of the Korean Physical Society,* 76**,** 848-854.

BELŠČAK-CVITANOVIĆ, A., DURGO, K., HUĐEK, A., BAČUN-DRUŽINA, V. & KOMES, D. 2018. 1 - Overview of polyphenols and their properties. *In:* GALANAKIS, C. M. (ed.) *Polyphenols: Properties, Recovery, and Applications*. Woodhead Publishing.

BHARALI, A., DEKA, B., SAHU, B. P. & LALOO, D. 2023. Major challenges and probable scientific solutions toward the large-scale production of plant-based metallic nanoparticles: a systematic review. *Nanotechnology for Environmental Engineering,* 8**,** 933-941.

BHARDWAJ, B., SINGH, P., KUMAR, A., KUMAR, S. & BUDHWAR, V. 2020. Eco-Friendly Greener Synthesis of Nanoparticles. *Adv PHarm Bull,* 10**,** 566-576.

BHAT, M. A., GEDIK, K. & GAGA, E. O. 2023. Chapter 23 - Environmental impacts of nanoparticles: pros, cons, and future prospects. *In:* OZTURK, M., ROY, A., BHAT, R. A., VARDAR-SUKAN, F. & POLICARPO TONELLI, F. M. (eds.) *Synthesis of Bionanomaterials for Biomedical Applications*. Elsevier.

BHATT, P., PANDEY, S. C., JOSHI, S., CHAUDHARY, P., PATHAK, V. M., HUANG, Y., WU, X., ZHOU, Z. & CHEN, S. 2022. Nanobioremediation: A sustainable approach for the removal of toxic pollutants from the environment. *Journal of Hazardous Materials,* 427**,** 128033.

BOJES, H. K. & POPE, P. G. 2007. Characterization of EPA's 16 priority pollutant polycyclic aromatic hydrocarbons (PAHs) in tank bottom solids and associated contaminated soils at oil exploration and production sites in Texas. *Regulatory Toxicology and PHarmacology,* 47**,** 288-295.

BORA, B., KAUSER, H. & GEED, S. R. 2025. Bioremediation strategies for xenobiotic degradation in petroleum-impacted industrial ecosystems: Practical challenges and future directions. *Journal of Water Process Engineering,* 70**,** 106877.

BORJA, J., NGO, M. A. S., SARANGLAO, C. C., TIONGCO, R. P. M., ROQUE, E. & DUGOS, N. 2015. Synthesis of green zero-valent iron using polyphenols from dried green tea extract. 10**,** 22-31.

BRODERICK, J. B. 1999. Catechol dioxygenases. *Essays Biochem,* 34**,** 173-89.

BUARKI, F., ABUHASSAN, H., HANNAN, F. & HENARI, F. 2022. Green Synthesis of Iron Oxide Nanoparticles Using Hibiscus rosa sinensis Flowers and Their Antibacterial Activity. *Journal of Nanotechnology,* 2022**,** 1-6.

CAKIR, E., SEVGILI, C. & FISKIN, R. 2021. An analysis of severity of oil spill caused by vessel accidents. *Transportation Research Part D: Transport and Environment,* 90**,** 102662.

CAO, B., NAGARAJAN, K. & LOH, K.-C. 2009. Biodegradation of aromatic compounds: Current status and opportunities for biomolecular approaches. *Applied Microbiology and Biotechnology,* 85**,** 207-28.

CAPORASO, J. G., KUCZYNSKI, J., STOMBAUGH, J., BITTINGER, K., BUSHMAN, F. D., COSTELLO, E. K., FIERER, N., PEÑA, A. G., GOODRICH, J. K., GORDON, J. I., HUTTLEY, G. A., KELLEY, S. T., KNIGHTS, D., KOENIG, J. E., LEY, R. E., LOZUPONE, C. A., MCDONALD, D., MUEGGE, B. D., PIRRUNG, M., REEDER, J., SEVINSKY, J. R., TURNBAUGH, P. J., WALTERS, W. A., WIDMANN, J., YATSUNENKO, T., ZANEVELD, J. & KNIGHT, R. 2010. QIIME allows analysis of high-throughput community sequencing data. *Nat Methods,* 7**,** 335-6.

CAPORASO, J. G., LAUBER, C. L., WALTERS, W. A., BERG-LYONS, D., HUNTLEY, J., FIERER, N., OWENS, S. M., BETLEY, J., FRASER, L., BAUER, M., GORMLEY, N., GILBERT, J. A., SMITH, G. & KNIGHT, R. 2012. Ultra-high-throughput microbial community analysis on the Illumina HiSeq and MiSeq platforms. *The ISME Journal,* 6**,** 1621-1624.

CAPPADONA, V. *Can wastewater treatment plants cope with future nanoparticle loading scenarios?* http://purl.org/coar/resource_type/c_db06.

CASTAÑO, A., PROSENKOV, A., BARAGAÑO, D., OTAEGUI, N., SASTRE, H., RODRÍGUEZ-VALDÉS, E., GALLEGO, J. L. R. & PELÁEZ, A. I. 2021. Effects of in situ Remediation With Nanoscale Zero Valence Iron on the Physicochemical Conditions and Bacterial Communities of Groundwater Contaminated With Arsenic. *Frontiers in Microbiology,* 12.

ČERNÍK, M., NOSEK, J., FILIP, J., HRABAL, J., ELLIOTT, D. W. & ZBOŘIL, R. 2019. Electric-field enhanced reactivity and migration of iron nanoparticles with implications for groundwater treatment technologies: Proof of concept. *Water Research,* 154**,** 361-369.

CHANG, M. C., SHU, H. Y., HSIEH, W. P. & WANG, M. C. 2005. Using nanoscale zero-valent iron for the remediation of polycyclic aromatic hydrocarbons contaminated soil. *J Air Waste Manag Assoc,* 55**,** 1200-7.

CHEMERYS, A., PELLETIER, E., CRUAUD, C., MARTIN, F., VIOLET, F. & JOUANNEAU, Y. 2014. Characterization of Novel Polycyclic Aromatic Hydrocarbon Dioxygenases from the Bacterial Metagenomic DNA of a Contaminated Soil. *Applied and Environmental Microbiology,* 80**,** 6591-6600.

CHEN, A., WANG, H., ZHAN, X., GONG, K., XIE, W., LIANG, W., ZHANG, W. & PENG, C. 2024. Applications and synergistic degradation mechanisms of nZVI-modified biochar for the remediation of organic polluted soil and water: A review. *Science of The Total Environment,* 911**,** 168548.

CHEN, H., LIU, Y., YAN, T., WANG, Q., JIN, N., WANG, X., LIU, X., ZHAO, Y., FENG, Y., LUO, H. & LI, W. 2025. Iron complexes synthesized from FeOCl with carboxylic acid based ligands as Fenton-like catalysts for the highly efficient degradation of organic dyes over a wide pH range. *Colloids and Surfaces A: Physicochemical and Engineering Aspects,* 705**,** 135697.

CHEN, H. & QIAN, L. 2024. Performance of field demonstration nanoscale zero-valent iron in groundwater remediation: A review. *Science of The Total Environment,* 912**,** 169268.

CHEN, S., BEDIA, J., LI, H., REN, L. Y., NALUSWATA, F. & BELVER, C. 2018. Nanoscale zero-valent iron@mesoporous hydrated silica core-shell particles with enhanced dispersibility, transportability and degradation of chlorinated aliphatic hydrocarbons. *Chemical Engineering Journal,* 343**,** 619-628.

CHERNIKOVA, T. N., BARGIELA, R., TOSHCHAKOV, S. V., SHIVARAMAN, V., LUNEV, E. A., YAKIMOV, M. M., THOMAS, D. N. & GOLYSHIN, P. N. 2020. Hydrocarbon-Degrading Bacteria Alcanivorax and Marinobacter Associated With Microalgae Pavlova lutheri and Nannochloropsis oculata. *Frontiers in Microbiology,* 11.

CHIKERE, C. B., OKPOKWASILI, G. C. & CHIKERE, B. O. 2011. Monitoring of microbial hydrocarbon remediation in the soil. *3 Biotech,* 1**,** 117-138.

CHUANG, F. W., LARSON, R. A. & WESSMAN, M. S. 1995. Zerovalent Iron-Promoted Dechlorination of Polychlorinated Biphenyls. *Environ. Sci. Technol.,* 29**,** 2463.

CHUNYAN, X., QARIA, M. A., QI, X. & DAOCHEN, Z. 2023. The role of microorganisms in petroleum degradation: Current development and prospects. *Science of The Total Environment,* 865**,** 161112.

CIAMPI, P., ZEPPILLI, M., LORINI, L., VILLANO, M., ESPOSITO, C., NIELSEN, C., LEDDA, L., OLIVIERI, S. & PETRANGELI PAPINI, M. 2024. Coupling Physical and Chemical-Biological Techniques for the Remediation of Contaminated Soils and Groundwater. *In:* ORTEGA-CALVO, J. J. & COULON, F. (eds.) *Soil Remediation Science and Technology*. Cham: Springer Nature Switzerland.

CLAUSER, N. M., FELISSIA, F. F., AREA, M. C. & VALLEJOS, M. E. 2022. Chapter 2 - Technological and economic barriers of industrial-scale production of nanocellulose. *In:* SHANKER, U., HUSSAIN, C. M. & RANI, M. (eds.) *Green Nanomaterials for Industrial Applications*. Elsevier.

COENYE, T. 2013. The Family Burkholderiaceae. *The Prokaryotes: Alphaproteobacteria and Betaproteobacteria***,** 759-776.

COENYE, T. 2014. The Family Burkholderiaceae. *In:* ROSENBERG, E., DELONG, E. F., LORY, S., STACKEBRANDT, E. & THOMPSON, F. (eds.) *The Prokaryotes: Alphaproteobacteria and Betaproteobacteria*. Berlin, Heidelberg: Springer Berlin Heidelberg.

COOK, S. M. 2009. Assessing the Use and Application of Zero-Valent Iron Nanoparticle Technology for Remediation at Contaminated Sites. USEPA: Office of Solid Waste and Emergency Response, Office of Superfund Remediation and Technology Innovation.

CRAMPON, M., JOULIAN, C., OLLIVIER, P., CHARRON, M. & HELLAL, J. 2019. Shift in Natural Groundwater Bacterial Community Structure Due to Zero-Valent Iron Nanoparticles (nZVI). *Frontiers in Microbiology,* 10.

CRANE, R. A. & SCOTT, T. B. 2012. Nanoscale zero-valent iron: Future prospects for an emerging water treatment technology. *Journal of Hazardous Materials,* 211-212**,** 112-125.

CZINNEROVA, M., NGUYEN, N. H. A., NEMECEK, J., MACKENZIE, K., BOOTHMAN, C., LLOYD, J., LASZLO, T., SPANEK, R., CERNIK, M. & SEVCU, A. 2020. In situ pilot application of nZVI embedded in activated carbon for remediation of chlorinated ethene-contaminated groundwater: effect on microbial communities. *Environmental Sciences Europe,* 32**,** 154.

D'ANDREA, M. & REDDY, K. 2014. Crude Oil Spill Exposure and Human Health Risks. *Journal of occupational and environmental medicine / American College of Occupational and Environmental Medicine,* 56**,** 1029-1041.

DAS, N. & CHANDRAN, P. 2011. Microbial degradation of petroleum hydrocarbon contaminants: an overview. *Biotechnol Res Int,* 2011**,** 941810.

DAS, S. & PATRA, C. R. 2021. Chapter 6 - Green synthesis of iron oxide nanoparticles using plant extracts and its biological application. *In:* KHARISOV, B. & KHARISSOVA, O. (eds.) *Handbook of Greener Synthesis of Nanomaterials and Compounds*. Elsevier.

DAVIDOVA, I. A., MARKS, C. R. & SUFLITA, J. M. 2018. Anaerobic Hydrocarbon-Degrading Deltaproteobacteria. *In:* MCGENITY, T. J. (ed.) *Taxonomy, Genomics and EcopHysiology of Hydrocarbon-Degrading Microbes*. Cham: Springer International Publishing.

DENG, Y., YANG, Y. & YANG, T. 2024. Three systems of the oil and gas formation in the world. *Petroleum Research*.

DEPETRIS, P. J., PASQUINI, A. I. & LECOMTE, K. 2014. Chemical Weathering Processes on the Earth's Surface. *In:* DEPETRIS, P. J., PASQUINI, A. I. & LECOMTE, K. L. (eds.) *Weathering and the Riverine Denudation of Continents*. Dordrecht: Springer Netherlands.

DEVATHA, C. P., THALLA, A. K. & KATTE, S. Y. 2016. Green synthesis of iron nanoparticles using different leaf extracts for treatment of domestic waste water. *Journal of Cleaner Production,* 139**,** 1425-1435.

DEVENDRAPANDI, G., LIU, X., BALU, R., AYYAMPERUMAL, R., VALAN ARASU, M., LAVANYA, M., MINNAM REDDY, V. R., KIM, W. K. & KARTHIKA, P. C. 2024. Innovative remediation strategies for persistent organic pollutants in soil and water: A comprehensive review. *Environmental Research,* 249**,** 118404.

DHAKA, A. & CHATTOPADHYAY, P. 2021. A review on physical remediation techniques for treatment of marine oil spills. *Journal of Environmental Management,* 288**,** 112428.

DONG, H., LI, L., LU, Y., CHENG, Y., WANG, Y., NING, Q., WANG, B., ZHANG, L. & ZENG, G. 2019. Integration of nanoscale zero-valent iron and functional anaerobic bacteria for groundwater remediation: A review. *Environment International,* 124**,** 265-277.

DU, C., CHEN, H., GAO, W., SUN, W., PENG, L. & XU, N. 2022. Green Synthesis of Nano-Zero Valence Iron with Green Tea and It's Implication in Lead Removal. *Bulletin of Environmental Contamination and Toxicology,* 110**,** 10.

EBRAHIMINEZHAD, A., ZARE-HOSEINABADI, A., SARMAH, A., TAGHIZADEH, S., YOUNES, G. & BERENJIAN, A. 2018. Plant-Mediated Synthesis and Applications of Iron Nanoparticles. *Molecular Biotechnology,* 60.

EDUOK, S. & COULON, F. 2017. Engineered Nanoparticles in the Environments: Interactions with Microbial Systems and Microbial Activity. *In:* CRAVO-LAUREAU, C., CAGNON, C., LAUGA, B. & DURAN, R. (eds.) *Microbial Ecotoxicology*. Cham: Springer International Publishing.

EL-KHAWAGA, A. M., ZIDAN, A. & EL-MAGEED, A. I. A. A. 2023. Preparation methods of different nanomaterials for various potential applications: A review. *Journal of Molecular Structure,* 1281**,** 135148.

ELGAZALI, A., ALTHALB, H., ELMUSRATI, I., AHMED, H. M. & BANAT, I. M. 2023. Remediation Approaches to Reduce Hydrocarbon Contamination in Petroleum-Polluted Soil. *Microorganisms,* 11.

ELJAMAL, R., ELJAMAL, O., KHALIL, A. M. E., SAHA, B. B. & MATSUNAGA, N. 2018. Improvement of the chemical synthesis efficiency of nano-scale zero-valent iron particles. *Journal of Environmental Chemical Engineering,* 6**,** 4727-4735.

ELJAMAL, R., ELJAMAL, O., MAAMOUN, I., YILMAZ, G. & SUGIHARA, Y. 2020. Enhancing the characteristics and reactivity of nZVI: Polymers effect and mechanisms. *Journal of Molecular Liquids,* 315**,** 113714.

ENSLEY, B. D. & GIBSON, D. T. 1983. Naphthalene dioxygenase: purification and properties of a terminal oxygenase component. *J Bacteriol,* 155**,** 505-11.

FAHMY, H., MOHAMED, F., MARZOUQ, M., BAHAA EL-DIN, A., ALSOUDI, A., ASHOOR, O., MOHAMED, M. & MAHMOUD, F. 2018. Review of Green Methods of Iron Nanoparticles Synthesis and Applications. *BioNanoScience,* 8.

FAJARDO, C., GARCÍA-CANTALEJO, J., BOTÍAS, P., COSTA, G., NANDE, M. & MARTIN, M. 2019. New insights into the impact of nZVI on soil microbial biodiversity and functionality. *J Environ Sci Health A Tox Hazard Subst Environ Eng,* 54**,** 157-167.

FALIH, K. T., MOHD RAZALI, S. F., ABDUL MAULUD, K. N., ABD RAHMAN, N., ABBA, S. I. & YASEEN, Z. M. 2024. Assessment of petroleum contamination in soil, water, and atmosphere: a comprehensive review. *International Journal of Environmental Science and Technology,* 21**,** 8803-8832.

FAN, Y.-Y., LI, B.-B., YANG, Z.-C., CHENG, Y.-Y., LIU, D.-F. & YU, H.-Q. 2018. Abundance and diversity of iron reducing bacteria communities in the sediments of a heavily polluted freshwater lake. *Applied Microbiology and Biotechnology,* 102**,** 10791-10801.

FAZLZADEH, M., RAHMANI, K., ZAREI, A., ABDOALLAHZADEH, H., NASIRI, F. & KHOSRAVI, R. 2017. A novel green synthesis of zero valent iron nanoparticles (NZVI) using three plant extracts and their efficient application for removal of Cr(VI) from aqueous solutions. *Advanced Powder Technology,* 28**,** 122-130.

FUCHS, G., BOLL, M. & HEIDER, J. 2011. Microbial degradation of aromatic compounds — from one strategy to four. *Nature Reviews Microbiology,* 9**,** 803-816.

FURUKAWA, K. & FUJIHARA, H. 2008. Microbial degradation of polychlorinated biphenyls: Biochemical and molecular features. *Journal of Bioscience and Bioengineering,* 105**,** 433-449.

GACEM, M. A. & ABD-ELSALAM, K. A. 2022. Chapter 27 - Strategies for scaling up of green-synthesized nanomaterials: Challenges and future trends. *In:* ABD-ELSALAM, K. A. (ed.) *Green Synthesis of Silver Nanomaterials*. Elsevier.

GALDAMES, A., RUIZ-RUBIO, L., ORUETA, M., SÁNCHEZ-ARZALLUZ, M. & VILAS-VILELA, J. L. 2020. Zero-Valent Iron Nanoparticles for Soil and Groundwater Remediation. *International Journal of Environmental Research and Public Health,* 17**,** 5817.

GARG, R., MITTAL, M., TRIPATHI, S. & EDDY, N. O. 2024. Core to concept: synthesis, structure, and reactivity of nanoscale zero-valent iron (NZVI) for wastewater remediation. *Environmental Science and Pollution Research,* 31**,** 67496-67520.

GAUVRY, E., MATHOT, A.-G., COUVERT, O., LEGUÉRINEL, I. & COROLLER, L. 2021. Effects of temperature, pH and water activity on the growth and the sporulation abilities of Bacillus subtilis BSB1. *International Journal of Food Microbiology,* 337**,** 108915.

GEDDES, J. A. & MURPHY, J. G. 2012. 10 - The science of smog: a chemical understanding of ground level ozone and fine particulate matter. *In:* ZEMAN, F. (ed.) *Metropolitan Sustainability*. Woodhead Publishing.

GHAFFARZADEH, M., KHORJESTAN, R., AFRADI, A., BANDEHPEY, A. & BEHBUDI, G. 2024. Recent advances in synthesis, properties, and applications of nano-zero valent iron: A promising material for environmental remediation. *Synthesis and Sintering,* 4**,** 226-240.

GIRARD, L., LOOD, C., HÖFTE, M., VANDAMME, P., ROKNI-ZADEH, H., VAN NOORT, V., LAVIGNE, R. & DE MOT, R. 2021. The Ever-Expanding Pseudomonas Genus: Description of 43 New Species and Partition of the Pseudomonas putida Group. *Microorganisms,* 9.

GÓMEZ-GIL, L., KUMAR, P., BARRIAULT, D., BOLIN, J. T., SYLVESTRE, M. & ELTIS, L. D. 2007. Characterization of biphenyl dioxygenase of Pandoraea pnomenusa B-356 as a potent polychlorinated biphenyl-degrading enzyme. *J Bacteriol,* 189**,** 5705-15.

GRIEGER, K., HJORTH, R., CARPENTER, A. W., KLAESSIG, F., LEFEVRE, E., GUNSCH, C., SORATANA, K., LANDIS, A. E., WICKSON, F., HRISTOZOV, D. & LINKOV, I. 2019. Sustainable Environmental Remediation Using NZVI by Managing Benefit-Risk Trade-Offs. *In:* PHENRAT, T. & LOWRY, G. V. (eds.) *Nanoscale Zerovalent Iron Particles for Environmental Restoration: From Fundamental Science to Field Scale Engineering Applications*. Cham: Springer International Publishing.

GRIEGER, K. D., FJORDBØGE, A., HARTMANN, N. B., ERIKSSON, E., BJERG, P. L. & BAUN, A. 2010. Environmental benefits and risks of zero-valent iron nanoparticles (nZVI) for in situ remediation: Risk mitigation or trade-off? *Journal of Contaminant Hydrology,* 118**,** 165-183.

GUAN, X., SUN, Y., QIN, H., LI, J., LO, I. M. C., HE, D. & DONG, H. 2015. The limitations of applying zero-valent iron technology in contaminants sequestration and the corresponding countermeasures: The development in zero-valent iron technology in the last two decades (1994–2014). *Water Research,* 75**,** 224-248.

GUERRA, F., ATTIA, M., WHITEHEAD, D. & ALEXIS, F. 2018. Nanotechnology for Environmental Remediation: Materials and Applications. *Molecules,* 23.

GUETTERMAN, T. C. 2019. Basics of statistics for primary care research. *Fam Med Community Health,* 7.

GUL, M. Z., RUPULA, K. & RAO, B. S. 2022. Chapter 45 - Nanobioremediation: a novel application of green-nanotechnology in environmental cleanup. *In:* MALIK, J. A. (ed.) *Microbes and Microbial Biotechnology for Green Remediation.* Elsevier.

GUPTA, D., BOORA, A., THAKUR, A. & GUPTA, T. K. 2023a. Green and sustainable synthesis of nanomaterials: Recent advancements and limitations. *Environmental Research,* 231**,** 116316.

GUPTA, K., SAINI, K. & MATHUR, J. 2023b. Eco-Friendly Synthesis of Iron Nanoparticles Using Green Tea Extract: Characterization and Evaluation of Their Catalytic, Anti-oxidant and Anti-bacterial Potentials. *ChemistrySelect,* 8**,** e202204421.

GUTIERREZ, T. 2017. Aerobic Hydrocarbon-Degrading Gammaproteobacteria: Xanthomonadales. *In:* MCGENITY, T. J. (ed.) *Taxonomy, Genomics and EcopHysiology of Hydrocarbon-Degrading Microbes*. Cham: Springer International Publishing.

GUTIERREZ, T. 2019. Marine, Aerobic Hydrocarbon-Degrading Gammaproteobacteria: Overview. *In:* MCGENITY, T. J. (ed.) *Taxonomy, Genomics and EcopHysiology of Hydrocarbon-Degrading Microbes*. Cham: Springer International Publishing.

HAAS, B. J., GEVERS, D., EARL, A. M., FELDGARDEN, M., WARD, D. V., GIANNOUKOS, G., CIULLA, D., TABBAA, D., HIGHLANDER, S. K., SODERGREN, E., METHÉ, B., DESANTIS, T. Z., PETROSINO, J. F., KNIGHT, R. & BIRREN, B. W. 2011. Chimeric 16S rRNA sequence formation and detection in Sanger and 454-pyrosequenced PCR amplicons. *Genome Res,* 21**,** 494-504.

HAIDER, F. U., ZULFIQAR, U., UL AIN, N., HUSSAIN, S., MAQSOOD, M. F., EJAZ, M., YONG, J. W. H. & LI, Y. 2024. Harnessing plant extracts for eco-friendly synthesis of iron nanoparticle (Fe-NPs): Characterization and their potential applications for ameliorating environmental pollutants. *Ecotoxicology and Environmental Safety,* 281**,** 116620.

HAJIPOUR, M. J., FROMM, K. M., AKBAR ASHKARRAN, A., JIMENEZ DE ABERASTURI, D., LARRAMENDI, I. R. D., ROJO, T., SERPOOSHAN, V., PARAK, W. J. & MAHMOUDI, M. 2012. Antibacterial properties of nanoparticles. *Trends in Biotechnology,* 30**,** 499-511.

HAN, Y., NAMBI, I. M. & PRABHAKAR CLEMENT, T. 2018. Environmental impacts of the Chennai oil spill accident – A case study. *Science of The Total Environment,* 626**,** 795-806.
HANEEF, T., UL MUSTAFA, M. R., RASOOL, K., HO, Y. C. & MOHAMED KUTTY, S. R. 2020. Removal of Polycyclic Aromatic Hydrocarbons in a Heterogeneous Fenton Like Oxidation System Using Nanoscale Zero-Valent Iron as a Catalyst. *Water,* 12**,** 2430.
HANO, C. & ABBASI, B. H. 2021. Plant-Based Green Synthesis of Nanoparticles: Production, Characterization and Applications. *Biomolecules,* 12.
HAO, R., LI, D., ZHANG, J. & JIAO, T. 2021. Green Synthesis of Iron Nanoparticles Using Green Tea and Its Removal of Hexavalent Chromium. *Nanomaterials,* 11**,** 650.
HARUNA, A., TANIMU, G., IBRAHIM, I., GARBA, Z. N., YAHAYA, S. M., MUSA, S. G. & MERICAN, Z. M. A. 2023. Mitigating oil and gas pollutants for a sustainable environment – Critical review and prospects. *Journal of Cleaner Production,* 416**,** 137863.
HAZEN, T. 2009. Biostimulation.
HE, F. & ZHAO, D. 2005. Preparation and Characterization of a New Class of Starch-Stabilized Bimetallic Nanoparticles for Degradation of Chlorinated Hydrocarbons in Water. *Environmental Science & Technology,* 39**,** 3314-3320.
HETTITHANTHRI, O., NGUYEN, T. B. T., FIEDLER, T., PHAN, C., VITHANAGE, M., PALLEWATTA, S., NGUYEN, T. M. L., NGUYEN, P. Q. A. & BOLAN, N. 2024. A review of oil spill dynamics: Statistics, impacts, countermeasures, and weathering behaviors. *Asia-Pacific Journal of Chemical Engineering,* 19**,** e3128.
HONDA, M. & SUZUKI, N. 2020. Toxicities of Polycyclic Aromatic Hydrocarbons for Aquatic Animals. *Int J Environ Res Public Health,* 17.
HOU, J., LI, Y., CI, H., MIAO, L., YOU, G., WU, J. & XU, Y. 2022. Influence of aggregation and sedimentation behavior of bare and modified zero-valent-iron nanoparticles on the Cr(VI) removal under various groundwater chemistry conditions. *ChemospHere,* 296**,** 133905.
HUANG, K.-C. & EHRMAN, S. 2007. Synthesis of Iron Nanoparticles via Chemical Reduction with Palladium Ion Seeds. *Langmuir : the ACS journal of surfaces and colloids,* 23**,** 1419-26.
HUANG, L., WENG, X., CHEN, Z., MEGHARAJ, M. & NAIDU, R. 2014. Green synthesis of iron nanoparticles by various tea extracts: Comparative study of the reactivity. *Spectrochimica Acta Part A: Molecular and Biomolecular Spectroscopy,* 130**,** 295-301.
HUSAIN, S. 2008. Literature overview: Microbial metabolism of high molecular weight polycyclic aromatic hydrocarbons. *Remediation Journal,* 18**,** 131-161.
HUSSAIN, C. M. 2022. *The Handbook of Environmental Remediation Classic and Modern Techniques*.
HUSSEIN, H. S. 2023. The state of the art of nanomaterials and its applications in energy saving. *Bulletin of the National Research Centre,* 47**,** 7.
IBRAHIM, H. M., AWAD, M., AL-FARRAJ, A. S. & AL-TURKI, A. M. 2020. Stability and Dynamic Aggregation of Bare and Stabilized Zero-Valent Iron Nanoparticles under Variable Solution Chemistry. *Nanomaterials (Basel),* 10.
IHEME, C. I., ASIKA, K. E., OLUGBUE, R. C., OKWARAEJESU, V., EZE, V. C., OBASI, U. K., IBEH, R. C., MORAH, A. C., ELEMIKE, E. E., CHIEGBOKA, N. A. & ALISI, C. S. 2025. Environmental remediation of petroleum-hydrocarbon-contaminated Avu mechanic village soil using green-synthesized iron oxide nanoparticles: Advance remediation technology. *Journal of Hazardous Materials Advances,* 17**,** 100566.
IMAM, A., KUMAR SUMAN, S., KANAUJIA, P. K. & RAY, A. 2022. Biological machinery for polycyclic aromatic hydrocarbons degradation: A review. *Bioresource Technology,* 343**,** 126121.
INOUE, K. & NOJIRI, H. 2014. Structure and Function of Aromatic-Ring Hydroxylating Dioxygenase System. *In:* NOJIRI, H., TSUDA, M., FUKUDA, M. & KAMAGATA, Y. (eds.) *Biodegradative Bacteria: How Bacteria Degrade, Survive, Adapt, and Evolve*. Tokyo: Springer Japan.

IQBAL, N., HAYAT, M. T., ZEB, B. S., ABBAS, Z. & AHMED, T. 2019. Chapter 21 - PHytoremediation of Cd-Contaminated Soil and Water. *In:* HASANUZZAMAN, M., PRASAD, M. N. V. & FUJITA, M. (eds.) *Cadmium Toxicity and Tolerance in Plants*. Academic Press.

IRAVANI 2011. Green synthesis of metal nanoparticles using plants. *Green Chemistry,* 13**,** 2638-2650.

ISIBOR, P. O. 2024. Regulations and Policy Considerations for Nanoparticle Safety. *In:* ISIBOR, P. O., DEVI, G. & ENUNEKU, A. A. (eds.) *Environmental Nanotoxicology: Combatting the Minute Contaminants*. Cham: Springer Nature Switzerland.

ISRAEEL, M., IQBAL, J., ABBASI, B. A., IJAZ, S., ULLAH, R., ZARSHAN, F., YASEEN, T., KHAN, G., MURTAZA, G., ALI, I., ALARJANI, K. M., ELSHIKH, M. S., RIZWAN, M., KHAN, S. & IQBAL, R. 2024. Potential biological applications of environment friendly synthesized iron oxide nanoparticles using Sageretia thea root extract. *Scientific Reports,* 14**,** 28310.

JABEEN, S., KHAN, T., JAISWAL, A. & BALA, S. 2024. Green Nanotechnology for Clean Energy and Environmental Sustainability. *In:* UDDIN, I. (ed.) *Sustainable Nanomaterials: Synthesis and Environmental Applications*. Singapore: Springer Nature Singapore.

JACQUELINE, O. S. 2013. *Investigation of Iron Reduction by Green Tea Polyphenols for Application in Soil Remediation*. Masters Masters Theses, University of Connecticut.

JAFARINEJAD, S. 2017. 6 - Treatment of Oily Wastewater. *In:* JAFARINEJAD, S. (ed.) *Petroleum Waste Treatment and Pollution Control*. Butterworth-Heinemann.

JANG, M. H., LIM, M. & HWANG, Y. S. 2014. Potential environmental implications of nanoscale zero-valent iron particles for environmental remediation. *Environ Health Toxicol,* 29**,** e2014022.

JAVED, R., ZIA, M., NAZ, S., AISIDA, S. O., AIN, N. U. & AO, Q. 2020. Role of capping agents in the application of nanoparticles in biomedicine and environmental remediation: recent trends and future prospects. *Journal of Nanobiotechnology,* 18**,** 172.

JAWED, A., SHARMA, S., GOLDER, A. K. & PANDEY, L. M. 2021. Chapter 6 - Plant-polyphenol-mediated synthesis of iron oxide nanomaterials for heavy metal removal: a review. *In:* SHAH, M. P., RODRIGUEZ COUTO, S. & KUMAR, V. (eds.) *New Trends in Removal of Heavy Metals from Industrial Wastewater*. Elsevier.

JI, Y., WANG, Y., WANG, X., LV, C., ZHOU, Q., JIANG, G., YAN, B. & CHEN, L. 2024. Beyond the promise: Exploring the complex interactions of nanoparticles within biological systems. *Journal of Hazardous Materials,* 468**,** 133800.

JIA, S. & KRAFT, K. 2023. Alicyclic Hydrocarbons. *Patty's Toxicology*.

JIA, W., DENG, Z., PAPINI, M. P., CHENG, L., JIN, N., ZHANG, D., LI, Z., ZHANG, D., ZHU, Y. & DING, A. 2025. Long-term response mechanism of bacterial communities to chemical oxidation remediation in petroleum hydrocarbon contaminated groundwater. *Journal of Hazardous Materials,* 488**,** 137239.

JOHN, R. C., ESSIEN, J. P., AKPAN, S. B. & OKPOKWASILI, G. C. 2012. Polycyclic Aromatic Hydrocarbon-degrading Bacteria from Aviation Fuel Spill Site at Ibeno, Nigeria. *Bulletin of Environmental Contamination and Toxicology,* 88**,** 1014-1019.

JOUANNEAU, Y., MARTIN, F., SERGE, K. & WILLISON, J. 2011. *Ring-hydroxylating dioxygenases involved in PAH biodegradation : structure, function, biodiversity*.

JOVANOVIĆ, T., PETROVIĆ, M., KOSTIĆ, M., BOJIC, D. & BOJIĆ, A. 2021. Chemical remediation technologies. *Facta universitatis - series: Physics, Chemistry and Technology,* 19**,** 1-15.

KAFLE, A., TIMILSINA, A., GAUTAM, A., ADHIKARI, K., BHATTARAI, A. & ARYAL, N. 2022. PHytoremediation: Mechanisms, plant selection and enhancement by natural and synthetic agents. *Environmental Advances,* 8**,** 100203.

KARISHMA, S., SARAVANAN, A., DEIVAYANAI, V. C., AJITHKUMAR, U., YAASHIKAA, P. R. & VICKRAM, A. S. 2024. Emerging strategies for enhancing microbial degradation of petroleum hydrocarbons: Prospects and challenges. *Bioresource Technology Reports,* 26**,** 101866.

KARLSSON, A., PARALES, J. V., PARALES, R. E., GIBSON, D. T., EKLUND, H. & RAMASWAMY, S. 2003. Crystal Structure of Naphthalene Dioxygenase: Side-on Binding of Dioxygen to Iron. *Science,* 299**,** 1039-1042.

KARN, B., KUIKEN, T. & OTTO, M. 2011. Nanotechnology and in situ remediation: a review of the benefits and potential risks. *Cien Saude Colet,* 16**,** 165-78.

KARNWAL, A., JASSIM, A. Y., MOHAMMED, A. A., SHARMA, V., AL-TAWAHA, A. & SIVANESAN, I. 2024. Nanotechnology for Healthcare: Plant-Derived Nanoparticles in Disease Treatment and Regenerative Medicine. *PHarmaceuticals (Basel),* 17.

KARTHICK, A., ROY, B. & CHATTOPADHYAY, P. 2019. Comparison of zero-valent iron and iron oxide nanoparticle stabilized alkyl polyglucoside pHospHate foams for remediation of diesel-contaminated soils. *Journal of Environmental Management,* 240**,** 93-107.

KEBEDE, G., TAFESE, T., ABDA, E. M., KAMARAJ, M. & ASSEFA, F. 2021. Factors Influencing the Bacterial Bioremediation of Hydrocarbon Contaminants in the Soil: Mechanisms and Impacts. *Journal of Chemistry,* 2021**,** 9823362.

KEN, D. S. & SINHA, A. 2020. Recent developments in surface modification of nano zero-valent iron (nZVI): Remediation, toxicity and environmental impacts. *Environmental Nanotechnology, Monitoring & Management,* 14**,** 100344.

KERTESZ, M. A., KAWASAKI, A. & STOLZ, A. 2017. Aerobic Hydrocarbon-Degrading Alphaproteobacteria: SpHingomonadales. *In:* MCGENITY, T. J. (ed.) *Taxonomy, Genomics and EcopHysiology of Hydrocarbon-Degrading Microbes*. Cham: Springer International Publishing.

KHADEMIAN, M. & IMLAY, J. A. 2021. How Microbes Evolved to Tolerate Oxygen. *Trends in Microbiology,* 29**,** 428-440.

KHAN, F., SHARIQ, M., ASIF, M., SIDDIQUI, M. A., MALAN, P. & AHMAD, F. 2022. Green Nanotechnology: Plant-Mediated Nanoparticle Synthesis and Application. *Nanomaterials (Basel),* 12.

KHAN, M. A. I., BISWAS, B., SMITH, E., NAIDU, R. & MEGHARAJ, M. 2018. Toxicity assessment of fresh and weathered petroleum hydrocarbons in contaminated soil- a review. *ChemospHere,* 212**,** 755-767.

KHARISOV, B. I., RASIKA DIAS, H. V., KHARISSOVA, O. V., MANUEL JIMÉNEZ-PÉREZ, V., OLVERA PÉREZ, B. & MUÑOZ FLORES, B. 2012. Iron-containing nanomaterials: synthesis, properties, and environmental applications. *RSC Advances,* 2**,** 9325-9358.

KHARISSOVA, O., DIAS, R., KHARISOV, B., PÉREZ, B. & JIMÉNEZ-PÉREZ, V. 2013a. The greener synthesis of nanoparticles. *Trends in biotechnology,* 31.

KHARISSOVA, O. V., DIAS, H. V. R., KHARISOV, B. I., PÉREZ, B. O. & PÉREZ, V. M. J. 2013b. The greener synthesis of nanoparticles. *Trends in Biotechnology,* 31**,** 240-248.

KHATOON, K. & MALIK, A. 2019. Screening of polycyclic aromatic hydrocarbon degrading bacterial isolates from oil refinery wastewater and detection of conjugative plasmids in polycyclic aromatic hydrocarbon tolerant and multi-metal resistant bacteria. *Heliyon,* 5**,** e02742.

KHUNTIA, B., ANWAR, M., ALAM, T., SAMIM, M., KUMARI, M. & ARORA, I. 2019. Synthesis and Characterization of Zero-Valent Iron Nanoparticles, and the Study of Their Effect against the Degradation of DDT in Soil and Assessment of Their Toxicity against Collembola and Ostracods. *ACS Omega,* 2019.

KIAMARSI, Z., SOLEIMANI, M., NEZAMI, A. & KAFI, M. 2019. Biodegradation of n-alkanes and polycyclic aromatic hydrocarbons using novel indigenous bacteria isolated from contaminated soils. *International Journal of Environmental Science and Technology,* 16**,** 6805-6816.

KIRUBAKARAN, D., WAHID, J. B. A., KARMEGAM, N., JEEVIKA, R., SELLAPILLAI, L., RAJKUMAR, M. & SENTHILKUMAR, K. J. 2025. A Comprehensive Review on the Green Synthesis of

Nanoparticles: Advancements in Biomedical and Environmental Applications. *Biomedical Materials & Devices*.
KOH, L. M. & KHOR, S. M. 2022. Biodegradation Process: Basics, Factors Affecting, and Industrial Applications. *In:* ALI, G. A. M. & MAKHLOUF, A. S. H. (eds.) *Handbook of Biodegradable Materials*. Cham: Springer International Publishing.
KOLAHALAM, L. A., KASI VISWANATH, I. V., DIWAKAR, B. S., GOVINDH, B., REDDY, V. & MURTHY, Y. L. N. 2019. Review on nanomaterials: Synthesis and applications. *Materials Today: Proceedings,* 18**,** 2182-2190.
KONADU-AMOAH, B., HU, R., NDÉ-TCHOUPÉ, A. I., GWENZI, W. & NOUBACTEP, C. 2022. Metallic iron (Fe0)-based materials for aqueous pHospHate removal: A critical review. *Journal of Environmental Management,* 315**,** 115157.
KONDAKINDI, V. R., PABBATI, R., ERUKULLA, P., MADDELA, N. R. & PRASAD, R. 2024. Bioremediation of heavy metals-contaminated sites by microbial extracellular polymeric substances – A critical view. *Environmental Chemistry and Ecotoxicology,* 6**,** 408-421.
KOSHLAF, E. & BALL, A. S. 2017. Soil bioremediation approaches for petroleum hydrocarbon polluted environments. *AIMS Microbiol,* 3**,** 25-49.
KOSTKA, J. E., TESKE, A. P., JOYE, S. B. & HEAD, I. M. 2014. The metabolic pathways and environmental controls of hydrocarbon biodegradation in marine ecosystems. *Frontiers in Microbiology,* 5.
KOTCHAPLAI, P., KHAN, E. & VANGNAI, A. 2019. Microbial Perspective of NZVI Applications: From Fundamental Science to Field Scale Engineering Applications.
KOTHARI, V., PANCHAL, M. & SRIVASTAVA, N. 2014. Microbial Degradation of Hydrocarbons. *National Science Digital Library*.
KOUL, B. & TAAK, P. 2018. Chemical Methods of Soil Remediation. *In:* KOUL, B. & TAAK, P. (eds.) *Biotechnological Strategies for Effective Remediation of Polluted Soils*. Singapore: Springer Singapore.
KOZMA, G., RÓNAVÁRI, A., KÓNYA, Z. & KUKOVECZ, Á. 2016. Environmentally Benign Synthesis Methods of Zero-Valent Iron Nanoparticles. *ACS Sustainable Chemistry & Engineering,* 4**,** 291-297.
KRIECH, A. J. & OSBORN, L. V. 2022. Review of the impact of stormwater and leaching from pavements on the environment. *Journal of Environmental Management,* 319**,** 115687.
KULSHRESHTHA, S., MATHUR, N. & BHATNAGAR, P. 2014. Mushroom as a product and their role in mycoremediation. *AMB Express,* 4**,** 29.
KUMAR, A., TYAGI, P. K., TYAGI, S. & GHORBANPOUR, M. 2024. Integrating green nanotechnology with sustainable development goals: a pathway to sustainable innovation. *Discover Sustainability,* 5**,** 364.
KUMAR, R., SINGH, N. & PANDEY, S. N. 2015. Potential of green synthesized zero-valent iron nanoparticles for remediation of lead-contaminated water. *International Journal of Environmental Science and Technology,* 12**,** 3943-3950.
KUMAR, V., KAUSHIK, N. K., TIWARI, S. K., SINGH, D. & SINGH, B. 2023. Green synthesis of iron nanoparticles: Sources and multifarious biotechnological applications. *International Journal of Biological Macromolecules,* 253**,** 127017.
KUMAR YADAV, K., SINGH, K., SINGH, A. & KUMAR, D. 2023. The Ecological Impact of Oil Spills on Soil Health. 93-96.
KUMARI, P. & KUMAR, A. 2023. ADVANCED OXIDATION PROCESS: A remediation technique for organic and non-biodegradable pollutant. *Results in Surfaces and Interfaces,* 11**,** 100122.
KUMARI, S., RATURI, S., KULSHRESTHA, S., CHAUHAN, K., DHINGRA, S., ANDRÁS, K., THU, K., KHARGOTRA, R. & SINGH, T. 2023. A comprehensive review on various techniques used for synthesizing nanoparticles. *Journal of Materials Research and Technology,* 27**,** 1739-1763.

KUPPAN, N., PADMAN, M., MAHADEVA, M., SRINIVASAN, S. & DEVARAJAN, R. 2024. A comprehensive review of sustainable bioremediation techniques: Eco friendly solutions for waste and pollution management. *Waste Management Bulletin,* 2**,** 154-171.

LAWSON, P. A. 2018. Chapter 1 - The Phylum Actinobacteria. *In:* MATTARELLI, P., BIAVATI, B., HOLZAPFEL, W. H. & WOOD, B. J. B. (eds.) *The Bifidobacteria and Related Organisms*. Academic Press.

LE, P. T., PONTAROTTI, P. & RAOULT, D. 2014. Alphaproteobacteria species as a source and target of lateral sequence transfers. *Trends in Microbiology,* 22**,** 147-156.

LEFEVRE, E., BOSSA, N., WIESNER, M. R. & GUNSCH, C. K. 2016. A review of the environmental implications of in situ remediation by nanoscale zero valent iron (nZVI): Behavior, transport and impacts on microbial communities. *Sci Total Environ,* 565**,** 889-901.

LETINSKI, D. J. & PRINCE, R. C. 2017. Volume 2: Hydrocarbon Extraction. *In:* MCGENITY, T. J., TIMMIS, K. N. & NOGALES, B. (eds.) *Hydrocarbon and Lipid Microbiology Protocols: Petroleum, Hydrocarbon and Lipid Analysis*. Berlin, Heidelberg: Springer Berlin Heidelberg.

LI, J., LUO, C., SONG, M., DAI, Q., JIANG, L., ZHANG, D. & ZHANG, G. 2017. Biodegradation of Phenanthrene in Polycyclic Aromatic Hydrocarbon-Contaminated Wastewater Revealed by Coupling Cultivation-Dependent and -Independent Approaches. *Environmental Science & Technology,* 51**,** 3391-3401.

LI, S., LI, L. & ZHANG, W. 2024. Nanoscale Zero-Valent Iron (nZVI) for Heavy Metal Wastewater Treatment: A Perspective. *Engineering,* 36**,** 16-20.

LI, S., LI, S.-K., GAN, R.-Y., SONG, F.-L., KUANG, L. & LI, H.-B. 2013. Antioxidant capacities and total phenolic contents of infusions from 223 medicinal plants. *Industrial Crops and Products,* 51**,** 289-298.

LI, X., ELLIOTT, D. & ZHANG, W.-X. 2006. Zero-Valent Iron Nanoparticles for Abatement of Environmental Pollutants: Materials and Engineering Aspects. *Critical Reviews in Solid State and Materials Sciences - CRIT REV SOLID STATE MAT SCI,* 31**,** 111-122.

LIBRALATO, G., COSTA DEVOTI, A., VOLPI GHIRARDINI, A. & VIGNATI, D. A. L. 2017. Environmental Effects of nZVI for Land and Groundwater Remediation. *In:* LOFRANO, G., LIBRALATO, G. & BROWN, J. (eds.) *Nanotechnologies for Environmental Remediation: Applications and Implications*. Cham: Springer International Publishing.

LIEN, H. L. & ZHANG, W. X. 2001. Nanoscale Iron Particles for Complete Reduction of Chlorinated Ethenes. *Colloids Surf., A,* 191**,** 105.

LIGHT, T., LICHT, S., BEVILACQUA, A. & MORASHC, K. 2005. The Fundamental Conductivity and Resistivity of Water. *Electrochemical and Solid State Letters - ELECTROCHEM SOLID STATE LETT,* 8.

LIN, K.-S., MDLOVU, N. V., CHEN, C.-Y., CHIANG, C.-L. & DEHVARI, K. 2018. Degradation of TCE, PCE, and 1,2–DCE DNAPLs in contaminated groundwater using polyethylenimine-modified zero-valent iron nanoparticles. *Journal of Cleaner Production,* 175**,** 456-466.

LIN, L., YANG, H. & XU, X. 2022. Effects of Water Pollution on Human Health and Disease Heterogeneity: A Review. *Frontiers in Environmental Science,* 10**,** 880246.

LIU, F., HE, C., JIANG, Y., YANG, Y., PENG, F., LIU, L., MEN, J., FENG, J., LI, L., TANG, G. & FENG, J. 2023. Carbon layer encapsulation strategy for designing multifunctional core-shell nanorod aerogels as high-temperature thermal superinsulators. *Chemical Engineering Journal,* 455**,** 140502.

LIU, J.-W., WEI, K.-H., XU, S.-W., CUI, J., MA, J., XIAO, X.-L., XI, B.-D. & HE, X.-S. 2021. Surfactant-enhanced remediation of oil-contaminated soil and groundwater: A review. *Science of The Total Environment,* 756**,** 144142.

LIU, M., CHEN, G., XU, L., HE, Z. & YE, Y. 2024. Environmental remediation approaches by nanoscale zero valent iron (nZVI) based on its reductivity: a review. *RSC Advances,* 14**,** 21118-21138.

LIU, Z. & LIU, J. 2013. Evaluating bacterial community structures in oil collected from the sea surface and sediment in the northern Gulf of Mexico after the Deepwater Horizon oil spill. *Microbiologyopen,* 2**,** 492-504.

LU, C., HONG, Y., LIU, J., GAO, Y., MA, Z., YANG, B., LING, W. & WAIGI, M. G. 2019. A PAH-degrading bacterial community enriched with contaminated agricultural soil and its utility for microbial bioremediation. *Environmental Pollution,* 251**,** 773-782.

MACAYA, C. C., DURÁN, R. E., HERNÁNDEZ, L., RODRÍGUEZ-CASTRO, L., BARRA-SANHUEZA, B., DOROCHESI, F. & SEEGER, M. 2019. Bioremediation of Petroleum. *Reference Module in Life Sciences*. Elsevier.

MACCHI, M., MARTINEZ, M., TAUIL, R. M. N., VALACCO, M. P., MORELLI, I. S. & COPPOTELLI, B. M. 2017. Insights into the genome and proteome of SpHingomonas paucimobilis strain 20006FA involved in the regulation of polycyclic aromatic hydrocarbon degradation. *World Journal of Microbiology and Biotechnology,* 34**,** 7.

MACHADO, S., PACHECO, J. G., NOUWS, H. P. A., ALBERGARIA, J. T. & DELERUE-MATOS, C. 2015. Characterization of green zero-valent iron nanoparticles produced with tree leaf extracts. *Science of The Total Environment,* 533**,** 76-81.

MACHADO, S., PINTO, S. L., GROSSO, J. P., NOUWS, H. P. A., ALBERGARIA, J. T. & DELERUE-MATOS, C. 2013. Green production of zero-valent iron nanoparticles using tree leaf extracts. *Science of The Total Environment,* 445-446**,** 1-8.

MACKENZIE, K. & GEORGI, A. 2019. NZVI Synthesis and Characterization. *In:* PHENRAT, T. & LOWRY, G. V. (eds.) *Nanoscale Zerovalent Iron Particles for Environmental Restoration: From Fundamental Science to Field Scale Engineering Applications*. Cham: Springer International Publishing.

MAHANAYAK, B. 2024. Environmental Restoration through Bioremediation: Methods, Advantages, and Challenges. *International Journal of Research Publication and Reviews,* 5**,** 6661-6664.

MAHMOUD, A. S., FARAG, R. S. & ELSHFAI, M. M. 2020. Reduction of organic matter from municipal wastewater at low cost using green synthesis nano iron extracted from black tea: Artificial intelligence with regression analysis. *Egyptian Journal of Petroleum,* 29**,** 9-20.

MAIER, R. M. 2019. Chapter 9 - Biological Processes Affecting Contaminants Transport and Fate. *In:* BRUSSEAU, M. L., PEPPER, I. L. & GERBA, C. P. (eds.) *Environmental and Pollution Science (Third Edition)*. Academic Press.

MALLAH, M. A., CHANGXING, L., MALLAH, M. A., NOREEN, S., LIU, Y., SAEED, M., XI, H., AHMED, B., FENG, F., MIRJAT, A. A., WANG, W., JABAR, A., NAVEED, M., LI, J.-H. & ZHANG, Q. 2022. Polycyclic aromatic hydrocarbon and its effects on human health: An overeview. *ChemospHere,* 296**,** 133948.

MAREEDU, T., POIBA, V. & VANGALAPATI, M. 2021. Green synthesis of iron nanoparticles by green tea and black tea leaves extract. *Materials Today: Proceedings,* 42**,** 1498-1501.

MARTIN, F., MALAGNOUX, L., VIOLET, F., JAKONCIC, J. & JOUANNEAU, Y. 2013. Diversity and catalytic potential of PAH-specific ring-hydroxylating dioxygenases from a hydrocarbon-contaminated soil. *Applied Microbiology and Biotechnology,* 97**,** 5125-5135.

MATHESON, L. J. & TRATNYEK, P. G. 1994. Reductive Dehalogenation of Chlorinated Methanes by Iron Metal. *Environ. Sci. Technol.,* 28**,** 2053.

MCELROY, J. A., KASSOTIS, C. D. & NAGEL, S. C. 2020. In Our Backyard: Perceptions About Fracking, Science, and Health by Community Members. *New Solut,* 30**,** 42-51.

MILLER, J. I., TECHTMANN, S., FORTNEY, J., MAHMOUDI, N., JOYNER, D., LIU, J., OLESEN, S., ALM, E., FERNANDEZ, A., GARDINALI, P., GARAJAYEVA, N., ASKEROV, F. S. & HAZEN, T. C. 2019. Oil Hydrocarbon Degradation by Caspian Sea Microbial Communities. *Front Microbiol,* 10**,** 995.

MIRANDA, M. H., MENEZES, D. B., VEGA-BAUDRIT, J. R., FERREIRA, L. F. R., BHARAGAVA, R. N., IQBAL, H. M. N. & BILAL, M. 2022. 1 - Nanobioremediation: An introduction. *In:* IQBAL, H. M. N., BILAL, M. & NGUYEN, T. A. (eds.) *Nano-Bioremediation : Fundamentals and Applications*. Elsevier.

MIRONOV, O. G. 1968. Hydrocarbon pollution of the sea and its influence on marine organisms. *Helgoländer wissenschaftliche Meeresuntersuchungen,* 17**,** 335-339.

MISHRA, M., SINGH, S. K. & KUMAR, A. 2021. Chapter 5 - Environmental factors affecting the bioremediation potential of microbes. *In:* KUMAR, A., SINGH, V. K., SINGH, P. & MISHRA, V. K. (eds.) *Microbe Mediated Remediation of Environmental Contaminants*. Woodhead Publishing.

MIYAZAWA, D., THANH, L. T. H., TANI, A., SHINTANI, M., LOC, N. H., HATTA, T. & KIMBARA, K. 2019. Isolation and Characterization of Genes Responsible for Naphthalene Degradation from ThermopHilic Naphthalene Degrader, Geobacillus sp. JF8. *Microorganisms,* 8.

MOHAMED AMINE, G. & ABD-ELSALAM, K. 2021. Chapter 27 - Strategies for scaling up of green-synthesized nanomaterials: Challenges and future trends.

MOHAMED, B. A. & SAMER, M. 2023. Chapter 8 - Biobutanol production from agricultural wastes. *In:* SELVASEMBIAN, R., WAN AZELEE, N. I., SHANMUGAM, S. R., VENKATACHALAM, P. & MISHRA, A. K. (eds.) *Valorization of Wastes for Sustainable Development*. Elsevier.

MOHAMMADIPANAH, F. & DEHHAGHI, M. 2017. Classification and Taxonomy of Actinobacteria. *In:* WINK, J., MOHAMMADIPANAH, F. & HAMEDI, J. (eds.) *Biology and Biotechnology of Actinobacteria*. Cham: Springer International Publishing.

MOHAPATRA, B., DHAMALE, T., SAHA, B. K. & PHALE, P. S. 2022. Chapter 18 - Microbial degradation of aromatic pollutants: metabolic routes, pathway diversity, and strategies for bioremediation. *In:* DAS, S. & DASH, H. R. (eds.) *Microbial Biodegradation and Bioremediation (Second Edition)*. Elsevier.

MOJIRI, A., ZHOU, J. L., OHASHI, A., OZAKI, N. & KINDAICHI, T. 2019. Comprehensive review of polycyclic aromatic hydrocarbons in water sources, their effects and treatments. *Science of The Total Environment,* 696**,** 133971.

MOKRANI, S., HOUALI, K., YADAV, K. K., ARABI, A. I. A., ELTAYEB, L. B., AWJANALRESHIDI, M., BENGUERBA, Y., CABRAL-PINTO, M. M. S. & NABTI, E.-H. 2024. Bioremediation techniques for soil organic pollution: Mechanisms, microorganisms, and technologies - A comprehensive review. *Ecological Engineering,* 207**,** 107338.

MONDAL, A., DUBEY, B. K., ARORA, M. & MUMFORD, K. 2021. Porous media transport of iron nanoparticles for site remediation application: A review of lab scale column study, transport modelling and field-scale application. *Journal of Hazardous Materials,* 403**,** 123443.

MONTCOUDIOL, N., ISHERWOOD, C., GUNNING, A., KELLY, T. & YOUNGER, P. L. 2017. Shale gas impacts on groundwater resources: Understanding the behavior of a shallow aquifer around a fracking site in Poland. *Energy Procedia,* 125**,** 106-115.

MORYA, R., SALVACHÚA, D. & THAKUR, I. S. 2020. Burkholderia: An Untapped but Promising Bacterial Genus for the Conversion of Aromatic Compounds. *Trends in Biotechnology,* 38**,** 963-975.

MU, X. 2019. Refining and Marketing. *In:* MU, X. (ed.) *The Economics of Oil and Gas*. Agenda Publishing.

MUKHOPADHYAY, S., PAL, D. & DAVE, V. 2025. Application of Bioremediation Using Nanoparticles. *In:* DAVE, V. & KUILA, A. (eds.) *Nanomaterials as a Catalyst for Biofuel Production*. Singapore: Springer Nature Singapore.

MÜLLER, A., ÖSTERLUND, H., MARSALEK, J. & VIKLANDER, M. 2020. The pollution conveyed by urban runoff: A review of sources. *Science of The Total Environment,* 709**,** 136125.

MUNDRA, S. & PROVIS, J. L. 2021. Mechanisms of passivation and chloride-induced corrosion of mild steel in sulfide-containing alkaline solutions. *Journal of Materials Science,* 56**,** 14783-14802.

MURGUEITIO, E., CUMBAL, L., ABRIL, M., IZQUIERDO, A., DEBUT, A. & TINOCO, O. 2018. Green Synthesis of Iron Nanoparticles: Application on the Removal of Petroleum Oil from Contaminated Water and Soils. *Journal of Nanotechnology*.

MYSTRIOTI, C., XANTHOPOULOU, T. D., TSAKIRIDIS, P., PAPASSIOPI, N. & XENIDIS, A. 2016. Comparative evaluation of five plant extracts and juices for nanoiron synthesis and application for hexavalent chromium reduction. *Science of The Total Environment,* 539**,** 105-113.

NADAGOUDA, M. N., CASTLE, A. B., MURDOCK, R. C., HUSSAIN, S. M. & VARMA, R. S. 2010. In vitro biocompatibility of nanoscale zerovalent iron particles (NZVI) synthesized using tea polyphenols. *Green Chemistry,* 12**,** 114-122.

NALWEYISO, A., NAGAWA, C. B., EMEL, Y., UZMAN, S., WANYAMA, J., KIRABIRA, J. B., ZZIWA, A., SAGALA, F., SSEBUGERE, P., OMWOMA, S., KYARIMPA, C., KIGGUNDU, N. & KABENGE, I. 2025. Green synthesis of zero-valent iron nanoparticles from cape gooseberry (pHysalis peruviana l.) Biomass for oil spill remediation. *Environmental Challenges,* 19**,** 101146.

NAMAKKA, M., RAHMAN, M. R., BIN MOHAMAD SAID, K. A. & MUHAMMAD, A. 2024. Insights into micro-and nano-zero valent iron materials: synthesis methods and multifaceted applications. *RSC Advances,* 14**,** 30411-30439.

NARYAL, S., RANA, M., SHARMA, N., AHMED, B., SHARMA, P., KUJUR, S., JAISWAL, S., GUPTA, S. D., PATEL, S. M. B., KAUSHAL, S., SAINI, N. & KAUR, I. P. 2024. Navigating Sustainable and Healthy Future: Green Nanotechnology, Regulatory Priorities, and Challenges. *In:* SOBTI, R. C. (ed.) *Role of Science and Technology for Sustainable Future: Volume 2-Applied Sciences and Technologies*. Singapore: Springer Nature Singapore.

NAZIR, R., BABA, U. & RATHER, S. 2021. Factors affecting bioremediation.

NGO, M. A. S., TIONGCO, R. P. M. & SARANGLAO, C. C. 2014. Synthesis of green zero-valent iron using polyphenols from dried green tea extract.

NJUGUNA, J., SIDDIQUE, S., BAKAH KWROFFIE, L., PIROMRAT, S., ADDAE-AFOAKWA, K., EKEH-ADEGBOTOLU, U., OLUYEMI, G., YATES, K., KUMAR MISHRA, A. & MOLLER, L. 2022. The fate of waste drilling fluids from oil & gas industry activities in the exploration and production operations. *Waste Management,* 139**,** 362-380.

NOOR, M., SAJID, A., BANGASH, K., ABBAS, M., AHMED, S., KAPLAN, A., IQBAL, S., KHAN, M., ADNAN, M., ALI, A., ZAMAN, F. & WAHAB, S. 2023. Potential and Challenges in Green Synthesis of Nanoparticles: A Review. *Xi'an Shiyou Daxue Xuebao (Ziran Kexue Ban)/Journal of Xi'an Shiyou University,* 19**,** 1155-1165.

NUNES, H. X., SILVA, D. L., RANGEL, C. M. & PINTO, A. M. F. R. 2021. Rehydrogenation of Sodium Borates to Close the NaBH4-H2 Cycle: A Review. *Energies,* 14**,** 3567.

NWANKWEGU, A. S., ZHANG, L., XIE, D., ONWOSI, C. O., MUHAMMAD, W. I., ODOH, C. K., SAM, K. & IDENYI, J. N. 2022. Bioaugmentation as a green technology for hydrocarbon pollution remediation. Problems and prospects. *Journal of Environmental Management,* 304**,** 114313.

OLADIPO, A., ALABI, V., MUSE, S., EHIZOJIE, O., SAHEED, E. & OLADOYE, P. O. 2025. 17 - Mycoremediation: A biobased approach toward environmental sustainability. *In:* WU, Q.-S. (ed.) *Management of Mycorrhizal Symbiosis for Mycoremediation and PHytostabilization*. Elsevier.

OLUSILE AKINYELE BABAYEJU, A. A., IFEANYI ONYEDIKA EKEMEZIE, OLUDAYO OLATOYE SOFOLUWE 2024. Advancements in predictive maintenance for aging oil and gas infrastructure. *World Journal of Advanced Research and Reviews,* 3**,** 252-266.

OREN, A. 2017. Aerobic Hydrocarbon-Degrading Archaea. *In:* MCGENITY, T. J. (ed.) *Taxonomy, Genomics and EcopHysiology of Hydrocarbon-Degrading Microbes*. Cham: Springer International Publishing.

ORTH, W. & GILLHAM, R. W. 1996. Dechlorination of Trichloroethene in Aqueous Solution Using Fe0. *Environmental Science & Technology,* 30**,** 66-71.

OSMAN, A. I., ZHANG, Y., FARGHALI, M., RASHWAN, A. K., ELTAWEIL, A. S., ABD EL-MONAEM, E. M., MOHAMED, I. M. A., BADR, M. M., IHARA, I., ROONEY, D. W. & YAP, P.-S. 2024. Synthesis of green nanoparticles for energy, biomedical, environmental, agricultural, and food applications: A review. *Environmental Chemistry Letters,* 22**,** 841-887.

PAISSE, S., GONI, M., STALDER, T., STADLER, T., BUDZINSKI, H. & DURAN, R. 2011. Ring-hydroxylating dioxygenase (RHD) expression in a microbial community during the early response to oil pollution. *FEMS microbiology ecology,* 80**,** 77-86.

PAL, G., RAI, P. & PANDEY, A. 2019. Chapter 1 - Green synthesis of nanoparticles: A greener approach for a cleaner future. *In:* SHUKLA, A. K. & IRAVANI, S. (eds.) *Green Synthesis, Characterization and Applications of Nanoparticles*. Elsevier.

PAL, K., CHAKROBORTY, S. & NATH, N. 2022. Limitations of nanomaterials insights in green chemistry sustainable route: Review on novel applications. *Green Processing and Synthesis,* 11**,** 951-964.

PÁL, R., JUHÁSZ, M. & STUMPF, Á. 1998. Detailed analysis of hydrocarbon groups in diesel range petroleum fractions with on-line coupled supercritical fluid chromatography–gas chromatography–mass spectrometry. *Journal of Chromatography A,* 819**,** 249-257.

PALIWAL, R., BABU, R. J. & PALAKURTHI, S. 2014. Nanomedicine scale-up technologies: feasibilities and challenges. *AAPS PHarmSciTech,* 15**,** 1527-34.

PAN, Y., QIN, R., HOU, M., XUE, J., ZHOU, M., XU, L. & ZHANG, Y. 2022. The interactions of polyphenols with Fe and their application in Fenton/Fenton-like reactions. *Separation and Purification Technology,* 300**,** 121831.

PANDOLFO, E., BARRA CARACCIOLO, A. & ROLANDO, L. 2023. Recent Advances in Bacterial Degradation of Hydrocarbons. *Water,* 15**,** 375.

PARALES, R. E. & RESNICK, S. M. 2006. Aromatic Ring Hydroxylating Dioxygenases. *In:* RAMOS, J.-L. & LEVESQUE, R. C. (eds.) *Pseudomonas: Volume 4 Molecular Biology of Emerging Issues*. Boston, MA: Springer US.

PATEL, A. B., SHAIKH, S., JAIN, K. R., DESAI, C. & MADAMWAR, D. 2020. Polycyclic Aromatic Hydrocarbons: Sources, Toxicity, and Remediation Approaches. *Front Microbiol,* 11**,** 562813.

PATOWARY, K., PATOWARY, R., KALITA, M. C. & DEKA, S. 2017. Characterization of Biosurfactant Produced during Degradation of Hydrocarbons Using Crude Oil As Sole Source of Carbon. *Frontiers in Microbiology,* Volume 8 - 2017.

PERRY, C., DE LOS SANTOS, E. L. C., ALKHALAF, L. M. & CHALLIS, G. L. 2018. Rieske non-heme iron-dependent oxygenases catalyse diverse reactions in natural product biosynthesis. *Nat Prod Rep,* 35**,** 622-632.

PHALE, P. S., BASU, A., MAJHI, P. D., DEVERYSHETTY, J., VAMSEE-KRISHNA, C. & SHRIVASTAVA, R. 2007. Metabolic diversity in bacterial degradation of aromatic compounds. *Omics,* 11**,** 252-79.

PHAM, A. N. & WAITE, T. D. 2008. Oxygenation of Fe(II) in natural waters revisited: Kinetic modeling approaches, rate constant estimation and the importance of various reaction pathways. *Geochimica et Cosmochimica Acta,* 72**,** 3616-3630.

PHENRAT, T., LONG, T. C., LOWRY, G. V. & VERONESI, B. 2009. Partial oxidation ("aging") and surface modification decrease the toxicity of nanosized zerovalent iron. *Environ Sci Technol,* 43**,** 195-200.

PHENRAT, T., LOWRY, G. V. & BABAKHANI, P. 2019. Nanoscale Zerovalent Iron (NZVI) for Environmental Decontamination: A Brief History of 20 Years of Research and Field-Scale

Application. *In:* PHENRAT, T. & LOWRY, G. V. (eds.) *Nanoscale Zerovalent Iron Particles for Environmental Restoration: From Fundamental Science to Field Scale Engineering Applications*. Cham: Springer International Publishing.
PIMENTEL, N. & DOS REIS, R. P. 2020. Nature and Occurrence of Hydrocarbons. *In:* LEAL FILHO, W., AZUL, A. M., BRANDLI, L., LANGE SALVIA, A. & WALL, T. (eds.) *Life Below Water*. Cham: Springer International Publishing.
PLESSL, K., RUSS, A. & VOLLPRECHT, D. 2023. Application and development of zero-valent iron (ZVI) for groundwater and wastewater treatment. *International Journal of Environmental Science and Technology,* 20**,** 6913-6928.
POOLE, Z. 2024. *HYDROCARBON POLLUTION: Spot it - Report it - Stop it* [Online]. Available: https://raleighnc.gov/stormwater/services/spot-report-and-stop-water-pollution/hydrocarbon-pollution [Accessed 25 November 2024 2024].
RAJABI, H., HADI MOSLEH, M., MANDAL, P., LEA-LANGTON, A. & SEDIGHI, M. 2020. Emissions of volatile organic compounds from crude oil processing – Global emission inventory and environmental release. *Science of The Total Environment,* 727**,** 138654.
RAJKUMAR, R., EZHUMALAI, G. & GNANADESIGAN, M. 2021. A green approach for the synthesis of silver nanoparticles by Chlorella vulgaris and its application in pHotocatalytic dye degradation activity. *Environmental Technology & Innovation,* 21**,** 101282.
RAKHMAWATY EDDY, D., NURSYAMSIAH, D., PERMANA, M. D., NOVIYANTI, A., SOLUHUDIN & RAHAYU, I. 2022. Green Production of Zero-Valent Iron (ZVI) Using Tea-Leaf Extracts for Fenton Degradation of Mixed Rhodamine B and Methyl Orange Dyes. *Materials,* 15**,** 332.
RANA, A., YADAV, K. & JAGADEVAN, S. 2020. A comprehensive review on green synthesis of nature-inspired metal nanoparticles: Mechanism, application and toxicity. *Journal of Cleaner Production,* 272**,** 122880.
RANI, N., SINGH, P., KUMAR, S., KUMAR, P., BHANKAR, V. & KUMAR, K. 2023. Plant-mediated synthesis of nanoparticles and their applications: A review. *Materials Research Bulletin,* 163**,** 112233.
RASHEED, Q. J., PANDIAN, K. & MUTHUKUMAR, K. 2011. Treatment of petroleum refinery wastewater by ultrasound-dispersed nanoscale zero-valent iron particles. *Ultrasonics Sonochemistry,* 18**,** 1138-1142.
RASHEED, T. 2022. Magnetic nanomaterials: Greener and sustainable alternatives for the adsorption of hazardous environmental contaminants. *Journal of Cleaner Production,* 362**,** 132338.
RAYAROTH, M. P., MARCHEL, M. & BOCZKAJ, G. 2023. Advanced oxidation processes for the removal of mono and polycyclic aromatic hydrocarbons – A review. *Science of The Total Environment,* 857**,** 159043.
RODRÍGUEZ-RASERO, C., ALEXANDRE-FRANCO, M. F., FERNÁNDEZ-GONZÁLEZ, C., MONTES-JIMÉNEZ, V. & CUERDA-CORREA, E. M. 2024. Valorizing Tea Waste: Green Synthesis of Iron Nanoparticles for Efficient Dye Removal from Water. *Antioxidants (Basel),* 13.
ROY, A., SHARMA, A., YADAV, S., JULE, L. T. & KRISHNARAJ, R. 2021. Nanomaterials for Remediation of Environmental Pollutants. *Bioinorg Chem Appl,* 2021**,** 1764647.
SAEEDI, M., MALEKMOHAMMADI, B. & TAJALLI, S. 2024. Interaction of benzene, toluene, ethylbenzene, and xylene with human's body: Insights into characteristics, sources and health risks. *Journal of Hazardous Materials Advances,* 16**,** 100459.
SAIF, S., TAHIR, A. & CHEN, Y. 2016. Green Synthesis of Iron Nanoparticles and Their Environmental Applications and Implications. *Nanomaterials (Basel),* 6.
SAJID, M., ASIF, M., BAIG, N., KABEER, M., IHSANULLAH, I. & MOHAMMAD, A. W. 2022. Carbon nanotubes-based adsorbents: Properties, functionalization, interaction mechanisms, and applications in water purification. *Journal of Water Process Engineering,* 47**,** 102815.
SAMANTA, I. & BANDYOPADHYAY, S. 2020. Chapter 23 - Pseudomonas. *In:* SAMANTA, I. & BANDYOPADHYAY, S. (eds.) *Antimicrobial Resistance in Agriculture*. Academic Press.

SANDER, R. 2015. Compilation of Henry's law constants (Version 4.0) for water as solvent. *Atmospheric Chemistry and Physics,* 15**,** 4399-4981.

SANJAY, S. S. 2019. Chapter 2 - Safe nano is green nano. *In:* SHUKLA, A. K. & IRAVANI, S. (eds.) *Green Synthesis, Characterization and Applications of Nanoparticles*. Elsevier.

SARAVANAN, A., KUMAR, P. S., KARISHMA, S., VO, D.-V. N., JEEVANANTHAM, S., YAASHIKAA, P. R. & GEORGE, C. S. 2021. A review on biosynthesis of metal nanoparticles and its environmental applications. *ChemospHere,* 264**,** 128580.

SARKAR, P., ROY, A., PAL, S., MOHAPATRA, B., KAZY, S. K., MAITI, M. K. & SAR, P. 2017. Enrichment and characterization of hydrocarbon-degrading bacteria from petroleum refinery waste as potent bioaugmentation agent for in situ bioremediation. *Bioresour Technol,* 242**,** 15-27.

SARMA, J., SENGUPTA, A., LASKAR, M. K., SENGUPTA, S., TENGURIA, S. & KUMAR, A. 2023. Chapter 13 - Microbial adaptations in extreme environmental conditions. *In:* KUMAR, A. & TENGURIA, S. (eds.) *Bacterial Survival in the Hostile Environment*. Academic Press.

SCOTCHMAN, I. C. 2016. Shale gas and fracking: exploration for unconventional hydrocarbons. *Proceedings of the Geologists' Association,* 127**,** 535-551.

SEMERÁD, J. & CAJTHAML, T. 2016. Ecotoxicity and environmental safety related to nano-scale zerovalent iron remediation applications. *Applied Microbiology and Biotechnology,* 100**,** 9809-9819.

SEMERAD, J., PACHECO, N. I. N., GRASSEROVA, A., PROCHAZKOVA, P., PIVOKONSKY, M., PIVOKONSKA, L. & CAJTHAML, T. 2020a. In Vitro Study of the Toxicity Mechanisms of Nanoscale Zero-Valent Iron (nZVI) and Released Iron Ions Using Earthworm Cells. *Nanomaterials,* 10**,** 2189.

SEMERAD, J., PIVOKONSKY, M. & CAJTHAML, T. 2020b. Nano-Bioremediation: Nanoscale Zero-Valent Iron for Inorganic and Organic Contamination.

SEO, J. S., KEUM, Y. S. & LI, Q. X. 2009. Bacterial degradation of aromatic compounds. *Int J Environ Res Public Health,* 6**,** 278-309.

SERNA-GALLÉN, P. & MUŽINA, K. 2024. Metallic nanoparticles at the forefront of research: Novel trends in catalysis and plasmonics. *Nano Materials Science*.

SHANKER, U., JASSAL, V. & RANI, M. 2017. Green synthesis of iron hexacyanoferrate nanoparticles: Potential candidate for the degradation of toxic PAHs. *Journal of Environmental Chemical Engineering,* 5**,** 4108-4120.

SHANNON, E., JAISWAL, A. & ABU-GHANNAM, N. 2017. Polyphenolic content and antioxidant capacity of white, green, black, and herbal teas: A kinetic study. *Food Research,* 2**,** 1-11.

SHARMA, K., SHAH, G., SINGHAL, K. & SONI, V. 2024. Comprehensive insights into the impact of oil pollution on the environment. *Regional Studies in Marine Science,* 74**,** 103516.

SHARMIN, S., RAHAMAN, M. M., SARKAR, C., ATOLANI, O., ISLAM, M. T. & ADEYEMI, O. S. 2021. Nanoparticles as antimicrobial and antiviral agents: A literature-based perspective study. *Heliyon,* 7**,** e06456.

SHEGOKAR, R. & NAKACH, M. 2020. Chapter 4 - Large-scale manufacturing of nanoparticles—An industrial outlook. *In:* SHEGOKAR, R. (ed.) *Drug Delivery Aspects*. Elsevier.

SHRESTHA, S., WANG, B. & DUTTA, P. 2020. Nanoparticle processing: Understanding and controlling aggregation. *Advances in Colloid and Interface Science,* 279**,** 102162.

SINGH, H., DESIMONE, M. F., PANDYA, S., JASANI, S., GEORGE, N., ADNAN, M., ALDARHAMI, A., BAZAID, A. S. & ALDERHAMI, S. A. 2023. Revisiting the Green Synthesis of Nanoparticles: Uncovering Influences of Plant Extracts as Reducing Agents for Enhanced Synthesis Efficiency and Its Biomedical Applications. *Int J Nanomedicine,* 18**,** 4727-4750.

SINGH, J., DUTTA, T., KIM, K.-H., RAWAT, M., SAMDDAR, P. & KUMAR, P. 2018a. 'Green' synthesis of metals and their oxide nanoparticles: applications for environmental remediation. *Journal of Nanobiotechnology,* 16**,** 84.

SINGH, N. B., KUMAR, B., USMAN, U. L. & SUSAN, M. A. B. H. 2024. Nano revolution: Exploring the frontiers of nanomaterials in science, technology, and society. *Nano-Structures & Nano-Objects,* 39**,** 101299.

SINGH, P., KIM, Y.-J., ZHANG, D. & YANG, D.-C. 2016. Biological Synthesis of Nanoparticles from Plants and Microorganisms. *Trends in Biotechnology,* 34**,** 588-599.

SINGH, S., KUMAR, V., ROMERO, R., SHARMA, K. & SINGH, J. 2019. Applications of Nanoparticles in Wastewater Treatment. *In:* PRASAD, R., KUMAR, V., KUMAR, M. & CHOUDHARY, D. (eds.) *Nanobiotechnology in Bioformulations*. Cham: Springer International Publishing.

SINGH, V., SINGH, A., SINGH, R. & KUMAR, A. 2018b. Iron oxidizing bacteria: insights on diversity, mechanism of iron oxidation and role in management of metal pollution. *Environmental Sustainability,* 1.

SLOOTWEG, J. C. 2024. Sustainable chemistry: Green, circular, and safe-by-design. *One Earth,* 7**,** 754-758.

SPEIGHT, J. G. 2017. Chapter 2 - Organic Chemistry. *In:* SPEIGHT, J. G. (ed.) *Environmental Organic Chemistry for Engineers*. Butterworth-Heinemann.

SRIVASTAVA, J., NARAIAN, R., KALRA, S. J. S. & CHANDRA, H. 2014. Advances in microbial bioremediation and the factors influencing the process. *International Journal of Environmental Science and Technology,* 11**,** 1787-1800.

STAROŃ, A. & DŁUGOSZ, O. 2021. Antimicrobial properties of nanoparticles in the context of advantages and potential risks of their use. *Journal of Environmental Science and Health, Part A,* 56**,** 680-693.

STEFANIUK, M., OLESZCZUK, P. & OK, Y. S. 2016. Review on nano zerovalent iron (nZVI): From synthesis to environmental applications. *Chemical Engineering Journal,* 287**,** 618-632.

SUNARDI, ASHADI, A., RAHARDJO, S. & INAYATI, I. 2017. Ecofriendly Synthesis of nano Zero Valent Iron from Banana Peel Extract. *Journal of Physics: Conference Series,* 795**,** 012063.

SURRIYA, O., SARAH SALEEM, S., WAQAR, K. & GUL KAZI, A. 2015. Chapter 1 - PHytoremediation of Soils: Prospects and Challenges. *In:* HAKEEM, K. R., SABIR, M., ÖZTÜRK, M. & MERMUT, A. R. (eds.) *Soil Remediation and Plants*. San Diego: Academic Press.

SWEENEY, R., HARRIES, N., BARDOS, P. & VAIOPOULOU, E. 2024. Analysis of sustainable remediation techniques and technologies based on 10 European case studies. *Remediation Journal,* 34**,** e21773.

TANG, S. C. N. & LO, I. M. C. 2013. Magnetic nanoparticles: Essential factors for sustainable environmental applications. *Water Research,* 47**,** 2613-2632.

TANWIR, K., AMNA, JAVED, M. T., SHAHID, M., AKRAM, M. S. & ALI, Q. 2021. Chapter 32 - Antioxidant defense systems in bioremediation of organic pollutants. *In:* HASANUZZAMAN, M. & PRASAD, M. N. V. (eds.) *Handbook of Bioremediation*. Academic Press.

THI MO, L., IRINA, P., NATALIA, S., IRINA, N., LENAR, A., ANDREY, F., EKATERINA, A., SERGEY, A. & OLGA, P. 2022. Hydrocarbons Biodegradation by Rhodococcus: Assimilation of Hexadecane in Different Aggregate States. *Microorganisms,* 10.

THIAGARAJAN, C. & DEVARAJAN, Y. 2025. The urgent challenge of ocean pollution: Impacts on marine biodiversity and human health. *Regional Studies in Marine Science,* 81**,** 103995.

THOMAS, R. S., PHILBERT, M. A., AUERBACH, S. S., WETMORE, B. A., DEVITO, M. J., COTE, I., ROWLANDS, J. C., WHELAN, M. P., HAYS, S. M., ANDERSEN, M. E., MEEK, M. E., REITER, L. W., LAMBERT, J. C., CLEWELL, H. J., 3RD, STEPHENS, M. L., ZHAO, Q. J., WESSELKAMPER, S. C., FLOWERS, L., CARNEY, E. W., PASTOOR, T. P., PETERSEN, D. D., YAUK, C. L. & NONG, A. 2013. Incorporating new technologies into toxicity testing and risk assessment: moving from 21st century vision to a data-driven framework. *Toxicol Sci,* 136**,** 4-18.

TRATNYEK, P. G. & JOHNSON, R. L. 2006. Nanotechnologies for environmental cleanup. *Nano Today,* 1**,** 44-48.
TRUSKEWYCZ, A., GUNDRY, T. D., KHUDUR, L. S., KOLOBARIC, A., TAHA, M., ABURTO-MEDINA, A., BALL, A. S. & SHAHSAVARI, E. 2019. Petroleum Hydrocarbon Contamination in Terrestrial Ecosystems—Fate and Microbial Responses. *Molecules,* 24**,** 3400.
TUKUR UMAR, A. & HAJJ OTHMAN, M. D. S. 2017. Causes and consequences of crude oil pipeline vandalism in the Niger delta region of Nigeria: A confirmatory factor analysis approach. *Cogent Economics & Finance,* 5**,** 1353199.
UL-ISLAM, M., ULLAH, M. W., KHAN, S., MANAN, S., KHATTAK, W. A., AHMAD, W., SHAH, N. & PARK, J. K. 2017. Current advancements of magnetic nanoparticles in adsorption and degradation of organic pollutants. *Environmental Science and Pollution Research,* 24**,** 12713-12722.
UNEP 2011. *Environmental Assessment of Ogoniland*, UNited Nations Environmental Programme.
USEPA. 2020a. *In Situ Flushing* [Online]. USEPA. Available: https://clu-in.org/techfocus/default.focus/sec/In_Situ_Flushing/cat/Overview/ [Accessed 12th July 2022].
USEPA. 2020b. *Nanotechnology: Applications for Environmental Remediation* [Online]. USEPA. Available: https://clu-in.org/techfocus/default.focus/sec/Nanotechnology%3A_Applications_for_Environmental_Remediation/cat/Overview/ [Accessed 27th June 2022].
USEPA. 2020c. *Remediation Technologies* [Online]. USEPA. Available: https://clu-in.org/remediation/ [Accessed 06/03/2023].
VAN DEELEN, T. W., HERNÁNDEZ MEJÍA, C. & DE JONG, K. P. 2019. Control of metal-support interactions in heterogeneous catalysts to enhance activity and selectivity. *Nature Catalysis,* 2**,** 955-970.
VARJANI, S. J. 2017. Microbial degradation of petroleum hydrocarbons. *Bioresource Technology,* 223**,** 277-286.
VIO, S. A., GARCÍA, S. S., CASAJUS, V., ARANGO, J. S., GALAR, M. L., BERNABEU, P. R. & LUNA, M. F. 2020. Chapter 15 - Paraburkholderia. *In:* AMARESAN, N., SENTHIL KUMAR, M., ANNAPURNA, K., KUMAR, K. & SANKARANARAYANAN, A. (eds.) *Beneficial Microbes in Agro-Ecology*. Academic Press.
WACKETT, L. P. 2002. Mechanism and applications of Rieske non-heme iron dioxygenases. *Enzyme and Microbial Technology,* 31**,** 577-587.
WACŁAWEK, S., NOSEK, J., CÁDROVÁ, L., ANTOŠ, V. & CERNIK, M. 2015. Use of Various Zero Valent Irons for Degradation of Chlorinated Ethenes and Ethanes. *Ecological Chemistry and Engineering S,* 22.
WAIGI, M. G., KANG, F., GOIKAVI, C., LING, W. & GAO, Y. 2015. Phenanthrene biodegradation by spHingomonads and its application in the contaminated soils and sediments: A review. *International Biodeterioration & Biodegradation,* 104**,** 333-349.
WANG, A., HOU, J., XU, Q., WU, J. & XING, B. 2023. Green synthesis of zero valent iron using tannins to activate persulphate for sulphamethoxazole degradation. *Environmental Pollution,* 336**,** 122418.
WANG, H., ZHANG, J., HUANG, H., WANG, X., YANG, X. & COULON, F. 2024. Physicochemical Remediation of Soil Contamination: From Laboratory to Field. *In:* ORTEGA-CALVO, J. J. & COULON, F. (eds.) *Soil Remediation Science and Technology*. Cham: Springer Nature Switzerland.
WANG, T., LIN, J., CHEN, Z., MEGHARAJ, M. & NAIDU, R. 2014. Green synthesized iron nanoparticles by green tea and eucalyptus leaves extracts used for removal of nitrate in aqueous solution. *Journal of Cleaner Production,* 83**,** 413-419.

WANG, X., CHE, Y., XU, Y., WU, Y., XU, H. & LI, L. 2025. Mechanisms of nano zero-valent iron in enhancing dibenzofuran degradation by a Rhodococcus sp.: Trade-offs between ATP production and protection against reactive oxygen species. *Journal of Hazardous Materials,* 481**,** 136502.

WANG, X., SUN, T., ZHU, H., HAN, T., WANG, J. & DAI, H. 2020. Roles of pH, cation valence, and ionic strength in the stability and aggregation behavior of zinc oxide nanoparticles. *Journal of Environmental Management,* 267**,** 110656.

WANI, A. K., AKHTAR, N., SHER, F., NAVARRETE, A. A. & AMÉRICO-PINHEIRO, J. H. P. 2022. Microbial adaptation to different environmental conditions: molecular perspective of evolved genetic and cellular systems. *Arch Microbiol,* 204**,** 144.

WIDDEL, F. & RABUS, R. 2001. Anaerobic biodegradation of saturated and aromatic hydrocarbons. *Current Opinion in Biotechnology,* 12**,** 259-276.

WISSNER, J. L., ESCOBEDO-HINOJOSA, W., VOGEL, A. & HAUER, B. 2021. An engineered toluene dioxygenase for a single step biocatalytical production of (-)-(1S,2R)-cis-1,2-dihydro-1,2-naphthalenediol. *Journal of Biotechnology,* 326**,** 37-39.

WOLFE, M. D., ALTIER, D. J., STUBNA, A., POPESCU, C. V., MÜNCK, E. & LIPSCOMB, J. D. 2002. Benzoate 1,2-Dioxygenase from Pseudomonas putida: Single Turnover Kinetics and Regulation of a Two-Component Rieske Dioxygenase. *Biochemistry,* 41**,** 9611-9626.

WU, L., ZHANG, J., CHEN, F., LI, J., WANG, W., LI, S. & HU, L. 2024. Mechanisms, Applications, and Risk Analysis of Surfactant-Enhanced Remediation of Hydrophobic Organic Contaminated Soil. *Water,* 16**,** 2093.

WU, M., DICK, W. A., LI, W., WANG, X., YANG, Q., WANG, T., XU, L., ZHANG, M. & CHEN, L. 2016. Bioaugmentation and biostimulation of hydrocarbon degradation and the microbial community in a petroleum-contaminated soil. *International Biodeterioration & Biodegradation,* 107**,** 158-164.

WU, M., WU, J., ZHANG, X. & YE, X. 2019. Effect of bioaugmentation and biostimulation on hydrocarbon degradation and microbial community composition in petroleum-contaminated loessal soil. *ChemospHere,* 237**,** 124456.

XIE, J., LEI, C., CHEN, W., XIE, Q., GUO, Q. & HUANG, B. 2021. Catalytic properties of transition metals modified nanoscale zero-valent iron for simultaneous removal of 4-chlorophenol and Cr(VI): Efficacy, descriptor and reductive mechanisms. *Journal of Hazardous Materials,* 403**,** 123827.

XIE, Y., DONG, H., ZENG, G., TANG, L., JIANG, Z., ZHANG, C., DENG, J., ZHANG, L. & ZHANG, Y. 2017. The interactions between nanoscale zero-valent iron and microbes in the subsurface environment: A review. *Journal of Hazardous Materials,* 321**,** 390-407.

XU, H., JIA, Y., SUN, Z., SU, J., LIU, Q. S., ZHOU, Q. & JIANG, G. 2022. Environmental pollution, a hidden culprit for health issues. *Eco-Environment & Health,* 1**,** 31-45.

XU, X., LIU, W., TIAN, S., WANG, W., QI, Q., JIANG, P., GAO, X., LI, F., LI, H. & YU, H. 2018. Petroleum Hydrocarbon-Degrading Bacteria for the Remediation of Oil Pollution Under Aerobic Conditions: A Perspective Analysis. *Front Microbiol,* 9**,** 2885.

YEH, W. K., GIBSON, D. T. & LIU, T.-N. 1977. Toluene dioxygenase: A multicomponent enzyme system. *Biochemical and Biophysical Research Communications,* 78**,** 401-410.

YEKEEN, N., PADMANABHAN, E., SYED, A. H., SEVOO, T. & KANESEN, K. 2020. Synergistic influence of nanoparticles and surfactants on interfacial tension reduction, wettability alteration and stabilization of oil-in-water emulsion. *Journal of Petroleum Science and Engineering,* 186**,** 106779.

YING, S., GUAN, Z., OFOEGBU, P. C., CLUBB, P., RICO, C., HE, F. & HONG, J. 2022. Green synthesis of nanoparticles: Current developments and limitations. *Environmental Technology & Innovation,* 26**,** 102336.

YU, B., YUAN, Z., YU, Z. & XUE-SONG, F. 2022. BTEX in the environment: An update on sources, fate, distribution, pretreatment, analysis, and removal techniques. *Chemical Engineering Journal,* 435**,** 134825.

YUSUF, E. O., AMBER, I., OFFICER, S. & OLUYEMI, G. F. 2024. Transport of nanoparticles in porous media and associated environmental impact: A review. *Journal of Engineering Research,* 12**,** 275-284.

ZAFAR, A. M., JAVED, M. A., HASSAN, A. A. & MOHAMED, M. M. 2021. Groundwater remediation using zero-valent iron nanoparticles (nZVI). *Groundwater for Sustainable Development,* 15**,** 100694.

ZAGOSKINA, N. V., ZUBOVA, M. Y., NECHAEVA, T. L., KAZANTSEVA, V. V., GONCHARUK, E. A., KATANSKAYA, V. M., BARANOVA, E. N. & AKSENOVA, M. A. 2023. Polyphenols in Plants: Structure, Biosynthesis, Abiotic Stress Regulation, and Practical Applications (Review). *Int J Mol Sci,* 24.

ZENG, G., YANG, R., ZHOU, Z., XU, Z. & LYU, S. 2024. Comparative study of naphthalene removal in different radicals-dominated systems: Kinetics, degradation intermediates, and pathways. *Journal of Water Process Engineering,* 57**,** 104659.

ZENG, J., ZHU, Q., WU, Y., CHEN, H. & LIN, X. 2017. Characterization of a polycyclic aromatic ring-hydroxylation dioxygenase from Mycobacterium sp. NJS-P. *ChemospHere,* 185**,** 67-74.

ZHANG, B., GUO, Y., HUO, J., XIE, H., XU, C. & LIANG, S. 2020. Combining chemical oxidation and bioremediation for petroleum polluted soil remediation by BC-nZVI activated persulphate. *Chemical Engineering Journal,* 382**,** 123055.

ZHANG, B., MATCHINSKI, E. J., CHEN, B., YE, X., JING, L. & LEE, K. 2019. Chapter 21 - Marine Oil Spills—Oil Pollution, Sources and Effects. *In:* SHEPPARD, C. (ed.) *World Seas: An Environmental Evaluation (Second Edition).* Academic Press.

ZHANG, C.-J., ZHOU, Z., CHA, G., LI, L., FU, L., LIU, L.-Y., YANG, L., WEGENER, G., CHENG, L. & LI, M. 2024. Anaerobic hydrocarbon biodegradation by alkylotropHic methanogens in deep oil reservoirs. *The ISME Journal,* 18.

ZHANG, S., YI, K., CHEN, A., SHAO, J., PENG, L. & LUO, S. 2022. Toxicity of zero-valent iron nanoparticles to soil organisms and the associated defense mechanisms: a review. *Ecotoxicology,* 31**,** 873-883.

ZHANG, W.-X. 2003. Nanoscale Iron Particles for Environmental Remediation: An Overview. *Journal of Nanoparticle Research,* 5**,** 323-332.

ZHANG, W. 2014. Nanoparticle Aggregation: Principles and Modeling. *In:* CAPCO, D. G. & CHEN, Y. (eds.) *Nanomaterial: Impacts on Cell Biology and Medicine.* Dordrecht: Springer Netherlands.

ZHAO, Y., ZHAO, Z., SONG, X., JIANG, X., WANG, Y., CAO, X., SI, Z. & PAN, F. 2020. Effects of nZVI dosing on the improvement in the contaminant removal performance of constructed wetlands under the dye stress. *Science of The Total Environment,* 703**,** 134789.

ZHOU, X., ZHOU, C., HUANG, M., WANG, Y., ZHAO, M., ZHANG, Y., FAN, Y., ZHU, Y. & ZHU, Z. 2025. Enhancing nano zero-valent iron (nZVI) performance for Cr(VI) removal through zeolite imidazole framework-8 (ZIF-8) coating. *Water Cycle*.

ZOGHI, P. & MAFIGHOLAMI, R. 2023. Optimisation of soil washing method for removal of petroleum hydrocarbons from contaminated soil around oil storage tanks using response surface methodology. *Scientific Reports,* 13**,** 15457.

Appendices

Appendix A1: TPH values of treated contaminated water with different doses of industrial and green nZVI.

Sample Type	TPH (C8-C40) (mg/L)	Average TPH (mg/L)	Standard Deviation	Average removal efficiency (%)
Contaminated Water	93.10	58.13	30.41	0.00
Contaminated Water	37.90			
Contaminated Water	43.40			
Contaminated Water + 0.004mg/L of Industrial nZVI after 2 h	20.68	19.23	1.38	66.92
Contaminated Water + 0.004mg/L of Industrial nZVI after 2 h	19.08			
Contaminated Water + 0.004mg/L of Industrial nZVI after 2 h	17.93			
Contaminated Water + 0.01mg/L of Industrial nZVI after 2 h	22.53	22.61	0.32	61.11
Contaminated Water + 0.01mg/L of Industrial nZVI after 2 h	22.96			
Contaminated Water + 0.01mg/L of Industrial nZVI after 2 h	22.34			
Contaminated Water + 0.02mg/L of Industrial nZVI after 2 h	28.70	25.83	2.67	55.56
Contaminated Water + 0.02mg/L of Industrial nZVI after 2 h	23.41			
Contaminated Water + 0.02mg/L of Industrial nZVI after 2 h	25.39			
Contaminated Water + 0.004mg/L of Industrial nZVI after 24h	12.10	15.74	3.19	72.92
Contaminated Water + 0.004mg/L of Industrial nZVI after 24h	17.04			
Contaminated Water + 0.004mg/L of Industrial nZVI after 24h	18.08			
Contaminated Water + 0.01mg/L of Industrial nZVI after 24 h	17.07	20.92	3.35	64.01
Contaminated Water + 0.01mg/L of Industrial nZVI after 24 h	22.70			
Contaminated Water + 0.01mg/L of Industrial nZVI after 24 h	23.01			
Contaminated Water + 0.02mg/L of Industrial nZVI after 24 h	17.65	19.66	2.72	66.18
Contaminated Water + 0.02mg/L of Industrial nZVI after 24 h	22.75			
Contaminated Water + 0.02mg/L of Industrial nZVI after 24 h	18.58			
Contaminated Water + 0.004mg/L of Green nZVI after 2 h	30.77	31.81	1.26	45.27
Contaminated Water + 0.004mg/L of Green nZVI after 2 h	31.46			
Contaminated Water + 0.004mg/L of Green nZVI after 2 h	33.22			
Contaminated Water + 0.01mg/L of Green nZVI after 2 h	35.38	36.64	1.15	36.97
Contaminated Water + 0.01mg/L of Green nZVI after 2 h	36.90			
Contaminated Water + 0.01mg/L of Green nZVI after 2 h	37.64			
Contaminated Water + 0.02mg/L of Green nZVI after 2 h	34.80	35.32	0.46	39.24
Contaminated Water + 0.02mg/L of Green nZVI after 2 h	35.67			
Contaminated Water + 0.02mg/L of Green nZVI after 2 h	35.50			
Contaminated Water + 0.004mg/L of Green nZVI after 24 h	20.29	20.98	0.94	63.90
Contaminated Water + 0.004mg/L of Green nZVI after 24 h	22.06			
Contaminated Water + 0.004mg/L of Green nZVI after 24 h	20.60			
Contaminated Water + 0.01mg/L of Green nZVI after 24 h	25.16	24.21	0.83	58.35
Contaminated Water + 0.01mg/L of Green nZVI after 24 h	23.66			
Contaminated Water + 0.01mg/L of Green nZVI after 24 h	23.81			
Contaminated Water + 0.02mg/L of Green nZVI after 24 h	27.19	25.05	2.64	56.92
Contaminated Water + 0.02mg/L of Green nZVI after 24 h	22.09			

Contaminated Water + 0.02mg/L of Green nZVI after 24 h	25.86			

Appendix A: Images from GC-FID results comparing contaminated water with different doses and formulations

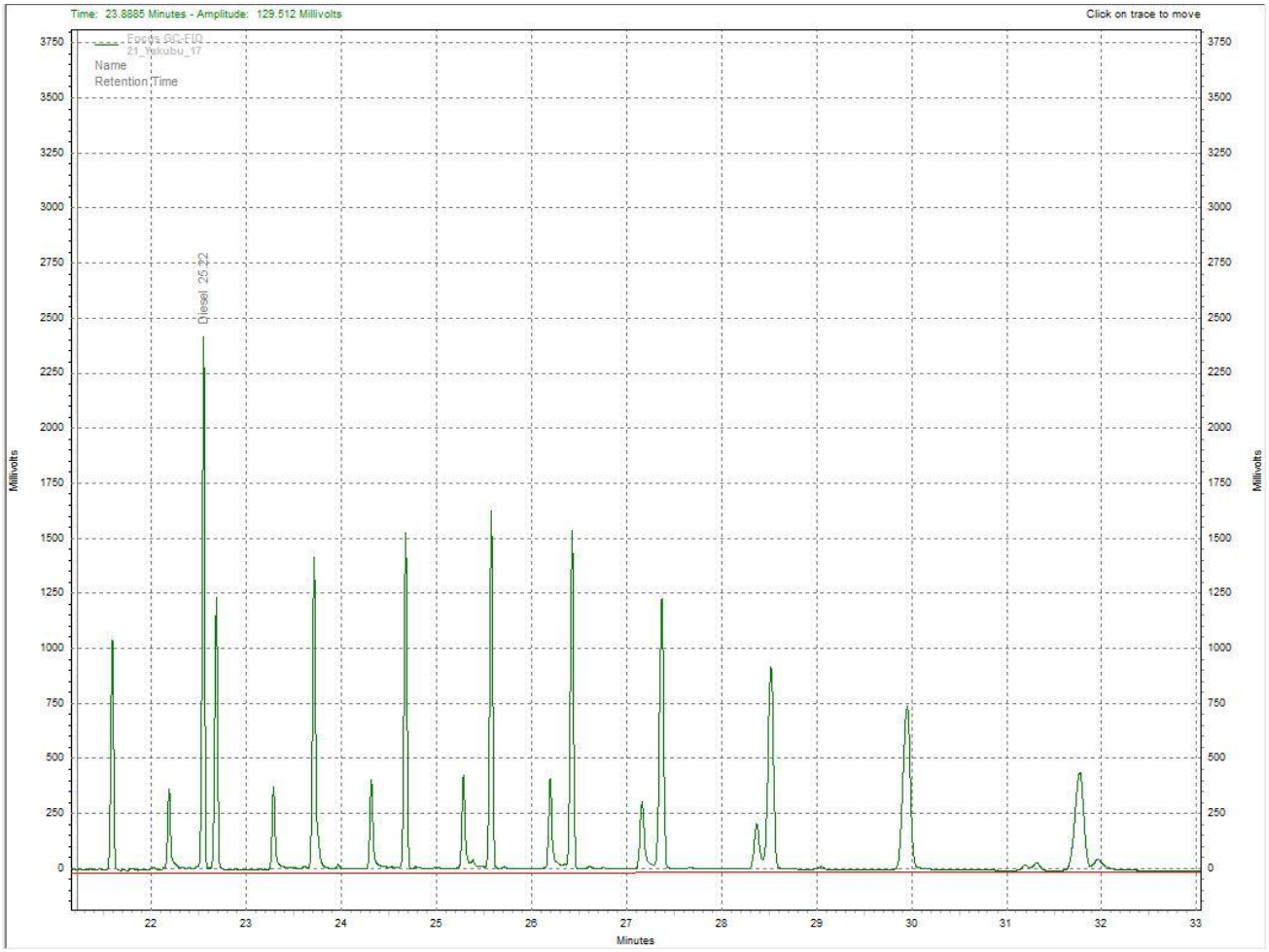

Appendix A.2: *GC-FID Image from Untreated Contaminated water sample*

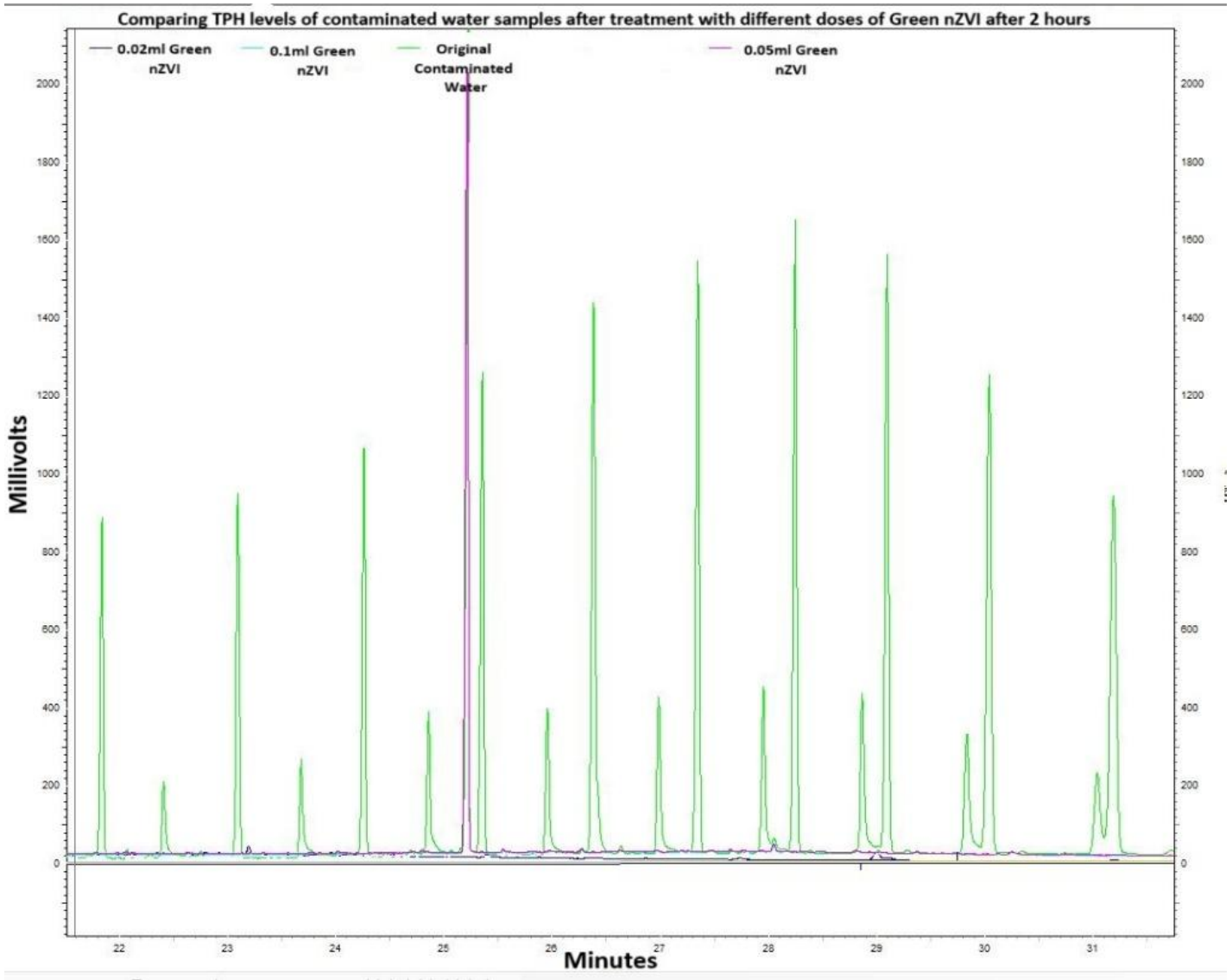

Appendix A.3: *GC-FID Image comparing TPH of contaminated water samples treated with 0.004mg/L, 0.01mg/L and 0.02mg/L doses of Green nZVI after 2 h*

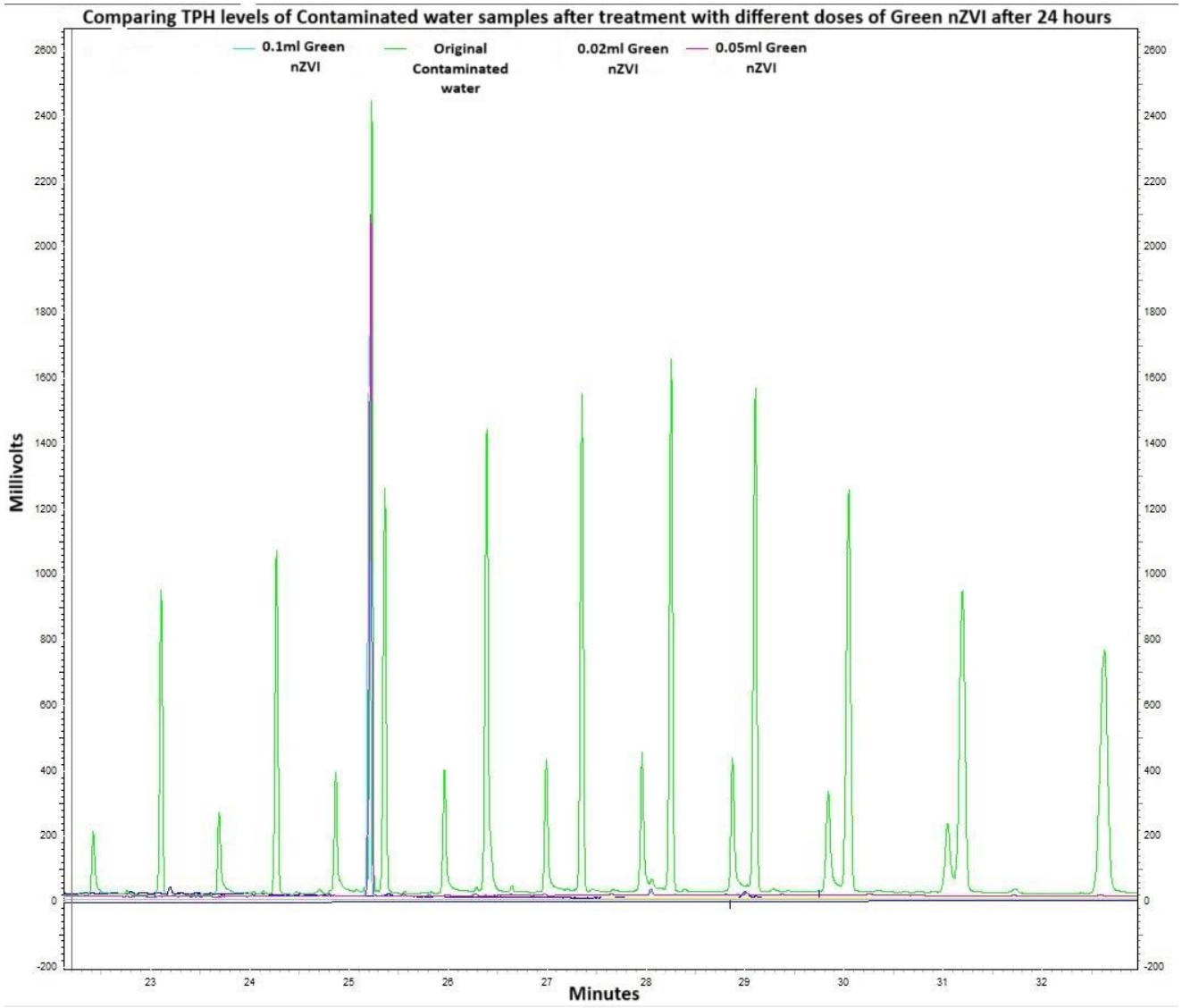

Appendix A.4*: GC-FID Image comparing TPH of contaminated water samples treated with 0.004mg/L, 0.01mg/L and 0.02mg/L doses of Green nZVI after 24 h*

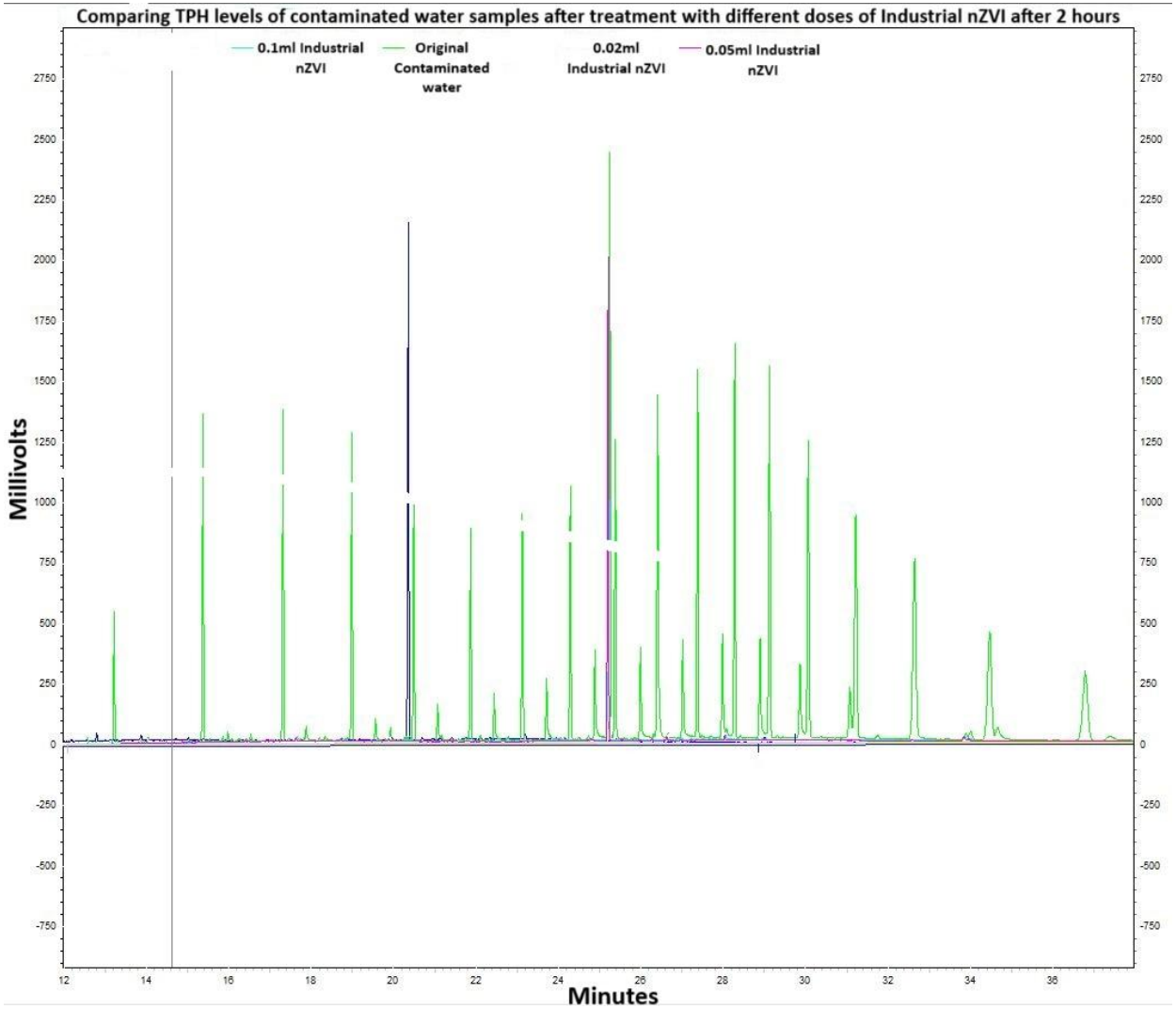

Appendix A.5: *GC-FID Image comparing TPH of contaminated water samples treated with 0.004mg/L, 0.01mg/L and 0.02mg/L doses of Industrial nZVI after 2 h*

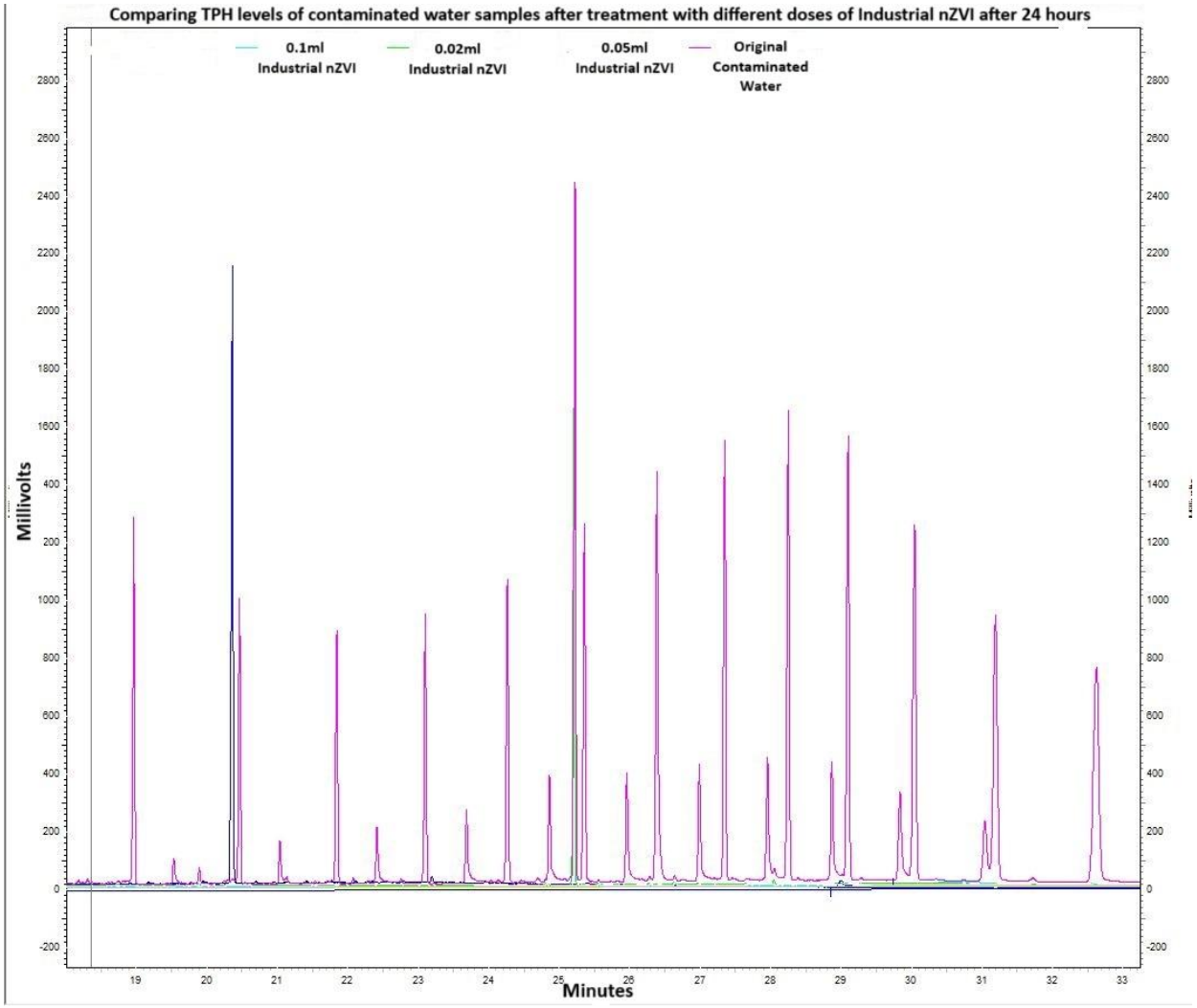

Appendix A.6: *GC-FID Image comparing TPH of contaminated water samples treated with 0.004mg/L, 0.01mg/L and 0.02mg/L doses of Industrial nZVI after 24 h*

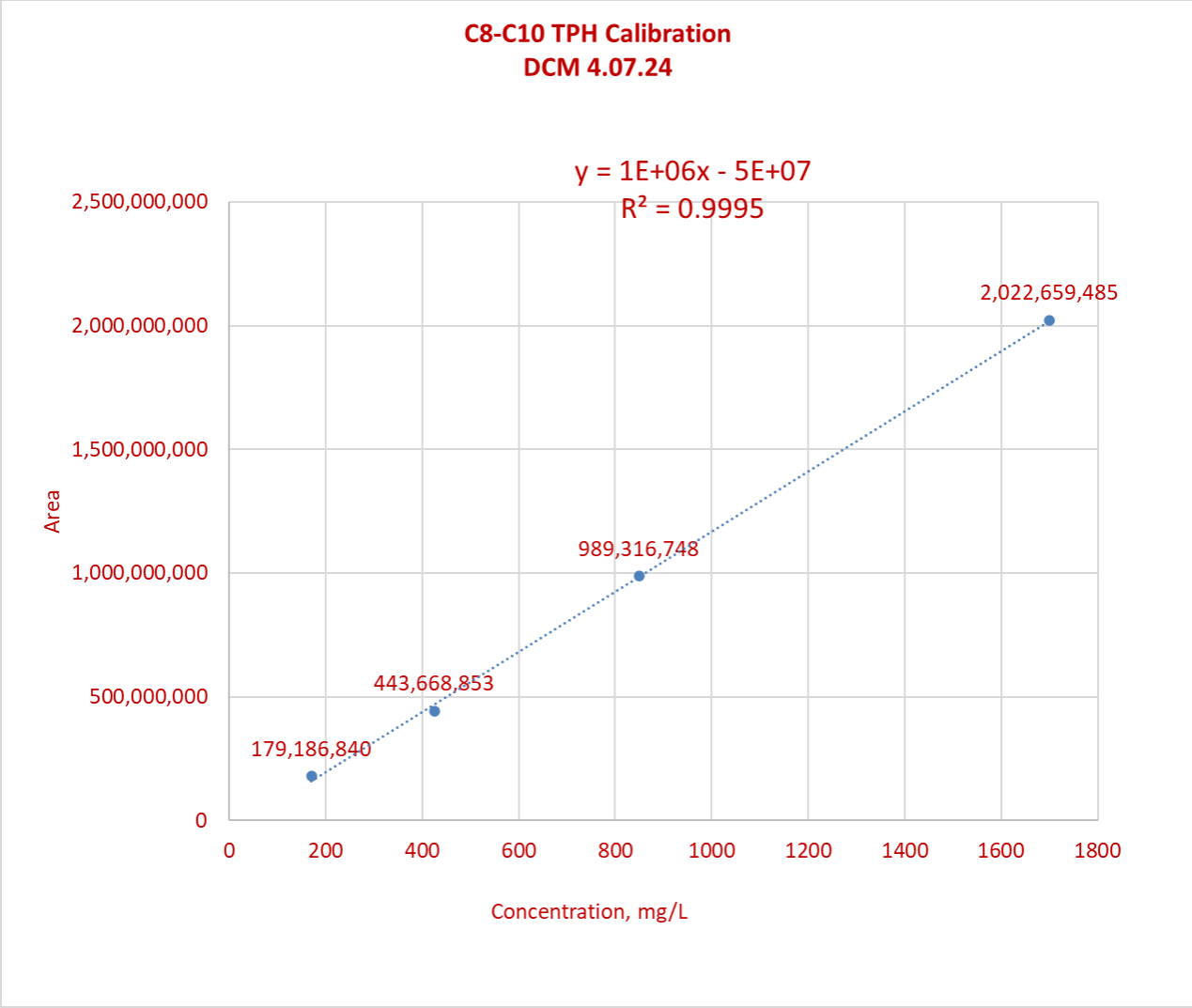

Appendix A.12: *Calibration curve for TPH (C8-C10)*

Appendix B: Data generated from Microbial Analysis

index		k__Archae	k__Archae	k__Bacteri	k__Bacteri	k__Bacteri	k__Bacteri	k__Bacteri	k__Bacteri	k__Bacteri	k__Bacteri	k__Bacteri	k__Bacteri	k__Bacteri	k__Bacteri	k__Bacteri	k__Bacteri	k__Bacteri	k__Bacteri	k__Bacteri	k__Bacteri	k__Bacteri	k__Bacteri	k__Bacteri	k__Bacteri	k__Bacteri	k__Bacteri	k__Bacteri	k__Bacteri	k__Bacteri	k__Bacteri	k__Bacteri	k__Bacteri	k__Bacteri	k__Bacteri	k__Bacteri	k__Bacteri	k__Bacteri
YS-CK-01	9510	0	0	0	0	6	0	1028	0	0	0	52	0	193	0	46	2536	40	0	0	0	0	0	79	0	0	0	0	0	153	14	0	4	0	102	15	1080	7
YS-CK-02	9318	0	0	0	0	95	2	1540	0	0	0	80	0	168	18	27	140	43	0	0	0	2	0	46	0	0	0	0	14	25	13	0	29	0	130	0	1193	11
YS-CK-03	8854	0	0	0	0	113	0	1595	0	0	3	83	0	186	0	24	218	18	0	0	0	0	0	29	0	0	0	0	14	16	17	0	32	0	127	0	1140	11
YS-CK-04	9578	0	0	0	0	93	0	1833	0	0	0	97	0	163	12	14	239	17	0	0	0	0	0	14	0	0	0	0	16	0	6	0	42	0	130	0	1146	16
YS-CK-05	6453	0	0	0	0	0	119	34	0	0	40	42	66	1205	0	71	181	724	6	2	16	33	0	8	0	0	20	0	167	289	66	2	0	0	589	0	371	0
YS-CK-06	7727	0	0	0	0	0	0	637	0	0	0	25	0	84	3	61	3086	38	0	0	0	5	0	37	0	0	0	6	0	54	10	0	8	0	60	6	747	11
YS-CK-07	7889	0	0	0	0	31	0	1020	0	0	0	58	0	156	2	39	2045	24	0	0	0	10	0	32	0	0	0	0	0	95	11	0	11	0	94	8	941	9
YS-CK-08	11599	0	0	0	0	86	0	2386	0	0	0	134	3	183	12	21	243	0	0	0	7	0	0	42	0	0	0	3	30	51	9	0	51	0	171	3	1572	0
YS-CK-09	18237	0	2	0	0	28	66	1607	0	0	76	44	10	1141	175	47	645	2536	0	0	16	38	0	91	0	0	0	261	176	166	29	0	12	0	577	0	2180	23
YS-CK-11	20949	0	0	0	0	20	38	946	0	0	55	18	0	1163	164	35	605	2574	4	0	2	8	0	80	0	0	0	195	126	109	16	0	14	2	741	4	2914	12
YS-CK-12	36851	0	0	0	0	146	45	8379	0	0	119	93	61	1638	92	86	367	1064	0	0	21	38	0	38	0	0	0	67	223	376	46	5	24	0	538	17	5625	38
YS-CK-13	34725	0	0	0	0	141	43	7025	0	0	137	79	48	1611	105	111	302	1003	2	1	23	41	0	47	0	0	0	65	193	304	48	5	37	0	519	17	5898	10
YS-CK-14	30917	0	0	0	0	143	45	4953	0	0	146	49	20	1674	115	280	327	1088	8	5	27	48	0	52	10	0	0	59	180	274	47	5	31	0	462	16	6161	9
YS-CK-01	BLANK Contaminated water sample	0.0%	0.0%	0.0%	0.0%	0.1%	0.0%	10.8%	0.0%	0.0%	0.0%	0.5%	0.0%	2.0%	0.0%	0.5%	26.7%	0.4%	0.0%	0.0%	0.0%	0.0%	0.0%	0.8%	0.0%	0.0%	0.0%	0.0%	0.0%	1.6%	0.1%	0.0%	0.0%	0.0%	1.1%	0.2%	11.4%	0.1%
YS-CK-02	Contaminated water + 0.02ml of InZVI after 2 hrs	0.0%	0.0%	0.0%	0.0%	1.0%	0.0%	16.5%	0.0%	0.0%	0.0%	0.9%	0.0%	1.8%	0.2%	0.3%	1.5%	0.5%	0.0%	0.0%	0.0%	0.0%	0.0%	0.5%	0.0%	0.0%	0.0%	0.0%	0.2%	0.3%	0.1%	0.0%	0.3%	0.0%	1.4%	0.0%	12.8%	0.1%
YS-CK-03	Contaminated water + 0.05ml of InZVI after 2 hrs	0.0%	0.0%	0.0%	0.0%	1.3%	0.0%	18.0%	0.0%	0.0%	0.0%	0.9%	0.0%	2.1%	0.0%	0.3%	2.5%	0.2%	0.0%	0.0%	0.0%	0.0%	0.0%	0.3%	0.0%	0.0%	0.0%	0.0%	0.2%	0.2%	0.2%	0.0%	0.4%	0.0%	1.4%	0.0%	12.9%	0.1%
YS-CK-04	Contaminated water + 0.1ml of InZVI after 2 hrs	0.0%	0.0%	0.0%	0.0%	1.0%	0.0%	19.1%	0.0%	0.0%	0.0%	1.0%	0.0%	1.7%	0.1%	0.1%	2.5%	0.2%	0.0%	0.0%	0.0%	0.0%	0.0%	0.1%	0.0%	0.0%	0.0%	0.0%	0.2%	0.0%	0.1%	0.0%	0.4%	0.0%	1.4%	0.0%	12.0%	0.2%
YS-CK-05	Contaminated water + 0.02ml of InZVI after 24 hrs	0.0%	0.0%	0.0%	0.0%	0.0%	1.8%	0.5%	0.0%	0.0%	0.6%	0.7%	1.0%	18.7%	0.0%	1.1%	2.8%	11.2%	0.1%	0.0%	0.2%	0.5%	0.0%	0.1%	0.0%	0.0%	0.3%	0.0%	2.6%	4.5%	1.0%	0.0%	0.0%	0.0%	9.1%	0.0%	5.7%	0.0%
YS-CK-06	Contaminated water + 0.05ml of InZVI after 24 hrs	0.0%	0.0%	0.0%	0.0%	0.0%	0.0%	8.2%	0.0%	0.0%	0.0%	0.3%	0.0%	1.1%	0.0%	0.8%	39.9%	0.5%	0.0%	0.0%	0.0%	0.1%	0.0%	0.5%	0.0%	0.0%	0.0%	0.1%	0.0%	0.7%	0.1%	0.0%	0.1%	0.0%	0.8%	0.1%	9.7%	0.1%
YS-CK-07	Contaminated water + 0.1ml of InZVI after 24hrs	0.0%	0.0%	0.0%	0.0%	0.4%	0.0%	12.9%	0.0%	0.0%	0.0%	0.7%	0.0%	2.0%	0.0%	0.5%	25.9%	0.3%	0.0%	0.0%	0.0%	0.1%	0.0%	0.4%	0.0%	0.0%	0.0%	0.0%	0.0%	1.2%	0.1%	0.0%	0.1%	0.0%	1.2%	0.1%	11.9%	0.1%
YS-CK-08	Contaminated water + 0.02ml of GnZVI after 2 hrs	0.0%	0.0%	0.0%	0.0%	0.7%	0.0%	20.6%	0.0%	0.0%	0.0%	1.2%	0.0%	1.6%	0.1%	0.2%	2.1%	0.0%	0.0%	0.0%	0.1%	0.0%	0.0%	0.4%	0.0%	0.0%	0.0%	0.0%	0.3%	0.4%	0.1%	0.0%	0.4%	0.0%	1.5%	0.0%	13.6%	0.0%
YS-CK-09	Contaminated water + 0.05ml of GnZVI after 2 hrs	0.0%	0.0%	0.0%	0.0%	0.2%	0.4%	8.8%	0.0%	0.0%	0.4%	0.2%	0.1%	6.3%	1.0%	0.3%	3.5%	13.9%	0.0%	0.0%	0.1%	0.2%	0.0%	0.5%	0.0%	0.0%	0.0%	1.4%	1.0%	0.9%	0.2%	0.0%	0.1%	0.0%	3.2%	0.0%	12.0%	0.1%
YS-CK-11	Contaminated water + 0.1ml of GnZVI after 2 hrs	0.0%	0.0%	0.0%	0.0%	0.1%	0.2%	4.5%	0.0%	0.0%	0.3%	0.1%	0.0%	5.6%	0.8%	0.2%	2.9%	12.3%	0.0%	0.0%	0.0%	0.0%	0.0%	0.4%	0.0%	0.0%	0.0%	0.9%	0.6%	0.5%	0.1%	0.0%	0.1%	0.0%	3.5%	0.0%	13.9%	0.1%
YS-CK-12	Contaminated water + 0.02ml of GnZVI after 24 hrs	0.0%	0.0%	0.0%	0.0%	0.4%	0.1%	22.7%	0.0%	0.0%	0.3%	0.3%	0.2%	4.4%	0.2%	0.2%	1.0%	2.9%	0.0%	0.0%	0.1%	0.1%	0.0%	0.1%	0.0%	0.0%	0.0%	0.2%	0.6%	1.0%	0.1%	0.0%	0.1%	0.0%	1.5%	0.0%	15.3%	0.1%
YS-CK-13	Contaminated water + 0.05ml of GnZVI after 24 hrs	0.0%	0.0%	0.0%	0.0%	0.4%	0.1%	20.2%	0.0%	0.0%	0.4%	0.2%	0.1%	4.6%	0.3%	0.3%	0.9%	2.9%	0.0%	0.0%	0.1%	0.1%	0.0%	0.1%	0.0%	0.0%	0.0%	0.2%	0.6%	0.9%	0.1%	0.0%	0.1%	0.0%	1.5%	0.0%	17.0%	0.0%
YS-CK-14	Contaminated water + 0.1ml of GnZVI after 24 hrs	0.0%	0.0%	0.0%	0.0%	0.5%	0.1%	16.0%	0.0%	0.0%	0.5%	0.2%	0.1%	5.4%	0.4%	0.9%	1.1%	3.5%	0.0%	0.0%	0.1%	0.2%	0.0%	0.2%	0.0%	0.0%	0.0%	0.2%	0.6%	0.9%	0.2%	0.0%	0.1%	0.0%	1.5%	0.1%	19.9%	0.0%

k__Bacteri	k__Bacteri	k__Bacteri	k__Bacteri	k__Bacteri	k__Bacteri	k__Bacteri	k__Bacteri	k__Bacteri	k__Bacteri	k__Bacteri	k__Bacteri	k__Bacteri	k__Bacteri	k__Bacteri	k__Bacteri	k__Bacteri	k__Bacteri	k__Bacteri	k__Bacteri	k__Bacteri	k__Bacteri	k__Bacteri	k__Bacteri	k__Bacteri	k__Bacteri	k__Bacteri	k__Bacteri	k__Bacteri	k__Bacteri	k__Bacteri
7	550	32	101	0	1916	0	0	0	65	56	0	2	0	15	0	0	0	587	0	7	0	0	13	72	714	0	25	0	0	0
11	227	27	100	7	1922	8	0	0	257	243	0	0	0	8	0	0	6	657	5	3	0	0	573	365	1325	0	0	0	9	0
11	200	22	80	0	1819	4	0	0	267	193	0	0	0	0	0	0	0	648	0	0	0	0	290	302	1374	0	0	0	25	4
16	242	23	95	6	1906	6	0	0	291	168	0	0	0	6	0	0	0	831	0	0	0	0	405	364	1364	0	5	0	24	4
0	16	0	88	10	546	0	963	0	0	0	0	0	0	21	0	0	0	0	0	0	0	0	672	0	36	0	0	0	50	0
11	330	11	86	0	1123	0	0	0	60	35	0	0	0	3	0	0	0	209	0	0	0	0	17	28	929	0	18	0	0	0
9	375	19	61	0	1405	0	0	0	119	50	0	0	0	0	0	0	4	400	0	9	0	0	11	52	774	0	19	0	5	0
0	341	33	103	7	2246	0	0	0	330	198	0	3	0	0	0	0	0	825	0	0	0	0	497	368	1618	0	0	3	16	4
23	371	8	347	0	3727	0	223	0	76	358	0	10	2	0	0	55	0	62	5	0	0	0	1659	107	1118	31	2	0	130	0
12	307	0	387	3	3985	0	203	0	48	286	0	0	2	5	0	74	2	66	255	0	0	0	3728	74	1590	8	0	0	81	0
38	893	224	1376	19	8731	0	22	0	576	1162	0	6	0	44	2	0	4	50	0	2	0	0	1302	576	2558	12	27	0	76	43
10	537	299	1008	6	8123	4	31	0	254	571	0	9	0	28	0	0	0	50	11	0	0	0	2891	305	2623	12	19	0	88	41
9	498	302	829	0	6027	12	57	0	180	392	0	9	0	22	0	0	0	40	40	0	0	0	3928	134	2061	14	4	0	92	42
0.1%	5.8%	0.3%	1.1%	0.0%	20.1%	0.0%	0.0%	0.0%	0.7%	0.6%	0.0%	0.0%	0.0%	0.2%	0.0%	0.0%	0.0%	6.2%	0.0%	0.1%	0.0%	0.0%	0.1%	0.8%	7.5%	0.0%	0.3%	0.0%	0.0%	0.0%
0.1%	2.4%	0.3%	1.1%	0.1%	20.6%	0.1%	0.0%	0.0%	2.8%	2.6%	0.0%	0.0%	0.0%	0.1%	0.0%	0.0%	0.1%	7.1%	0.1%	0.0%	0.0%	0.0%	6.1%	3.9%	14.2%	0.0%	0.0%	0.0%	0.1%	0.0%
0.1%	2.3%	0.2%	0.9%	0.0%	20.5%	0.0%	0.0%	0.0%	3.0%	2.2%	0.0%	0.0%	0.0%	0.0%	0.0%	0.0%	0.0%	7.3%	0.0%	0.0%	0.0%	0.0%	3.3%	3.4%	15.5%	0.0%	0.0%	0.0%	0.3%	0.0%
0.2%	2.5%	0.2%	1.0%	0.1%	19.9%	0.1%	0.0%	0.0%	3.0%	1.8%	0.0%	0.0%	0.0%	0.1%	0.0%	0.0%	0.0%	8.7%	0.0%	0.0%	0.0%	0.0%	4.2%	3.8%	14.2%	0.0%	0.1%	0.0%	0.3%	0.0%
0.0%	0.2%	0.0%	1.4%	0.2%	8.5%	0.0%	14.9%	0.0%	0.0%	0.0%	0.0%	0.0%	0.0%	0.3%	0.0%	0.0%	0.0%	0.0%	0.0%	0.0%	0.0%	0.0%	10.4%	0.0%	0.6%	0.0%	0.0%	0.0%	0.8%	0.0%
0.1%	4.3%	0.1%	1.1%	0.0%	14.5%	0.0%	0.0%	0.0%	0.8%	0.5%	0.0%	0.0%	0.0%	0.0%	0.0%	0.0%	0.0%	2.7%	0.0%	0.0%	0.0%	0.0%	0.2%	0.4%	12.0%	0.0%	0.2%	0.0%	0.0%	0.0%
0.1%	4.8%	0.2%	0.8%	0.0%	17.8%	0.0%	0.0%	0.0%	1.5%	0.6%	0.0%	0.0%	0.0%	0.0%	0.0%	0.0%	0.1%	5.1%	0.0%	0.1%	0.0%	0.0%	0.1%	0.7%	9.8%	0.0%	0.2%	0.0%	0.1%	0.0%
0.0%	2.9%	0.3%	0.9%	0.1%	19.4%	0.0%	0.0%	0.0%	2.8%	1.7%	0.0%	0.0%	0.0%	0.0%	0.0%	0.0%	0.0%	7.1%	0.0%	0.0%	0.0%	0.0%	4.3%	3.2%	13.9%	0.0%	0.0%	0.0%	0.1%	0.0%
0.1%	2.0%	0.0%	1.9%	0.0%	20.4%	0.0%	1.2%	0.0%	0.4%	2.0%	0.0%	0.1%	0.0%	0.0%	0.0%	0.3%	0.0%	0.3%	0.0%	0.0%	0.0%	0.0%	9.1%	0.6%	6.1%	0.2%	0.0%	0.0%	0.7%	0.0%
0.1%	1.5%	0.0%	1.8%	0.0%	19.0%	0.0%	1.0%	0.0%	0.2%	1.4%	0.0%	0.0%	0.0%	0.0%	0.0%	0.4%	0.0%	0.3%	1.2%	0.0%	0.0%	0.0%	17.8%	0.4%	7.6%	0.0%	0.0%	0.0%	0.4%	0.0%
0.1%	2.4%	0.6%	3.7%	0.1%	23.7%	0.0%	0.1%	0.0%	1.6%	3.2%	0.0%	0.0%	0.0%	0.1%	0.0%	0.0%	0.0%	0.1%	0.0%	0.0%	0.0%	0.0%	3.5%	1.6%	6.9%	0.0%	0.1%	0.0%	0.2%	0.1%
0.0%	1.5%	0.9%	2.9%	0.0%	23.4%	0.0%	0.1%	0.0%	0.7%	1.6%	0.0%	0.0%	0.0%	0.1%	0.0%	0.0%	0.0%	0.1%	0.0%	0.0%	0.0%	0.0%	8.3%	0.9%	7.6%	0.0%	0.1%	0.0%	0.3%	0.1%
0.0%	1.6%	1.0%	2.7%	0.0%	19.5%	0.0%	0.2%	0.0%	0.6%	1.3%	0.0%	0.0%	0.0%	0.1%	0.0%	0.0%	0.0%	0.1%	0.1%	0.0%	0.0%	0.0%	12.7%	0.4%	6.7%	0.0%	0.0%	0.0%	0.3%	0.1%

Appendix B.1: *Raw data showing Microbial OTUs as extracted from QIIME2*

S/No	Taxon	Abundance (OTUs)
1	k__Bacteria;p__Bacteroidetes;c__Flavobacteriia;o__Flavobacteriales	2536
2	k__Bacteria;p__Proteobacteria;c__Betaproteobacteria;o__Burkholderiales	1916
3	k__Bacteria;p__Proteobacteria;c__Alphaproteobacteria;o__Rhizobiales	1080
4	k__Bacteria;p__Actinobacteria;c__Actinobacteria;o__Actinomycetales	1028
5	k__Bacteria;p__Proteobacteria;c__Gammaproteobacteria;o__Xanthomonadales	714
6	k__Bacteria;p__Proteobacteria;c__Gammaproteobacteria;o__Chromatiales	587
7	k__Bacteria;p__Proteobacteria;c__Alphaproteobacteria;o__Rhodospirillales	550
8	k__Bacteria;p__Bacteroidetes;c__[Saprospirae];o__[Saprospirales]	193
9	k__Bacteria;p__Planctomycetes;c__Planctomycetia;o__Gemmatales	153
10	k__Bacteria;p__Proteobacteria;c__Alphaproteobacteria;o__Caulobacterales	102

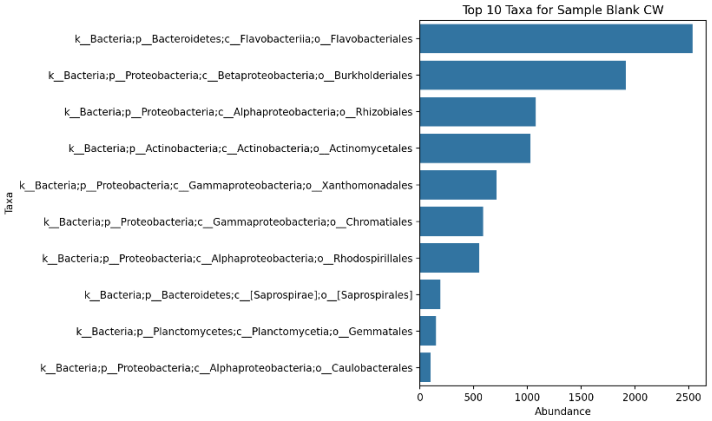

***Appendix B.2**: Figures from Top 10 Microbial Taxa in untreated contaminated water sample and the corresponding Bar chart*

S/No	Taxon	Abundance (OTUs)
1	k__Bacteria;p__Proteobacteria;c__Betaproteobacteria;o__Burkholderiales	1922
2	k__Bacteria;p__Actinobacteria;c__Actinobacteria;o__Actinomycetales	1540
3	k__Bacteria;p__Proteobacteria;c__Gammaproteobacteria;o__Xanthomonadales	1325
4	k__Bacteria;p__Proteobacteria;c__Alphaproteobacteria;o__Rhizobiales	1193
5	k__Bacteria;p__Proteobacteria;c__Gammaproteobacteria;o__Chromatiales	657
6	k__Bacteria;p__Proteobacteria;c__Gammaproteobacteria;o__Pseudomonadales	573
7	k__Bacteria;p__Proteobacteria;c__Gammaproteobacteria;o__PYR10d3	365
8	k__Bacteria;p__Proteobacteria;c__Betaproteobacteria;o__Nitrosomonadales	257
9	k__Bacteria;p__Proteobacteria;c__Betaproteobacteria;o__Rhodocyclales	243
10	k__Bacteria;p__Proteobacteria;c__Alphaproteobacteria;o__Rhodospirillales	227

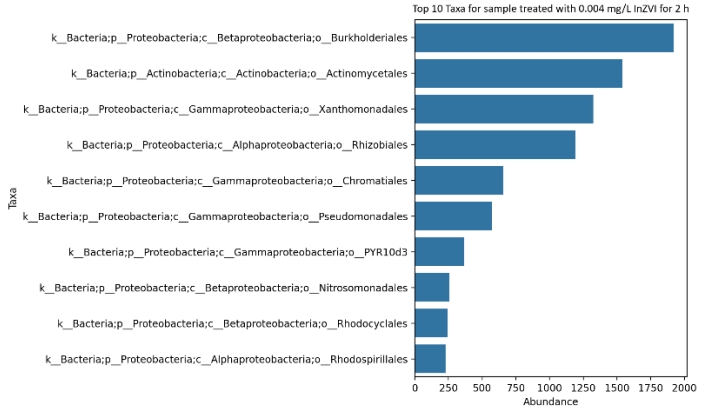

***Appendix B.3**: Figures from Top 10 Microbial Taxa in contaminated water sample treated with 0.004mg/L industrial nZVI after 2 h and the corresponding Bar chart*

S/No	Taxon	Abundance (OTUs)
1	k__Bacteria;p__Proteobacteria;c__Betaproteobacteria;o__Burkholderiales	1819
2	k__Bacteria;p__Actinobacteria;c__Actinobacteria;o__Actinomycetales	1595
3	k__Bacteria;p__Proteobacteria;c__Gammaproteobacteria;o__Xanthomonadales	1374
4	k__Bacteria;p__Proteobacteria;c__Alphaproteobacteria;o__Rhizobiales	1140
5	k__Bacteria;p__Proteobacteria;c__Gammaproteobacteria;o__Chromatiales	648
6	k__Bacteria;p__Proteobacteria;c__Gammaproteobacteria;o__PYR10d3	302
7	k__Bacteria;p__Proteobacteria;c__Gammaproteobacteria;o__Pseudomonadales	290
8	k__Bacteria;p__Proteobacteria;c__Betaproteobacteria;o__Nitrosomonadales	267
9	k__Bacteria;p__Bacteroidetes;c__Flavobacteriia;o__Flavobacteriales	218
10	k__Bacteria;p__Proteobacteria;c__Alphaproteobacteria;o__Rhodospirillales	200

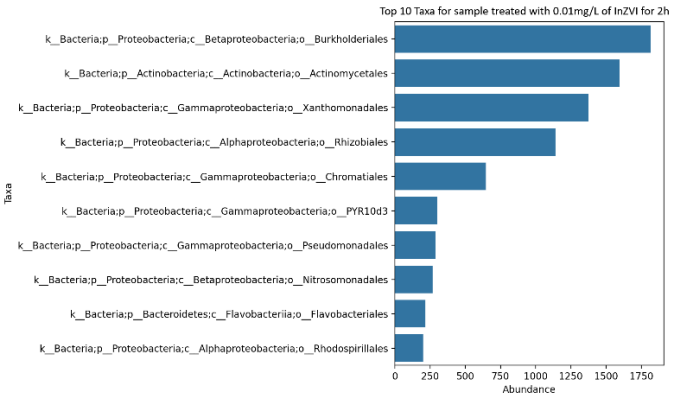

***Appendix B.4**: Figures from Top 10 Microbial Taxa in contaminated water sample treated with 0.01mg/L industrial nZVI after 2 h and the corresponding Bar chart*

S/No	Taxon	Abundance (OTUs)
1	k__Bacteria;p__Proteobacteria;c__Betaproteobacteria;o__Burkholderiales	1906
2	k__Bacteria;p__Actinobacteria;c__Actinobacteria;o__Actinomycetales	1833
3	k__Bacteria;p__Proteobacteria;c__Gammaproteobacteria;o__Xanthomonadales	1364
4	k__Bacteria;p__Proteobacteria;c__Alphaproteobacteria;o__Rhizobiales	1146
5	k__Bacteria;p__Proteobacteria;c__Gammaproteobacteria;o__Chromatiales	831
6	k__Bacteria;p__Proteobacteria;c__Gammaproteobacteria;o__Pseudomonadales	405
7	k__Bacteria;p__Proteobacteria;c__Gammaproteobacteria;o__PYR10d3	364
8	k__Bacteria;p__Proteobacteria;c__Betaproteobacteria;o__Nitrosomonadales	291
9	k__Bacteria;p__Proteobacteria;c__Alphaproteobacteria;o__Rhodospirillales	242
10	k__Bacteria;p__Bacteroidetes;c__Flavobacteriia;o__Flavobacteriales	239

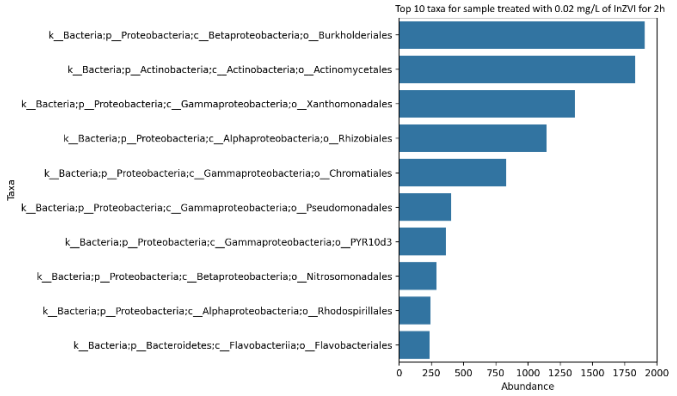

***Appendix B.5**: Figures from Top 10 Microbial Taxa in contaminated water sample treated with 0.02mg/L industrial nZVI after 2 h and the corresponding Bar chart*

S/No	Taxon	Abundance (OTUs)
1	k__Bacteria;p__Bacteroidetes;c__[Saprospirae];o__[Saprospirales]	1205
2	k__Bacteria;p__Proteobacteria;c__Betaproteobacteria;o__Methylophilales	963
3	k__Bacteria;p__Bacteroidetes;c__Sphingobacteriia;o__Sphingobacteriales	724
4	k__Bacteria;p__Proteobacteria;c__Gammaproteobacteria;o__Pseudomonadales	672
5	k__Bacteria;p__Proteobacteria;c__Alphaproteobacteria;o__Caulobacterales	589
6	k__Bacteria;p__Proteobacteria;c__Betaproteobacteria;o__Burkholderiales	546
7	k__Bacteria;p__Proteobacteria;c__Alphaproteobacteria;o__Rhizobiales	371
8	k__Bacteria;p__Planctomycetes;c__Planctomycetia;o__Gemmatales	289
9	k__Bacteria;p__Bacteroidetes;c__Flavobacteriia;o__Flavobacteriales	181
10	k__Bacteria;p__OD1;c__;o__	167

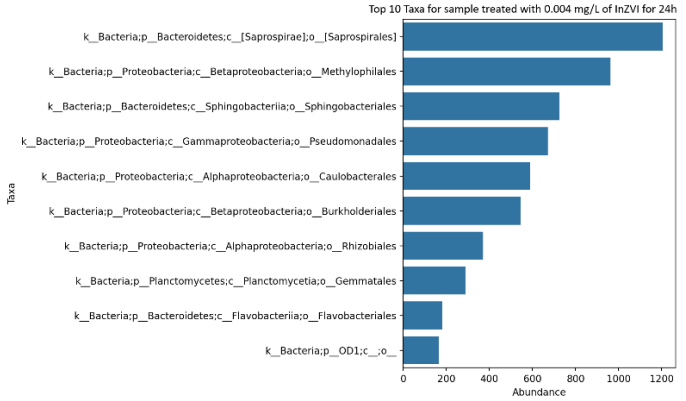

***Appendix B.6**: Figures from Top 10 Microbial Taxa in contaminated water sample treated with 0.004mg/L industrial nZVI after 24 h and the corresponding Bar chart*

S/No	Taxon	Abundance (OTUs)
1	k__Bacteria;p__Bacteroidetes;c__Flavobacteriia;o__Flavobacteriales	3086
2	k__Bacteria;p__Proteobacteria;c__Betaproteobacteria;o__Burkholderiales	1123
3	k__Bacteria;p__Proteobacteria;c__Gammaproteobacteria;o__Xanthomonadales	929
4	k__Bacteria;p__Proteobacteria;c__Alphaproteobacteria;o__Rhizobiales	747
5	k__Bacteria;p__Actinobacteria;c__Actinobacteria;o__Actinomycetales	637
6	k__Bacteria;p__Proteobacteria;c__Alphaproteobacteria;o__Rhodospirillales	330
7	k__Bacteria;p__Proteobacteria;c__Gammaproteobacteria;o__Chromatiales	209
8	k__Bacteria;p__Proteobacteria;c__Alphaproteobacteria;o__Sphingomonadales	86
9	k__Bacteria;p__Bacteroidetes;c__[Saprospirae];o__[Saprospirales]	84
10	k__Bacteria;p__Bacteroidetes;c__Cytophagia;o__Cytophagales	61

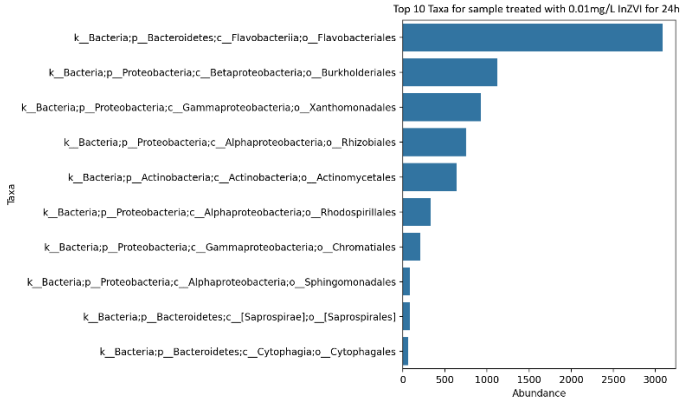

***Appendix B.7**: Figures from Top 10 Microbial Taxa in contaminated water sample treated with 0.01mg/L industrial nZVI after 24 h and the corresponding Bar chart*

S/No	Taxon	Abundance (OTUs)
1	k__Bacteria;p__Bacteroidetes;c__Flavobacteriia;o__Flavobacteriales	2045
2	k__Bacteria;p__Proteobacteria;c__Betaproteobacteria;o__Burkholderiales	1405
3	k__Bacteria;p__Actinobacteria;c__Actinobacteria;o__Actinomycetales	1020
4	k__Bacteria;p__Proteobacteria;c__Alphaproteobacteria;o__Rhizobiales	941
5	k__Bacteria;p__Proteobacteria;c__Gammaproteobacteria;o__Xanthomonadales	774
6	k__Bacteria;p__Proteobacteria;c__Gammaproteobacteria;o__Chromatiales	400
7	k__Bacteria;p__Proteobacteria;c__Alphaproteobacteria;o__Rhodospirillales	375
8	k__Bacteria;p__Bacteroidetes;c__[Saprospirae];o__[Saprospirales]	156
9	k__Bacteria;p__Proteobacteria;c__Betaproteobacteria;o__Nitrosomonadales	119
10	k__Bacteria;p__Planctomycetes;c__Planctomycetia;o__Gemmatales	95

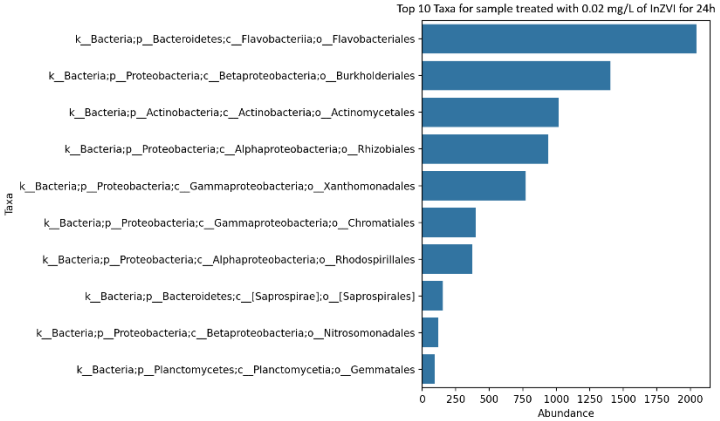

***Appendix B.8**: Figures from Top 10 Microbial Taxa in contaminated water sample treated with 0.02mg/L industrial nZVI after 24 h and the corresponding Bar chart*

S/No	Taxon	Abundance (OTUs)
1	k__Bacteria;p__Actinobacteria;c__Actinobacteria;o__Actinomycetales	2386
2	k__Bacteria;p__Proteobacteria;c__Betaproteobacteria;o__Burkholderiales	2246
3	k__Bacteria;p__Proteobacteria;c__Gammaproteobacteria;o__Xanthomonadales	1618
4	k__Bacteria;p__Proteobacteria;c__Alphaproteobacteria;o__Rhizobiales	1572
5	k__Bacteria;p__Proteobacteria;c__Gammaproteobacteria;o__Chromatiales	825
6	k__Bacteria;p__Proteobacteria;c__Gammaproteobacteria;o__Pseudomonadales	497
7	k__Bacteria;p__Proteobacteria;c__Gammaproteobacteria;o__PYR10d3	368
8	k__Bacteria;p__Proteobacteria;c__Alphaproteobacteria;o__Rhodospirillales	341
9	k__Bacteria;p__Proteobacteria;c__Betaproteobacteria;o__Nitrosomonadales	330
10	k__Bacteria;p__Bacteroidetes;c__Flavobacteriia;o__Flavobacteriales	243

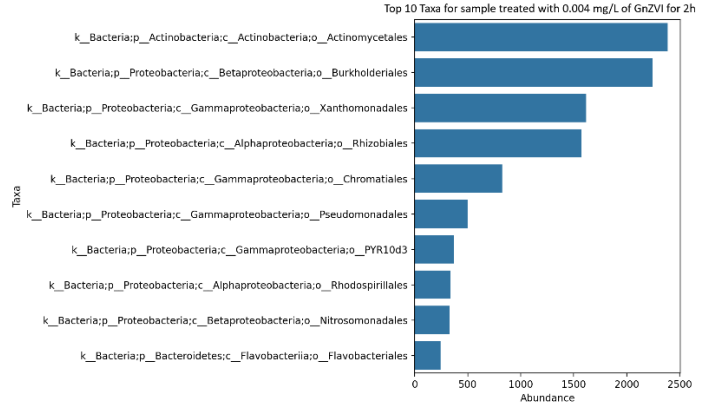

***Appendix B.9**: Figures from Top 10 Microbial Taxa in contaminated water sample treated with 0.004mg/L Green nZVI after 2 h and the corresponding Bar chart*

S/No	Taxon	Abundance (OTUs)
1	k__Bacteria;p__Proteobacteria;c__Betaproteobacteria;o__Burkholderiales	3727
2	k__Bacteria;p__Bacteroidetes;c__Sphingobacteriia;o__Sphingobacteriales	2536
3	k__Bacteria;p__Proteobacteria;c__Alphaproteobacteria;o__Rhizobiales	2180
4	k__Bacteria;p__Proteobacteria;c__Gammaproteobacteria;o__Pseudomonadales	1659
5	k__Bacteria;p__Actinobacteria;c__Actinobacteria;o__Actinomycetales	1607
6	k__Bacteria;p__Bacteroidetes;c__[Saprospirae];o__[Saprospirales]	1141
7	k__Bacteria;p__Proteobacteria;c__Gammaproteobacteria;o__Xanthomonadales	1118
8	k__Bacteria;p__Bacteroidetes;c__Flavobacteriia;o__Flavobacteriales	645
9	k__Bacteria;p__Proteobacteria;c__Alphaproteobacteria;o__Caulobacterales	577
10	k__Bacteria;p__Proteobacteria;c__Alphaproteobacteria;o__Rhodospirillales	371

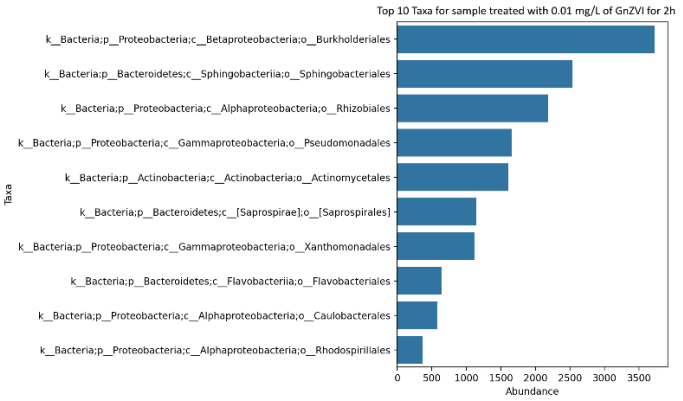

***Appendix B.10**: Figures from Top 10 Microbial Taxa in contaminated water sample treated with 0.01mg/L Green nZVI after 2 h and the corresponding Bar chart*

S/No	Taxon	Abundance (OTUs)
1	k__Bacteria;p__Proteobacteria;c__Betaproteobacteria;o__Burkholderiales	3985
2	k__Bacteria;p__Proteobacteria;c__Gammaproteobacteria;o__Pseudomonadales	3728
3	k__Bacteria;p__Proteobacteria;c__Alphaproteobacteria;o__Rhizobiales	2914
4	k__Bacteria;p__Bacteroidetes;c__Sphingobacteriia;o__Sphingobacteriales	2574
5	k__Bacteria;p__Proteobacteria;c__Gammaproteobacteria;o__Xanthomonadales	1590
6	k__Bacteria;p__Bacteroidetes;c__[Saprospirae];o__[Saprospirales]	1163
7	k__Bacteria;p__Actinobacteria;c__Actinobacteria;o__Actinomycetales	946
8	k__Bacteria;p__Proteobacteria;c__Alphaproteobacteria;o__Caulobacterales	741
9	k__Bacteria;p__Bacteroidetes;c__Flavobacteriia;o__Flavobacteriales	605
10	k__Bacteria;p__Proteobacteria;c__Alphaproteobacteria;o__Sphingomonadales	387

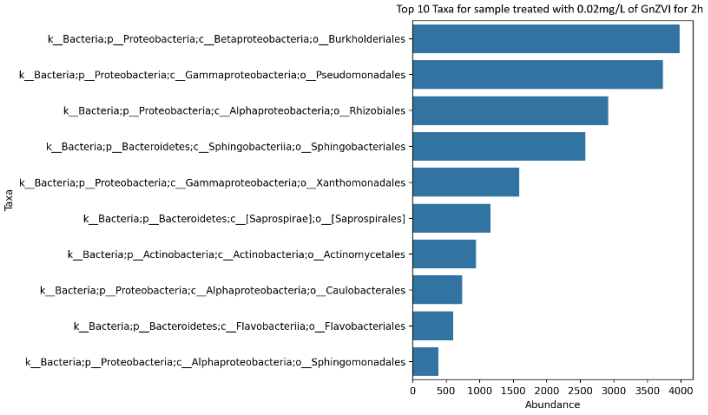

***Appendix B.11**: Figures from Top 10 Microbial Taxa in contaminated water sample treated with 0.02mg/L Green nZVI after 2 h and the corresponding Bar chart*

S/No	Taxon	Abundance (OTUs)
1	k__Bacteria;p__Proteobacteria;c__Betaproteobacteria;o__Burkholderiales	8731
2	k__Bacteria;p__Actinobacteria;c__Actinobacteria;o__Actinomycetales	8379
3	k__Bacteria;p__Proteobacteria;c__Alphaproteobacteria;o__Rhizobiales	5625
4	k__Bacteria;p__Proteobacteria;c__Gammaproteobacteria;o__Xanthomonadales	2558
5	k__Bacteria;p__Bacteroidetes;c__[Saprospirae];o__[Saprospirales]	1638
6	k__Bacteria;p__Proteobacteria;c__Alphaproteobacteria;o__Sphingomonadales	1376
7	k__Bacteria;p__Proteobacteria;c__Gammaproteobacteria;o__Pseudomonadales	1302
8	k__Bacteria;p__Proteobacteria;c__Betaproteobacteria;o__Rhodocyclales	1162
9	k__Bacteria;p__Bacteroidetes;c__Sphingobacteriia;o__Sphingobacteriales	1064
10	k__Bacteria;p__Proteobacteria;c__Alphaproteobacteria;o__Rhodospirillales	893

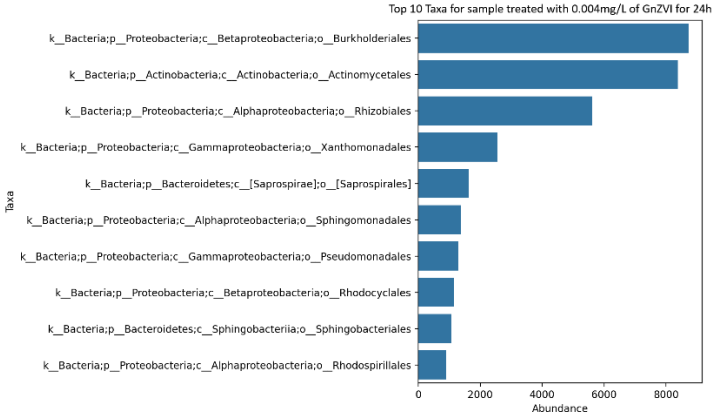

***Appendix B.12**: Figures from Top 10 Microbial Taxa in contaminated water sample treated with 0.004mg/L Green nZVI after 24 h and the corresponding Bar chart*

S/No	Taxon	Abundance (OTUs)
1	k__Bacteria;p__Proteobacteria;c__Betaproteobacteria;o__Burkholderiales	8123
2	k__Bacteria;p__Actinobacteria;c__Actinobacteria;o__Actinomycetales	7025
3	k__Bacteria;p__Proteobacteria;c__Alphaproteobacteria;o__Rhizobiales	5898
4	k__Bacteria;p__Proteobacteria;c__Gammaproteobacteria;o__Pseudomonadales	2891
5	k__Bacteria;p__Proteobacteria;c__Gammaproteobacteria;o__Xanthomonadales	2623
6	k__Bacteria;p__Bacteroidetes;c__[Saprospirae];o__[Saprospirales]	1611
7	k__Bacteria;p__Proteobacteria;c__Alphaproteobacteria;o__Sphingomonadales	1008
8	k__Bacteria;p__Bacteroidetes;c__Sphingobacteriia;o__Sphingobacteriales	1003
9	k__Bacteria;p__Proteobacteria;c__Betaproteobacteria;o__Rhodocyclales	571
10	k__Bacteria;p__Proteobacteria;c__Alphaproteobacteria;o__Rhodospirillales	537

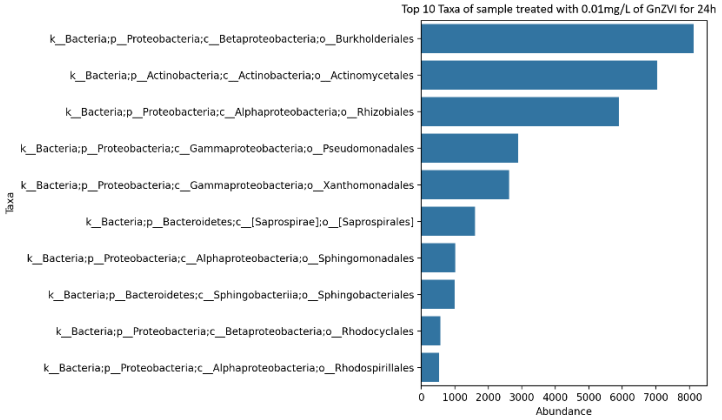

***Appendix B.13**: Figures from Top 10 Microbial Taxa in contaminated water sample treated with 0.01mg/L Green nZVI after 24 h and the corresponding Bar chart*

S/No	Taxon	Abundance (OTUs)
1	k__Bacteria;p__Proteobacteria;c__Alphaproteobacteria;o__Rhizobiales	6161
2	k__Bacteria;p__Proteobacteria;c__Betaproteobacteria;o__Burkholderiales	6027
3	k__Bacteria;p__Actinobacteria;c__Actinobacteria;o__Actinomycetales	4953
4	k__Bacteria;p__Proteobacteria;c__Gammaproteobacteria;o__Pseudomonadales	3928
5	k__Bacteria;p__Proteobacteria;c__Gammaproteobacteria;o__Xanthomonadales	2061
6	k__Bacteria;p__Bacteroidetes;c__[Saprospirae];o__[Saprospirales]	1674
7	k__Bacteria;p__Bacteroidetes;c__Sphingobacteriia;o__Sphingobacteriales	1088
8	k__Bacteria;p__Proteobacteria;c__Alphaproteobacteria;o__Sphingomonadales	829
9	k__Bacteria;p__Proteobacteria;c__Alphaproteobacteria;o__Rhodospirillales	498
10	k__Bacteria;p__Proteobacteria;c__Alphaproteobacteria;o__Caulobacterales	462

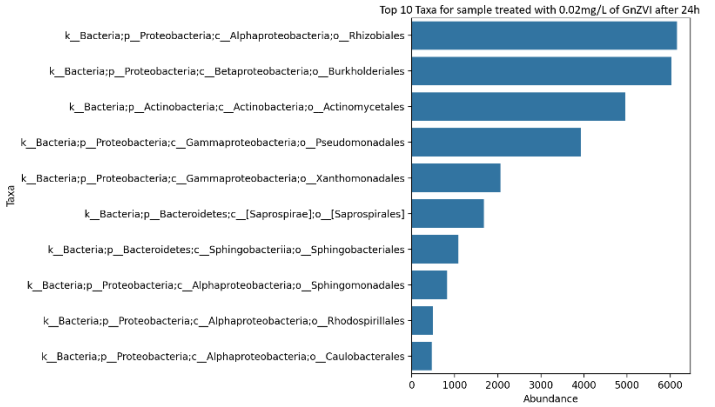

Appendix B.14*: Figures from Top 10 Microbial Taxa in contaminated water sample treated with 0.02mg/L Green nZVI after 24 h and the corresponding Bar chart*